RUTTING PERFORMANCE OF AIRPORT HOT-MIX ASPHALT CHARACTERIZED BY LABORATORY PERFORMANCE TESTING, FULL-SCALE ACCELERATED PAVEMENT TESTING, AND FINITE ELEMENT MODELING

A Dissertation

by

JOHN FORD RUSHING

Submitted to the Office of Graduate and Professional Studies of
Texas A&M University
in partial fulfillment of the requirements for the degree of

DOCTOR OF PHILOSOPHY

Chair of Committee,	Dallas N. Little
Committee Members,	E. Ray Brown
	Charles J. Glover
	Robert L. Lytton
	Eyad A. Masad
Head of Department,	Robin L. Autenrieth

May 2014

Major Subject: Civil Engineering

ABSTRACT

Hot Mix Asphalt (HMA) laboratory mixture design is intended to provide a durable, rut-resistant mixture for a given traffic type. Current mixture design procedures using the Superpave Gyratory Compactor (SGC) rely on volumetric properties of the compacted mixture to assure reliable performance; however, a definitive performance test does not exist. This study provides guidance for selecting a laboratory performance test for airport HMA mixture designs based on; (a) data analyses of results from four potential laboratory tests, (b) comparisons of laboratory tests results to full-scale accelerated pavement test results, and (c) analyses of results from finite element simulations.

The laboratory study evaluated of the repeated load test, the static creep test, the dynamic modulus test, and the Asphalt Pavement Analyzer (APA) test as potential performance tests to accompany airport HMA mixture design with a goal of providing acceptable threshold test results that predict rutting performance under aircraft traffic. Over 340 specimens were tested from 34 asphalt mixtures. Specific criteria for each test method were developed.

Next, the test methods and criteria were applied to an HMA mixture design selected for accelerated pavement testing. The full-scale tests applied wheel loads that simulated both military fighter aircraft and heavy cargo aircraft traffic to a pavement constructed to meet typical airport design standards. In the first test, simulating fighter jet aircraft, the tire inflation pressure was 2241 kPa, and the pavement temperature was maintained at 43°C. The second test, simulating cargo aircraft, used a tire inflation pressure of 980 kPa

and a pavement temperature of 25°C. As expected, rutting was much more severe in the first test.

The full-scale tests were then simulated computationally using finite element modeling. The asphalt layer was modeled using the nonlinear viscoelastic, viscoplastic components of the Pavement Analysis Using Nonlinear Damage Approach (PANDA) model. The pavement sections and wheel loads from the field-tests were recreated using two-dimensional simulations within ABAQUS. The simulations resulted in very high rates of viscoplastic strain for the conditions of the first test, but almost no permanent deformation in the second test. Finally, recommendations for implementing APA criteria into airfield HMA mixture design are presented.

DEDICATION

This dissertation is dedicated to my children, Reagan and Kyle. Dare to dream big; never give up. If you believe in yourself, work hard, and be persistently determined, you will find that anything is possible.

ACKNOWLEDGEMENTS

I sincerely thank my committee chair, Dr. Dallas N. Little, for providing continuous support and guidance. His advice, encouragement, and direction have been invaluable during my studies. I also express my appreciation to Dr. Ray Brown for his friendship and mentoring and to my committee members, Dr. Charles Glover, Dr. Robert Lytton, and Dr. Eyad Masad, for their guidance and support throughout the course of this research.

I am grateful to Mr. Tim McCaffrey and the team at ERDC for outstanding technical support throughout the laboratory and field-testing processes. I appreciate Ms. Cheri Loden for her help in preparing this document and all my colleagues who provided guidance on its content.

I thank Dr. Masoud Darabi, Eisa Rahmani, and Taesun You for patiently helping me through the technical and software challenges of computational simulations. Without you, this work would not have been possible.

I express my gratitude to the Federal Aviation Administration, William J. Hughes Technical Center for its financial contributions and support of laboratory testing and to the U.S. Air Force Civil Engineer Center for its financial contributions to field-tests. I am also grateful to the management at ERDC for allowing me to pursue my educational goals.

Finally, I offer my appreciation to my parents for their encouragement and my gratitude to my wife, Casey, for her patience, love, and commitment to me, allowing me to follow my dreams.

NOMENCLATURE

AASHTO	American Association of State Highway Transportation Officials
AIMS	Aggregate Image Measurement System
AMPT	asphalt mixture performance tester
ANOVA	analysis of variance
APA	Asphalt Pavement Analyzer
CBR	California Bearing Ratio
DoD	Department of Defense
DSR	Dynamic Shear Rheometer
ERDC	U.S. Army Engineer Research and Development Center
FAA	Federal Aviation Administration
FN	flow number
FT	flow time
HMA	Hot Mix Asphalt
HVS	heavy vehicle simulator
JMF	Job Mix Formula
LVDT	Linear variable differential transformer
MEPDG	Mechanistic Empirical Pavement Design Guide
MMPT	mean monthly pavement temperature
NCAT	National Center for Asphalt Technology
NCHRP	National Cooperative Highway Research Program

PANDA	Pavement Analysis Using Nonlinear Damage Approach
PG	Performance grade
PUI	Panda User Interface
RCRT-CLT	repeated creep-recovery test with constant loading time
RCRT-VS	Repeated creep-recovery at various stress level
SGC	Superpave Gyratory Compactor
Superpave	Superior Performing Asphalt Pavements
TF	tertiary flow number
USCS	Unified Soil Classification System

TABLE OF CONTENTS

Page

LIST OF FIGURES

Page

LIST OF TABLES

Page

CHAPTER I

INTRODUCTION

Superpave HMA Mixture Design Procedure

Rut minimization on airport hot mix asphalt (HMA) pavements is a topic that has been studied for many years. The development of aircraft with heavier wheel loads and higher tire pressures has contributed to refinement of material selection and pavement design procedures. Aircraft with higher tire pressures are more likely to cause rutting to occur. New generation aircraft continue to necessitate modifications in the procedures by which HMA mixtures are designed so that rutting does not become a prevalent distress on airport pavements.

The Federal Aviation Administration (FAA) has predominantly required use of the Marshall method for designing HMA mixtures for airfield pavements although several other mixture design methods have been developed over the years. The Superior Performing Asphalt Pavements (Superpave) laboratory mixture design and analysis system was introduced in the mid 1990s. This method is based on compaction of asphalt concrete specimens using a Superpave gyratory compactor (SGC). The SGC was selected because it produced compacted specimens with particle orientation more closely simulating the results of field compaction (Consuega et al. 1989).

The Superpave HMA mixture design procedure has been adopted by nearly every state department of transportation in the United States. Consequently, contractors and testing laboratories maintain testing capabilities for, and are experienced in using the

Superpave method. In the future, organizations continuing to use the Marshall mixture design method will encounter increasing difficulty in finding contractors and testing laboratories experienced and accredited in the Marshall mixture design method.

Originally, the Superpave mixture design method consisted of three proposed phases: (1) materials selection, (2) aggregate blending, and (3) volumetric analysis on specimens compacted using the SGC. A fourth step that would provide a method to analyze the mixture properties and to determine performance potential is needed. National Cooperative Highway Research Program (NCHRP) Project 9-19 identified potential performance tests to complement the Superpave mixture design method (Witczak et al. 2002). Most state departments of transportation have not yet adopted these procedures, and no guidance for applying these tests to airport HMA exists.

Research and experimental construction projects have shown that the Superpave volumetric mixture design method alone is not sufficient to ensure reliable mixture performance over a wide range of materials, traffic, and climatic conditions. Good field performance cannot be ensured by controlling volumetric properties (Brown et al. 2001).

Correlations between Marshall and Superpave Gyratory Compaction

Rushing (2009) recently reported results of a study conducted to recommend a value for the number of design gyrations in the SGC (N_{design}) with which to design asphalt mixtures for airport pavements using the SGC. The value for N_{design} was selected as the number of gyrations resulting in an air void content of 3.5 percent. This compaction was performed at the same binder content required to compact samples to 3.5 percent air voids using the Marshall 75-blow manual compaction effort. Fifty-two HMA mixtures

were evaluated in the study. The number of gyrations required to produce equivalent density had a mean value of 69 and one standard deviation of 25. Mortar sand content, aggregate type and gradation, and binder type all contributed to significant differences in the number of gyrations required to compact mixtures to the target air void content of 3.5 percent. While the mean value was selected for N_{design}, further analysis showed that changing the N_{design} value by 10 gyrations resulted in less than a 0.5-percent change in air void content. An N_{design} value of 70 was recommended for implementation along with monitoring the performance of in-service pavements. Rushing recommended the adoption of a performance test to evaluate mixtures in the laboratory.

Cooley et al. (2007) conducted a study for the Airfield Asphalt Pavement Technology Program to create a specification for designing asphalt paving mixtures for airport pavements. One of the primary objectives for the study was to determine the required compaction effort for the SGC. HMA mixtures from 10 airports were collected and compacted in the laboratory at different compaction efforts. Additionally, performance testing using the flow number test was conducted to characterize the rutting potential of the mixtures. Recommendations from the study included using three different compaction efforts depending on the anticipated tire pressures of the aircraft using the pavement. Gyration levels of 50, 65, and 80 were recommended for design aircraft tire pressures of less than 690 kPa, 690 to 1380 kPa, and more than 1380 kPa, respectively. However, actual data from the study indicated an average of 49 gyrations in the SGC produced equivalent density to the 75-blow Marshall compaction. Cooley also

stated the importance of including a proof test in the specification that would test the properties of the HMA mixture.

A third study also compared the SGC to the Marshall device to correlate compaction efforts. This study used HMA mixtures from eight airport paving projects. Christensen (2010) reported an average value of 62 gyrations required to produce a density equivalent to the 75-blow Marshall compaction. Recommendations from the study included using 70 gyrations as recommended by Rushing.

Problem Statement

The proportion of aggregate and binder used in an HMA mixture has a significant influence on asphalt mixture performance in the field. A laboratory design procedure is used to select good quality materials in a proportion that will result in optimal mixture performance. Traditionally, the Marshall design procedure has been used by the FAA to design mixtures in the laboratory. The Marshall method uses requirements of volumetric properties as well as performance index tests to determine if a HMA mixture is acceptable. The FAA is currently adopting an optional laboratory design procedure that uses the SGC for compaction. In this procedure, the proportion of aggregate and binder is selected only from the volumetric properties of compacted specimens. There is no method available to assess the performance of the selected mixture in response to loading. Several studies have been completed to identify a simple performance test for HMA mixtures for roadway pavements. The applicability of these tests and associated acceptance limits for airport pavements is not known.

Objective and Scope of Study

The objective of this study was to develop a laboratory procedure for testing HMA designed for airfield pavement that can identify mixtures prone to permanent deformation, or rutting. A selected suite of performance tests was performed on HMA mixtures with an expected broad range of rutting performance potential with the goal of identifying preliminary criteria for using the test results to screen airport HMA paving mixtures. The ability of each performance test to appropriately rank mixture performance was a primary factor in test selection. The preliminary criteria developed from laboratory testing were assessed by comparing laboratory test results of one HMA mixture to field performance from accelerated pavement testing using two different loading and environmental conditions. Further, finite element simulations of the field-test pavements provided insight into the material properties affecting rutting to enhance the designer's ability to design rut-resistant mixtures for any specific loading scenario.

Outline of the Dissertation

Chapter II of this dissertation presents a literature review of permanent deformation in asphalt concrete pavement layers and material properties that influence its occurrence. Models used to predict permanent deformation in asphalt concrete are discussed. This chapter also presents laboratory tests used for quantifying an asphalt mixture's susceptibility to permanent deformation. The principles of each laboratory performance test are described along with the benefits and limitations according to the literature.

Chapter III describes the materials used in this study. Three aggregate types were mixed with both an unmodified binder and a polymer-modified binder to prepare the

asphalt concrete mixtures used in the study. Aggregate gradation and maximum size of aggregate, along with the percentage of natural sand used in the mixture, were varied to provide a broad range of mixture rutting performance. The airport pavement mixture design procedure is also described in this chapter.

Chapter IV provides a plan of study including descriptions of the materials selected for use, the HMA mixture designs, the modeling procedures and performance tests used to identify the potential for permanent deformation of the mixtures, and the full-scale accelerated pavement testing.

Chapter V discusses the different performance tests selected for this study. Three tests—the Asphalt Pavement Analyzer test, the repeated load test, and the static creep test—were modified to account for the higher tire pressures experienced by airport pavements compared to roadway pavements. The modifications included increasing the loading stress for each test and increasing the confining stress for triaxial tests. The dynamic modulus test was performed according to standard procedures.

Chapter VI presents results from the laboratory performance tests. Results from the triaxial repeated load and static creep tests were used to identify four different numerical indices that can be extracted from test data. Each of these indices was evaluated based on its ability to rank mixture performance. Results from the dynamic modulus test are often imported into a modeling procedure such as the mechanistic-empirical pavement design guide (MEPDG) and used to determine structural designs as well as to predict damage from traffic. For this study, critical response values from dynamic modulus data were investigated as a mixture ranking system. The Asphalt Pavement Analyzer (APA)

test produced data for accumulated rut depth as a function of number of simulated traffic passes. Criterion for APA testing typically states that a mixture must not exceed a specified level of rutting after a given number of passes. Analysis of the data from this study followed this approach for making recommendations for high-pressure APA testing. Chapter VII provides an assessment of the laboratory performance tests based upon the results from this study.

Chapter VIII describes full-scale accelerated pavement testing that was performed on one asphalt mixture using two different loading and environmental conditions. The first test applied simulated military fighter aircraft traffic to a pavement at an elevated temperature (43°C). This portion of the study represented the case particularly prone to rutting because of high tire pressure (2241 kPa) and warm temperature. A second test applied simulated military cargo aircraft traffic at a moderate temperature of 25°C. The cargo aircraft scenario represented heavy gross loads, but lower tire pressure (980 kPa), at moderate temperature. These conditions typically result in low rutting potential. Laboratory performance test results from the asphalt mixture used in accelerated pavement testing were compared to field performance observations to validate proposed criteria developed from the initial work.

Chapter IX describes the finite element modeling procedures used in this study. A nonlinear viscoelastic, viscoplastic asphalt material model was selected to characterize mixture performance. Finite element simulations were performed on the pavement structures from accelerated pavement testing using the material properties measured for the different pavement layers. The user-defined material model, PANDA, was applied to

the asphalt concrete layer. Loading simulations were selected to mimic accelerated pavement tests. The rutting predictions are compared with field results.

Chapter X discusses the considerations for selecting a performance test for airport HMA mixture design. Chapter XI provides conclusions and recommendations from this study.

CHAPTER II

LITERATURE REVIEW

Permanent Deformation in Airport HMA Pavements

Rutting is the occurrence and accumulation of permanent deformation upon application of cyclic loading. Gabrielson (1993) reported four types of rutting:

1. shear failure in the base, subbase, or subgrade,
2. consolidation of the HMA,
3. plastic flow in the HMA, and
4. pavement surface wear.

Chou (1977) reported two types of rutting:

1. densification and
2. plastic flow.

With properly designed airport pavements, the primary causes of permanent deformation are those reported by Chou, densification and plastic flow. Figures 1 and 2 illustrate these types of permanent deformation.

Consolidation (Figure 1) primarily occurs in the first two to three years of service life. Consolidation is more prominent in HMA with high air void content. Typical air void content of airport HMA is approximately 6 percent immediately after construction. Traffic loads cause the HMA to densify, reducing the air void content to around 4 percent. As consolidation takes place, the stability of the mixture increases, further resisting additional consolidation. Unstable mixtures continuing to densify below

2 percent air voids have been shown to be more prone to additional rutting. Using proper construction techniques can minimize rutting resulting from consolidation.

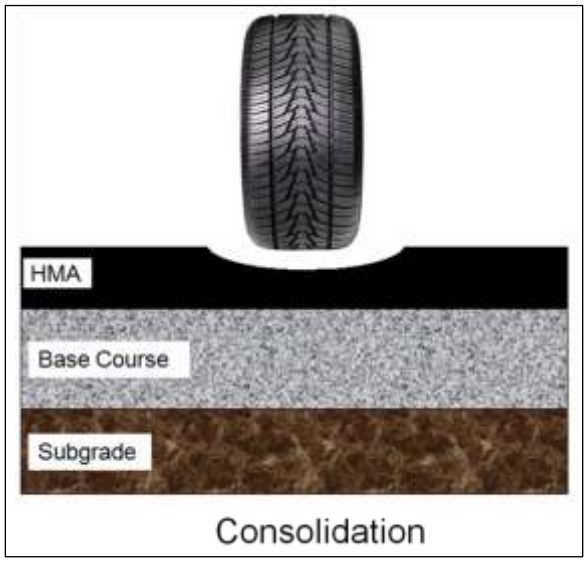

Figure 1. Densification in HMA

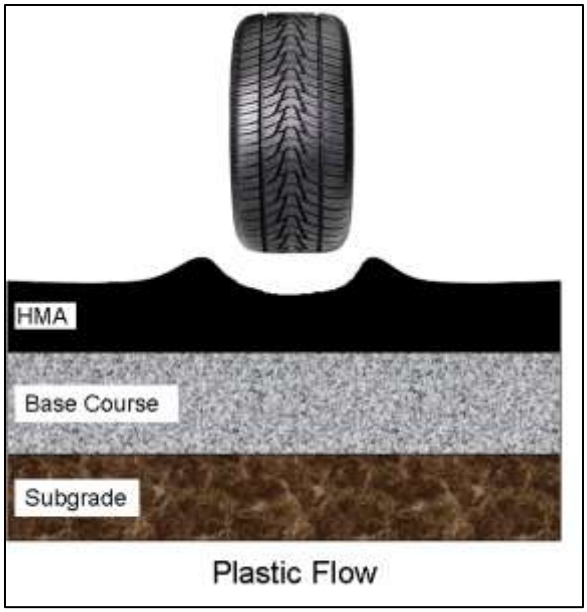

Figure 2. Plastic flow in HMA

Plastic flow (Figure 2) in HMA occurs when traffic loads cause the mixture to become unstable and flow laterally within the HMA due to shear. Either excessive binder content or poor aggregate quality or structure is typically the cause of permanent deformation caused by shear movement. Plastic flow can be limited by ensuring the mixture contains quality aggregate, proper aggregate gradation, proper binder grade, and proper binder content.

Influence of HMA Components on Permanent Deformation

Aggregate properties

Aggregate, whether measured by mass or volume, represents the major component of HMA and has a significant effect on the properties of the compacted mixture. Aggregate properties such as shape, gradation, and type, along with binder type and grade affect HMA compaction and performance. Some of the influences of aggregate properties on the HMA mixture properties are described in the following paragraphs.

Gradation

Numerous research efforts have been devoted to correlating aggregate gradation with HMA performance. Studies have been conducted on the effects of gradation on HMA properties, including permanent deformation (Elliot et al. 1991; Moore and Welke 1979; Kim et al. 1992; Krutz and Sebaaly 1993). Mixture gradations near the maximum density curve provide greater resistance to permanent deformation.

Shape

Aggregate particle shape refers to the form and contour of the individual aggregate particles (ASTM D 946). The preferred aggregate shape is cubical with mechanically

fractured faces. The percentage of flat and elongated particles in the aggregate should be limited in HMA mixtures. Angular particles provide greater particle interlock and mechanical stability.

Studies evaluating the effect of mechanically crushed particles in dense-graded asphalt concrete mixtures show that mixtures with crushed particles, as opposed to smooth, weathered particles, are more resistant to permanent deformation (Wedding and Gaynor 1961; Field 1957; Gaudette and Welke 1977).

Natural sand content

Fine aggregates are typically described as being either manufactured or natural. Manufactured aggregates are those obtained by crushing larger particles. Natural aggregates are from natural deposits and tend to have rounded particles. Numerous research studies have been conducted to determine how compacted HMA mixture properties are impacted by the use of natural sands in the mix. These studies show that natural sand increases the potential for plastic deformation in asphalt concrete and lowers the strength (Button et al. 1990; Ahlrich 1996). Typically, studies recommend that natural sand be limited to no more than10 to 15 percent by mass of total aggregate to reduce rutting.

In general, natural sands aid in compaction but reduce the strength of mixtures. The presence of excess natural sand in the aggregate is indicated by a ~~h~~ump" in the gradation curve around the No. 30 sieve size (Bureau of Public Roads 1962). Efforts to limit the amount of natural sand in the mixture have included controlling the gradation at

specific sieve size, placing numerical limits on the percentage of natural sand used in a mixture, and adopting the fine aggregate angularity test.

Binder grade

Asphalt cement is a product of crude oil distillation. Because sources of crude oil vary, so do the properties of asphalt cements. Asphalt binders are characterized according to their properties to ensure that they will perform as desired at in-service temperatures. There have been several major approaches to characterizing asphalt binders in recent history, including the penetration grading procedure (ASTM D 5) and the viscosity grading procedure (ASTM D 3381).

Most binders in the U.S. are currently characterized according to the performance grading (PG) procedure. The PG system includes physical property measurements at high, intermediate, and low temperatures. The particular properties are selected to correspond with pavement failure mechanisms at these temperatures. The system also includes an aging procedure to forecast long-term oxidative degradation of binders. Binders with greater stiffness at high temperatures are usually more resistant to permanent deformation. However, other distress mechanisms such as thermal or fatigue cracking are more prevalent when binder stiffness is higher at low temperatures; therefore, a proper grade for the climatic region should be selected.

Intermediate temperature measurements are intended to represent average high pavement service temperatures. The grading criteria are intended to ensure PG binders provide adequate stiffness at operating temperatures to resist flow and permanent deformation in the HMA. The Dynamic Shear Rheometer (DSR) is used to measure the

viscoelastic properties of the binder to determine how it will react to loading with variations in time and temperature.

The PG system was developed to grade binders for characteristics during production, construction, and long-term performance. The system also evaluates binder properties at extreme service temperatures to examine potential for typical pavement failure mechanisms. The PG system applies to both unmodified and modified binders. The PG system, along with supporting grade selection software, provides a reasonable method for selecting binder for use in HMA. The FAA uses PG graded binders for airport pavements. The FAA recommends using the PG grade used by the state highway department as long as the low temperature grade is as low as -22. The high temperature grade is recommended to be increased by one grade for airport pavements with aircraft tire pressures between 690 and 1380 kPa. For tire pressures greater than 1380 kPa, a two-grade bump is recommended. Grade bumping refers to selecting a higher-temperature grade asphalt cement so that that the binder has greater stiffness and better rutting resistance at high temperatures.

Environmental Influences on Permanent Deformation

Asphalt binders become less viscous with increasing temperature. The reduced viscosity at high temperature promotes shear flow in HMA pavements. Hofstra and Klomp (1972) investigated permanent deformation using a laboratory test track. Simulated traffic was applied at temperatures ranging from 20 to 60°C. Over this range of temperatures, the asphalt concrete modulus decreased by a factor of approximately 60 but permanent deformation increased by a factor of 250 to 350. Brown et al. (2004)

concluded that permanent deformation essentially stopped when air temperatures were below 28°C during accelerated pavement testing at the National Center for Asphalt Technology Test Track.

Permanent deformation is expected to occur early in the pavement life because oxidation, volatilization, and steric hardening of the asphalt binder stiffen the mixture over time, improving the resistance to permanent deformation.

Predicting Permanent Deformation in HMA

Models to predict permanent deformation

Mechanistic Empirical Pavement Design Guide (MEPDG)

The Mechanistic Empirical Pavement Design Guide, a comprehensive tool used to design highway pavements, is currently being implemented by many agencies. A portion of the design guide is dedicated to predicting rutting in asphalt concrete. One study used in the development of the MEPDG was conducted by Leahy (1989). She produced a model to predict permanent deformation based on properties of the asphalt mixture. The model used the form of Equation 1,

$$\frac{\varepsilon_p}{\varepsilon_r} = aN^b \quad (1)$$

where

ε_p = Accumulated permanent strain

ε_r = Resilient strain

N = Number of load applications

a = regression coefficient

b = regression coefficient

The model assumes that permanent deformation is proportional to the number of applied traffic repetitions raised to some power. This nonlinear relationship accounts for the reduced rate of accumulated permanent deformation with increasing traffic repetitions. Over 250 HMA specimens were included in Leahy's study. The repeated load versus permanent deformation behavior was used to determine the regression coefficients for the model. Further analysis was performed to expand the model to include mixture properties and testing conditions. The final equation for the ratio of permanent to resilient strain is Equation 2.

$$log\left(\frac{\varepsilon_p}{\varepsilon_r}\right) = -6.631 + 0.435\,log\,(N) + 2.767\,log\,(T) + 0.110\,log\,(S) + 0.118\,log\,(\eta) + 0.930\,log(V_{beff}) + 0.5011\,log\,(V_a) \quad (2)$$

where

T = test temperature (°F)

S = deviatoric stress (psi)

η = viscosity of binder at 70°F (106 poise)

V_{beff} = effective binder content by volume (%)

V_a = air void content (%)

The ratio of plastic (permanent) strain to resilient strain is a function of temperature and number of load cycles. The equation is also based on properties of the mixture, including the effective binder content, the air void content, and the viscosity of the

binder. The effect of load is governed by the deviatoric stress. The resilient strain can be determined from Equation 3:

$$\varepsilon_r = \frac{1}{E} \cdot (\zeta_z - \mu \cdot \zeta_x - \mu \cdot \zeta_y) \quad (3)$$

where

E = elastic modulus

ζ = stress

μ = Poisson's ratio

Vertical resilient strain is a function of the dynamic modulus (which, in turn, is a function of mixture properties, rate of load, and temperature) the stress state, and Poisson's ratio. The total rut depth is a summation of the individual plastic strain over the entire asphalt layer and is determined according Equation 4:

$$Rd = \sum_{i=1}^{n} (\varepsilon_{pi} \cdot \Delta h_i) \quad (4)$$

where

Rd = rut depth

h = thickness

Rut depth can be predicted using a range of environmental and loading conditions. Design conditions are expected to include high tire pressure traffic and high temperatures. The model was validated using repeated load testing in the laboratory. The measured permanent strain was compared to the total strain predicted by the model.

Transfer functions were assigned in the MEPDG to relate field results to model predictions.

Pavement Analysis Using Nonlinear Damage Approach (PANDA)

The asphalt research consortium initiated a program in 2007 with one of its goals being the development of a continuum damage model for predicting distresses in asphalt concrete. The model produced by the consortium was the Pavement Analysis Using Nonlinear Damage Approach (PANDA). PANDA is a thermo-viscoelasitc-viscoplastic-viscodamage constitutive model for asphaltic materials (Darabi 2011). The model couples Schaprey's nonlinear viscoelasticity model (Schaprey 1969), Perzyna's viscoplasticy model (Perzyna 1971), and a viscodamage model in order to model the nonlinear constitutive behavior of asphalt mixes. Implementation of the model has been successfully demonstrated through accurate numerical predictions of experimental laboratory data from triaxial tests on asphalt mixtures (Huang 2011). The PANDA model has been implemented in a user material subroutine within the commercial finite element code ABAQUS (2012) to allow modeling using an established software platform. Implementing the material model in ABAQUS allows the user to define other layers of the pavement structure and the magnitude and area of the loading to precisely simulate any desired type of vehicle traffic, environmental condition, or pavement design.

Material parameters for the nonlinear viscoelastic, viscoplastic model are determined through repeated creep-recovery laboratory tests (Darabi 2011). The time-temperature superposition principle can be used to perform simulations at various conditions by

applying a time-temperature shift factor. The resulting changes in material parameters will result in different magnitudes of pavement distresses.

Abu Al-Rub (2012) described simulations using both two-dimensional and three-dimensional models and noted that two-dimensional models predict much larger permanent deformations than equivalent simulations using the three-dimensional model. Ongoing studies to relate field traffic data to PANDA simulations will provide better distress prediction capabilities.

The PANDA development team has been optimizing several factors to allow the most accurate model predictions within the finite element software. The recent incorporation of healing and aging functions provides more accurate simulations. Supporting software has been developed to assist with determining the appropriate model parameters from laboratory test data (PPI 2013) and to provide a simple user-interface to generate ABAQUS input files (PUI 2013).

Laboratory tests to identify HMA mixtures prone to permanent deformation

The major objective of laboratory performance testing is to predict the behavior of HMA under field service conditions. In order to achieve an accurate correlation, laboratory testing conditions should match field service conditions as closely as possible. Attaining strong correlations between laboratory and field results allows for the development of constitutive equations that can explain responses in terms of the stress and strain states. Most laboratory testing determines the response of a material using one set of loading conditions. These testing conditions represent only one point in the pavement and one loading configuration with a given set of environmental conditions.

Analysis of the total pavement response requires a summation of the response at multiple locations affected by a change in stress state.

Results from many studies have provided algorithms to predict pavement rutting. The major focus of these studies has been to reproduce stress conditions encountered during the design loading. However, it is equally important that the material tested represents field conditions. Aggregate orientation, mixture volumetrics, and confinement are examples of properties that can influence test results. The SGC was selected as a laboratory compaction device most closely representing field compaction.

In 2002, NCHRP Report 465 recommended the dynamic modulus (E*), repeated load (flow number) and the static creep (flow time) as the top three candidate simple performance tests to accompany the Superpave highway mixture design system for evaluating resistance to permanent deformation. The criteria for selecting candidate tests were accuracy, reliability, ease of use, and reasonableness of equipment cost. This series of tests have been termed the simple performance test procedures (Witczak 2002). E* has been used for hot-mix asphalt materials characterization for pavement structural design using the MEPDG, while the flow number and flow time have been considered potential performance tests that might be used to indicate rutting resistance. The ability of these tests to predict permanent deformation has been evaluated in several studies. In 2004, the NCHRP Project 9-19 panel recommended the dynamic modulus (E*) test as the primary simple performance test for predicting permanent deformation (Witczak 2007). The panel also recommended the flow number test as a complementary procedure for evaluating the resistance of an HMA mixture design to tertiary flow.

Finally, the Asphalt Pavement Analyzer (APA) test has been evaluated and used by several agencies and contractors with good success. Preliminary performance criteria have been established by the National Center for Asphalt Technology (NCAT) (Zhang et al. 2002) and the WesTrack Forensic Team (1998).

Repeated load

Several studies have suggested that triaxial repeated load testing offers the best practical method for evaluating rutting in HMA because it allows for measurements of resilient and permanent strains. The testing limitation is that only principle stresses can be applied to the test specimen. Additionally, two of the principle stresses are equal because of the test configuration. Uniaxial compression and/or tension can be applied during triaxial testing.

The flow number test is a specific repeated load test protocol, and it was recommended as a potential simple performance test. The flow number test is performed on compacted asphalt concrete specimens using a servo-hydraulic testing machine capable of producing a controlled compressive loading. During the test, a specimen is subjected to repeated haversine load cycles, each applied for 0.1 sec, followed by a rest period of 0.9 sec. Permanent axial strain is measured as a function of the number of cycles. The flow number is defined as the number of load cycles corresponding to the minimum permanent strain rate. A high flow number indicates a more rut-resistant mix. According to AASHTO TP 79-09, the test is performed on three replicate specimens that are 150 mm high by 100 mm in diameter. Specimens may be obtained by coring gyratory-compacted samples. A confining pressure of 69 kPa is sometimes used for this

test, and research continues to evaluate whether confined samples simulate field conditions better than unconfined samples. The recommended test temperature is the effective temperature (T_{eff}) for a given climate (Witczak 2002).

Studies from WesTrack and the FHWA's Accelerated Loading Facility have shown reasonable correlations between flow number values and in-service pavement rutting. Recent studies at the NCAT Pavement Test Track showed moderate correlations between flow number and field rut depths and also rate of rutting, which could be useful in the mixture design process for determining flow number criteria at different design traffic levels. NCHRP 9-30-A researchers recommended using results from the flow number test to determine coefficients in the rut depth transfer function included in the MEPDG software. The coefficients to the transfer function are adjusted or shifted to correlate with field conditions (Von Quintus 2012).

Static creep

The static creep test is used to measure the creep compliance and the flow time of HMA mixtures. In this test, a cylindrical sample of HMA mixture is subjected to a static axial load. Permanent axial strains are recorded throughout the test and used to calculate compliance parameters and flow time.

Creep compliance is a measure of strain as a function of time when a constant stress is applied. It is calculated as the ratio of the strain to the applied stress. When performing a static creep test, three regions of response are generated: the primary, secondary, and tertiary regions. In the primary region, strain rate decreases as a function of time. In the secondary region, strain rate is constant with time. In the tertiary region, strain rate

asymptotically increases with time. Typically, the linear portion of the creep compliance versus time curve is considered most important. The slope of this portion of the curve is an important property of HMA mixtures. Creep compliance relates to a mixture's susceptibility to permanent deformation, thermal cracking, fatigue cracking, and other HMA distresses. The flow time is defined as the time corresponding to the minimum rate of compliance change. It is the postulated time when shear deformation, under constant volume, starts (Witczak et al. 2002).

Creep tests can be performed with or without confinement. Unconfined creep tests are typically performed using a static axial stress of 100 kPa applied to a specimen for a period of 1 hr at a temperature of 40°C. The applied pressure usually cannot exceed 207 kPa, and the test temperature usually cannot exceed 40°C, or the sample may fail prematurely (Brown et al. 2001). Actual roadway pavements are typically exposed to tire pressures of up to 828 kPa and temperatures in excess of 60°C. Thus, the unconfined test does not closely simulate field conditions. Confined static creep tests commonly use a confining pressure of about 138 kPa, which allows test conditions to more closely match field conditions. Research suggests that the confined static creep test does a better job of predicting field performance than the unconfined static creep test (Roberts et al. 1996).

Dynamic modulus

Dynamic modulus, $|E^*|$, is a measure of the linear viscoelastic stress-strain relationship for materials. Dynamic modulus is mathematically defined as the absolute value of the maximum (peak-to-peak) dynamic stress, ζ_o, divided by the recoverable (peak-to-peak) axial strain, ε_o (Equation 5). The real and imaginary portions of the

complex modulus are given in Equation 6. These portions are often the storage and loss components, E′ and E′′, respectively. For purely elastic materials, E′′ = 0; for purely viscous materials, E′ = 0.

$$|E^*| = \frac{\zeta_o}{\varepsilon_o} \tag{5}$$

$$E^* = E' + iE'' \tag{6}$$

American Association of State Highway and Transportation Officials (AASHTO) TP-62-07 described the test method for determining the dynamic modulus of hot mix asphalt. This test consisted of the application of a sinusoidal axial compressive stress to a specimen at a given temperature and loading frequency. Axial strains were continuously monitored to capture the response. The recommended dynamic modulus test consisted of testing at five different temperatures and at six different frequencies to develop master curves for use in pavement response and performance analysis. Each specimen was tested at each of the 30 combinations of temperature and loading frequency, starting with the lowest temperature and proceeding to the highest. Testing at a given temperature began with the highest frequency of loading and proceeded to the lowest (Mohammad et al. 2006).

The dynamic modulus is one of the fundamental inputs in the MEPDG developed in NCHRP Project 1-37A. Three levels of |E*| input are used in the MEPDG, which are related nominally to the reliability of pavement performance estimates generated by the guide. Level 1 |E*| inputs require laboratory-measured |E*| values, and Levels 2 and 3

|E*| inputs are estimated using a predictive equation. A comprehensive research effort conducted by Tran and Hall (2006) evaluated different |E*| testing protocols to provide the laboratory-measured |E*| inputs for implementation of the MEPDG. The protocols consisted of varying the number of linear variable differential transformers (LVDTs) per specimen, the number of replicates, the aggregate source, the nominal maximum aggregate size, the binder grade, the test temperature, and the loading frequency. Results from this study indicated that the optimal |E*| test protocol was the one using four LVDTs and two replicate specimens. The study also showed that increasing the number of replicates did not significantly reduce the test variability. Test variability was affected more by the test protocols at extreme low and high temperatures, and it was more significant for HMA mixes that had larger nominal maximum aggregate sizes.

Mohammad et al. (2006) also found that |E*| was sensitive to the nominal maximum aggregate size in an HMA mixture. The study revealed that larger aggregates combined with aged reclaimed asphalt pavement (RAP) materials tended to overestimate |E*| values at high temperatures.

Studies recommended using the confined |E*| test to rank and compare the expected field performances of different mixtures. Analyses were conducted on NCHRP Project 9-19 test data comparing the confined and unconfined |E*| tests. Shenoy and Romero (2002) analyzed the WesTrack data and showed that confined |E*| test results correlated better with field performance.

Sotil et al. (2004) proposed two methods (point-slope and slope-proportion) to predict confined |E*| values from unconfined |E*| results. The methods were developed

based on the fact that the unconfined |E*| and confined |E*| test results showed linear relationships with the applied bulk stress. Furthermore, the linear relationships were almost parallel, regardless of the confinement level. The authors found that the slope-proportion method provided better correlations between predicted and measured values. This method provided a potential decrease in laboratory testing time by at least 50 percent for confined |E*| testing by using a linear trend and reducing the required number of confined tests to one or two instead of five as required by current test protocols.

NCHRP Report 580 provided recommendations for implementing the dynamic modulus test to assess the adequacy of an HMA mixture according to the following modes:

- Mode 1 – The full use of MEPDG developed under NCHRP Project 1-37A, along with full use of the E* methodology developed under NCHRP Project 9-19
- Mode 2 – Use of an appropriate rut depth model based upon the MEPDG, and full use of the E* methodology
- Mode 3 – Use of E* as a mixture design tool
- Mode 4 – Use of E* as a construction quality control (QC)/quality assurance (QA) tool

Mode 1 provided the highest level of accuracy. This mode required detailed user input and assessed the total distress formation using MEPDG software.

Asphalt Pavement Analyzer (APA)

The APA has been used successfully by several agencies to determine HMA mixture suitability, and it is one of the most widely accepted laboratory accelerated wheel trafficking devices available. The APA attempts to mimic the action of a moving wheel to simulate traffic. Tests that simulate or mimic traffic action are often used in lieu of traditional laboratory testing because the action of a moving wheel load, in which there is a rotation of principal stresses and a transition from compression to extension, is difficult to recreate even with sophisticated triaxial laboratory tests (Zhang et al. 2005). For this reason, empirical tests such as the APA offer an alternative approach for determining rutting potential which is favored by many.

The APA provides for an accelerated evaluation of rutting potential after volumetric design. A typical duration for a complete rutting evaluation is 135 min (8,000 cycles). The test consists of placing a beam or a cylindrical sample under repetitive wheel loads and measuring permanent deformation. The APA features steel wheels which travel atop pressurized contact hoses that simulate tire contact on the specimens. A controllable load is applied to the wheel and the contact hose pressure is adjusted to represent actual field tire loading conditions. Each specimen can be subjected to different load levels up to 1113 N. Contact hose pressure can exceed 2067 kPa. Six cylindrical samples in three sample molds can be tested under controlled temperature and in dry or submerged environments. Specimens are commonly compacted with a Superpave Gyratory Compactor to 4 or 7 percent air void contents. The test can also be performed on cores or slabs taken from in-service pavement.

The WesTrack Forensic Team conducted a study on the performance of coarse graded mixes at WesTrack sections (WesTrack Forensic Team 1998). Results from this study showed that the use of the APA helped ensure that a satisfactory mixture was designed and produced. Results also indicated that a laboratory rut depth of 6 mm was indicative of a field rut depth of 12.5 mm. Criteria have also been developed in the past for some other test conditions. Some states have specified a maximum rut depth of 5 mm for HMA mixtures as the pass/fail criteria at a temperature of 50ºC (Shami et al. 1997). Zhang et al. (2002) conducted a study at the NCAT that provided a criterion of 8.2 mm for the APA rut test at standard PG temperature for the location in which the HMA will be used. This higher value for pass/fail criteria is associated with the higher PG temperature used.

Another study conducted by Huang and Shu (2009) evaluated mixtures from 26 test sections of the NCAT test track. Results indicated that APA rutting at 500 cycles correlated strongly to the final APA rut depth at 8,000 cycles. Regression analyses revealed that the APA rutting for Superpave gyratory compacted specimens at 7 percent air voids correlated reasonably well with the field-measured rut depths; whereas the APA results from lab-compacted specimens at 4 percent air voids had a weak correlation with the field rutting measurement. The authors suggested that for QC/QA purposes, the number of cycles in an APA rutting test might be significantly reduced from the current 8,000 cycles, and specimens at 7 percent air voids were recommended for rutting evaluation.

The APA test does have potential to be adopted as a performance test (Brown et al. 2001). It has been used by over 60 agencies and contractors with good success, and preliminary performance criteria have been established. The APA is a good empirical tool for measuring rutting susceptibility, and the test results are reasonably repeatable and reliable.

Previous Studies Evaluating Airport HMA Performance

Ahlrich performed repeated load tests using an axial stress of 1380 kPa with a confining stress of 276 kPa to assess the influence of aggregate properties on rutting performance of airport HMA (Ahlrich 1996). These tests were performed on individual Marshall specimens 100 mm in diameter and 68 mm high. The test temperature was 60°C, and 3,600 load cycles were applied to each specimen. Eighteen different HMA mixtures with a wide range of anticipated quality were prepared and tested using three replicates. The average total strain in specimens for each mixture ranged from 1.5 to 8.5 percent after testing. The majority of the mixtures experienced between 2 and 4 percent strain. Ahlrich also noted a significant improvement in rutting performance, particularly for lower quality mixtures, when using a polymer-modified binder. He concluded that the repeated load test can be used to evaluate the effects of aggregate property changes on mixture rutting performance for airport HMA.

Cooley et al. performed similar tests using deviator stress levels of 690, 1380, and 2413 kPa with 276 kPa confinement (Cooley 2009). Testing was performed on ten HMA mixtures from airports in the United States. The flow number test was performed with each mixture at the three deviator stress levels for two to four different compactive

efforts. Changing the compactive effort produced specimens with varying asphalt contents. The asphalt content typically varied between 0.2 and 0.5 percent with a change in compactive effort. Higher asphalt contents typically reduced the rutting resistance during flow number testing. In this study, the axial load pulse was repeated for 20,000 cycles or until failure occurred. The test temperature was the high pavement temperature determined from the local climate data. Testing was performed according to AASHTO TP 79. The data from this study showed that most mixtures achieved 20,000 cycles for 1380 kPa deviator stress at one or more asphalt contents (compactive effort). Increasing asphalt content or deviator stress caused sharp reductions in performance.

CHAPTER III

MATERIALS

Overview of Materials and Mixtures

This chapter provides properties of all materials tested as part of this study. Twenty-six mixtures using a neat binder were designed and tested. Eight additional mixtures were prepared using a polymer-modified binder. The nomenclature system used to identify each mixture is described below.

Mixture Nomenclature System

Two maximum aggregate sizes, two gradations, three aggregate types, and three different percentages of natural sand were used to produce mixtures included in this study. A nomenclature system was established to identify each mixture according to the variables identified above. The mixture identifier begins with a number representing the maximum aggregate size, followed by three letters representing the gradation and the aggregate type, and ends with a numerical value of either 0, 10, or 30 representing the percentage of natural sand. The maximum aggregate size of the mixture is identified as either

- 19 (Maximum aggregate size of 19 mm) or
- 12.5 (Maximum aggregate size of 12.5 mm).

The first letter in the mixture identifier indicates whether the mixture is fine- or coarse-graded relative to the allowable gradation band used by the FAA. The two possible characters are

- F (Fine-graded mixture) or
- C (Coarse-graded mixture).

The next two letters in the mixture identifier indicate the aggregate type. The possible designations are

- GN (Granite aggregate) or
- GV (Chert Gravel aggregate) or
- LS (Limestone aggregate).

Finally, the number at the end of the mixture identifier indicates the percentage of natural sand used in the mixture. For this study, possible values are

- 0 (No natural sand; the aggregate is 100 percent crushed) or
- 10 (The mixture contains 10 percent natural sand by mass of aggregate) or
- 30 (The mixture contains 30 percent natural sand by mass of aggregate.)

For example, 12.5 CGN10 identifies a mixture with a maximum aggregate size of 12.5 mm that is graded along the coarse side of the allowable gradation band and is composed of granite aggregate with 10 percent natural sand by mass of aggregate. Table 1 provides designations for all mixtures used in this study. Eight of the 26 mixtures from this study were selected and also prepared using a polymer-modified binder, for a total of 34 tested mixtures. These mixtures were prepared using the same design binder content as their unmodified counterparts to measure the change in performance achieved by using a premium binder. The mixtures made with unmodified and modified binders are noted in Table 1 by an asterisk after the mixture designation.

Table 1. Aggregate mixture designations and design binder content

Aggregate Type	Maximum Aggregate Size	Gradation	Natural Sand (%)	Design Binder Content (%)	Effective Binder Content (%)	Mixture Designation
Granite	12.5 mm	Fine	0	6.7	6.0	12.5 FGN0*
			10	6.8	6.2	12.5 FGN10
			30	7.2	6.7	12.5 FGN30
		Coarse	0	6.3	5.6	12.5 CGN0*
			10	5.9	5.3	12.5 CGN10
			30	6.8	6.3	12.5 CGN30
	19 mm	Fine	0	6.2	5.5	19 FGN0
			10	6.1	5.5	19 FGN10
			30	7	6.5	19 FGN30*
		Coarse	0	5.9	5.2	19 CGN0
			10	4.9	4.3	19 CGN10
			30	7.1	6.6	19 CGN30
Limestone	12.5 mm	Fine	0	6.1	5.6	12.5 FLS0
			10	5.2	4.7	12.5 FLS10
		Coarse	0	5.5	5.0	12.5 CLS0*
			10	5	4.5	12.5 CLS10
	19 mm	Fine	0	5.7	5.2	19 FLS0
			10	4.8	4.3	19 FLS10*
		Coarse	0	5.4	4.9	19 CLS0*
			10	5.4	4.9	19 CLS10
Chert Gravel	12.5 mm	Center	0	6.8	5.3	12.5 GV0*
			10	6.2	4.8	12.5 GV10
	19 mm	Fine	0	6.8	5.3	19 FGV0
			10	5.9	4.5	19 FGV10
		Coarse	0	6.4	4.9	19 CGV0*
			10	5.3	3.9	19 CGV10
* Mixture also prepared and tested with polymer-modified binder.						

Asphalt Binder

Two asphalt binders were used in this study. Both were obtained from Ergon Asphalt and Emulsions, Inc. Tests by the distributor indicated the two were a PG 64-22 neat binder and a PG 76-22 styrene-butadiene-styrene (SBS) polymer-modified binder. Distributor tests indicated both binders had a specific gravity of 1.038. Recommended mixing and compaction temperatures for the PG 64-22 binder were 154°C and 145°C, respectively, and recommended mixing and compaction temperatures for the PG 76-22 binder were 182°C and 168°C, respectively. Mixing and compaction temperatures for the modified binder were higher than those typically used during construction; however, these temperatures were used in this study to provide equivalent Brookfield viscosities of the binders. Figure 3 shows Brookfield viscosity versus temperature relationships for the two binders.

Aggregate

Aggregates used in this study included limestone, granite, and chert gravel. The limestone aggregate was from a Vulcan Materials quarry in Calera, Alabama. The granite aggregate was from Granite Mountain Quarries in Little Rock, Arkansas. The chert gravel aggregate was obtained from Green Brothers Gravel Company in Hazlehurst, Mississippi. Additionally, some mixtures were blended with selected percentages of natural sand obtained from Mississippi Materials Corporation in Vicksburg, Mississippi. Aggregates were blended to meet allowable FAA gradations reported in Tables 2 and 3. Aggregate absorption was 0.5, 0.6, and 1.4 percent for limestone, granite, and chert gravel aggregates, respectively.

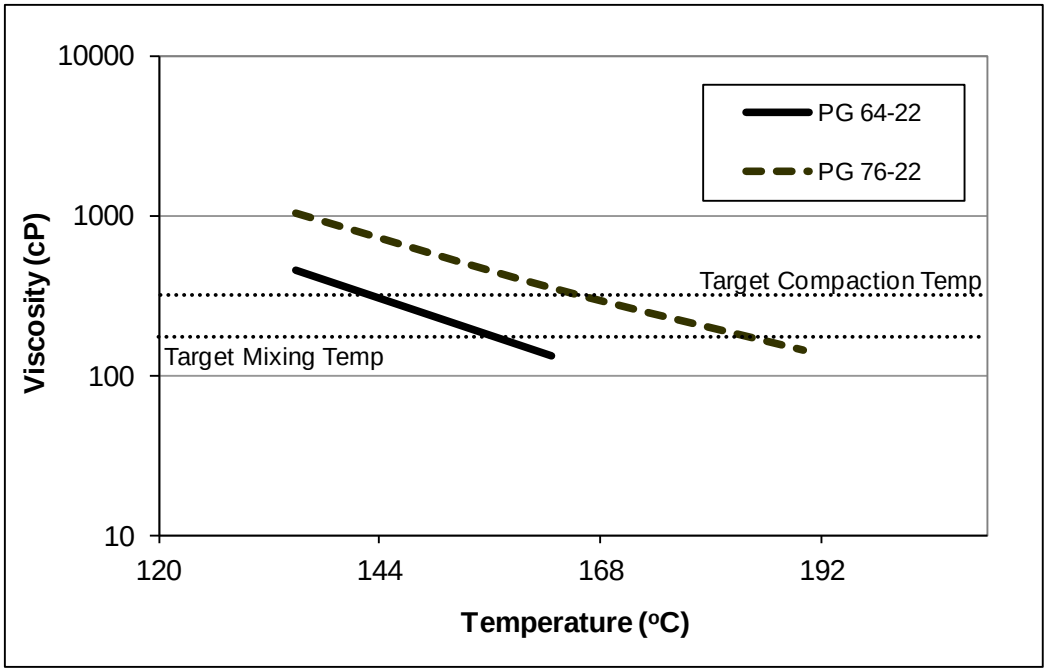

Figure 3. Brookfield temperature-viscosity curve for asphalt binders

Table 2. 12.5-mm aggregate blend gradations

Agg. Type	Sand (%)	Mix	Sieve sizes (percent passing)									
			19 mm	12.5 mm	9.5 mm	#4	#8	#16	#30	#50	#100	#200
Granite	0	12.5 FGN0	100	100	96	75	54	41	27	17	10	6.0
		12.5 CGN0	100	99	91	63	44	31	20	13	7	4.5
	10	12.5 FGN10	100	100	97	76	57	45	32	18	8	5.3
		12.5 CGN10	100	99	90	65	49	38	28	15	7	4.4
	30	12.5 FGN30	100	100	97	79	63	52	42	18	5	3.0
		12.5 CGN30	100	99	91	68	55	47	39	16	4	2.4
Gravel	0	12.5 GV0	100	100	88	69	53	39	28	20	9	4.6
	10	12.5 GV10	100	100	87	67	47	32	29	23	9	4.3
Limestone	0	12.5 FLS0	100	98	89	73	58	38	25	16	9	6.0
		12.5 CLS0	100	97	82	59	45	29	20	13	8	5.4
	10	12.5 FLS10	100	98	87	69	53	38	28	16	8	5.9
		12.5 CLS10	100	97	84	62	48	34	26	14	7	5.2
P-401 Specification Limits			100	100	79 - 99	58 - 78	39 - 59	26 - 46	19 - 35	12 - 24	7 - 17	3 - 6

Table 3. 19-mm aggregate blend gradations

Agg. Type	Sand (%)	Mix	Sieve sizes (percent passing)									
			19 mm	12.5 mm	9.5 mm	#4	#8	#16	#30	#50	#100	#200
Granite	0	19 FGN0	100	93	85	64	48	36	23	14	9	6.0
		19 CGN0	99	83	73	53	37	26	16	10	6	3.9
	10	19 FGN10	100	94	85	66	50	39	28	15	7	4.7
		19 CGN10	99	83	74	57	44	35	25	13	6	4.0
	30	19 FGN30	100	94	87	70	55	46	38	15	4	2.2
		19 CGN30	99	84	76	62	50	42	36	14	3	1.8
Gravel	0	19 FGV0	100	95	81	65	51	38	26	18	8	4.0
		19 CGV0	100	87	70	54	42	30	20	13	6	3.1
	10	19 FGV10	100	95	81	64	47	29	26	20	8	3.7
		19 CGV10	100	87	71	54	41	28	26	20	8	3.7
Limestone	0	19 FLS0	100	98	86	67	52	34	23	15	9	5.8
		19 CLS0	98	83	69	50	38	25	17	11	7	4.7
	10	19 FLS10	100	97	82	58	45	33	28	13	7	4.8
		19 CLS10	99	92	76	53	41	30	23	12	6	4.4
P-401 Specification Limits			100	79 - 99	68 - 88	48 - 68	33 - 53	20 - 40	14 - 30	9 - 21	6 - 16	3 - 6

Multiple stockpiles represented each aggregate type and were proportioned to meet the target gradations. Blends were adjusted to roughly follow the upper or lower limits of the Item P-401 gradation band. Blended gradations are shown in Tables 2 and 3. A graphical depiction of the representative aggregate gradations and of the specification limitation is given in Figure 4.

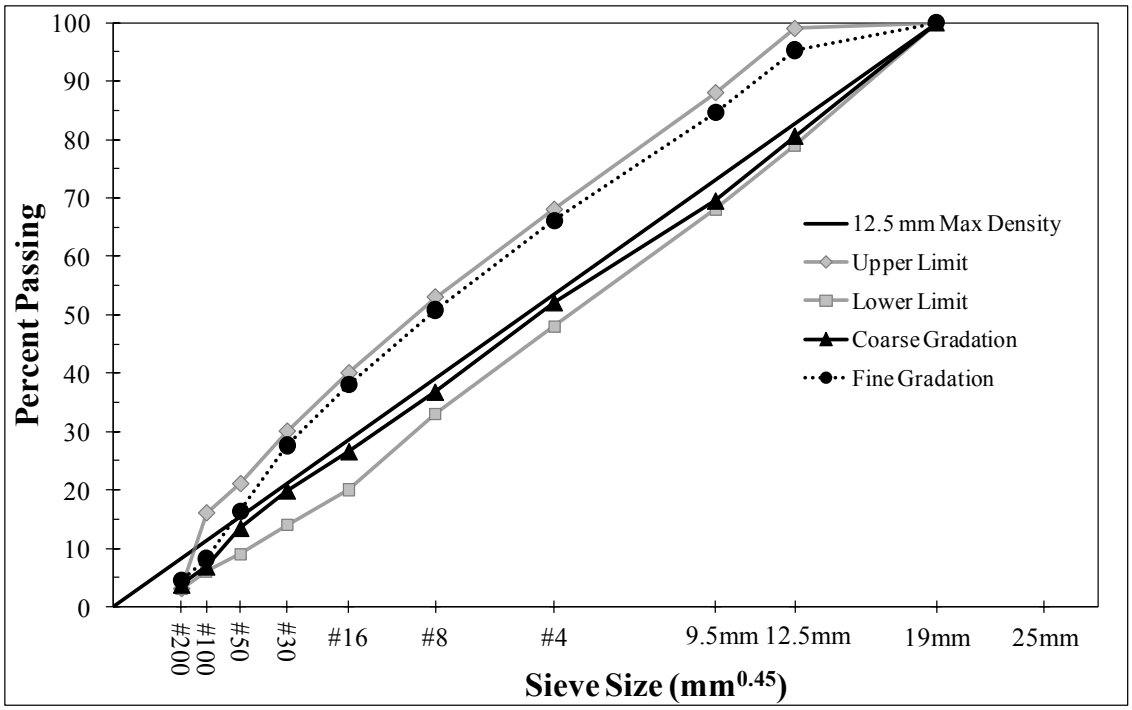

Figure 4. Representative aggregate gradations

The percentages of aggregate with at least two fractured faces (U.S. Army Corps of Engineers 1994) were 100, 100, and 97 percent for the limestone, granite, and chert gravel, respectively. The maximum percentages of flat and elongated particles according to ASTM D 4791was 1.6 percent for the limestone aggregate. The maximum percentages of flat and elongated particles were 1.0 and 0.3 percent for the granite and chert gravel, respectively. Each of the blends met the FAA requirements for flat and elongated particles (8 percent maximum).

The fine aggregate angularity for the limestone, granite, chert gravel, and natural sand aggregates was determined by Method A of ASTM C 1252. The limestone, granite, and chert gravel aggregates had fine aggregate angularities of 47, 47, and 46 percent,

respectively. These values were above the minimum value of 45 percent required by many agencies. The fine aggregate angularity of the natural sand was 40 percent. This value is characteristic of rounded aggregate particles and is typical for natural sands (Kandhal et al. 1991).

Additional testing of the aggregates was performed using the Aggregate Image Measurement System (AIMS). AIMS determines shape characteristics of aggregates through image processing and analysis techniques (Masad 2005). AIMS is a computer automated system that includes a lighting table where aggregates are placed in order to measure their physical characteristics (shape, angularity, and texture). It is equipped with an autofocus microscope and a digital camera and is capable of analyzing the characteristics of aggregates retained on the No. 100 (0.15-mm) sieve up to aggregates retained on the 25.4-mm sieve. Texture is measured by analyzing gray-scale images captured at the aggregate surface using the wavelet analysis method. The surface irregularities manifest themselves as variations in gray-level intensities that range from 0 to 255. Large variations in gray-level intensity mean a rough surface texture; whereas, smaller variation in gray-level intensity indicates smooth-surfaced particles. The wavelet transform analyzes the image as a two-dimensional signal of gray-scale intensities, and it gives a higher texture index for particles with rougher surfaces. Angularity is measured using the gradient analysis method, which basically quantifies the change in angles along the circumference of a particle. A higher change in angle means a more angular particle. Masad et al. (2005) gives detailed background information about AIMS operations and analysis methods. Six size fractions for each of the three aggregate types were tested

using AIMS. These fractions included aggregates retained on 12.5-mm, 9.5-mm, No. 4, No. 8, No. 16, and No. 30 U.S. standard sieves during a washed sieve analysis. Table 4 shows the average results for angularity and texture indices measured by AIMS.

Table 4. Aggregate data from AIMS analysis

	Angularity			Texture		
Sieve Size	**Limestone**	**Granite**	**Chert Gravel**	**Limestone**	**Granite**	**Chert Gravel**
12.5 mm	2607	3200	2721	359	535	153
9.5 mm	2668	3167	2912	345	493	164
No. 4	2841	3461	2960	274	362	130
No. 8	3162	3709	3212	Texture is measured only on coarse aggregate		
No. 16	3164	3907	3348			
No. 30	3176	3876	3282			

Mixture Design

For mixture designs, individual batches for each mixture were prepared by weighing the percentages of the target batch weight for each stockpile or sieve size into a shallow mixing pan. Aggregate batches were placed in an oven overnight at the mixing temperature of the binder prior to performing mixture designs. To perform the mixture design, the binder was heated to the mixing temperature of the asphalt cement. The aggregate was weighed into a mixing bowl, and binder was added to achieve the target binder content for the mixture. The sample was mixed using a Univex® commercial mixer until the aggregate was thoroughly coated with binder. The mixture was placed into a shallow pan and stored in the oven at the compaction temperature for two hours before placing it into the preheated compaction molds. A Pine Instruments Company model AFGC125X gyratory compactor was used in the mixture designs during this

study to compact cylindrical asphalt concrete specimens with a diameter of 150 mm at a target height of 115 mm. Compaction was performed using a ram pressure of 600 kPa and an internal angle of gyration of 1.16 deg ± 0.02 deg. Asphalt mixtures were compacted to 70 gyrations at a rate of 30 revolutions per minute. Seventy gyrations are recommended for N_{design} for HMA mixtures designed for high tire pressure aircraft (Rushing 2009).

The optimum binder content for each mixture was determined by compacting specimens using at least three different binder contents. The theoretical maximum density was measured for each mixture in accordance with ASTM D 2041. The bulk specific gravity was determined in accordance with ASTM D 2726. The percentage of air voids in the specimen was determined in accordance with ASTM D 3203. The percentage of air voids was plotted versus the percentage of binder in the mixture to determine the percentage of binder required to compact the mixture to 3.5 percent air voids at the design compactive effort. The air void content of 3.5 percent was selected since it is the center of the allowable design range in FAA specifications. This percentage of binder was considered the design binder content. Specimens for further testing were prepared using this design binder content.

CHAPTER IV

PLAN OF STUDY

The plan of study contained three major components. The first component was the selection of asphalt mixtures and their characterization through laboratory testing. The laboratory-testing program was intended to evaluate four test methods with potential for use in the mixture design section of asphalt concrete pavement construction specifications. Asphalt mixtures with an expected range of very poor to very good rutting performance were selected for testing to assess each laboratory test's ability to effectively rank the mixtures according to their expected resistance to permanent deformation. The goal of the testing was to identify preliminary criteria to screen airport HMA paving mixtures.

The second component of this study was full-scale, accelerated pavement testing of simulated military aircraft traffic on one asphalt mixture under two different loading cases. The asphalt mixture represented quality in terms of rutting performance near the lower end of those tested in the laboratory characterization component of this work. The full-scale testing provided validation of the proposed acceptance thresholds.

The third component of this study was finite element simulations using a nonlinear viscoelastic, viscoplastic asphalt model to determine material parameters that affect rutting. Simulations were performed according to the pavement structure, loads, and material properties used in the full-scale testing. Using finite element simulations allowed for determining the specific material properties needed to resist rutting under

any unique loading scenario. Figure 5 provides a flow chart of the efforts included in this study.

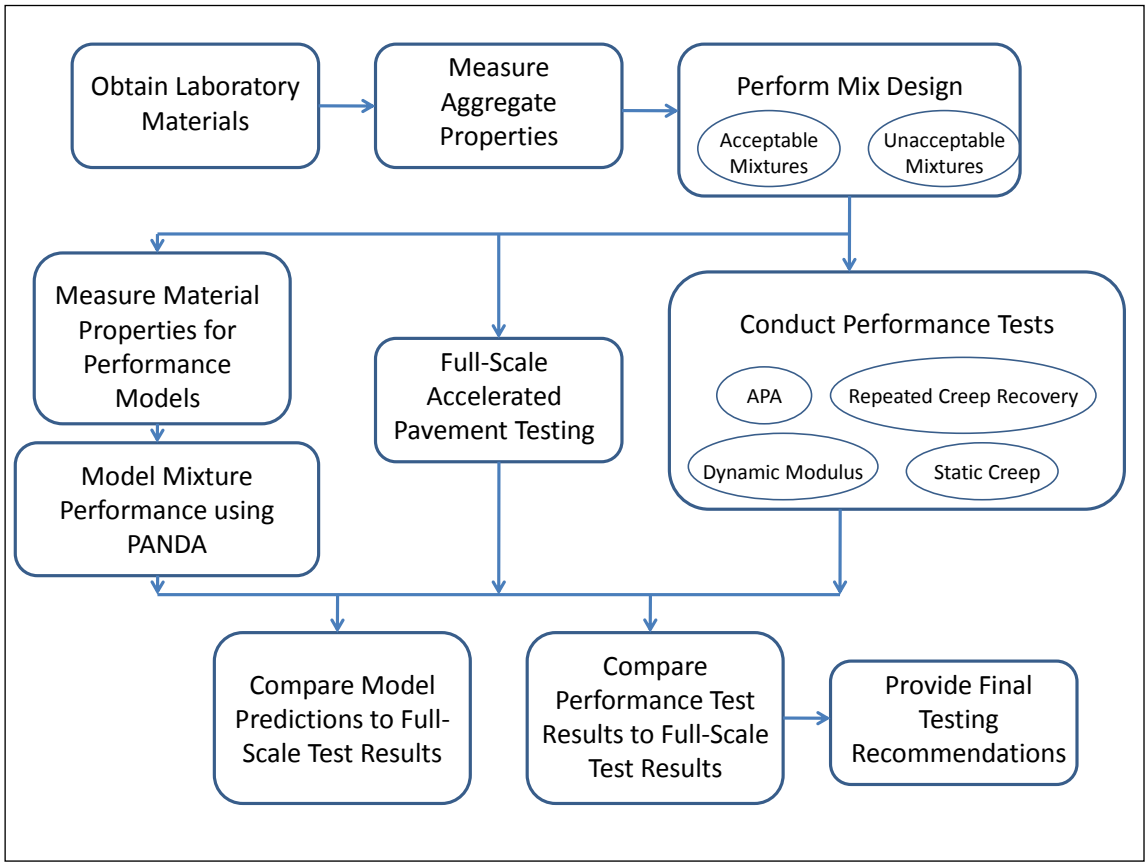

Figure 5. Research plan flow chart

Materials

Chapter III describes the materials used in this study. Aggregates were selected from stockpiles from a previous study used to define compaction requirements for using the SGC in mixture design (Rushing 2009). Aggregate blends were selected to provide a range of performance from very good to very poor in terms of rutting resistance.

Aggregate properties specified by the FAA mixture design procedure and others known to influence rutting susceptibility were measured. These properties are discussed in Chapter II.

HMA Mixture Designs

Mixture designs were performed according to FAA AC 5370/10G. Chapter III provides details of the mixture design procedures. Thirty-four different mixtures were included in the study. Twenty-two of these HMA mixtures were from previous research (Rushing 2009). From these, eight were reproduced using polymer-modified binder. These mixtures are listed in Table 5. The materials meet all requirements for FAA airport HMA paving mixtures (Federal Aviation Administration 2009).

Five additional HMA mixtures were prepared using the same granite aggregate with 30 percent natural sand by mass of aggregate. Table 6 includes a list of these mixtures. These mixtures do not meet FAA material requirements because the percentage of natural sand exceeds 15 percent. In addition, introducing 30 percent natural sand by mass will cause the aggregate gradation to fall outside of the allowable limits described by the FAA. Incorporating excessive natural sand is expected to produce mixtures that are susceptible to permanent deformation. These mixtures are needed to produce acceptance limits for the potential performance tests. The design binder content was determined by the method previously described.

Table 5. HMA mixtures meeting FAA requirements

Asphalt Binder	Natural Sand Content (%)	Aggregate Type	Maximum Aggregate Size	Gradation[1]
PG 64-22	0	Limestone	19 mm	Coarse
				Fine
			12.5 mm	Coarse
				Fine
		Granite	19 mm	Coarse
				Fine
			12.5 mm	Coarse
				Fine
		Chert Gravel	19 mm	Coarse
				Fine
			12.5 mm	Center
	10	Limestone	19 mm	Coarse
				Fine
			12.5 mm	Coarse
				Fine
		Granite	19 mm	Coarse
				Fine
			12.5 mm	Coarse
				Fine
		Chert Gravel	19 mm	Coarse
				Fine
			12.5 mm	Center
PG 76-22	0	Granite	12.5 mm	Coarse
				Fine
		Limestone	19 mm	Coarse
			12.5 mm	Coarse
		Chert Gravel	12.5 mm	Center
			19 mm	Coarse
	10	Limestone	19 mm	Fine

[1] Coarse and fine refer to gradations near the upper and lower band limit of P-401 specification, respectively.

Table 6. HMA mixtures failing to meet FAA requirements

Asphalt Binder	Natural Sand Content (%)	Aggregate Type	Maximum Aggregate Size	Gradation[1]
PG 64-22	30	Granite	19 mm	Coarse
				Fine
			12.5 mm	Coarse
				Fine
PG 76-22	30	Granite	19 mm	Fine
[1] Coarse and Fine refer to gradations near the upper and lower band limit of P-401 specification, respectively.				

Performance Tests for Permanent Deformation

Four laboratory-performance tests were performed on compacted mixtures. Details of these tests are given in Chapter V. The tests included in the study are listed below.

- Repeated Load Test
- Static Creep Test
- Dynamic Modulus Test
- Asphalt Pavement Analyzer

Repeated load testing involved applying repeated axial loads to cylindrical asphalt concrete specimens. Axial LVDTs measured the strain within each specimen. The axial strain was measured as a function of time and was easily associated with a number of load cycles knowing the frequency of the load pulse.

Static creep testing involved applying constant axial load to cylindrical asphalt concrete specimens. Axial LVDTs measured the strain within each specimen. The axial strain was measured and reported as a function of time.

Dynamic modulus testing involved applying non-destructive (within the elastic region) repeated axial loads to cylindrical asphalt concrete specimens. Axial LVDTs measured the strain within each specimen. The complex modulus was measured as the peak-to-peak stress divided by the peak-to-peak strain. The absolute value of the complex modulus was the dynamic modulus.

The APA applied repetitive, simulated wheel loads onto the surface of confined cylindrical asphalt concrete specimens. The wheel loads were transferred through a pressurized rubber hose to imitate a rubber tire. The vertical position of the loading device was recorded to provide instantaneous rut depth within the specimen. The rut depth as a function of number of load cycles was reported.

Full-Scale Accelerated Pavement Testing

Full-scale accelerated pavement tests from ongoing research studies were used to provide rutting performance data for different loading conditions. The first study, Field Trial 1, applied high tire pressure and wheel load (2,241 kPa and 142 kN) military fighter aircraft traffic to an HMA pavement at a constant temperature of 43°C. The second study, Field Trial 2, applied heavy cargo aircraft traffic (980 kPa tire pressure and 200 kN wheel load) to an HMA pavement at 25°C. Rutting performances at these two conditions were used to assess the preliminary threshold values for the mixture design performance tests. The first study represented severe loading conditions that promoted rutting (high tire pressure and elevated temperature). The second study represented moderate loading conditions where rutting was less likely to occur.

Modeling HMA Rutting Under Aircraft Loads

The properties of the asphalt mixture at the two different field-test temperatures were used to model the expected behavior under field loading conditions. The PANDA model was selected as the best available model to simulate aircraft loading. This model required measured material parameters relating to the viscoelastic and viscoplastic properties of the HMA. The pavement structure and loading conditions were created in the finite element software to replicate field-test conditions.

Viscoelastic and viscoplastic material parameters were obtained from dynamic modulus and repeated creep-recovery tests. Dynamic modulus test data were used to determine the Prony series coefficients for the linear elastic material response. Repeated creep-recovery test at various stress level (RCRT-VS) test data were used to determine the nonlinear viscoelastic response parameters and viscoplastic material parameters. A repeated creep-recovery test using a constant loading rate but having various rest periods was used to capture the hardening-relaxation model parameters.

Comparing Laboratory Performance Test Data to Field-Test Results and Model Simulations

The results from each of the performance tests were used to determine threshold acceptance values by delineating performance among mixtures with expected good and poor performance. These threshold values were validated by full-scale testing. The ability of the PANDA to accurately predict rutting during full-scale tests was determined based on measured material parameters and comparisons of simulations to field testing. Finally, the usefulness of the model as a method to identify proper material properties

from an asphalt mixture was determined by examining material parameters affecting rutting from model simulations.

CHAPTER V

PERFORMANCE TESTS

Performance tests selected for this study were among those most recommended by previous research. Because the purpose of this study was to recommend one or more performance tests for incorporation into construction specifications, certain considerations were made in selecting the test procedures and test specimen properties. The selected test methods required commercially available equipment. Some positive historical experience with the test methods or equipment was desired. The test specimen properties were selected to be as simple as possible to prepare while maintaining sufficient precision in the test results to separate acceptable and unacceptable performance. The specimen geometries required for the selected tests were unchanged from the accepted standards. For example, the APA required specimens approximately 75 mm in height because of equipment limitations. Further, the height-to-diameter ratio for dynamic modulus and triaxial testing (i.e., repeated load or static creep tests) was maintained from accepted testing standards to ensure viability of the data. The air void content of the test specimens was selected to be approximately 3.5 percent, the design air void content. Some researchers preferred to use a higher air void content (i.e., 7 percent) for performance testing because they believe it more closely represents the air void content of a newly-constructed HMA pavement. However, using a different air void content from the mixture design requires an adjustment of the compactive effort and further burdened the designer as he prepared specimens. Additionally, test specimens

prepared at higher air void contents experienced densification during the test, while specimens prepared and tested at the design air void content were able to be sufficiently ranked according to the mixture stability. Table 7 provides the measured voids in mineral aggregate (VMA) and air void content (V_a) of the specimens used for performance testing. The following sections describe the details of the four performance tests used in this study.

Repeated Load Test

The repeated load triaxial test measured permanent deformation as axial load cycles were applied to cylindrical HMA specimens. Cumulative permanent deformation was reported as a function of number of load cycles. Cumulative permanent deformation historically has been categorized for a wide range of materials—such as metals, polymers and some composites—into three zones: primary, secondary, and tertiary, as indicated on the illustrative creep data curve (Figure 6). The primary zone was characterized by a decreasing rate of accumulated permanent deformation during specimen densification. In the secondary zone, permanent strain accumulated in a relatively linear fashion. The tertiary zone occurred as the specimen failed and was characterized by an increasing rate of accumulated permanent deformation.

The repeated load test was used to determine the flow number (FN) for HMA in the asphalt mixture performance tester (AMPT) according to AASHTO TP 79-09. The procedure allowed performing the test on unconfined or confined cylindrical specimens, 100 mm in diameter by 150 mm high, cored from gyratory compacted mixtures.

Table 7. Volumetric properties of specimens

Binder	Agg. Type	Sand (%)	Mix Designation	RCR1		RCR2		SC1		SC2		DM1		DM2		DM3		APA1		APA2	
				VMA	Va	VMA	Va	VMA	Va	VMA	Va	VMA	Va	VMA	Va	VMA	Va	VMA	Va	VMA	Va
64-22	Granite	0	12.5 FGN0	16.6	3.1	17.2	3.8	17.6	4.2	17.8	4.5	16.6	2.6	16.7	2.8	16.9	3.0	17.5	3.7	17.5	3.7
			12.5 CGN0	16.2	3.2	15.9	2.9	16.2	3.2	16.0	2.9	15.8	2.7	15.7	2.6	16.3	3.3	16.7	3.8	16.9	4.0
			19 FGN0	14.8	4.4	14.7	4.4	15.7	5.4	13.6	3.1	14.2	1.1	13.9	0.7	14.6	1.5	15.3	2.4	15.9	3.0
			19 CGN0	16.1	5.4	14.7	3.9	15.4	4.7	15.2	4.5	14.3	2.4	15.2	3.4	14.7	2.9	16.3	4.7	17.7	6.3
		10	12.5 FGN10	17.9	3.9	17.8	3.9	18.2	4.4	17.7	3.7	18.2	4.3	17.4	3.4	17.1	3.1	17.1	3.1	17.2	3.1
			12.5 CGN10	15.4	2.9	16.1	3.6	16.6	4.2	16.1	3.6	16.1	3.6	16.6	4.2	16.5	4.1	16.3	3.9	16.1	3.6
			19 FGN10	17.2	4.8	16.5	3.9	15.9	3.3	15.5	2.8	14.8	2.0	14.8	2.0	15.6	2.9	15.3	2.6	13.8	0.8
			19 CGN10	13.7	3.2	13.1	2.5	14.1	3.6	15.1	4.8	14.8	4.5	13.3	2.7	14.4	4.0	14.7	4.3	15.3	4.9
		30	12.5 FGN30	19.7	4.5	20.7	5.7	21.0	6.1	21.1	6.3	21.2	5.9	19.4	5.4	19.5	5.6	20.5	5.5	20.9	6.0
			12.5 CGN30	19.1	4.9	18.0	5.0	18.8	4.8	19.3	5.1	18.3	4.9	18.7	4.7	19.4	5.1	19.1	4.9	18.0	3.5
			19 FGN30	18.9	4.2	19.2	4.5	19.2	4.5	18.4	3.6	17.8	3.4	18.1	4.2	17.7	3.9	17.0	2.5	17.6	3.2
			19 CGN30	19.9	3.5	19.5	4.6	19.1	4.2	18.9	3.8	19.6	3.9	19.2	4.1	20.1	5.2	19.9	5.0	19.5	4.6
	Gravel	0	12.5 GV0	16.1	3.9	16.3	4.0	16.0	3.6	16.1	3.8	15.5	3.2	15.8	3.5	15.5	3.1	15.8	3.5	15.7	3.3
			19 FGV0	16.2	3.9	15.8	3.5	15.5	3.2	16.2	3.9	15.9	3.6	15.8	3.5	15.3	2.9	16.0	3.7	16.0	3.7
			19 CGV0	15.0	3.3	14.8	3.1	15.2	3.5	15.5	3.9	14.5	2.7	14.4	2.6	14.4	2.6	15.3	3.7	15.5	3.9
		10	12.5 GV10	18.0	2.2	17.8	1.9	17.9	2.1	18.1	2.3	17.4	1.6	17.7	1.8	17.6	1.7	18.2	2.5	18.0	2.3
			19 FGV10	16.2	3.9	15.8	3.5	15.5	3.2	16.2	3.9	17.1	2.4	17.5	2.8	17.3	2.6	16.0	3.7	16.0	3.7
			19 CGV10	16.0	2.5	16.3	2.9	15.8	2.3	15.6	2.1	16.4	3.0	16.8	3.4	16.2	2.8	16.7	3.3	16.6	3.2
	Limestone	0	12.5 FLS0	16.4	3.0	17.2	4.0	16.7	3.4	17.7	4.6	17.5	4.4	17.3	4.1	17.0	3.8	17.4	4.3	17.3	4.1
			12.5 CLS0	15.5	3.5	15.3	3.3	15.7	3.8	14.9	2.8	15.2	3.2	14.7	2.7	16.9	5.2	16.5	4.7	16.9	5.1
			19 FLS0	17.5	5.3	17.5	5.3	17.2	4.9	17.2	4.9	15.9	3.5	17	4.8	16.1	3.7	16.8	4.5	16.9	4.6
			19 CLS0	14.1	1.4	14.1	1.9	14.5	1.4	14.5	1.4	15.3	2.8	14.6	2.0	15.1	2.6	15.3	2.8	15.6	3.2
		10	12.5 FLS10	15.3	3.1	14.6	3.0	14.8	3.6	14.6	2.9	15.2	3.5	15.1	3.5	15.3	3.7	15.3	3.7	15.1	3.5
			12.5 CLS10	14.4	3.4	13.9	2.8	14.4	3.4	14.0	2.9	14.1	3.1	14.7	3.8	14.2	3.2	15.0	4.1	14.6	3.6
			19 FLS10	14.1	3.5	14.1	3.5	13.7	3.1	13.7	3.1	14.5	4.0	14.0	3.4	13.8	3.2	14.5	3.9	14.9	4.4
			19 CLS10	13.4	1.3	13.1	0.9	14.0	2.0	13.2	1.1	13.7	1.6	13.8	1.8	13.6	1.6	14.0	2.0	14.4	2.5

Table 7 Continued

Binder	Agg. Type	Sand (%)	Mix Designation	RCR1		RCR2		SC1		SC2		DM1		DM2		DM3		APA1		APA2	
				VMA	Va	VMA	Va	VMA	Va	VMA	Va	VMA	VMA	Va	VMA	Va	VMA	Va	VMA	Va	VMA
76-22	Granite	0	12.5 FGN0	16.7	3.1	16.3	2.7	17.3	3.9	16.5	3.0	16.6	3.0	16.9	3.4	16.6	3.1	17.6	3.8	18.4	4.8
			12.5 CGN0	16.1	3.1	16.4	3.4	16.6	3.6	16.3	3.2	16.2	3.2	16.7	3.8	16.6	3.5	17.6	4.7	17.1	4.2
		30	19 FGN30	18.1	3.3	19.4	4.8	19.9	5.3	18.9	4.2	17.7	2.7	18.3	3.5	19.3	4.7	19.3	5.3	18.4	4.2
	Gravel	0	12.5 GV0	15.6	3.2	15.2	2.8	15.3	2.9	15.5	3.2	15.5	3.1	15.6	3.2	15.6	3.2	16.3	4.0	15.8	3.5
			19 CGV0	14.9	3.2	15.8	4.3	15.1	3.4	15.2	3.5	14.3	2.5	14.9	3.2	14.6	2.9	16.1	4.5	16.0	4.4
	Limestone	0	12.5 CLS0	14.8	2.8	15.4	3.4	15.5	3.6	14.8	2.7	14.6	2.5	15.9	4.0	15.1	3.1	16.3	4.5	16.9	5.1
			19 CLS0	14.5	1.8	14.2	1.6	14.1	1.4	14.8	2.2	14.7	2.1	14.8	2.2	14.5	1.9	16.9	4.6	16.9	4.6
		10	19 FLS10	13.8	3.1	13.4	2.7	13.5	2.8	13.4	2.7	13.6	2.9	13.8	3.2	14.7	4.2	13.9	3.3	13.7	3.0

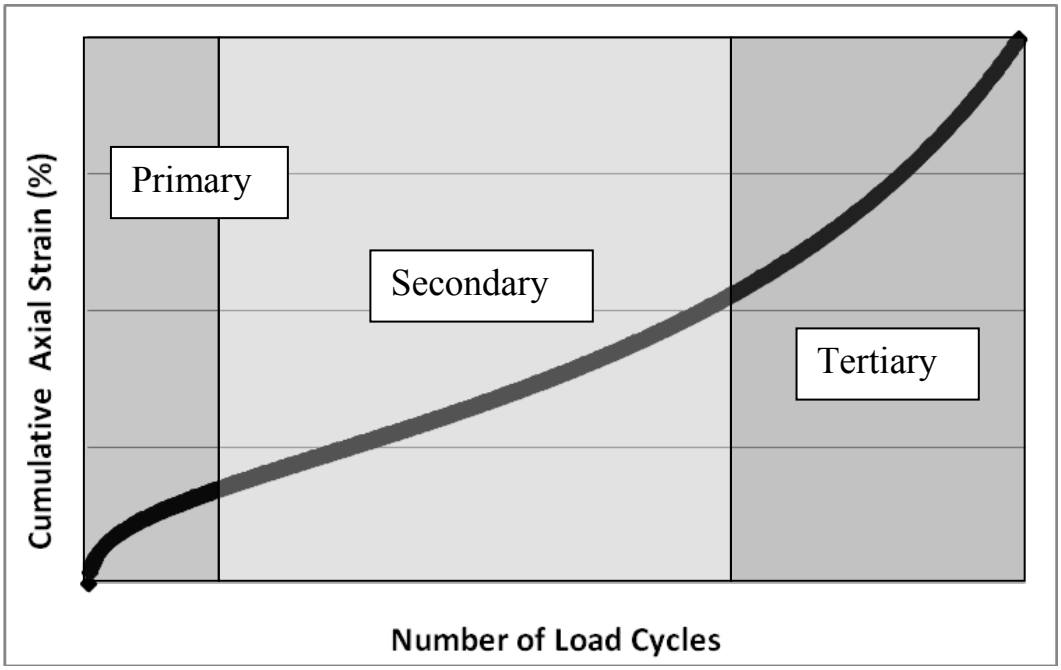

Figure 6. Typical permanent deformation behavior of asphalt mixtures

The basic principles of the AASHTO FN test were used in this study. Variations in stress conditions were incorporated to be more applicable to airfield pavements. The confined test was selected to more closely represent field conditions. A confining stress of 276 kPa and deviator stress of 1380 kPa were selected. Simulations of stress distributions in a typical pavement structure loaded by a heavy commercial airliner using simple linear elastic computer programs such as Kenlayer suggested these conditions were reasonable for triaxial testing. Although the stress distributions within an HMA surface layer on a loaded airfield pavement are very complex, one single, representative confinement level and axial stress combination was selected to serve as a basis for ranking mixture performance. The load pulse consisted of a 0.1-sec load followed by 0.9-sec dwell time. The test temperature was selected to be the mean monthly pavement

temperature (MMPT) and was defined by Witczak (1996). The MMPT was 43°C in Vicksburg, Mississippi, the selected climate.

The FN was defined as the number of cycles corresponding to the minimal rate of change of permanent axial strain during the repeated load test. The FN for each specimen was determined by fitting the repeated load test data to the Francken model by a least sum of squares method. The Francken model (Equation 7) fit the permanent strain data by using a combination of a power law and an exponential model. Four fitting coefficients were used to fit the model to experimental data (Figure 7). The FN was defined as the number of cycles when the second derivative of the model (Equation 8) changed from negative to positive.

$$\varepsilon_p = An^B + C(e^{Dn} - 1) \tag{7}$$

where

A, B, C, and D = fitting coefficients

$$\frac{d^2\varepsilon_p}{dn^2} = AB(B-1)n^{(B-2)} + CD^2e^{Dn} \tag{8}$$

The FN for each mixture was determined according to the previously described procedure and occurred near the beginning of the secondary flow region in all cases for this set of testing conditions. The data were further analyzed to determine the number of load cycles where tertiary flow began. To determine this point, a line was first drawn along the slope of the secondary flow region. Next, a line was drawn following the slope of the tertiary flow region. The intercept of these lines was defined to be the tertiary flow

number (TF) for these data. Figure 8 illustrates the procedure for defining the TF value. Figure 9 shows an example of the FN (indicated by a star) and TF (indicated by a triangle) values along a typical data curve. Appendix A contains all of the repeated load test data in this format.

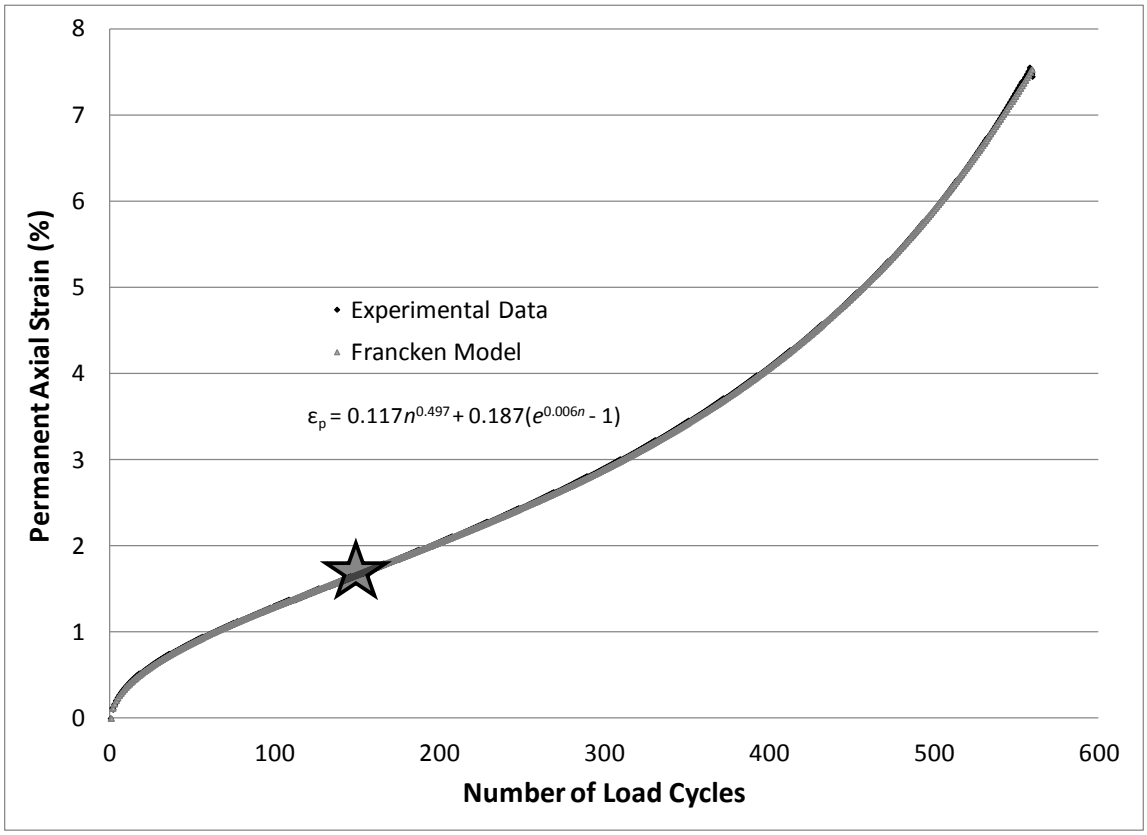

Figure 7. Example of determining flow number

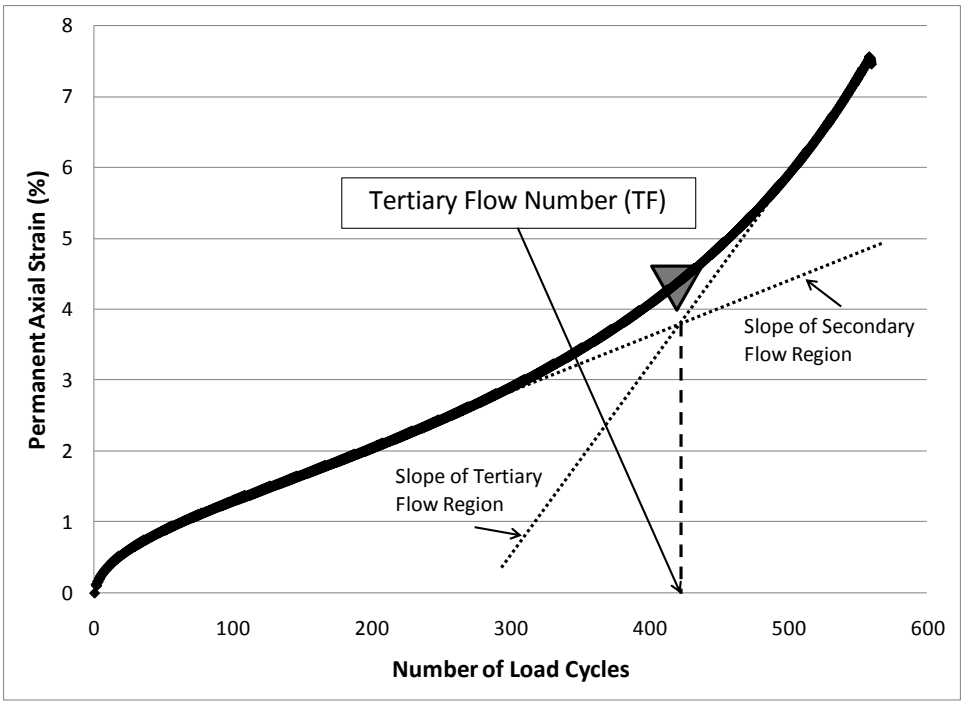

Figure 8. Example of determining tertiary flow value

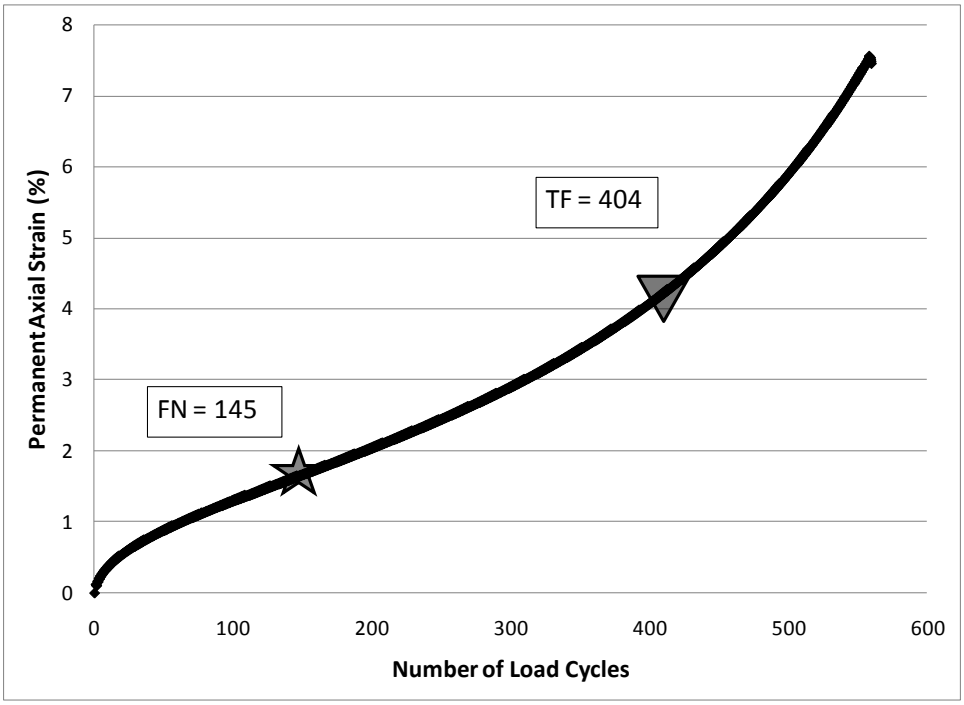

Figure 9. Example performance parameters for repeated load test

The rate of accumulated permanent deformation was also mathematically expressed using the classic power-law model, shown in Equation 9.

$$\varepsilon_p = a \times N^b \tag{9}$$

where

ε_p = permanent strain

a = regression constant

N = number of load cycles

b = regression constant

Figure 10 shows test data plotted on a log-log scale. The slope, *b*, and the intercept, *a*, are noted on the figure. The slope and intercept values for each specimen were determined according to this procedure from repeated load test data.

Static Creep Test

The static creep triaxial test measured permanent deformation as a function of time when a constant load was applied to cylindrical HMA specimens. Cumulative permanent deformation was reported as a function of time during loading. Representative static creep data from this study is shown in Figure 11.

NCHRP Report 465 provided a procedure for measuring the flow time of HMA using static creep tests (Witczak et al. 2002). The procedure was based on application of statec loads to unconfined or confined cylindrical specimens, 100 mm in diameter and 150 mm in height, cored from gyratory compacted mixtures.

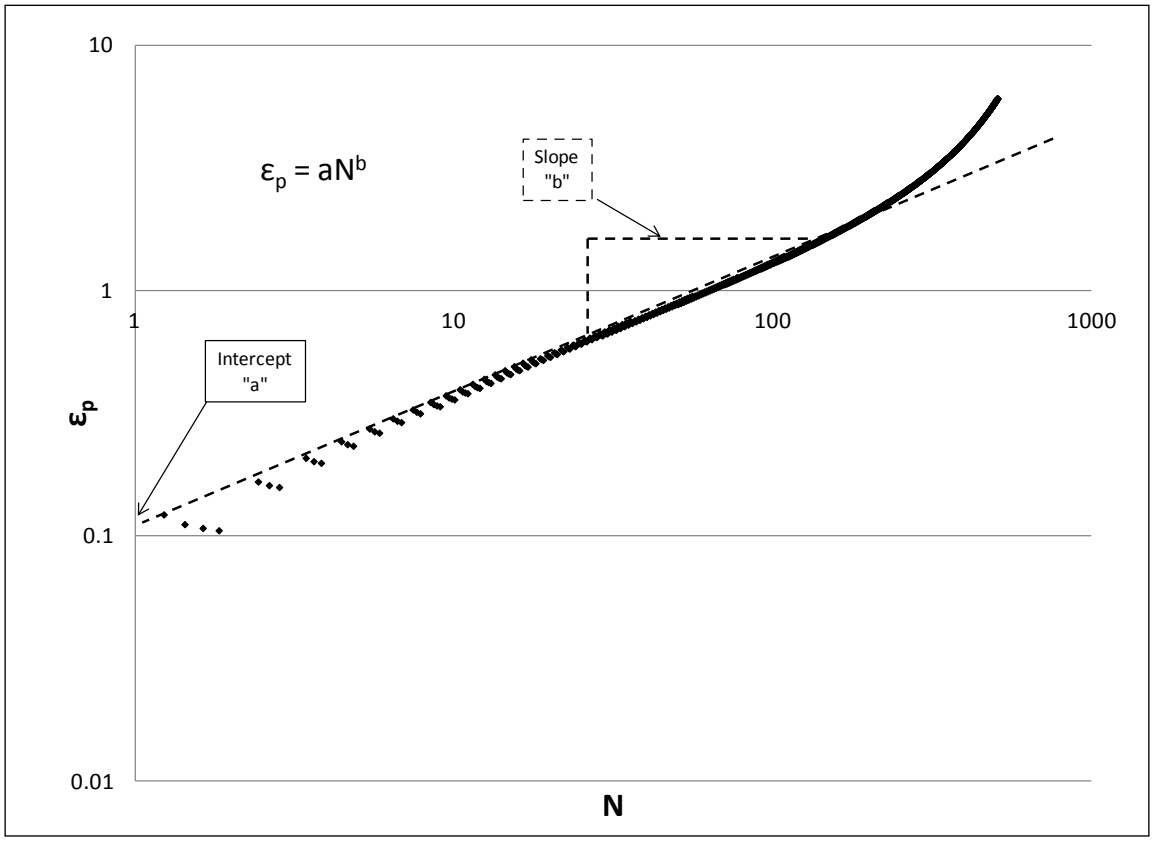

Figure 10. Example of determining slope and intercept value from repeated load data

The basic principles related to the static creep test as stipulated in NCHRP Report 465 for flow time testing were applied in this study. Variations in stress conditions and test temperatures were considered in order to apply more directly to airfield pavements. The confined test was selected in lieu of the unconfined compression test, because it better simulated field conditions. Specifically, a confining stress of 276 kPa and a deviator stress of 1380 kPa were selected. The test temperature was selected to be the MMPT as defined by Witczak (1996). An MMPT of 43°C was used for Vicksburg, Mississippi.

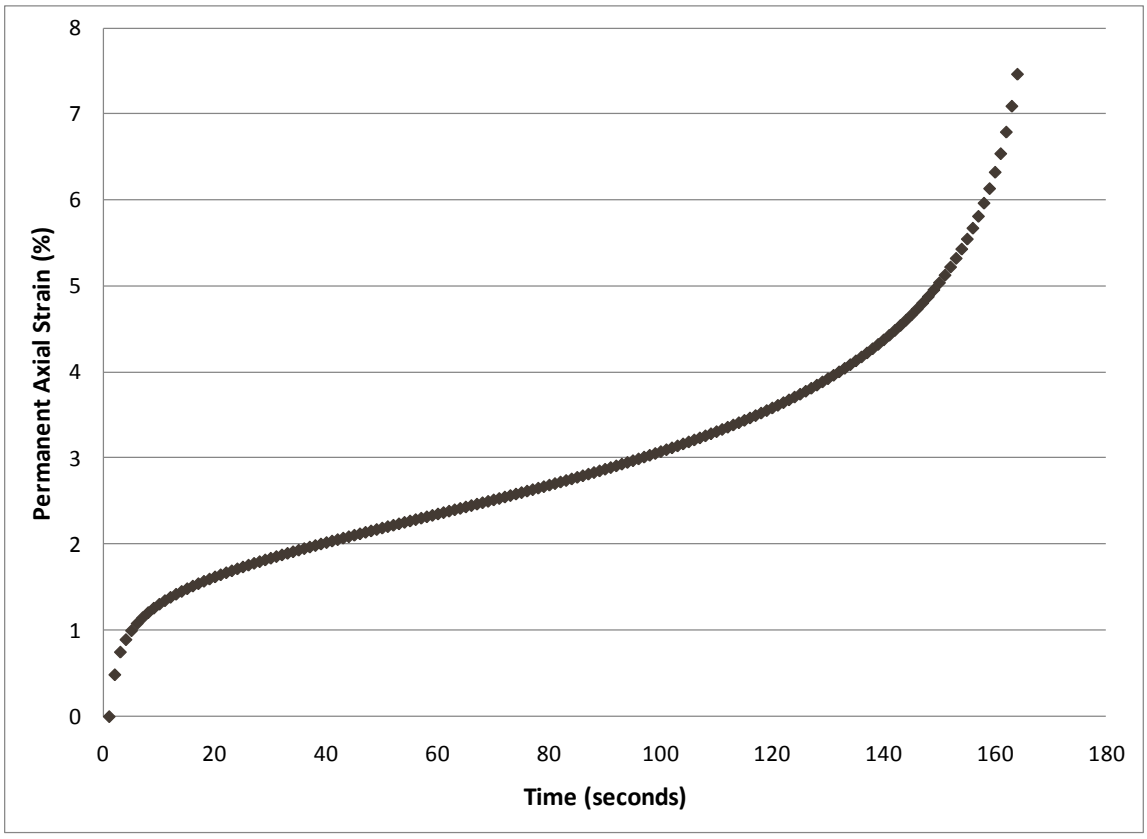

Figure 11. Example of static creep test data

The flow time (FT) was defined as the time corresponding to the minimal rate of change of permanent axial strain during the static creep test. The FT for each specimen was determined by fitting the data to the Francken model by a least sum of squares method. The Francken model (Equation 7) fit the permanent strain data by using a combination of a power law and an exponential model. Four fitting coefficients were used to fit the model to experimental data (Figure 12). The flow time was defined as the time when the second derivative of the model (Equation 8) changes from negative to positive.

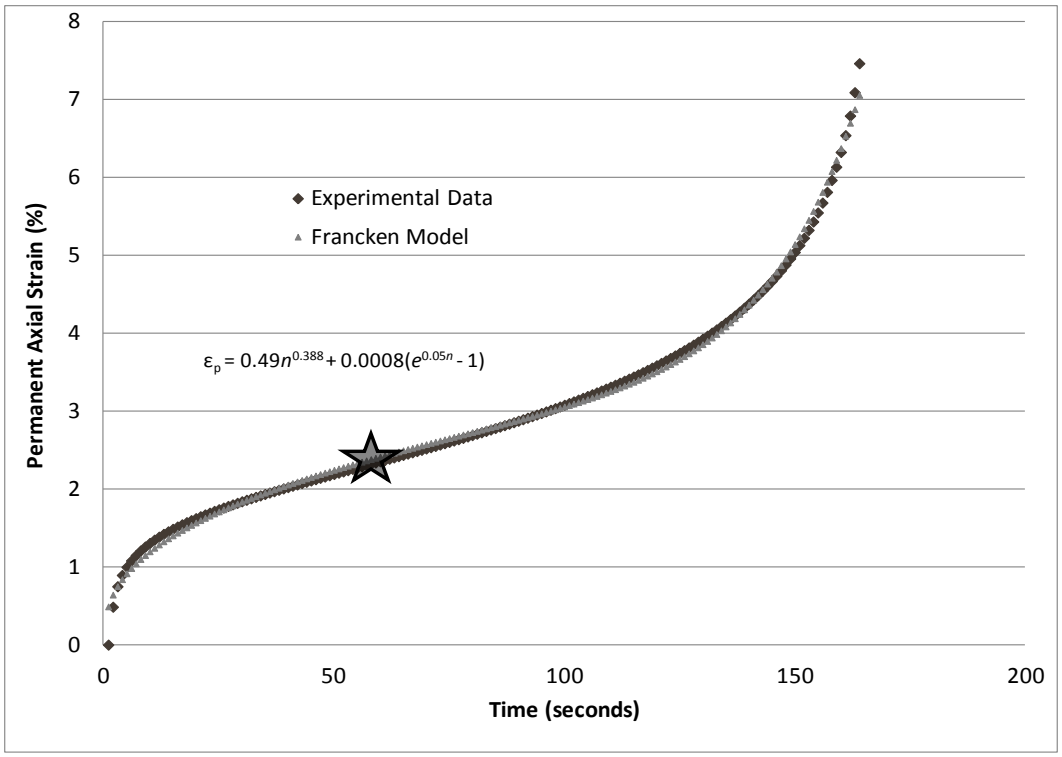

Figure 12. Example of determining flow time from static creep data

Similar to the FN, the FT for each mixture occurred near the beginning of the secondary flow region in all cases for this set of testing conditions. These data were also analyzed to determine the time of loading when tertiary flow began. To determine this point, the previously described graphical procedure was used. First, a line was drawn along the slope of the secondary flow region. Next, a line was drawn following the slope of the tertiary flow region. The intercept of these lines was defined to be the tertiary flow number (TF) for these data. Figure 13 illustrates the procedure for defining the TF value. Figure 14 shows an example of the FT (indicated by a star) and TF (indicated by a triangle) values along a typical data curve. Appendix B contains all of the static creep test data in this format.

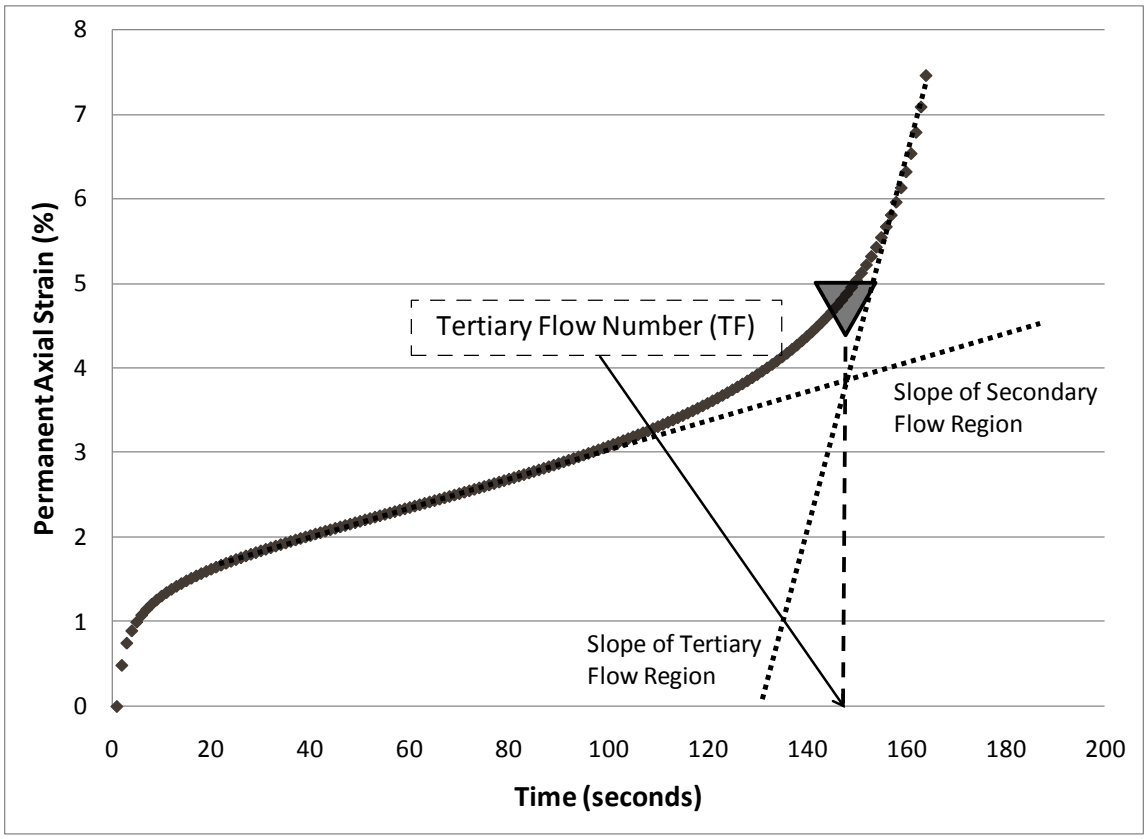

Figure 13. Example of determining tertiary flow value from static creep data

Another common method for analyzing creep test data is to plot the accumulated permanent strain versus time on a log-log scale. The secondary phase of the creep curve typically has a relatively linear shape. The data from the secondary phase of the curve plotted on a log-log scale can be approximated using Equation 10 to express permanent strain as a function of time.

$$\varepsilon_p = a * t^m \tag{10}$$

where

t = loading time (s)

a, m = material regression coefficients

Figure 15 shows test data plotted on a log-log scale. The slope, m, and the intercept, a, are noted on the figure. The slope and intercept values for each specimen were determined according to this procedure from static creep test data.

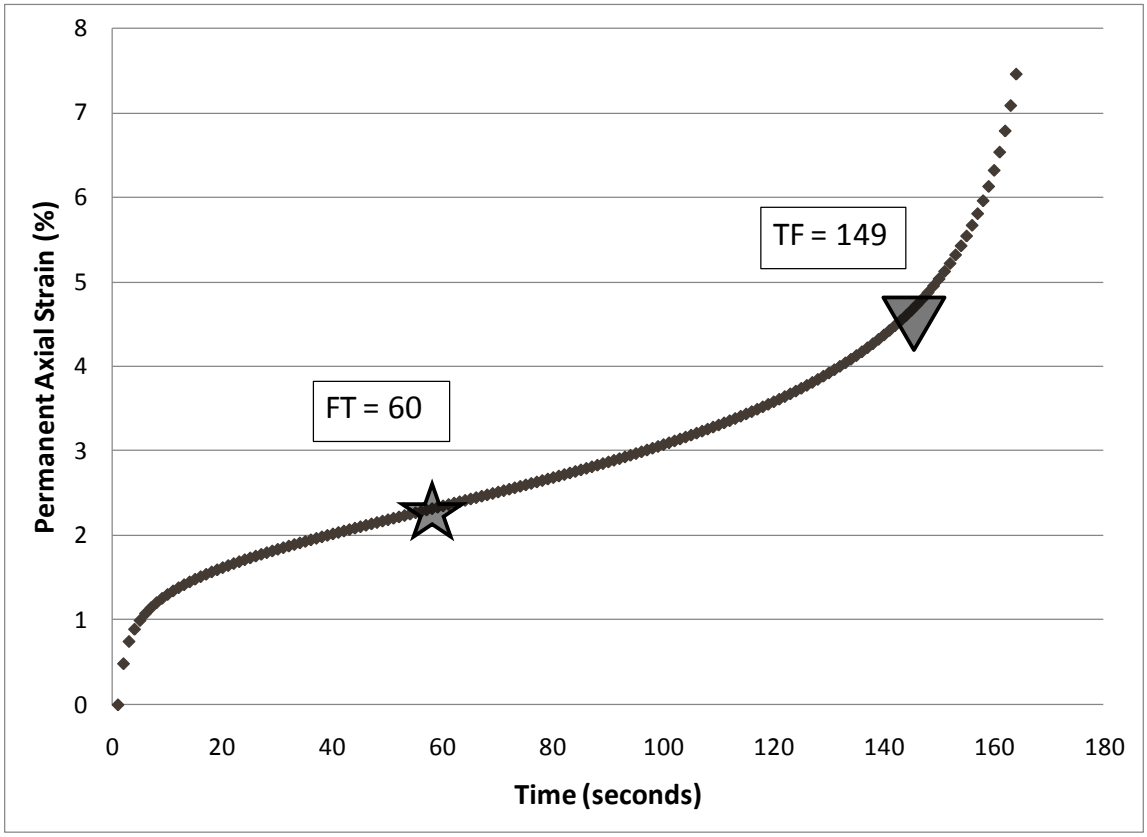

Figure 14. Example of performance parameters from static creep data

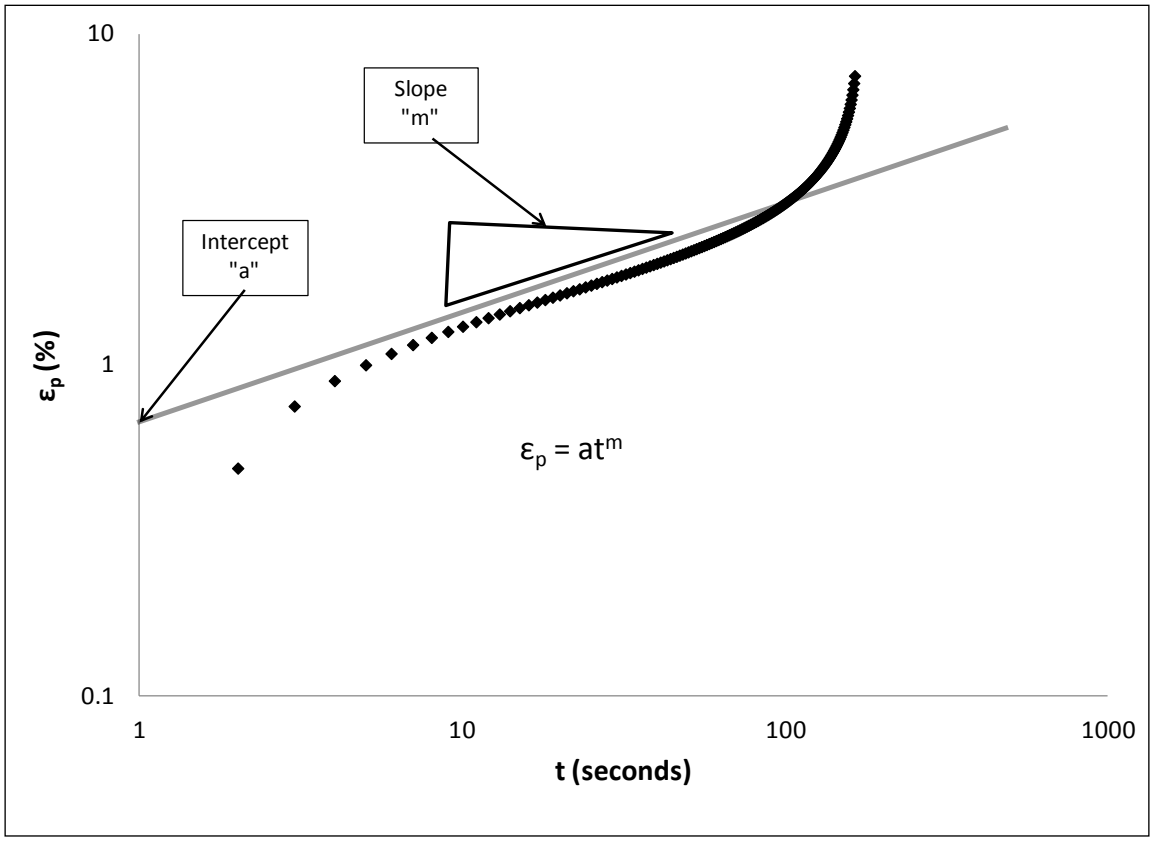

Figure 15. Example of determining slope and intercept value from static creep data

Dynamic Modulus Test

AASHTO TP 62-07 provided the procedure for determining dynamic modulus. The procedure allowed testing unconfined or confined cylindrical specimens, 100 mm diameter by 150 mm high, cored from gyratory compacted mixtures. The stress conditions were adjusted to result in 50 to 150 microstrain. Specimens were typically tested at 5 temperatures and 6 frequencies, resulting in 30 combinations of testing. The suggested test temperatures were -10, 4, 21, 37, and 54°C. The suggested test frequencies were 25, 10, 5, 1, 0.5, and 0.1 Hz. For this study, testing was performed at

18 combinations of test conditions. No testing was performed at -10 or 4°C. Testing at low temperatures was not performed because rutting was the primary pavement distress investigated in this study and because rutting in the HMA layer does not typically occur at low temperatures.

AASHTO PP 62-10 provided guidance on developing dynamic modulus master curves. The master curves were developed to enable material characterization on a single response scale. Data were typically shown as modulus over a range of reduced frequency at a reference temperature (Equation 11). The time-temperature superposition principle was used to shift the measured responses at various temperatures to this reduced frequency according to Equation 12.

$$log\left|E^*\right| = \delta + \frac{(\alpha)}{1+e^{\beta+\gamma log\, f_r}} \tag{11}$$

where

$|E^*|$ = dynamic modulus (MPa)

$\alpha, \beta, \delta, \gamma$ = fitting coefficients

f_r = reduced frequency (Hz)

$$log\ f_r = log\ f + a_1(T_R - T) + a_2(T_R - T)^2 \tag{12}$$

where

f = loading frequency at test temperature

a_1, a_2 = fitting coefficients

T_R = reference temperature (°C)

T = test temperature (°C)

$$log\left|\hat{E}^*\right| = \delta + \frac{(\alpha)}{1+e^{\beta+\gamma\left[log\, f + a_1(T_R - T) + a_2(T_R - T)^2\right]}} \quad (13)$$

The selected reference temperature was 21°C. All dynamic modulus data were shifted to the reduced frequency by using Equation 13. A numerical optimization procedure was used to minimize the error between the predicted and actual dynamic modulus measurements to determine the fitting coefficients as shown in Equation 14. The procedure was accomplished using the solver function in Microsoft Excel software.

$$\sum error^2 = \sum_1^n \left(log\left|\hat{E}^*\right|_i - log\left|E^*\right|_i \right)^2 \quad (14)$$

Figure 16 shows an example of a dynamic modulus master curve along with the plot of temperature shift factors. Appendix C contains all dynamic modulus master curves in this format.

Asphalt Pavement Analyzer Test

The APA used in this study was designed specifically to simulate high tire pressures associated with aircraft. An APA tube or hose pressure of 1724 kPa under a wheel load of 1113 N was used for testing. These conditions are more severe than those typically used in APA testing and were selected to better represent aircraft loads. The test temperature was 64°C, which was the high temperature PG grade for the neat binder. Mixtures containing polymer-modified binder were tested at the same temperature to

quantify the benefit of using premium binders in a given climatic region. Figure 17 shows the APA test configuration. Cylindrical asphalt concrete specimens with a target air void content of 3.5 percent were prepared and tested. The air void content was selected as the midpoint of the allowable range in the FAA mixture design procedure. Two replicate specimens were tested for each mix. The APA reported the average rut depth of the two specimens.

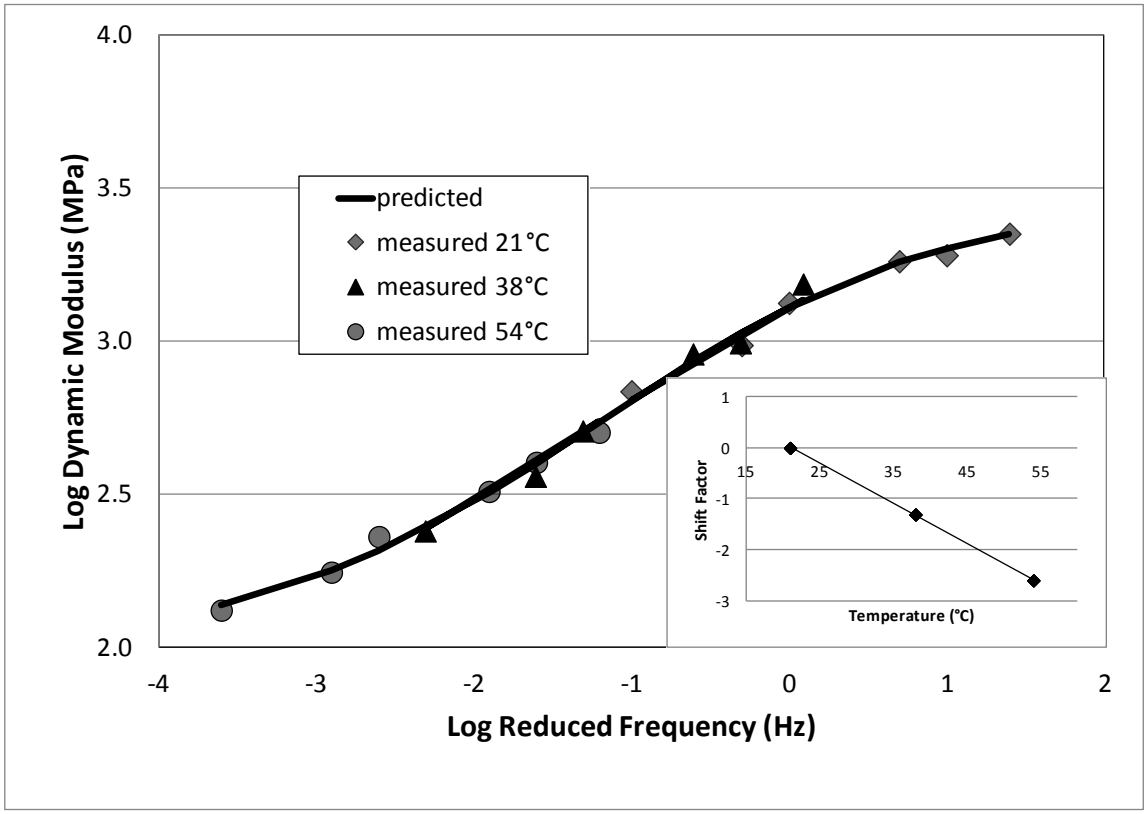

Figure 16. Example of dynamic modulus master curve

Figure 17. APA test configuration

The APA applied cyclic loads at a rate of one cycle per second. The terminal rut depth of the specimens was set at 12 mm. The test was performed until the terminal rut depth was reached or until 8,000 APA cycles were applied. Once one of the two specimens reached terminal rut depth, the test was stopped. However, since the APA reported the average rut depth for the two specimens, some average rut depths were less than 12 mm. Figure 18 shows specimens after the test was complete.

Figure 18. HMA specimens after testing in the APA

CHAPTER VI

PERFORMANCE TEST RESULTS*

Repeated Load Test Results

Repeated load testing was performed as described in Chapter V. The permanent deformation was recorded after each load cycle. Results from two specimens were averaged and are presented in Figures 19 through 22. The data were separated into groups to reduce the number of mixtures presented on each graph for easier interpretation. The mixtures containing neat binder were presented first, separated by the percent of natural sand in the mix. Figure 19 shows data for those with no natural sand, while Figures 20 and 21 show data for mixtures with 10 and 30 percent natural sand, respectively. Figure 22 shows data for mixtures prepared with the polymer-modified binder.

Figure 19 shows varying performance of the mixes with no natural sand, with failure (exceeding strain limit of LVDTs) occurring from approximately 200 to 1,300 load cycles. The performance for mixtures with gravel and granite aggregate was poorest, while mixtures with limestone aggregate had the greatest performance. All gravel mixtures and all but one granite mixture experienced failure within 500 load cycles. All limestone mixtures withstood at least 700 load cycles before failure.

---

* Part of the data reported in this chapter is reprinted with permission from "Asphalt Pavement Analyzer Used to Assess Rutting Susceptibility of Hot-Mix Asphalt Designed for High Tire Pressure Aircraft" by J. Rushing, D. Little, and N. Garg, 2013. *Transportation Research Record: Journal of the Transportation Research Board*, No. 2296, pp 98-101, Copyright 2013 by Transportation Research Board.

The data for mixtures containing 10 percent natural sand were similar to data from mixtures with no natural sand, but failures occurred within a narrower range of load cycles. Failure occurred between approximately 400 and 900 cycles for these mixtures. Like the mixtures without natural sand, the gravel mixtures had the poorest performance while the limestone mixtures had the greatest performance.

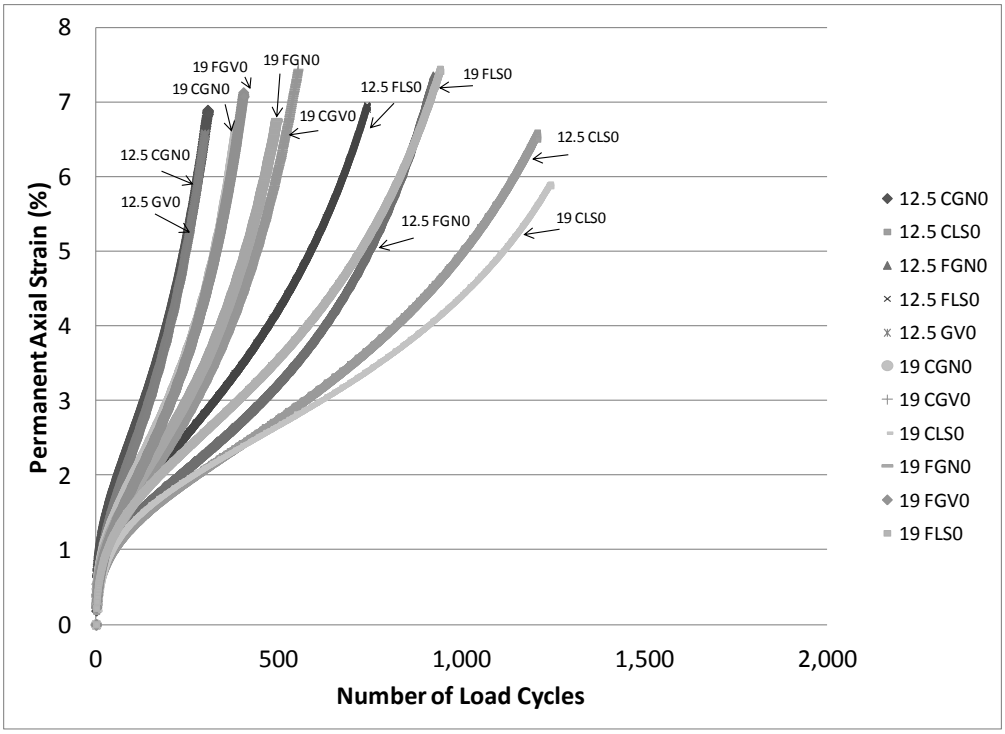

Figure 19. Repeated load data for mixtures containing 100 percent crushed aggregate

Test results for selected mixtures prepared with polymer-modified binder (Figure 22) show significant improvement in number of load cycles to failure over mixtures with neat binder. The mixture containing 30 percent natural sand failed around 200 load cycles, while all other mixtures withstood at least 1,000 load cycles. The three mixtures

containing limestone aggregate did not experience tertiary flow (failure) within 2,000 load cycles. The performance of the granite mixtures exceeded that of the gravel mixtures.

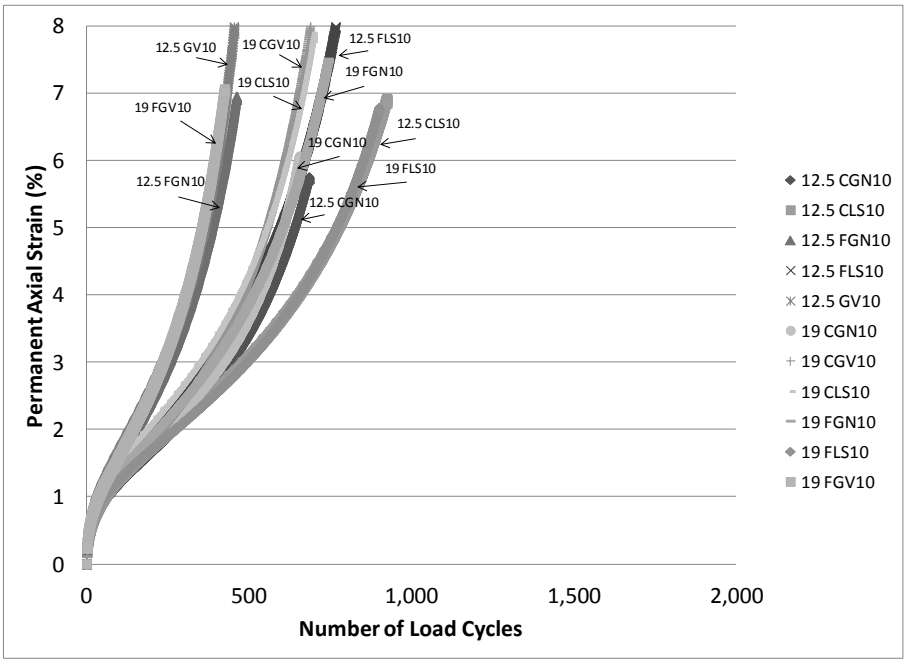

Figure 20. Repeated load data for mixtures containing 10 percent natural sand

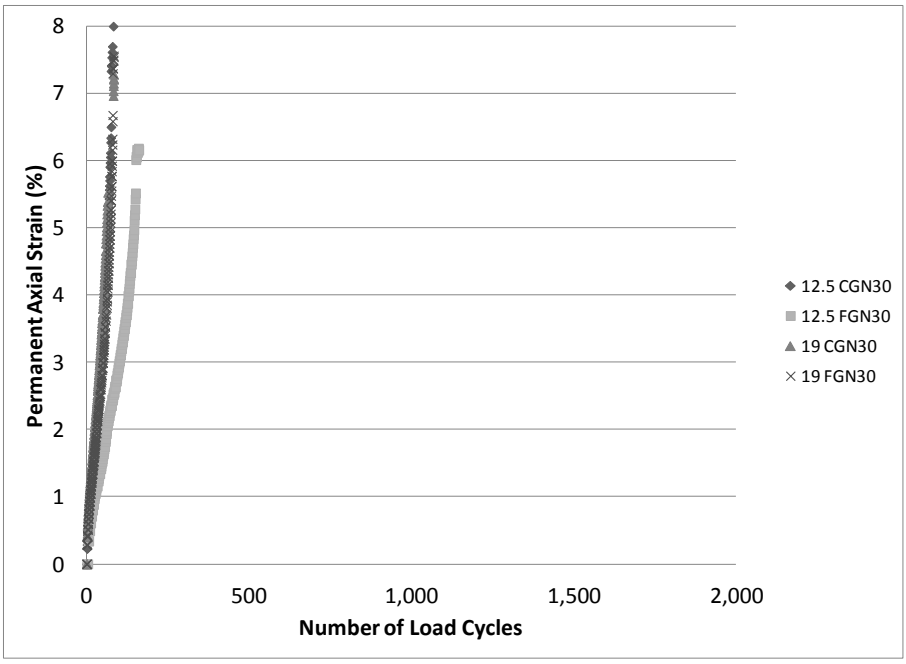

Figure 21. Repeated load data for mixtures containing 30 percent natural sand

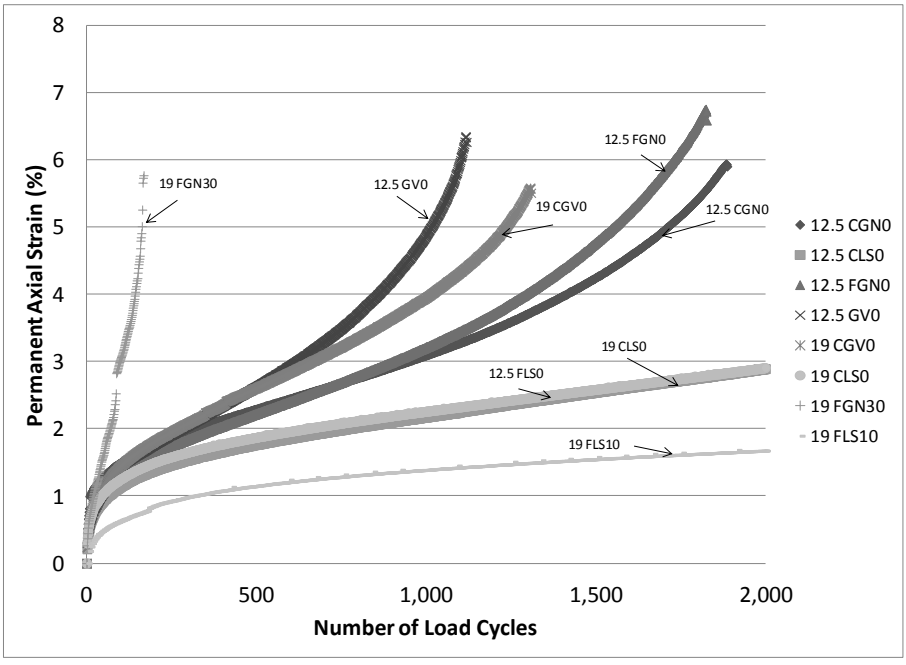

Figure 22. Repeated load data for mixtures prepared using polymer-modified binder

The four index parameters extracted from repeated load data are given in Table 8. These parameters include the slope and intercept values from the data plotted on a log-log scale and the flow number and tertiary flow values. The intercept values, *a*, ranged from 0.145 to 0.382. Slope values, *b*, ranged from 0.254 to 0.712. Typically, smaller slope and intercept values were indicative of greater rutting resistance. The mixtures expected to have the poorest rutting resistance in this study were those with 30 percent natural sand. The intercept values ranged from 0.166 to 0.331 for these mixtures, similar to the range of the overall data set. The slope values for these mixtures ranged from 0.558 to 0.712, excluding the mixture with 30 percent natural sand with a polymer-modified binder. This slope value was 0.495. Given that these mixtures are very susceptible to rutting, the intercept value does a poor job of differentiating these mixtures from other mixtures containing better quality aggregate. Further, when mixtures were ranked according to the smallest intercept value, the top five mixtures were 19 CGV10, 12.5 CGN30, 12.5 CGN10, 12.5 GV10, and 12.5 CLS10. Intuitively, these mixtures were not expected to provide the greatest rutting resistance. The slope values provided a much stronger association with rutting performance since the slopes of mixtures containing 30 percent natural sand were greater than the slope of any other mixture. The improvement in rutting resistance from using a polymer-modified binder was also observed, with the slope of the 19 FGN30 mixture reducing from 0.604 to 0.495 when the polymer-modified binder was used. A ranking of mixtures according to increasing slope value included 19 CGN10, 12.5 FGN0, 19 FLS10, 19 FLS0, and 19 FGN10 as the top performers for mixtures with the unmodified binder.

Table 8. Repeated load performance parameters

Binder	Agg. Type	Sand (%)	Mix	a	b	FN	TF
64-22	Granite	0	12.5 FGN0	0.29	0.36	285	690
			12.5 CGN0	0.37	0.42	87	237
			19 FGN0	0.29	0.45	165	369
			19 CGN0	0.28	0.43	148	315
		10	12.5 FGN10	0.21	0.44	135	355
			12.5 CGN10	0.18	0.41	221	646
			19 FGN10	0.22	0.40	231	544
			19 CGN10	0.29	0.35	255	592
		30	12.5 FGN30	0.26	0.65	21	44
			12.5 CGN30	0.17	0.71	28	56
			19 FGN30	0.25	0.60	22	54
			19 CGN30	0.33	0.56	15	51
	Gravel	0	12.5 GV0	0.29	0.44	110	244
			19 FGV0	0.22	0.46	140	312
			19 CGV0	0.21	0.44	186	399
		10	12.5 GV10	0.18	0.44	186	459
			19 FGV10	0.21	0.44	143	314
			19 CGV10	0.15	0.49	165	391
	Limestone	0	12.5 FLS0	0.23	0.43	286	594
			12.5 CLS0	0.20	0.41	451	962
			19 FLS0	0.25	0.41	386	706
			19 CLS0	0.25	0.37	629	1,236
		10	12.5 FLS10	0.19	0.43	237	559
			12.5 CLS10	0.18	0.42	323	729
			19 FLS10	0.24	0.36	320	701
			19 CLS10	0.27	0.43	128	379
76-22	Granite	0	12.5 FGN0	0.32	0.30	813	1,793
			12.5 CGN0	0.37	0.28	951	2,242
		30	19 FGN30	0.22	0.50	172	296
	Gravel	0	12.5 GV0	0.24	0.36	567	1365
			19 CGV0	0.30	0.33	842	1,875
	Limestone	0	12.5 CLS0	0.30	0.29	2,017	3,905
			19 CLS0	0.38	0.25	1,711	4,224
		10	19 FLS10	0.21	0.37	1,509	2,937

This ranking was more intuitively correct since quarried aggregates with a larger maximum size are known to provide better rutting resistance.

The FN values ranged from 15 to 629, and the TF values ranged from 44 to 1,236 for mixtures containing neat binder. Higher values indicated greater rutting resistance. In general, the TF values were a little more than twice the FN values for most mixtures. A ranking of the mixtures according to either of these parameters produced nearly identical results. In both cases, the mixtures with the poorest performances were those with 30 percent natural sand. The top five performers according to both values were 19 CLS0, 12.5 CLS0, 12.5 CLS10, 19 FLS, and 19 FSL10. Either index value showed limestone mixtures to have the greatest rutting resistance. Gravel mixtures tended to have lower performance compared to other aggregate types. The 19 FGN30 mixture with polymer-modified binder had an FN value of 172 and a TF value of 296. Other FN and TF values for mixtures with polymer-modified binder ranged from 567 to 1,509 and from 1,365 to 4,224, respectively. The improvement in rutting resistance by using a polymer-modified binder was clearly observed.

Static Creep Test Results

Creep testing was performed as described in Chapter V. The permanent deformation was recorded with time after the static load was applied. Results from two specimens were averaged and were presented in Figures 23 through 26. The data were grouped to reduce the number of mixtures presented on each graph for easier interpretation. The mixtures containing neat binder were presented first and are separated by the percent of natural sand in the mix. Figure 23 shows data for those with no natural sand, while

Figures 24 and 25 show data for mixtures with 10 and 30 percent natural sand, respectively. Figure 26 shows data for mixtures prepared with the polymer-modified binder.

Figure 23 shows varying performance of the mixes with no natural sand, with failure (exceeding strain limit of LVDTs) occurring from approximately 60 to 400 sec. In general, performance was poorest for mixtures with gravel and greatest for mixtures with limestone aggregate. All gravel mixtures experienced failure within the first 120 sec. All limestone mixtures survived at least 350 sec of loading before failure. The time to fail the granite mixtures ranged from approximately 100 to 300 sec.

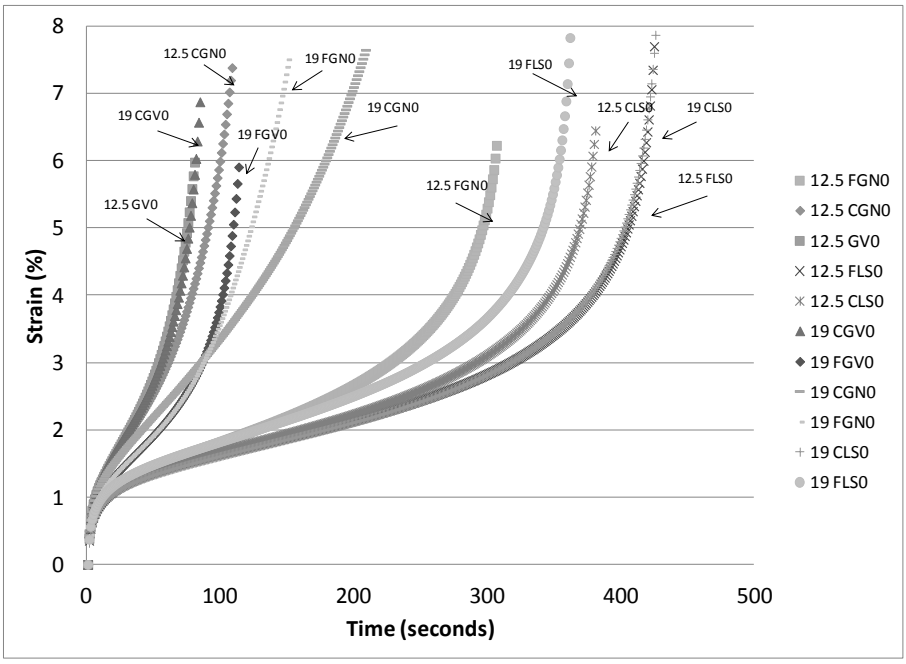

Figure 23. Static creep data for mixtures containing 100 percent crushed aggregate

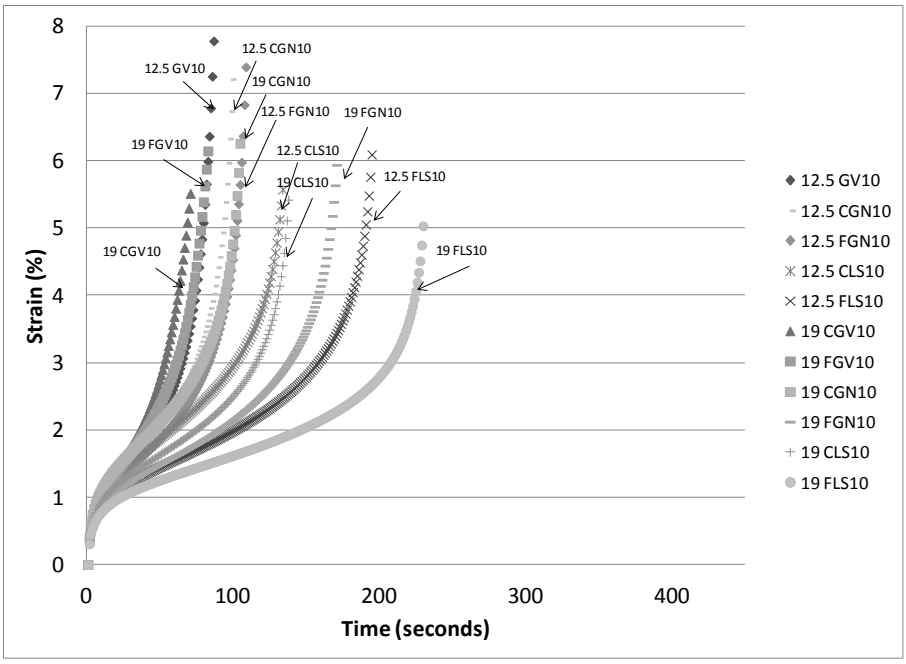

Figure 24. Static creep data for mixtures containing 10 percent natural sand

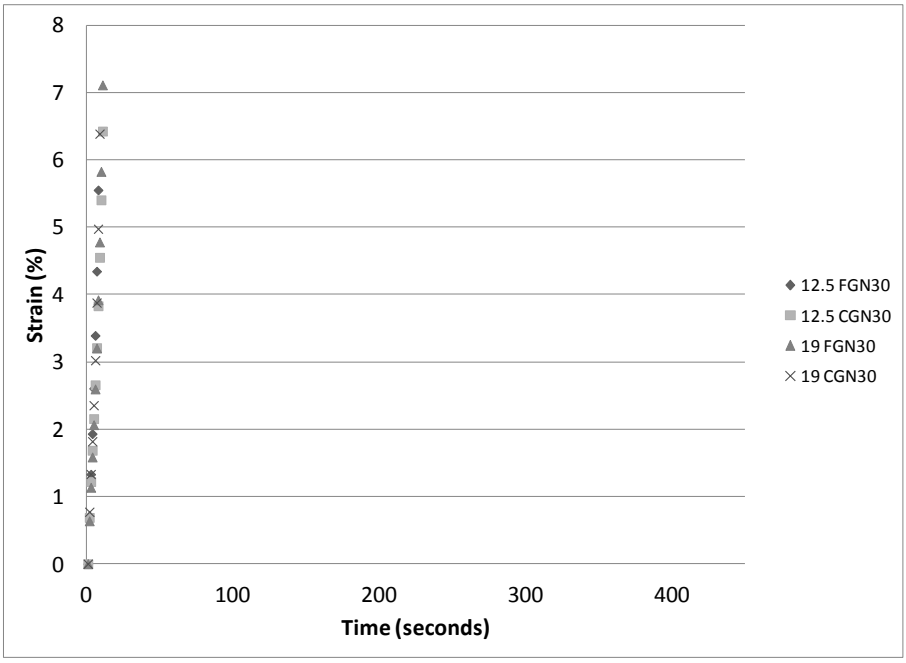

Figure 25. Static creep data for mixtures containing 30 percent natural sand

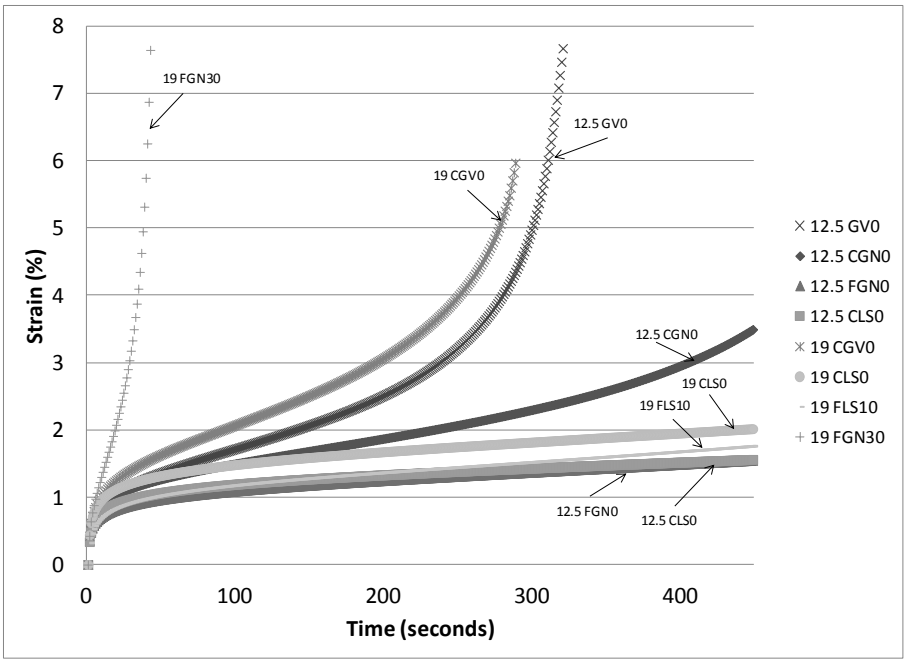

Figure 26. Static creep data for mixtures prepared using polymer-modified binder

The data for mixtures containing 10 percent natural sand were similar to data for mixtures with no natural sand, but the range was narrower. Failure occurred between approximately 50 and 230 sec for these mixtures. Similarly, the gravel mixtures had the poorest performance, while the limestone mixtures had the greatest performance.

Mixtures containing 30 percent natural sand experienced failure within the first 10 sec of loading. These mixtures were unable to withstand the applied load.

As expected, test results for mixtures prepared with polymer-modified binder (Figure 26) showed significant improvement in time to failure over mixtures with neat binder. The mixture containing 30 percent natural sand failed at around 25 sec, while the mixtures containing gravel aggregate achieved at least 275 sec. The remaining mixtures did not experience tertiary flow within 400 sec.

The four index parameters extracted from creep data are given in Table 9. These parameters include the slope and intercept values from the data plotted on a log-log scale and the flow time and tertiary flow values. The intercept values, *a*, ranged from 0.253 to 0.671. Slope values, *m*, ranged from 0.153 to 1.469. Typically, smaller slope and intercept values are indicative of greater rutting resistance. The mixtures with the poorest rutting performance in this study were those with 30 percent natural sand. The intercept values for three of these mixtures were the lowest in the data set, falsely indicating greatest rutting resistance. The slope values for these mixtures ranged from 1.006 to 1.469, excluding the mixture with 30 percent natural sand with a polymer-modified binder, whose slope value was 0.613. Given that these mixtures were very susceptible to rutting, the intercept value does a poor job, while the slope value does a good job of differentiating these mixtures from other mixtures containing better quality aggregate. When mixtures were ranked according to the smallest intercept value, the five top performing mixtures were 12.5 FGN30, 19 CGN30, 12.5 CGN30, 12.5 GV10, and 19 CGV10. Intuitively, these mixtures were expected to provide poor rutting resistance. The slope values provided a strong association with rutting performance since the slopes of mixtures containing 30 percent natural sand were greater than the slope of any other mixture. The improvement in rutting resistance by using a polymer-modified binder was also observed, with the slope of the 19 FGN30 mixture decreasing from 1.006 to 0.613 when the polymer-modified binder was used. A ranking of mixtures according to the lowest slope value includes 12.5 CLS0, 19 CLS0, 12.5 FLS0, 12.5 FGN0, and 19 FLS0 as the top performers from mixtures with the unmodified binder.

Table 9. Static creep performance parameters

Binder	Agg. Type	Sand (%)	Mix	a	m	FT	TF
64-22	Granite	0	12.5 FGN0	0.46	0.29	104	286
			12.5 CGN0	0.50	0.39	29	80
			19 FGN0	0.47	0.35	36	101
			19 CGN0	0.50	0.39	39	109
		10	12.5 FGN10	0.38	0.41	33	89
			12.5 CGN10	0.41	0.42	32	79
			19 FGN10	0.39	0.34	57	159
			19 CGN10	0.45	0.39	40	98
		30	12.5 FGN30	0.25	1.47	4	6
			12.5 CGN30	0.30	1.16	5	9
			19 FGN30	0.54	1.01	3	7
			19 CGN30	0.27	1.32	3	6
	Gravel	0	12.5 GV0	0.39	0.47	28	70
			19 FGV0	0.41	0.39	40	111
			19 CGV0	0.46	0.43	30	71
		10	12.5 GV10	0.34	0.45	27	74
			19 FGV10	0.35	0.46	28	72
			19 CGV10	0.34	0.47	25	63
	Limestone	0	12.5 FLS0	0.51	0.29	110	302
			12.5 CLS0	0.51	0.26	125	359
			19 FLS0	0.55	0.31	90	243
			19 CLS0	0.50	0.28	130	342
		10	12.5 FLS10	0.40	0.33	69	181
			12.5 CLS10	0.40	0.40	53	132
			19 FLS10	0.37	0.31	95	218
			19 CLS10	0.40	0.36	51	134
76-22	Granite	0	12.5 FGN0	0.47	0.15	402	1,435
			12.5 CGN0	0.44	0.27	188	533
		30	19 FGN30	0.30	0.61	18	44
	Gravel	0	12.5 GV0	0.39	0.33	95	267
			19 CGV0	0.45	0.33	106	284
	Limestone	0	12.5 CLS0	0.59	0.18	545	1,534
			19 CLS0	0.67	0.17	564	1,502
		10	19 FLS10	0.46	0.20	360	938

The FT values ranged from 3 to 30, and the TF values ranged from 6 to 359 for mixtures containing neat binder. Higher values indicated greater rutting resistance. A ranking of the mixtures according to either of these values produced nearly identical results. In both cases, the mixtures with the poorest performance were those with 30 percent natural sand. The top five mixtures according to both values were 19 CLS0, 12.5 CLS0, 12.5 FLS0, 12.5 FGN0, and 19 FLS10. Either index value showed limestone mixtures to have the greatest rutting resistance. Gravel mixtures tended to have lower performance compared to other aggregate types. The 19 FGN30 mixture with polymer-modified binder had an FT value of 18 and a TF value of 44. Other FT and TF values for mixtures with polymer-modified binder ranged from 95 to 564 and from 267 to 1,534, respectively. The improvement in rutting resistance by using a polymer-modified binder was clearly observed.

Dynamic Modulus Test Results

Dynamic modulus master curves were developed as described in Chapter V by fitting the test data to Equation 13. Table 10 provides the fitting parameters for each of the mixtures included in this study.

Dynamic modulus data from three selected test conditions are presented in Table 11 along with a predicted result based on calculations from the master curves. These test data included results for tests performed at 21°C using a frequency of 25 Hz (the lowest temperature and highest frequency from this study), 37°C using a frequency of 1.0 Hz, and 54°C using a frequency of 0.1 Hz (the highest temperature and lowest frequency from this study). The stiffness value was predicted for the conditions of 64°C using a

frequency of 1.0 Hz. Rutting was more likely to occur at higher temperatures and under lower frequency loading conditions.

The condition 64°C and 1.0 Hz was determined using Equation 15. The reduced frequency was determined using Equation 14 with the fitting parameters for each mixture and a reference temperature of 21°C. Fitting parameters are given in Table 10. These test conditions were selected because 64°C was the performance grade of the neat Binder, and 1.0-Hz loading was applicable for slow-moving aircraft traffic. Calculating the dynamic modulus at the performance grade temperature allowed determination of appropriate dynamic modulus values for any climatic region. Since the objective of this study was to recommend test parameters for application across any region of the United States, the evaluation of the dynamic modulus at a temperature related to the selected binder grade was reasonable. If modified binders were selected for their superior performance, the analysis of the test parameters would still take place at the high PG base grade for a selected climate to ensure the enhanced performance of the premium binder was measured.

Table 10. Dynamic modulus master curve fitting parameters

Binder	Agg. Type	Sand (%)	Mix	α	β	δ	ϒ	a1	a2
64-22	Granite	0	12.5 FGN0	1.582	-0.884	4.118	-0.890	0.036	-7.98E-05
			12.5 CGN0	1.477	-1.128	4.156	-0.930	0.044	8.02E-06
			19 FGN0	1.511	-1.083	4.138	-0.909	0.030	-2.46E-04
			19 CGN0	1.387	-1.132	4.216	-1.008	0.039	-2.92E-05
		10	12.5 FGN10	1.415	-0.990	4.213	-0.947	0.042	-4.24E-06
			12.5 CGN10	1.502	-1.084	4.172	-0.880	0.049	8.32E-05
			19 FGN10	1.398	-1.065	4.244	-0.974	0.040	4.73E-06
			19 CGN10	1.415	-0.990	4.213	-0.947	0.042	2.12E-07
		30	12.5 FGN30	6.091	-1.530	0.168	-0.295	0.023	-2.50E-04
			12.5 CGN30	6.002	-1.808	0.089	-0.345	0.028	-2.47E-04
			19 FGN30	5.967	-1.874	0.069	-0.343	0.024	-3.34E-04
			19 CGN30	5.960	-1.926	0.055	-0.361	0.028	-2.84E-04
	Gravel	0	12.5 GV0	1.693	-1.097	4.001	-0.789	0.046	2.28E-05
			19 FGV0	1.626	-1.107	4.010	-0.799	0.044	7.00E-05
			19 CGV0	1.501	-1.164	4.101	-0.866	0.047	7.27E-05
		10	12.5 GV10	1.620	-1.203	4.010	-0.781	0.036	-8.35E-05
			19 FGV10	1.372	-1.402	4.198	-0.961	0.042	-2.29E-05
			19 CGV10	1.519	-1.420	4.085	-0.788	0.050	1.05E-04
	Limestone	0	12.5 FLS0	1.403	-0.907	4.307	-0.940	0.046	1.73E-04
			12.5 CLS0	1.283	-0.923	4.360	-1.064	0.032	-2.81E-05
			19 FLS0	1.224	-1.176	4.380	-1.075	0.045	9.13E-05
			19 CLS0	1.363	-0.839	4.328	-0.922	0.043	1.14E-04
		10	12.5 FLS10	1.229	-1.062	4.355	-1.042	0.038	-7.55E-06
			12.5 CLS10	1.348	-1.062	4.308	-0.960	0.042	7.68E-05
			19 FLS10	1.171	-1.232	4.385	-1.146	0.030	-1.30E-04
			19 CLS10	1.280	-0.868	4.318	-0.970	0.025	-1.93E-04
76-22	Granite	0	12.5 FGN0	1.454	-0.962	4.153	-0.712	0.040	4.28E-06
			12.5 CGN0	1.685	-0.718	4.017	-0.576	0.041	3.83E-05
		30	19 FGN30	2.700	-0.222	3.457	-0.351	0.028	-1.12E-05
	Gravel	0	12.5 GV0	1.733	-0.781	3.994	-0.561	0.047	9.71E-05
			19 CGV0	1.427	-0.965	4.102	-0.699	0.038	5.64E-06
	Limestone	0	12.5 CLS0	2.257	-0.595	3.822	-0.405	0.041	4.88E-05
			19 CLS0	1.385	-0.681	4.318	-0.667	0.047	1.53E-04
		10	19 FLS10	1.612	-0.672	4.169	-0.561	0.044	1.61E-04

Table 11. Selected dynamic modulus data

Binder	Agg. Type	Sand (%)	Mix	Test Data (MPa)			Predicted Result (MPa)
				25 Hz	1 Hz	0.1 Hz	1.0 Hz
				21°C	37°C	54°C	64°C
64-22	Granite	0	12.5 FGN0	2,370	508	126	110
			12.5 CGN0	2,246	509	132	118
			19 FGN0	2,149	600	128	108
			19 CGN0	2,127	542	144	130
		10	12.5 FGN10	2,160	495	130	130
			12.5 CGN10	2,421	524	134	128
			19 FGN10	2,282	566	153	144
			19 CGN10	2,160	495	130	141
		30	12.5 FGN30	2,092	550	72	29
			12.5 CGN30	2,307	576	53	18
			19 FGN30	2,162	620	59	17
			19 CGN30	2,347	604	50	14
	Gravel	0	12.5 GV0	2,275	510	103	96
			19 FGV0	2,075	528	122	106
			19 CGV0	1,996	494	118	114
		10	12.5 GV10	2,007	634	130	106
			19 FGV10	1,974	604	132	130
			19 CGV10	2,150	665	143	131
	Limestone	0	12.5 FLS0	2,621	606	198	182
			12.5 CLS0	2,467	640	209	183
			19 FLS0	2,310	613	210	188
			19 CLS0	2,526	588	208	185
		10	12.5 FLS10	2,101	603	198	177
			12.5 CLS10	2,497	624	202	174
			19 FLS10	1,966	682	203	182
			19 CLS10	2,101	603	198	162
76-22	Granite	0	12.5 FGN0	1,784	584	174	150
			12.5 CGN0	1,697	534	164	142
		30	19 FGN30	1,223	402	133	117
	Gravel	0	12.5 GV0	1,791	535	163	141
			19 CGV0	1,458	533	162	143
	Limestone	0	12.5 CLS0	2,389	744	257	193
			19 CLS0	2,006	635	252	225
		10	19 FLS10	2,042	686	251	231

The dynamic modulus at 64°C and 1.0 Hz provided a reasonable ranking of mixture rutting performance. The mixtures with the lowest values were those containing high percentages of natural sand. The next three mixtures in the performance ranking were those with gravel aggregate, which was expected to be more rut-susceptible. The eight mixtures with limestone aggregate ranked as best performers.

Similar rankings were noted for mixtures containing polymer-modified binder. The limestone mixtures performed the best, followed by granite mixtures and then gravel mixtures. The mixture containing 30 percent natural sand had the poorest performance. In all cases, the polymer-modified binder increased the dynamic modulus at the test temperature of 64°C using a frequency of 1.0 Hz. Increased stiffness at high temperatures is one primary reason that polymer-modified binders are used to improve rutting performance.

The data from other test conditions where the mixtures were stiffer did not provide a rational mixture ranking. For example, ranking the dynamic modulus data at 21°C using a frequency of 25 Hz ranked the 19 CGN30 mixture as being seventh stiffest and the 19 FLS10 mixture as being least stiff. The dynamic modulus data at 37°C using a frequency of 1 Hz ranked 19 CGV10 as being the second stiffest mixture and 19 FGN30 as being the sixth stiffest mixture. These rankings were intuitively incorrect given the mixture properties and the known influence of natural sand and aggregate type on rutting performance. The binder properties appeared to dominate the material response at lower temperatures as evidenced by the similar test values measured for all mixtures using the PG 64-22 binder. At these test conditions, the binder appeared to provide most of the

elastic response, not allowing aggregate particle interactions to have a significant effect on mixture stiffness.

APA Test Results

The APA records the average rut depth of the two specimens with each load cycle into a Microsoft Excel spreadsheet. The average rut depth was plotted versus the number of load cycles to produce a curve of accumulated rutting. Figure 27 shows the number of load cycles versus APA rut depth for all 26 mixtures using the neat binder. As previously stated, the test was ceased after one of the two specimens reached the terminal rut depth of 12 mm. The values shown in Figure 27 were the average rut depth of the two specimens. The mixture designation was not included on this figure because of the large number of data sets. Data from Figure 27 were extracted in subsequent figures with mixture designations included for analysis.

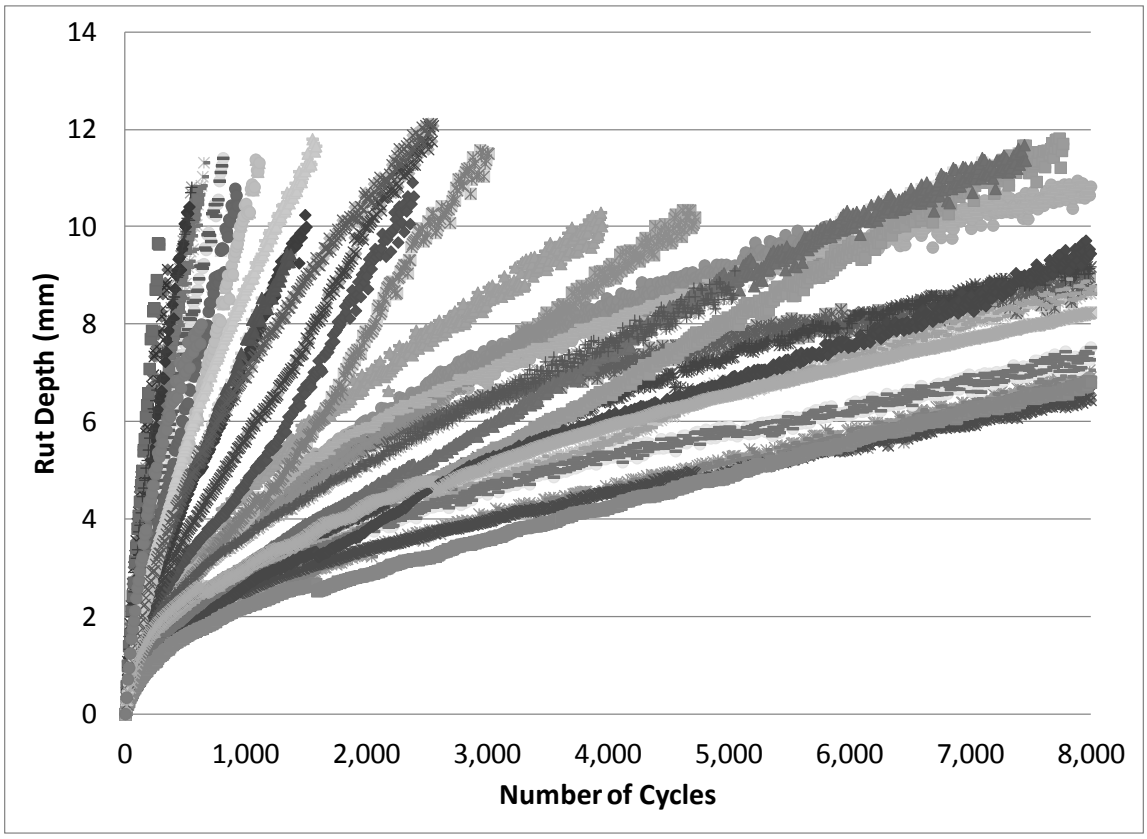

Figure 27. APA results for all mixtures

During APA testing, a more rapid rutting rate took place during the initial load cycles. After about 1 mm of rut development, specimen behavior was observed to be more closely linked to mixture characteristics as evidenced by variable rates of rut depth accumulation. Some mixtures had a slow rate of rut depth accumulation while others failed very quickly. The rutting rate appeared to become somewhat linear after approximately two mm of rutting. The rutting behavior in the APA followed the same general pattern as commonly observed in static creep and repeated load experiments with a primary and secondary flow. Tertiary flow was not observed during the experiments.

Although mixture designations were not shown in Figure 27, analysis of the data indicated general trends in the mixture variables that impacted the rate of rut depth accumulation. These mixture variables were investigated in the following paragraphs.

An analysis was conducted to determine the effect of natural sand on the APA results. Figure 28 shows the APA results for mixtures containing no natural sand. These mixtures, as expected, were among the best performers in the APA test. Incorporating natural sand promoted rutting in HMA (Button et al. 1990; Ahlrich 1996). For mixtures containing no natural sand, rut depth accumulation was related to the aggregate type. Mixtures containing crushed chert gravel aggregate rutted much more quickly than the other mixtures. The crushed gravel met the FAA requirements for the mass percentage of aggregate particles having at least two fractured faces (70 percent for coarse aggregate). However, these aggregates also had low levels of angularity and relatively smooth textures. Interparticle friction, although not directly measured, was expected to be lower for chert gravel than for quarried aggregate. In addition, chert gravel mixtures commonly had a higher VMA than quarried aggregate mixtures; thus, more binder was required to compact mixtures to equivalent air void content.

Mixtures containing crushed limestone aggregate performed best in the APA test. In general, the crushed granite mixtures rutted more quickly than the crushed limestone mixtures. The crushed granite mixtures, on average, had higher design binder content than the crushed limestone mixtures. The differences in design binder content or binder demand were likely to be influenced by factors such as aggregate shape, texture, and breakdown during compaction or mixture VMA.

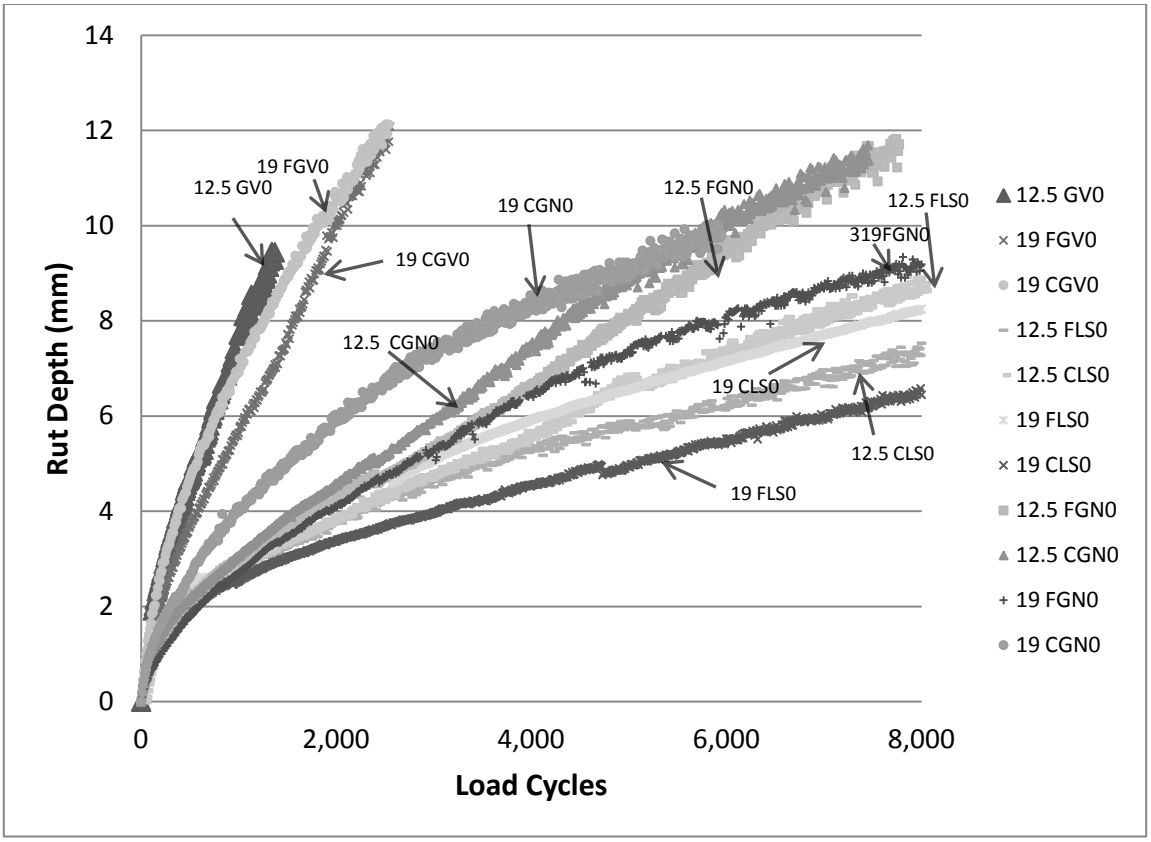

Figure 28. APA results for mixtures containing 100 percent crushed aggregate

Figure 29 shows the APA results for mixtures containing 10 percent natural sand. These mixtures rutted more quickly than those containing no natural sand. Once again, mixtures produced with crushed gravel rutted more quickly than other mixtures. Similarly, mixtures produced with crushed limestone performed best by demonstrating the greatest resistance to rutting.

Figure 30 shows the APA results for mixtures containing 30 percent natural sand. These mixtures contained a higher percentage of natural sand than is allowed by FAA specifications (maximum of 15 percent). The mixtures were included in the analysis because they were expected to rut quickly and could provide guidance for performance

threshold levels within the specifications. All mixtures containing 30 percent natural sand failed quickly in the APA.

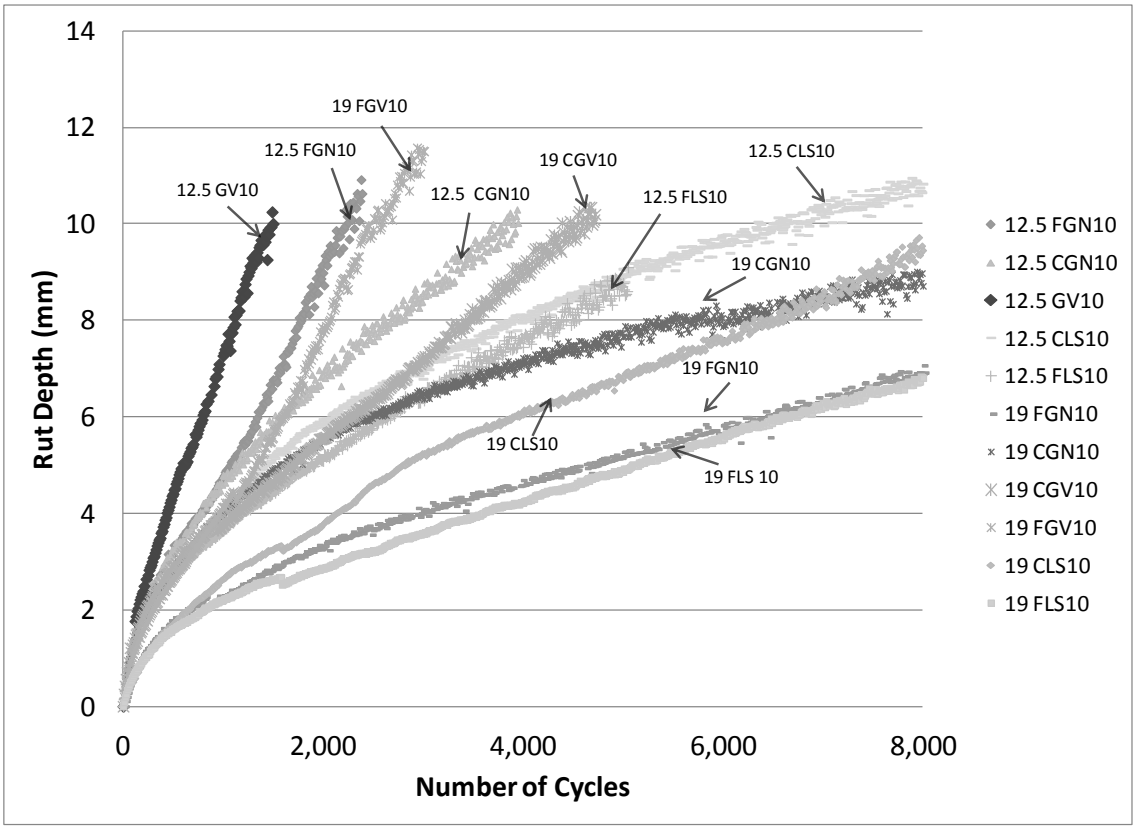

Figure 29. APA results for mixtures containing ten percent natural sand

Figure 31 shows the APA results for mixtures containing polymer-modified binder. Only the mixture containing 30 percent natural sand failed before the 8,000 cycle test duration was complete. The 19 FGN30 mixture with the polymer-modified binder reached the terminal rut depth after approximately 1,600 APA cycles compared to 800 cycles when the mixture was prepared with the neat binder. The rank order from APA testing of mixtures with polymer-modified binder was similar to results from

mixtures with neat binder, as the top three performers were the 12.5 CLS, 19 CLS, and 19 FLS10 mixtures in both cases. The two granite mixtures performed better than the two gravel mixtures. The rate of rutting of polymer-modified mixtures was approximately half the rutting rate of mixtures with neat binder.

In general, the percentage of natural sand influenced the APA test results more than any other variable. High percentages of natural sand caused premature failure in the APA. Additionally, aggregate type influenced the APA test results. Mixtures containing chert gravel rutted more quickly than mixtures with granite or limestone aggregate.

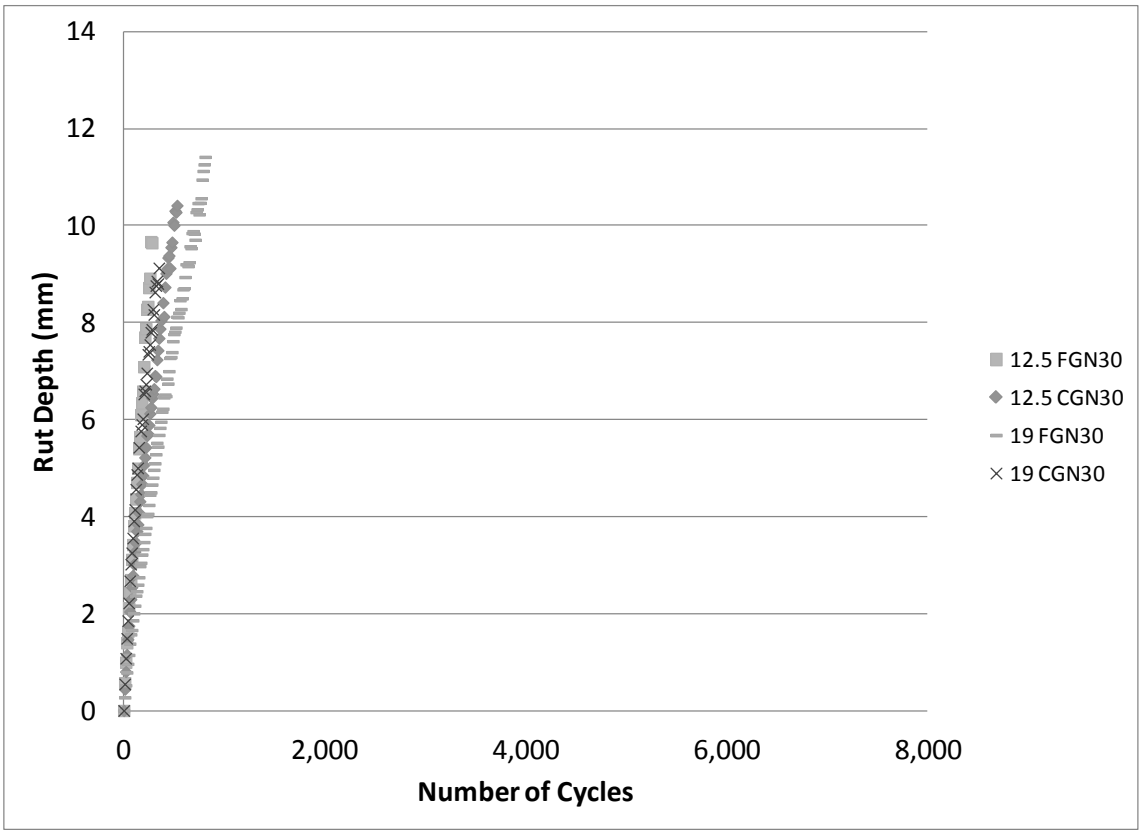

Figure 30. APA results for mixtures containing 30 percent natural sand

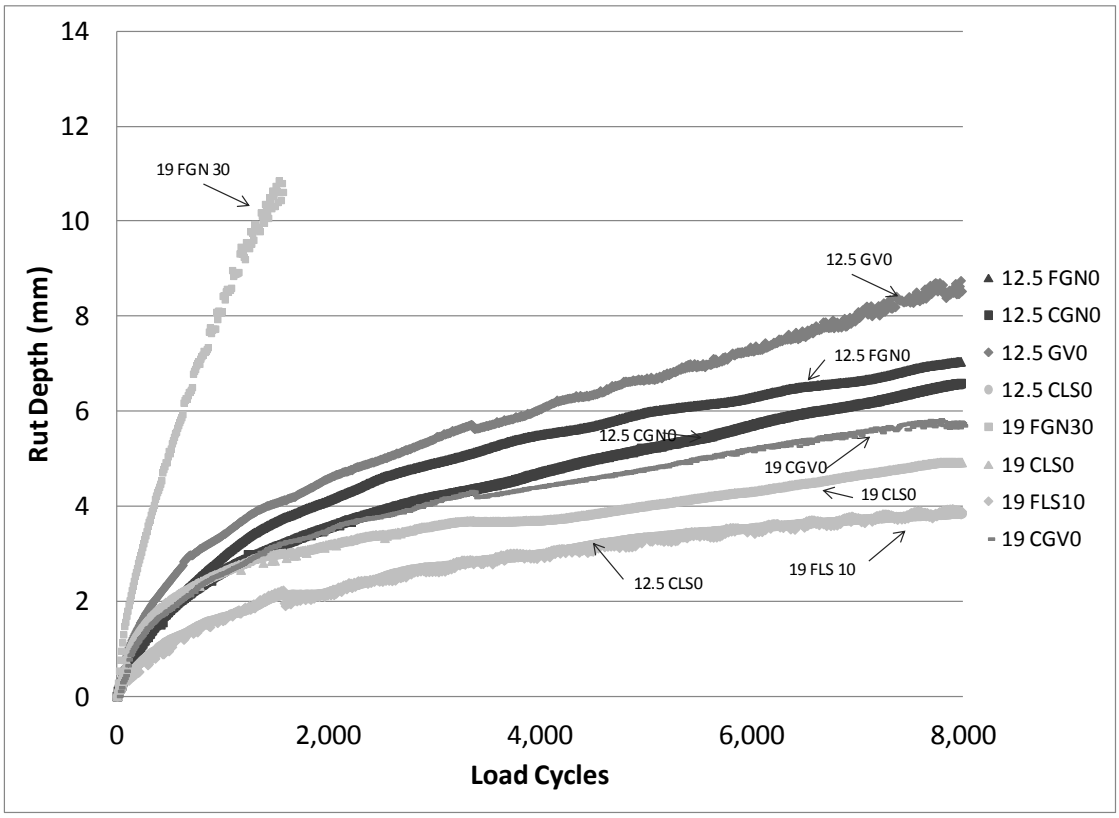

Figure 31. APA results for mixtures prepared using polymer-modified binder

Statistical Considerations

Analyses were performed to evaluate the impact of mixture variables on rutting performance considering statistical significance. All analyses were performed using SigmaStat® software at a 95 percent confidence level. The analysis of variance (ANOVA) procedure, including the Tukey test for all pairwise comparison, was used to evaluate data sets. For repeated load and static creep tests, the slope and intercept parameters along with the flow number or flow time and tertiary flow value were analyzed. For dynamic modulus test data, the value at 64°C using 1.0-Hz loading was considered. The number of load cycles to reach an average rut depth of ten mm was used

as a metric to quantify mixture behavior for APA analyses. A rut depth of ten mm was selected because it is near the maximum average rut depth reported in the APA samples. Table 12 shows the numerical values from the performance tests that were used in all analyses.

Table 12. Average test values for statistical analysis

Aggregate	Natural Sand (%)	a	b	FN	TF	a	m	FT	TF	Dynamic Modulus (MPa)	APA Cycles to 10-mm Rut Depth
Granite	0	0.306	0.412	171	403	0.484	0.357	52	144	117	6,530
	10	0.224	0.397	211	534	0.407	0.390	40	106	136	5,518
	30	0.251	0.631	21	51	0.340	1.239	4	7	20	490
Gravel	0	0.241	0.447	145	318	0.420	0.429	32	84	105	1,740
	10	0.179	0.456	164	388	0.342	0.461	27	70	122	2,850
Limestone	0	0.219	0.405	438	874	0.519	0.285	114	311	184	8,000
	10	0.222	0.413	252	592	0.392	0.351	67	180	174	7,033

The main objective of the statistical analyses was to verify the assumption that different aggregate types and different percentages of natural sand would influence mixture properties sufficiently to provide a broad range of performance to adequately assess each of the performance tests considered in this study. Grouping the test results according to the variables of aggregate type and natural sand percentage was expected to reduce the statistical power because the influence of other important properties such as gradation and mixture volumetrics was not considered. This study represented only a very small fraction of construction materials encountered throughout the United States. Analyzing broad groupings provided an objective assessment of the mixture properties to meet the purpose of this study.

The statistical analyses considered the following factors: (1) the influence of aggregate type (limestone, chert gravel or granite); (2) the influence of shape and textural factors (angularity, surface texture and flat and elongated shape factors); and (3) the impact of the presence and amount of natural sand (uncrushed). First, the influence of aggregate type was investigated. The p-values from all pairwise comparisons using Tukey's test were shown in Table 13. The values less than the 0.05 significance level are shown in bold text. These values were statistically significant.

Table 13. Statistical results from mixture comparisons

	p-value									
Comparison	**a**	**b**	**FN**	**TF**	**a**	**m**	**FT**	**TF**	**DM**	**APA**
GN0 vs. GN10	0.19	1.00	0.99	0.91	0.51	1.00	0.97	0.95	0.07	0.95
GN0 vs. GN30	0.61	**<0.001**	0.16	0.08	**0.03**	**<0.001**	**0.02**	**0.02**	**<0.001**	**<0.001**
GN0 vs. GV0	0.50	0.89	1.00	0.99	0.76	0.92	**<0.001**	**<0.001**	0.62	**0.01**
GN0 vs. LS0	0.28	1.00	**0.00**	**0.01**	0.97	0.89	0.79	0.75	**<0.001**	0.76
GN10 vs. GN30	0.98	**<0.001**	**0.04**	**0.01**	0.64	**<0.001**	0.12	0.17	**<0.001**	**0.00**
GN10 vs. GV10	0.84	0.45	0.99	0.90	0.75	0.92	0.95	0.97	0.42	0.23
GN10 vs LS10	1.00	1.00	0.99	1.00	1.00	0.99	0.41	0.47	**<0.001**	0.74
GV0 vs GV10	0.63	1.00	1.00	1.00	0.65	1.00	1.00	1.00	0.25	0.96
GV0 vs. LS0	1.00	0.78	**0.00**	**0.00**	0.30	0.34	**<0.001**	**<0.001**	**<0.001**	**<0.001**
GV10 vs LS10	0.90	0.75	0.78	0.67	0.91	0.63	0.11	0.15	**<0.001**	**0.02**
LS0 vs. LS10	1.00	1.00	**0.05**	0.24	0.07	0.93	**0.03**	**0.03**	0.62	0.96

The repeated load test data showed no statistical difference in aggregate type for the slope or intercept parameters. Both the FN and TF average values for mixtures with limestone aggregate were statistically different from the mixtures with granite or chert

gravel. There was no statistical difference between mixtures with granite and chert gravel.

The static creep test data showed the same results as the repeated load data. The slope and intercept values indicated no statistical difference among any of the three aggregate types. The limestone aggregate mixtures had statistically different FN and TF values from the mixtures with granite or chert gravel aggregate, while the granite and chert gravel mixtures were not different from each other.

The average dynamic modulus of granite, limestone, and chert gravel mixtures at 64°C and 1.0 Hz was 117, 184, and 105 MPa, respectively. The dynamic modulus data indicated the stiffness of mixtures with limestone aggregate was statistically different from that of mixtures containing granite or chert gravel aggregate. The dynamic modulus of granite aggregate mixtures was not statistically different than from chert gravel mixtures.

Granite, limestone, and chert gravel mixtures containing no natural sand required statistically different numbers of load cycles to reach 10 mm of rutting in the APA. The average number of load cycles required to reach 10-mm rutting for these respective mixtures was 6,530; 8,000; and 1,740. It is important to note that the value of 8,000 cycles was the terminal test value and no data were extrapolated.

Further analyses on the influence of aggregate type on rutting were performed on the AIMS data. The indices of shape and angularity were investigated and considered to be the aggregate characteristics most closely related to rutting in HMA. Aggregate angularity was measured for three sizes of coarse aggregate and three sizes of fine

aggregate for each aggregate type using AIMS. Coarse and fine aggregate were compared independently using ANOVA. Angularity was not found to be statistically different among the three size fractions within a specific aggregate type. The difference between the coarse aggregate fraction of limestone and chert gravel aggregates was not statistically significant. For each coarse size fraction, the granite aggregate was more angular than limestone. Granite was statistically more angular than chert gravel aggregate on 12.5-mm and No. 4 sieve sizes, but not the 9.5-mm sieve. Similarly, no statistically significant difference in angularity was detected between limestone and chert gravel fine aggregate. All size fractions of fine granite aggregate were statistically more angular than all size fractions of limestone or chert gravel aggregate.

Aggregate texture was only measured on coarse aggregate by AIMS. Statistical analyses of AIMS texture data indicate all sizes of chert gravel have a statistically lower texture index than any size fraction of limestone or granite aggregate. For all equal size fractions, granite aggregate has a higher texture than limestone aggregate.

In summary, the AIMS data ranked the aggregates the same by both angularity and texture, with granite having the highest indices and chert gravel having the lowest indices, although the angularity of limestone and chert gravel are very similar. Higher angularity and texture indices are expected to result in greater rutting resistance. On this basis, the degree of angularity and texture are consistent in terms of identifying chert gravel mixtures as the most rut susceptible, but inconsistent in predicting granite as the most rut resistant mixtures. Performance test data indicate aggregate texture may be a better indicator of rutting resistance than angularity. The lower resistance of the granite

mixtures to rutting compared to limestone mixtures likely results from higher design binder contents. Higher rut resistance resulted from increased aggregate texture and lower binder content.

The addition of neither ten nor 30 percent natural sand to the mixtures impacted the rank order of rutting sensitivity among the three aggregate types for any of the performance tests. The trend of performance for each test was the same for mixtures containing no natural sand as for mixtures containing 10 percent natural sand. Limestone mixtures performed best while chert gravel mixtures performed worst. However, the repeated load and creep tests did not show significant difference among any aggregate types. Further, only limestone and chert gravel were statistically different from each other according to Dynamic Modulus and APA tests.

The effect of the percentage of natural sand contained in the mixtures on the rutting performance was analyzed independently. Adding 10 percent natural sand had no statistically significant impact on the dynamic modulus or the number of APA load cycles to reach 10-mm rut depth for any aggregate type compared to the results of mixtures with no natural sand. The FN from the repeated load test and the FT and TF from creep tests show that the limestone aggregate's performance was statistically different with the addition of 10 percent natural sand.

Granite mixtures containing 30 percent natural sand were statistically different from mixtures containing either no natural sand or 10 percent natural sand according to the slope of the repeated load and creep test data, the dynamic modulus, and APA load cycles to 10-mm rutting. These mixtures were statistically different only from granite

mixtures with 10 percent natural sand according to FN and TF values from the repeated load test, and different only from granite mixtures with no natural sand according to FT and TF values from the creep test.

CHAPTER VII

PERFORMANCE TEST ASSESSMENT

Ultimately, the rutting threshold established for the selected performance test must be correlated to field results. However, in the interim it is important to establish a viable and realistic threshold acceptance rutting relationship between a performance test parameter and rut depth. In order to do this, the following factors were considered: (1) the number of applied aircraft loading relative to highway truck loading, (2) the tire pressure of airfield traffic relative to highway truck traffic, and (3) results of the mixtures that were tested in this study and the historical performance of these mixtures in airfield situations. Recommended threshold values for each performance test are given in Table 14 and discussed in the following paragraphs.

Table 14. Potential performance test acceptance threshold values

Repeated Load	**Static Creep**	**Dynamic Modulus**	**APA**
Maximum slope of 0.45 when data is plotted on a log-log scale or Minimum Flow Number (FN) of 200	Maximum slope of 0.45 when data is plotted on a log-log scale or Minimum Flow Time (FT) of 30 s	Minimum of 124 MPa dynamic modulus at PG high temp grade and 1.0-Hz loading	Less than 10-mm rutting after 4,000 APA cycles using 1113-N load and 1724-kPa pressure

Rushing (2012) recommended a maximum of 10-mm rutting after 4,000 APA cycles as an interim threshold value for accepting mixtures when testing them with the APA. This value was based on an analysis of rutting accumulation for the 34 mixtures from this study. The rutting accumulation was relatively linear after about 2 mm of rutting,

and the 10-mm criterion allowed significant damage to occur to delineate poorly-performing mixtures from well-performing mixtures. The recommended threshold value would eliminate those mixtures seemingly prone to rutting and was reasonable based on a review of available agency specifications for testing mixtures with the APA. This criterion rejects all mixtures containing 30 percent natural sand as well as mixtures 12.5 GV0, 19 FGV0, 19 CGV0, 12.5 GV10, 12.5 FGN10, 19 FGV10, and 12.5 CGN10.

A similar approach was considered for identifying threshold values for the other performance tests considered in this study. The intercept values from the repeated load and static creep tests did not provide reasonable mixture rankings and were not considered. Further, since the tertiary flow values produced nearly identical rankings to flow number, FN, or flow time, FT, values, these parameters were not considered. The flow number and flow time parameters can be mathematically defined and are not as subjective at the tertiary flow values. The dynamic modulus at the high temperature performance grade for the selected climate under a 1.0-Hz load was selected for comparison.

The slope of the repeated load data on a log-log scale ranged from 0.254 to 0.712. The maximum slope for mixtures meeting current FAA requirements was 0.490 for the 19 CGV10 mixture. Other mixtures with higher slopes were those containing 30 percent natural sand. The slope of the data for the mixture with 30 percent natural sand using a polymer-modified binder was 0.495.

An acceptance criterion for repeated load slope values should eliminate those mixtures with excessive natural sand, even when a premium binder is used. This

criterion should also reject mixtures that meet volumetric requirements but may be susceptible to rutting. For these reasons, a maximum slope value of 0.45 is recommended. This criterion would eliminate all mixtures with 30 percent natural sand along with mixtures 19 FGV0 and 19 CGV10.

An alternative criterion for repeated load data would contain a minimum value for FN. For these mixtures, FN ranged from 15 to 2,017. The minimum FN for mixtures meeting current FAA criteria was 87 for the 12.5 CGN0 mixture. Mixtures containing 30 percent natural sand with the neat binder had FN values ranging from 15 to 28. The mixture with 30 percent natural sand using a polymer-modified binder had a FN of 172. A potential criterion that would eliminate mixtures potentially susceptible to rutting is a minimum allowable FN of 200. This criterion would eliminate all mixtures with 30 percent natural sand. It would also eliminate mixtures 12.5 CGN0, 19 FGN0, 19 CGN, 12.5 FGN10, 12.5 GV0, 19 FGV0, 19 CGV0, 12.5 GV10, 19 FGV10, 19 CGV10, and 19 CLS10.

The FN criterion is much more exclusive than the criterion based on the slope of the data. The FN is influenced by the primary flow region when rapid permanent deformation occurs, while the slope value is primarily governed by the secondary flow region. Further, the variability of FN values is greater than that of slope values.

The slope of the static creep data on a log-log scale ranged from 0.153 to 1.469. The maximum slope for mixtures meeting current FAA requirements was 0.474 for the 19 CGV10 mixture. Other mixtures with higher slopes were those containing 30 percent

natural sand. The slope of the data for the mixture with 30 percent natural sand using a polymer-modified binder was 0.613.

An acceptance criterion for static creep slope values should eliminate those mixtures with excessive natural sand, even when a premium binder is used. This criterion should also reject mixtures that meet volumetric requirements but may be susceptible to rutting. For these reasons, a criterion of a maximum slope value of 0.45 is recommended. This criterion would eliminate all mixtures with 30 percent natural sand along with mixtures 12.5 GV0, 19 FGV10 and 19 CGV10.

An alternative criterion for static creep data would contain a minimum value for the FT. For these mixtures, the FT ranged from 3 to 564. The minimum FT for mixtures meeting current FAA criteria was 25 for the 19 CGV10 mixture. The mixture with 30 percent natural sand using a polymer-modified binder had a FT of 18. A reasonable criterion would have a minimum allowable FT of 30. This criterion would eliminate all mixtures with excessive natural sand. It would also eliminate mixtures 12.5 CGN0, 12.5 GV0, 12.5 GV10, 19 FGV10, and 19 CGV10.

This criterion is slightly more exclusive than the criterion based on the slope of the data. The FT is influenced by the primary flow region when rapid permanent deformation occurs, while the slope value is primarily governed by the secondary flow region. Also, the FT value is more variable than the slope value.

Dynamic modulus master curves were used to predict responses at the high performance grade binder temperature of 64°C using a 1.0-Hz load. An acceptance criterion for dynamic modulus data should require a minimum stiffness. Criterion that

uses the high performance grade temperature for a given climate allows for a singular stiffness threshold for any binder.

The predicted dynamic modulus at the selected conditions ranged from 14 to 188 MPa. The dynamic modulus of the mixtures containing 30 percent natural sand with the neat binder ranged from 14 to 29 MPa. An acceptance criterion should exclude these mixtures. The next lowest dynamic modulus value was 96 MPa for the 12.5 GV0 mixture. The 19 FGN30 mixture with the polymer-modified binder had a predicted dynamic modulus value of 117 MPa at these conditions. An acceptance criterion of a minimum dynamic modulus of 124 MPa when tested at the required performance grade temperature for the climate and using a 1.0-Hz load would reject all mixtures containing excessive natural sand. This criterion would also reject mixtures 12.5 GV0, 12.5 GV10, 19 FGV0, 19 FGN0, 12.5 FGN0, 19 CGV0, and 12.5 CGN0.

CHAPTER VIII

FULL-SCALE ACCELERATED PAVEMENT TESTING

Data from full-scale field-tests from ongoing research studies were used to evaluate the proposed laboratory performance test criteria. The first study, Field Trial 1, applied high tire pressure (2,241 kPa) and wheel load (142 kN) military fighter aircraft traffic to an HMA surface at 43°C. The second study, Field Trial 2, applied heavy cargo aircraft traffic (980 kPa tire pressure and 200 kN wheel load) to an HMA surface at ambient temperature (25°C). Rutting performance under these two conditions was used to assess the preliminary threshold values for the mixture design performance tests. The first study represents severe loading conditions that promote rutting (high tire pressure and elevated temperature). The second study represents moderate loading conditions where rutting is less likely to occur.

Materials

Foundation soil materials

For both Field Trial 1 and Field Trial 2, the subgrade consisted of a clay material classified as high-plasticity clay (CH) by the Unified Soil Classification System (USCS) described in ASTM D 2487. This material was procured from a local source in Vicksburg, Mississippi, and was selected for its ability to retain its moisture condition over long periods of time. Field Trial 1 also had a clay-gravel sub-base material procured from a local source in Vicksburg, Mississippi, and its USCS classification was clayey sand (SC) with gravel. Both pavement sections incorporated a limestone base course

material classified as gravel with silt and sand (GP-GM). This material was stockpiled at a local facility, but it was previously transported by barge to Vicksburg from its source in western Kentucky.

Asphalt concrete

Both field studies incorporated an HMA pavement surface layer comprised of the same HMA mixture, which was expected to be somewhat susceptible to rutting because the aggregate contained significant quantities of chert gravel and natural sand. Only 60 percent of the aggregate by mass was comprised of a quarried aggregate with more rut resistant physical properties, i.e., higher levels of angularity and texture.

An aggregate blend was designed to meet Job Mix Formula (JMF) gradation requirements for a 12.5-mm nominal maximum aggregate size mixture according to FAA Advisory Circular 150/5370 10 E. The blend consisted of 25 percent crushed gravel, 60 percent limestone, and 15 percent natural sand (maximum allowed by FAA specification). The aggregate sources and blend were selected based on materials available for plant production. The fine aggregate angularity value for this blend was 42.6 percent. Although fine aggregate angularity was not a test requirement for the specification, values below 45.0 percent are considered to indicate increased propensity for rutting. Gradation and aggregate properties for the JMF aggregate blend are provided in Figure 32.

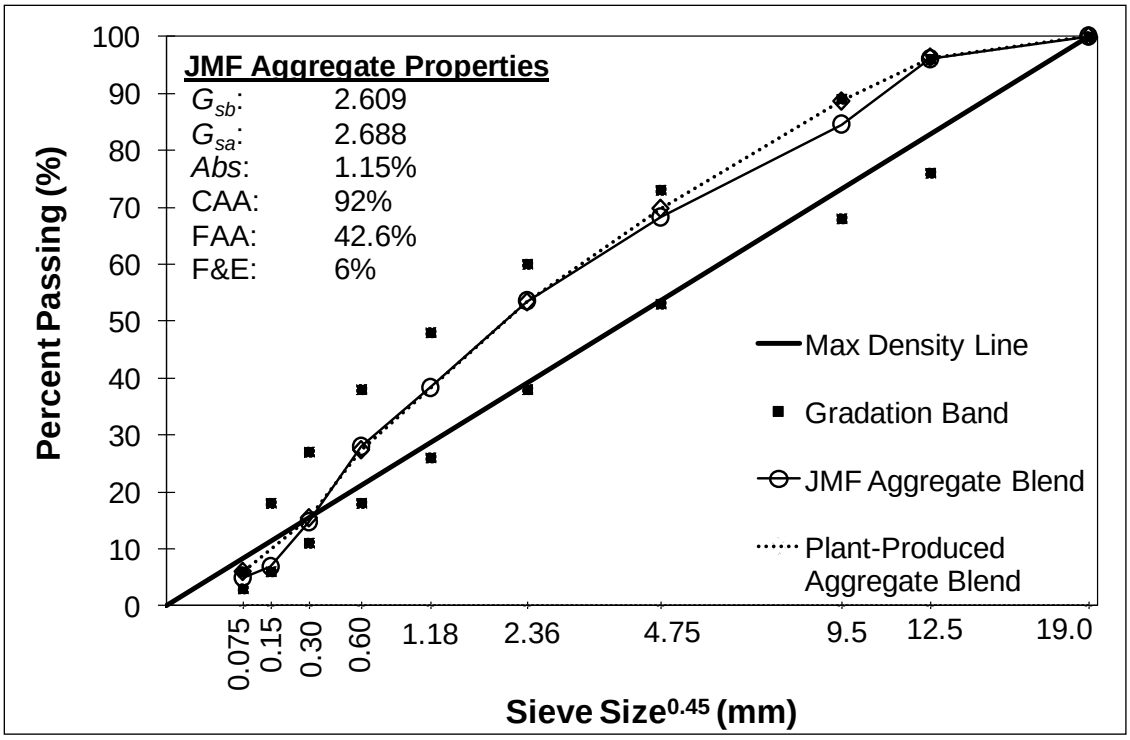

Figure 32. Properties of JMF aggregate blend.

The binder used for this project was an unmodified PG 64-22. Asphalt mixtures were designed using 75 gyrations in the SGC to achieve 4.0 percent air void content. The design compaction effort (75) was selected from military airfield construction specifications and is expected to result in a binder content nearly identical to that selected using the FAA draft design compaction effort of 70 gyrations. Theoretical maximum specific gravity (G_{mm}) of each mixture was determined on duplicate specimens according to AASHTO T 209, and the average value was reported. Bulk specific gravity (G_{mb}) of compacted cylindrical specimens was determined according to AASHTO T 331 and used to determine specimen air voids (V_a). For this mixture, the design binder content was 5.3 percent.

After the volumetric design was complete, test specimens were prepared with the HMA mixture for performance testing using all four potential test methods. Results from these tests compared against preliminary criteria are given in Table 15. The HMA mixture used for field-testing performed almost exactly at the minimum threshold criteria for each test method. Any mixture with poorer rutting resistance potential should fail to meet these criteria. Evaluating this mixture in the field study provided an indication of how well the criteria protected against using unsuitable mixtures in terms of rutting performance. All four test methods assessed the mixture as being borderline acceptable.

Table 15. Recommended performance test criteria

		Recommended Criterion	**Test Result**
APA	Rut depth after 4,000 cycles	<10 mm	10.5 mm
Dynamic Modulus	Dynamic modulus at 60°C, 1.0 Hz	>124 MPa	123 MPa
Creep	Slope on log-log scale	<0.45	0.44
	Flow time	>30	34
Repeated Load	Slope on log-log scale	<0.45	0.45
	Flow number	>200 FN	199

Field-Test Section Construction

Pavement structures for the tests were constructed under shelter in ERDC's Hangar 4 test facility. The subgrade was constructed by excavating a test pit to a minimum 1.2-m depth below the existing finished grade. The soil at the bottom of the excavation was a low plasticity silt material (ML) having a CBR less than 20 percent. The existing ML

material was leveled with a bulldozer and compacted with a pneumatic tire roller and a vibratory compactor to ensure that the remainder of the test section was constructed over a stable foundation. The bottom and sides of the test pit were lined with impervious 6-mil polyethylene sheeting to minimize moisture migration from the new soil serving as the test section subgrade.

The CH was processed at a nearby preparatory site to achieve a uniform distribution of moisture throughout the material. Once the CH had been processed to the target moisture content, the material was spread by a bulldozer in 200-mm lifts and compacted with a pneumatic-tired roller to a target depth of 150 mm. A rotary tiller was used to scarify the surface between lifts to ensure good bond. Final grade was established using a motor grader. The surface was rolled smooth using a steel-wheel roller.

For Field Trial 1, the sub-base soil was constructed over the compacted subgrade in two, 150-mm lifts. The soil was processed at a nearby preparatory site using a rotary tiller to adjust the moisture content to the desired percentage. The processed material was spread by a bulldozer in 200-mm lifts and compacted with a pneumatic-tired roller to a target depth of 150 mm. A motor grader was used to achieve proper grade. The surface was rolled smooth using a steel-wheel roller.

The base course soil was constructed in two lifts. The stockpiled material was spread by a bulldozer, and a motor grader was used to achieve proper grade. The material was compacted with a pneumatic-tired roller and then rolled smooth using a steel-wheel roller.

The asphalt was produced by APAC Mississippi, Inc. from a local drum mix plant in Vicksburg, Mississippi, and delivered to the construction site. Approximately 14,000 kg of the HMA was wasted from the beginning of the production run for each mixture to ensure the plant was producing a uniform material. The asphalt mixture was delivered to the laydown site within an hour of mixing; no material was stored in the silo for an extended period of time. Aggregate samples were collected from the feed belts at the plant to verify properties. Samples of the mixtures were collected from elevated platforms at the plant to verify that the mixture design had been achieved.

The asphalt concrete pavement layers were constructed on the prepared base course using conventional paving equipment in two 50-mm lifts. Paving was accomplished using at Caterpillar AP655D asphalt paver (Figure 33). Breakdown rolling was performed using a Caterpillar CB-534D XW vibratory steel-wheel asphalt compactor. An Ingersol Rand PT125R pneumatic roller was used for intermediate rolling. The steel-wheel roller with no vibration was used for finish rolling. A CRS-2 asphalt emulsion tack coat was applied between lifts.

Cores were extracted from the asphalt concrete pavement sections to determine the in-situ volumetric properties. The average values for ten cores taken from each test item are reported. The theoretical maximum specific gravity, G_{mm}, and percent binder, P_b, values were determined from QA lab testing. The G_{mb} was measured according to AASHTO T 166.

Figure 33. Paving test section in covered test facility

Simulated Aircraft Traffic

Each test item was trafficked in a bi-directional, normally distributed traffic pattern using a heavy vehicle simulator (HVS-A model). The HVS-A is a fully automated machine that simulates accelerated aircraft traffic on pavement test sections while allowing control of the pavement temperature with an integrated climate control system (Figure 34).

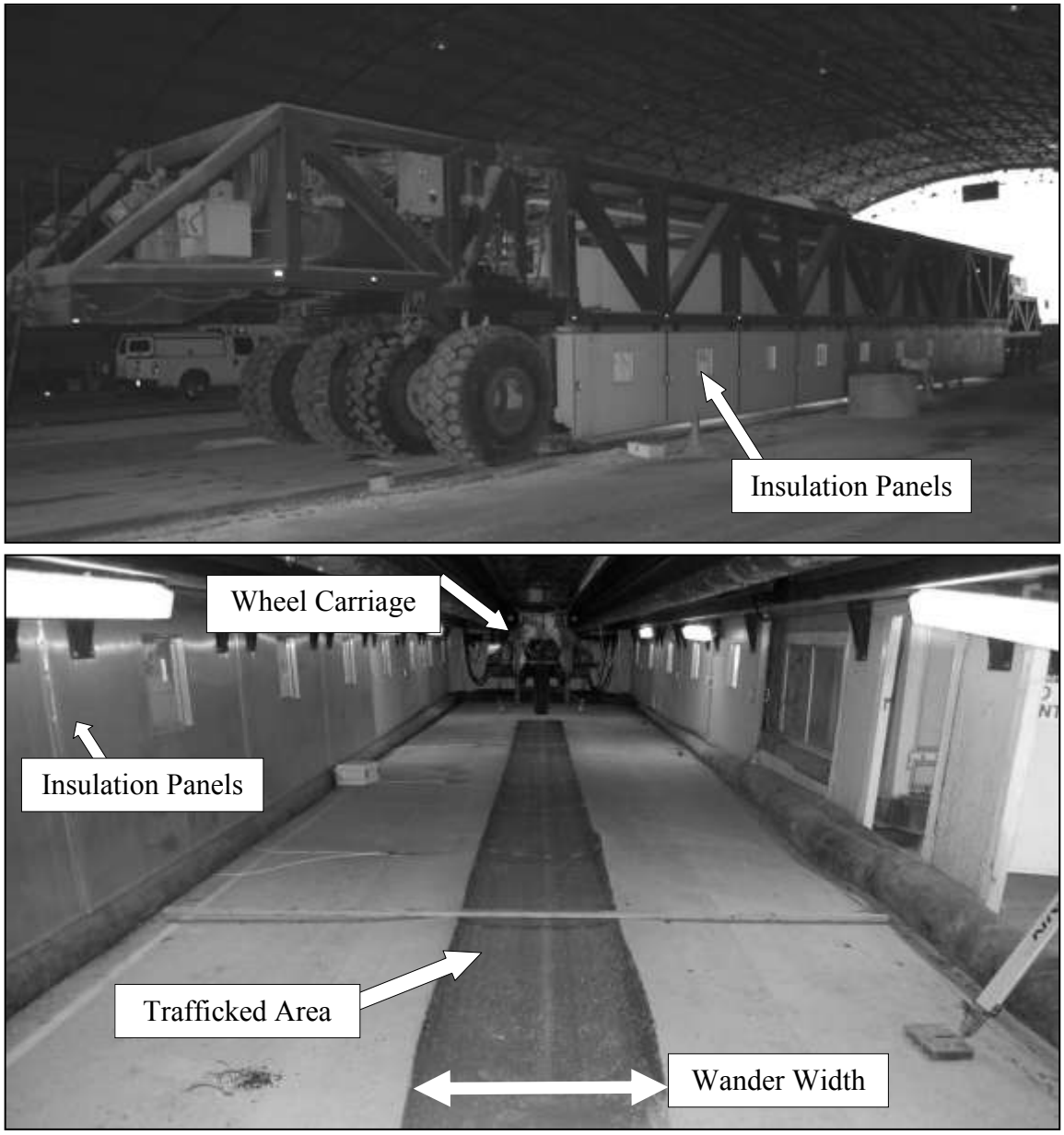

Figure 34. Overview and inside view of the HVS-A.

The wheel carriage travels forward and backward at a speed of approximately 7-km/hr over a 12-m traffic span length. The HVS has the capacity to apply up to 444-kN vertical loads. For Field Trial 1, the pavement was trafficked with a single

F-15E wheel loaded to approximately 142 kN with 2241-kPa tire pressure. The pavement for Field Trial 2 was trafficked with a single C-17 wheel loaded to approximately 200 kN with 980-kPa tire pressure. These conditions represented the normal range of loads that are expected in the field. Prior to testing, an externally calibrated aircraft scale was used to calibrate the hydraulically actuated wheel loading system of the HVS-A. During testing, the wheel load was monitored by the HVS-A's onboard control system. Prior to each day's testing, the tire inflation pressure was checked using a tire pressure gauge and adjusted if necessary. Figure 35 shows the loaded F-15E wheel. Figure 36 shows the loaded C-17 wheel.

Figure 35. Loaded F-15E wheel

Figure 36. Loaded C-17 wheel

A pass is defined as one movement of the aircraft wheel down the length of the test section. A normally distributed traffic wander pattern was used for this testing by programming a defined pass pattern into the HVS-A control system. The wander width for this traffic pattern was 0.81 m for Field Trial 1 and 1.22 m for Field Trial 2. Traffic was applied in accordance with the testing schedule provided in Table 16.

Table 16. Traffic operations sequence

Test Period (includes inactive days)	Test Item	Traffic Application Period (days)	Total Passes Applied
02/05/13 – 02/12/13	HMA Field Trial 1	6	3,326
07/03/12 – 10/24/12	HMA Field Trial 2	54	180,000

For this study, permanent deformation was defined as change in elevation of the pavement surface relative to its initial position; in other words, depth of the rut valley was considered, but uplift on the edges of the rutted areas was not. Uplift was measured as part of the survey process but was not considered as part of the failure criterion for the purposes of this study. The U.S. Department of Defense (DoD) failure criterion for flexible pavements is typically based upon 25 mm of permanent deformation. To ensure that the failure criterion was exceeded, both test items were trafficked until the average permanent deformation was approximately 30 mm.

Data Collection

The data collected at different traffic intervals included pavement and air temperature measurements and surface permanent deformation measurements at the centerline and cross-sections using a robotic total station.

Temperature monitoring

I-buttons were used as data loggers for continuously measuring and recording air and pavement temperature throughout each testing phase. Data were downloaded from all three I-buttons at each location periodically to monitor the temperatures. Prior to the application of traffic, data were downloaded to ensure that the high temperature condition was consistent throughout the asphalt pavement layer before applying any traffic. During traffic, data were downloaded to monitor any changes in the pavement temperature. After traffic, the full set of data was downloaded for analysis.

Centerline and cross-section profiles

A robotic total station established surveyed centerline and cross section profiles after selected traffic intervals (Figure 37) to aid in the calculation of the surface elevation change Measurements on the centerline were collected at 0.3-m intervals, while the cross-section profile measurements were collected in 0.3-m intervals outside of the traffic area and 0.15-m intervals in the center 1.3 m of the traffic lane. The results were used to illustrate the permanent surface deformation with increasing traffic applications.

Figure 37. Cross-section readings with robotic total station

Field Trial 1

Generally speaking, moderately loaded aircraft with high tire pressures and relatively small footprints (e.g., fighter aircraft) produce higher stresses near the top of a pavement structure, while heavily loaded aircraft with moderate tire pressures and larger footprints

(e.g., cargo aircraft) produce higher stresses in the lower portions of the structure. Hence, a high-tire-pressure aircraft is more likely to cause rutting as a result of shear stress in materials near the pavement surface.

For a properly proportioned asphalt mixture and properly constructed pavement, temperature is arguably the most important factor contributing to rutting performance. The higher the temperature a flexible pavement is exposed to, the greater the propensity for rutting. If temperature can be controlled, using a single test temperature is efficient as it greatly reduces testing time as well as the analytical efforts in the mixture evaluation process. The presence of a single test temperature at which asphalt mixtures can be evaluated has been termed the ―effective temperature" by Witczak (1992). Effective temperature has been defined as a single test temperature at which an amount of a given type of distress, within a given pavement system, would be equivalent to that which would occur from the seasonal temperature fluctuation throughout the annual temperature cycle (Witczak and Moulthrop, 2011). For Field Trial 1, a test temperature of 43ºC was selected as it is the Witczak effective test temperature for Vicksburg, Mississippi.

The flexible pavement structure for Field Trial 1 was designed to withstand over 100,000 passes of a fully loaded F-15E fighter jet aircraft (approximately 142-kN wheel load and 2,241-KPa tire pressure) without failure according to DoD criteria (UFC 3-260-02). Failure for this analysis was defined as 25 mm of rutting in the subgrade or subbase. The design procedure did not consider distresses developed in the asphalt surface layer. The resulting pavement structure (Figure 38) consisted of 100 mm of

asphalt concrete over 250 mm of limestone base course with a California Bearing Ratio (CBR) of 100, over a 300-mm-thick clay-gravel sub-base course with a CBR of 30. The subgrade was high plasticity clay and had an average CBR of 15. The test item was 15.2 m long and 3.7 m wide.

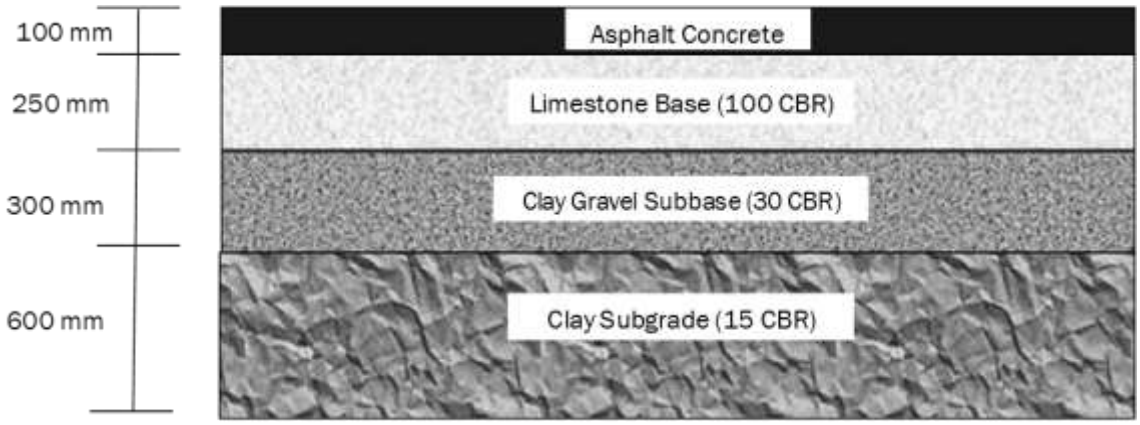

Figure 38. Pavement structure of Field Trial 1

The average volumetric properties of the asphalt layer were determined from ten 100-mm-thick cores. The average air void content of 3.8 percent was slightly below the target range of 4.0 to 6.0 percent for DoD specifications. The average VMA, VFA, and binder content were 14.3 percent, 73 percent and 5.3 percent, respectively. Simulated traffic was applied using the HVS-A. Insulated panels encapsulated the traffic area, and a heating unit provided a constant test temperature of 43°C during traffic. A total of 3,326 traffic passes were applied over a period of six days.

Temperature measurements

I-buttons were installed on the asphalt layer to continuously measure temperature. They were installed at three locations (north, center and south) on each test item and at three different depths in the asphalt layer (near the surface or top, mid depth and at the bottom). I-buttons were also used to monitor the air temperature inside the chamber (one on the north end and one on the south end) and also the outside temperature. These average temperatures were calculated using only the data that were collected when traffic was applied to the pavement. Figure 39 presents the average temperatures at the three locations as measured at the top, mid-depth, and bottom of the asphalt layer on the test item. Average air temperatures measured at the north and south ends of the test items are also included in the figures for comparison.

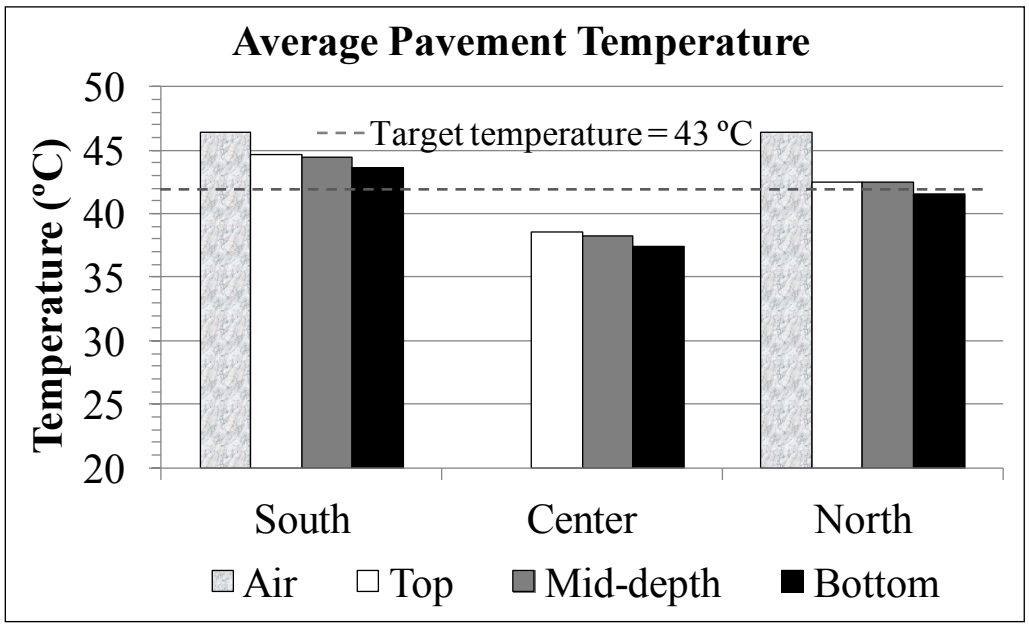

Figure 39. Average pavement temperatures as measured at the top, middle, and bottom of the asphalt layer during traffic

The target pavement temperature for this study was 43ºC, indicated by a dashed line in the figures. An almost linear temperature gradient was observed in most cases going from a higher temperature at the top of the asphalt layer to a lower temperature at the bottom. The inside air temperature varied slightly from the north end to the south. This slight difference was reflected in an average difference in pavement temperatures between the north and south ends of 2ºC.

A temperature variation within the test item is observed in Figure 39. Higher temperatures were observed at both ends of the test items compared to the center. The south end was generally the hottest area. During testing, it was noted that more hot air was coming out the heating vent 5 m from the south end than from the other vents. The hot air was introduced to the pavement through four vents: two were located in the south end of the HVS and the other two in the north end. There were no vents at the center of the HVS; furthermore, the vents were not symmetrically located in relation to the traffic area. A slightly uneven temperature distribution was noted, although the majority of the pavement was near the target value of 43ºC during testing.

An infrared camera was used to capture the surface temperature variation as shown in Figure 40. The photograph was taken from the south end of the test item. From this photograph, it is evident that the pavement temperature varied throughout the test area. The temperature difference between the warmest and coolest test areas was a little more than 5ºC.

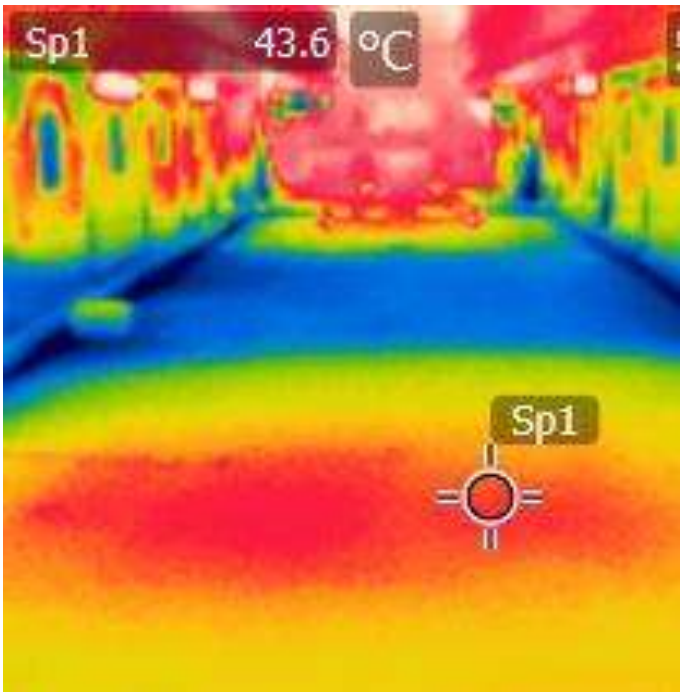

Figure 40. Typical surface temperatures as measured with infrared camera during Field-Test 1

Rutting performance

Rutting is a load-related distress caused by an accumulation of vertical compressions (Collop 1995). The presence of rutting indicates that a permanent deformation occurred in one or more of the layers of the pavement structure. This deformation occurs as a result of densification or shear flow or a combination of both. Figure 41 shows the rutting on the HMA after 3,326 passes. The HMA experienced pavement uplift along the sides of the rut and at the ends of the traffic lane (Figure 42). Upheaval typically indicates that there is shear, or an outward and upward movement of material, somewhere within the pavement structure. The pavement uplifts at the ends of the traffic lane were generated as the wheel stopped to change directions during traffic.

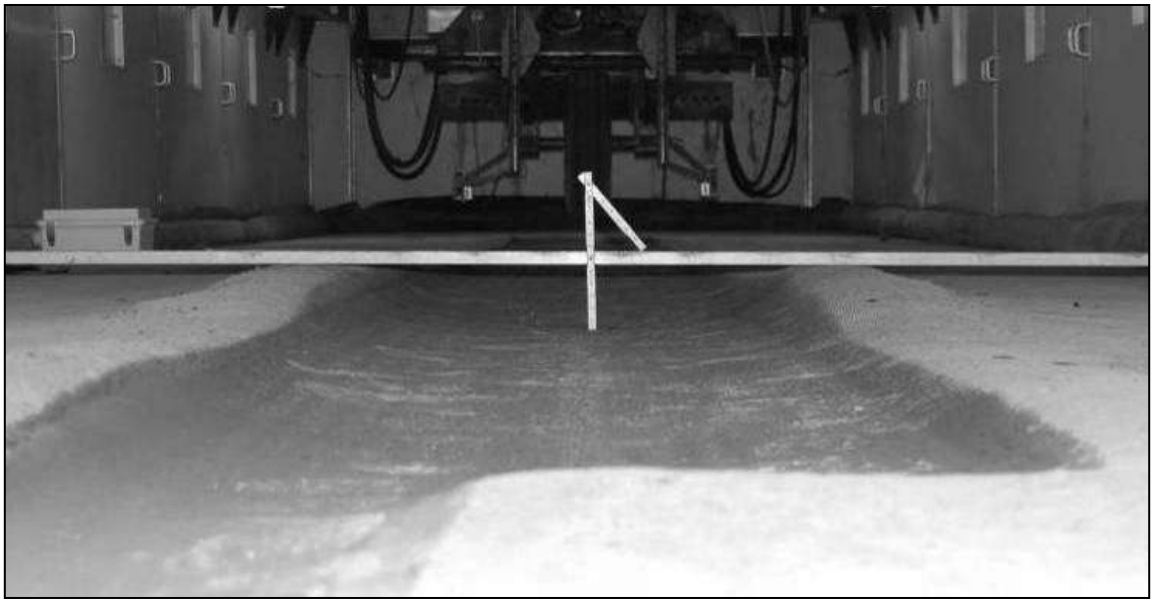

Figure 41. HMA rutting after 3,326 passes

Figure 42. Upheaval on side of the rut

Figure 43 presents the permanent deformation centerline profile. The data were normalized to zero elevation starting at 0 passes. Greater permanent deformations were observed at the locations where instrumentation for a separate study was installed. Also, a difference in permanent deformation between the south and north ends of the traffic lane was observed. The south end had greater permanent deformation than the rest of the traffic lane. This increase in permanent deformation was attributed to the higher temperature.

A cross-section showing the representative permanent deformation is presented in Figure 44. This cross-section shows the typical rutting failure that was experienced under the F-15E simulated traffic. The humps on the sides show that there was upheaval of the asphalt pavement during traffic.

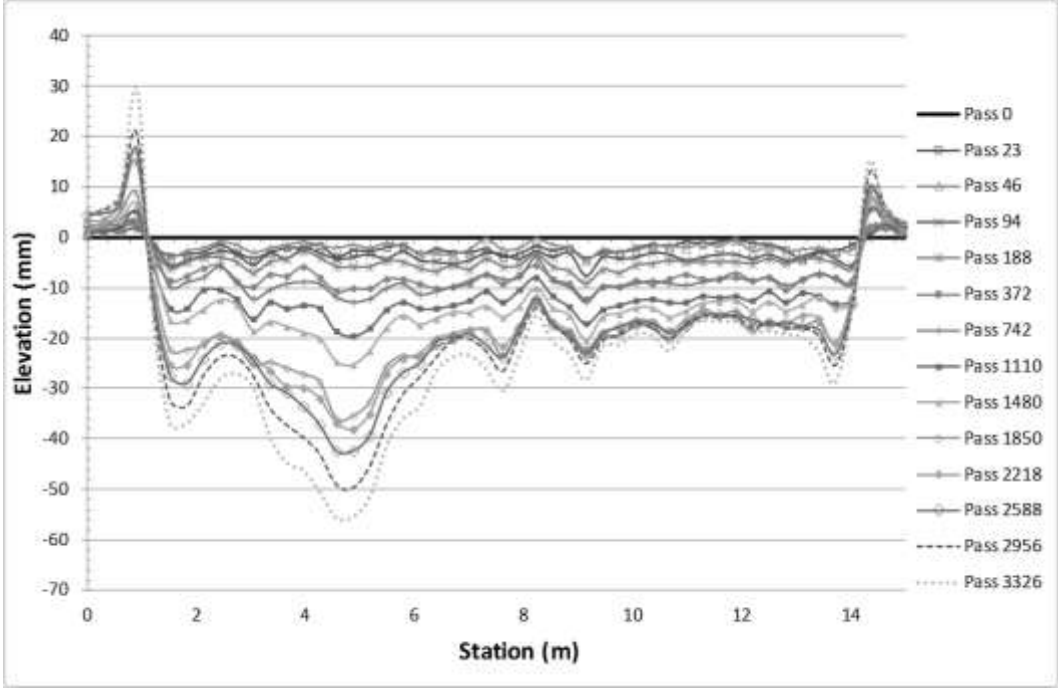

Figure 43. Field Trial 1 centerline profile

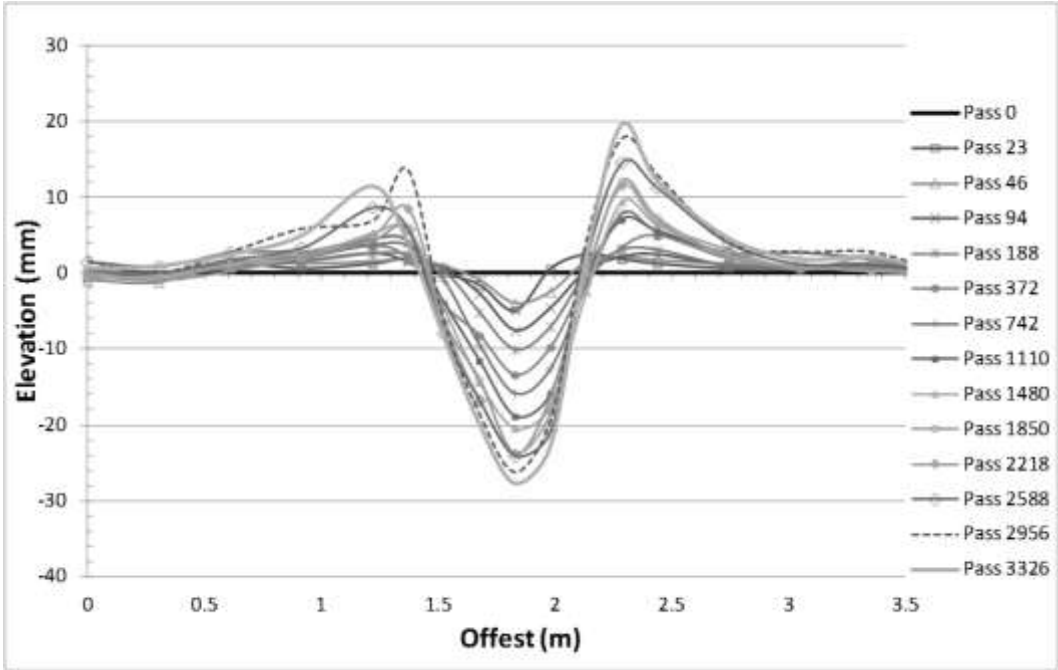

Figure 44. Field Trial 1 example cross-section profile

Forensic evaluation

The shape of the rut and the evidence of upheaval adjacent to the traffic area suggested that rutting occurred predominately in the asphalt concrete layer. A trench was dug across the pavement section after traffic was complete to verify this claim. The forensic investigation showed that rutting was mostly isolated in the asphalt concrete layer and that supporting pavement layers were not deformed (Figure 45).

Figure 45. Trench cut in Field Trial 1 pavement after traffic was complete

The final survey data collected from the trench is presented in Figure 46. These figures show the as-built (or before traffic) layer surface for reference (dotted lines). The changes in thickness observed on the subgrade and sub-base layers were negligible.

The average centerline permanent deformation as traffic progressed is shown in Figure 47. Failure was determined by interpolating the number of passes that caused 25 mm of average permanent deformation at the centerline. The HMA for Field Trial 1 failed after 2,900 passes. Even though the asphalt concrete layer rutted, underlying layers experienced minimal permanent deformation, indicating the overall pavement design was sufficient.

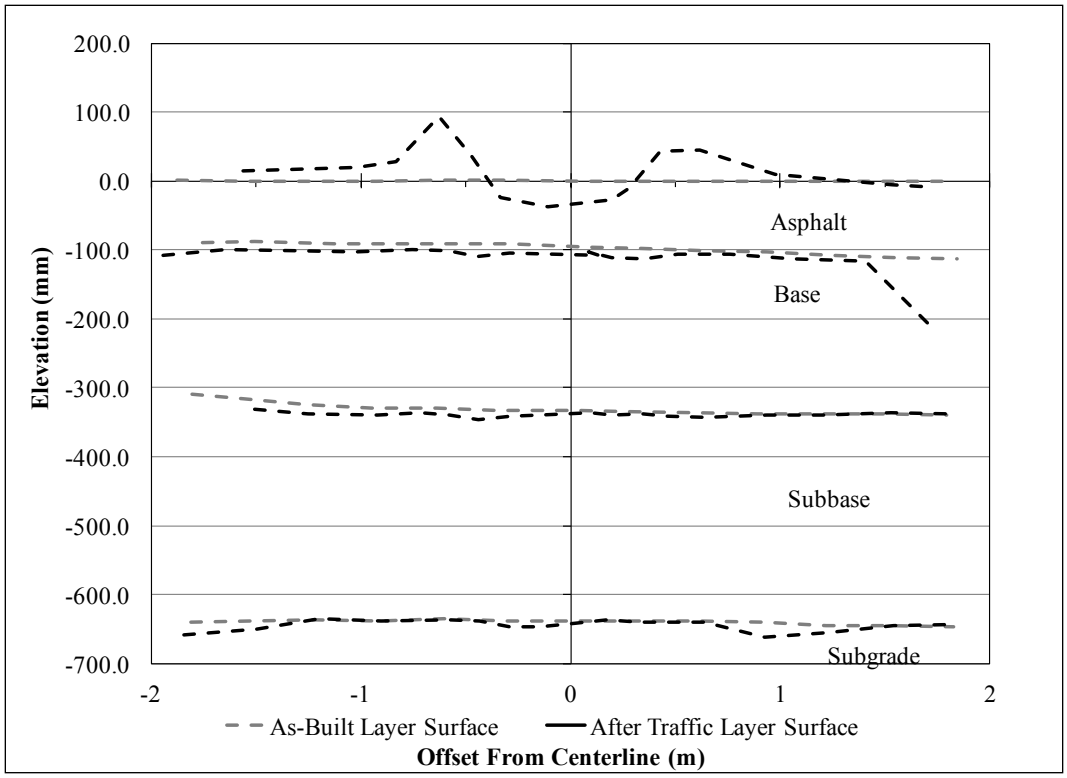

Figure 46. Field Trial 1 post traffic survey

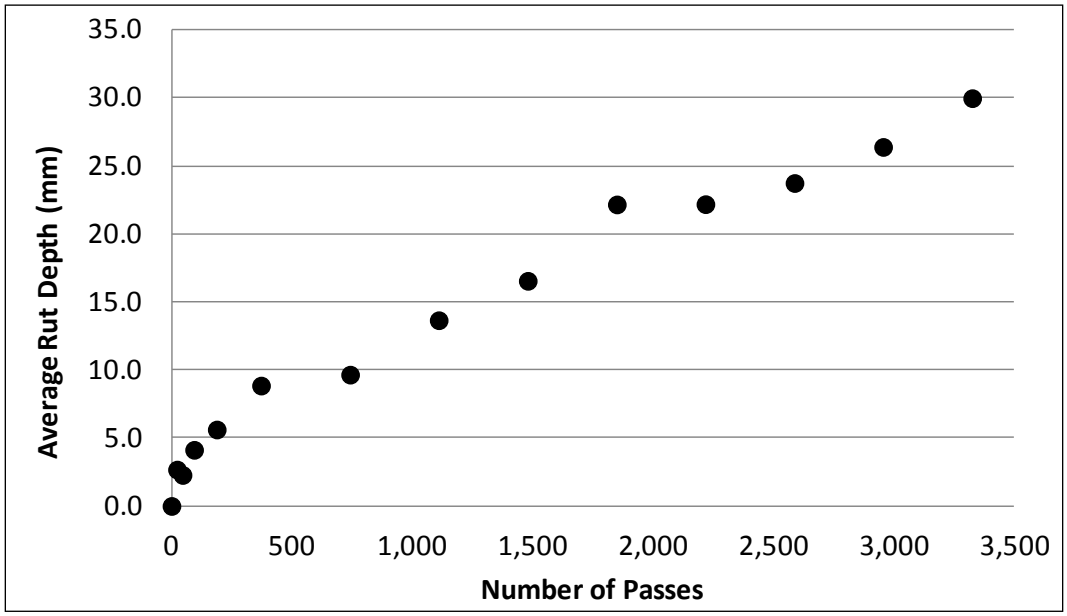

Figure 47. Rut depth accumulation during Field Trial 1

Field Trial 2

For Field Trial 2, a flexible pavement was designed that would withstand over 100,000 passes without failure (according to DoD criteria UFC 3-260-02) of a single wheel from a fully loaded C-17 cargo aircraft (approximately 200-kN wheel load and 980-kPa tire pressure). Failure for this trial was defined as 25 mm of rutting in the subgrade or subbase. The pavement structure (Figure 48) consisted of 100 mm of asphalt concrete over 350 mm of limestone base course with a CBR of 100, over a high plasticity clay subgrade with an average CBR of 8. The test item was 15.2 m long and 3.6 m wide.

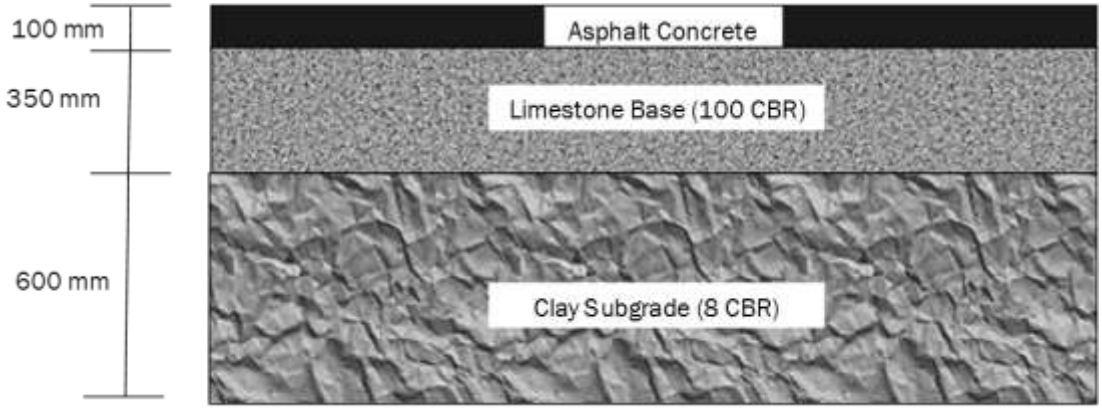

Figure 48. Pavement structure from Field Trial 2

The average volumetric properties of the asphalt layer were determined from ten 100-mm-thick cores. The average air void content was 5.8 percent, typical for a newly constructed pavement. The average VMA, VFA, and binder content were 15.8 percent, 64 percent, and 5.2 percent, respectively. Simulated traffic was applied using the HVS-A. Insulated panels encapsulated the traffic area, and conditioned air provided a

constant test temperature of 25°C during traffic. A normally distributed wander pattern was used to distribute traffic transversely within the center 1.22 m of the pavement lane. A total of 180,000 traffic passes were applied over a period of three months, including intervals for equipment maintenance.

Temperature measurements

Average pavement temperature was determined for the locations where the I-buttons were installed. These average temperatures were calculated using only the data that were collected when traffic was applied to the pavement. The average temperature at the mid-depth and bottom of the asphalt layer as well as the air temperature was measured. The average air temperature was 25.4°C. The average mid-depth asphalt temperature was 25.5°C, while the temperature at the bottom of the asphalt layer was 25°C. These data show that the target test temperature was maintained by the HVS-A during traffic.

An infrared camera was used to capture the surface temperature during traffic (Figure 49). The photograph was taken from the south end of the test item. The temperature outside the traffic lane is represented by the pointer shown. From this photograph, it is evident that the environmental chamber maintained the target environmental temperature but that the pavement temperature in the traffic lane was slightly higher due to heat generated by the wheel traversing the section. The pavement temperature was

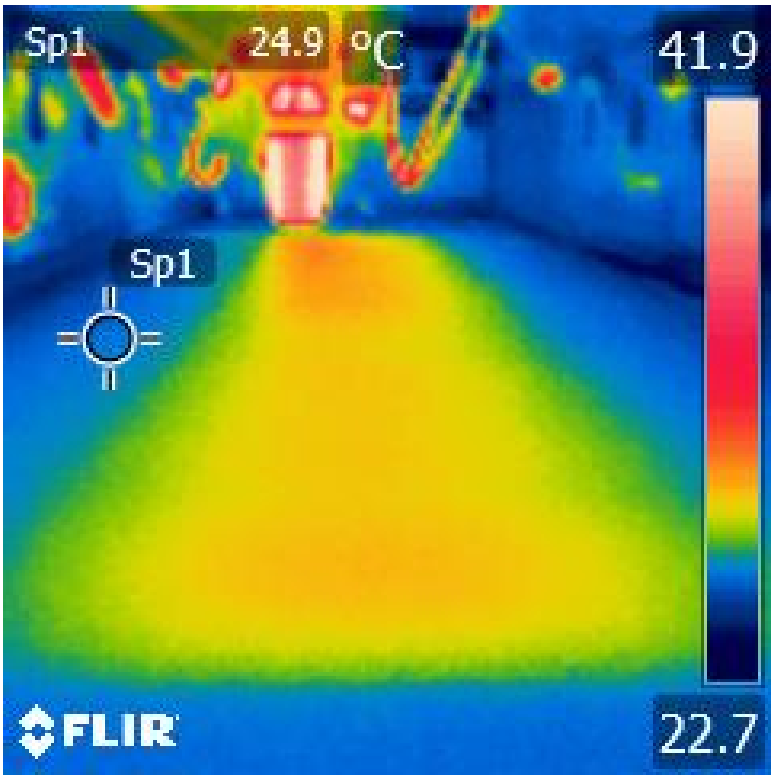

Figure 49. Typical surface temperatures measured with infrared camera during Field-Test 2

uniform in the traffic lane and not likely high enough to induce significant rutting. The temperature difference between the traffic lane and surrounding pavement was approximately 5°C. This difference was not noted by the I-button data because the device was located 50 mm deep in the pavement.

Rutting performance

Figure 50 shows the rutting on the HMA after 180,000 passes. The HMA experienced a shallow, bowl-shaped depression that spread to the outer edges of the wheel wander. No upheaval on the sides of the traffic area was observed.

Figure 50. Field Trial 2 rutting after 180,000 passes

Figure 51 presents the permanent deformation centerline profile. The data were normalized to zero prior to applying traffic. The failure criterion was 25 mm of permanent deformation. The amount of permanent deformation was relatively constant across the test item for a given traffic interval. The traffic interval for which data were collected became much longer later in the test because of the slow rate of permanent deformation occurring during the test.

A cross-section showing the representative permanent deformation is presented in Figure 52. This cross-section shows the typical rutting failure that was experienced under the C-17 simulated traffic.

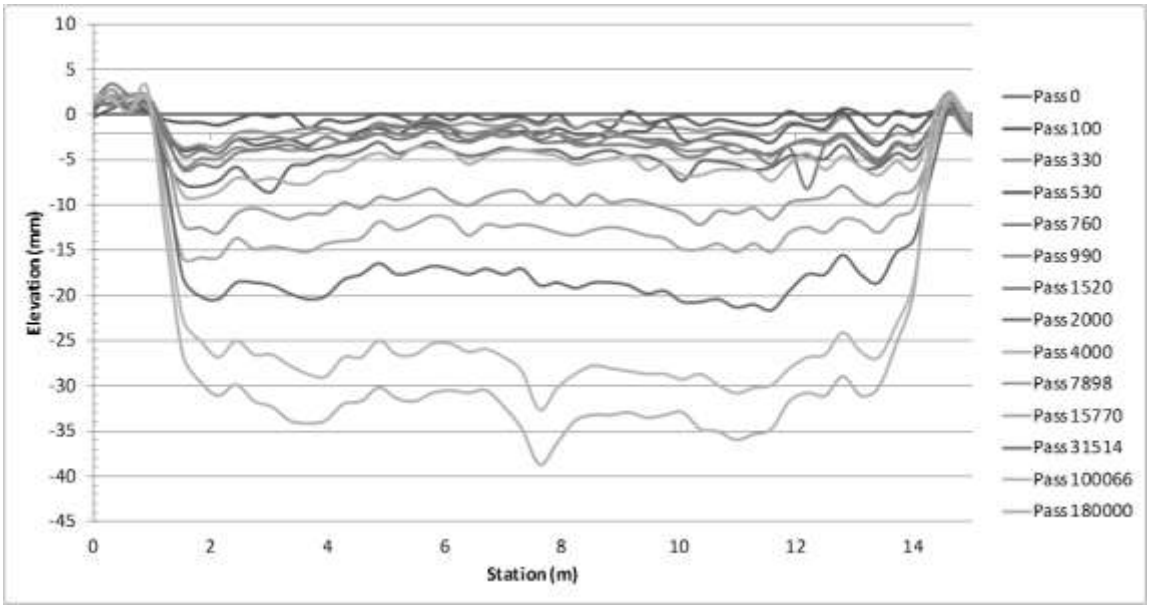

Figure 51. Field Trial 2 centerline profile

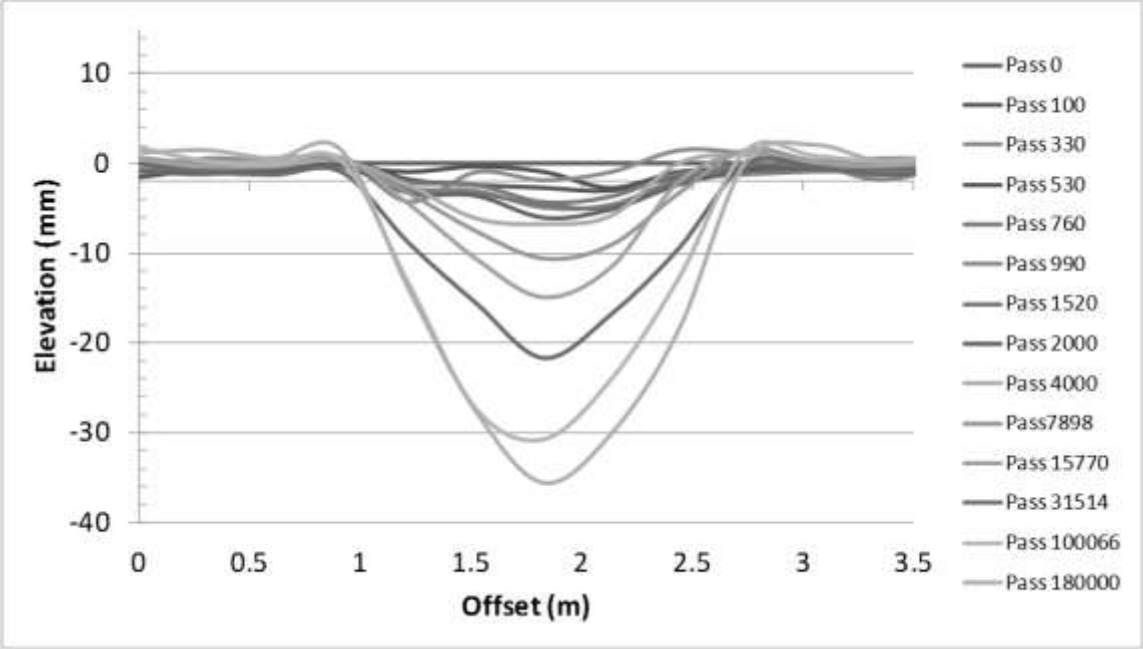

Figure 52. Example Field Trial 2 cross-section profile

Forensic evaluation

The shape of the rut from Field-test 2 was a shallow, wide bowl. This shape of rut is commonly associated with pavement failure deep within the soil layers (typically subgrade). The research study for which this pavement section was constructed was incomplete at the time of this publication. Since the HVS-A was still being moved around the pavement section, trenching was not possible. The large number of passes of simulated traffic achieved on this item suggests that rutting in the asphalt layer is not significant. Given that the pavement was constructed on an 8-CBR subgrade and trafficked with a relatively heavy wheel load, the location of failure is most likely in the subgrade.

The average centerline permanent deformation as traffic progressed is shown in Figure 53. Failure was determined by interpolating the number of passes that caused 25 mm of average permanent deformation at the centerline. The HMA for Field Trial 1 failed after approximately 75,000 passes.

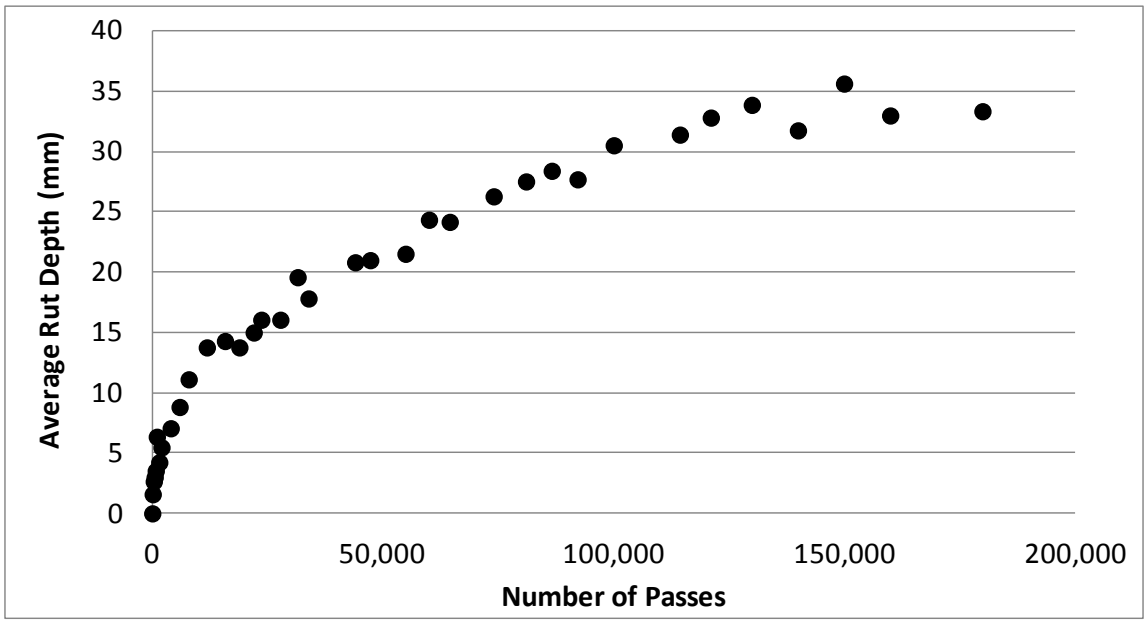

Figure 53. Rut depth accumulation during Field Trail 2

Comparison of Field Trial 1 and Field Trial 2

Results from the two field studies using the same asphalt mixture show very different rutting performance depending on the traffic and environmental conditions. Field Trial 1 represents an extremely severe condition that promotes high levels of rutting within the asphalt concrete layer. Applying 3,000 aircraft load applications at high temperatures is considered a reasonable, conservative method to test a mixture's rutting performance. An actual in-service pavement would not generally receive this level of traffic in such short duration. If one considers that the highest pavement temperatures only exist for about three months of the year, and only for an average of approximately 5 hours per day, then the actual number of hours that a pavement would experience such conditions would be about 450 hours per year. Assuming that most of the rutting occurs in the first year, the applied traffic represents approximately seven load applications per hour. This

type of traffic is reasonable for an active military airfield housing fighter jets. Many facilities receive much lower traffic levels and would have better rutting performance.

On the other hand, Field Trial 2 represents moderate loading conditions. The tire pressure of the C-17 cargo aircraft is typical of many commercial aircraft, although it is also common for tire pressures of commercial aircraft to reach 1380 kPa or even higher. The gear load of the C-17 is heavy and requires a substantial pavement structure. Traffic with the C-17 tire required 180,000 passes to achieve 33 mm of rutting in the pavement. Very little of this rutting was thought to result from shear flow in the asphalt layer, although verification would require trenching the pavement to observe the cross-section. The lower tire pressure and moderate temperature improved performance considerably compared to Field-test 1. These results are included to show that an asphalt mixture, even with marginal properties, can exhibit adequate or even exemplary rutting performance when loading conditions are moderate. The fact that most traffic occurs at moderate conditions is the reason that rutting is not typically a problem on airfields.

Based on the results of the full-scale field tests, the proposed criteria for mixture design performance tests are reasonable. They are conservative enough to eliminate any mixtures that would perform worse than the HMA tested in Field Trial 1 with very high tire pressure at elevated temperature. This performance was acceptable given that most pavements do not experience the type of traffic exposure used in the accelerated pavement test. Further, if traffic conditions did exist at a similar or higher level, a polymer-modified binder should be selected during design to provide better rutting performance.

Results from all four performance tests provided the same assessment of the mixture; which was questionable rutting performance according to the recommended acceptance criterion. Test results were nearly equal to the minimum thresholds for each test method. Since each test was capable of identifying the mixture as having some rutting susceptibility, selection of a performance test for use in mixture design specifications should include other factors such as the cost to perform the test, the time required to determine results, the complexity of the test and data analysis, and the variability of the test.

CHAPTER IX

MODELING HMA RUTTING UNDER AIRCRAFT LOADS

The full-scale accelerated pavement testing of one asphalt mixture under different loading and temperature scenarios supported the proposed performance test acceptance criteria that were developed through the laboratory study. It was desired to apply a rutting model using laboratory-measured material properties to simulate field conditions in order to enhance the ability to design mixtures for unique loading scenarios based on the materials. The Leahy model used in the MEPDG was considered, but the software did not include user-defined inputs for loads that represent aircraft traffic. The available range of traffic for the model is based on highway loading scenarios.

The option to apply a user-defined material model for asphalt coupled with embedded material models for other pavement layers in the ABAQUS software program was selected.

To accomplish this task, the Pavement Analysis Using Non-Linear Damage Approach (PANDA) model was used. The PANDA model is a thermo-viscoelastic-viscoplastic-viscodamage constitutive model for asphaltic materials (Darabi 2011). Schapery's non-linear viscoelastic theory, Perzyna's viscoplasticity model, and a Viscoplastic Hardening-Relaxation model are merged to simulate the non-linear mechanical response of HMA. The response at loading conditions representative of aircraft were modeled by implementing the PANDA model as a user-defined material for the HMA layer in ABAQUS.

Schaprey's nonlinear viscoelastic theory can be used to model the recoverable component of an asphalt mixture under an applied stress, ζ^t, using Equation 15:

$$\varepsilon^{nve}\ \ t\ = g_0 D_0 \zeta^{\,t} + g_1 \int_0^t \Delta D(\psi^t - \psi^{\eta}) \frac{d(g_2 \zeta^{\,\eta})}{d\eta} d\eta \tag{15}$$

The nonlinear viscoelastic strain is related to D_0, the instantaneous elastic compliance, ΔD, the transient compliance, and g_0, g_1, and g_2, nonlinear parameters related to stress or strain level. The reduced time, ψ^t, can be expressed in terms of the temperature shift factor, α_T. according to Equation 16:

$$\psi^t = \int_0^t \frac{d\xi}{\alpha_T} \tag{16}$$

The transient compliance is represented by a Prony series according to Equation 17:

$$\Delta D^{\psi^t} = \sum_{n=1}^{N} D_n\ \ 1 - exp\ \ -\lambda_n \psi^t \tag{17}$$

Perzyna's viscoplastic model with modified Drucker-Prager yield surface is used by PANDA for viscoplastic analysis. The viscoplastic flow rule is given in Equation 18:

$$\dot{\varepsilon}_{ij}^{vp} = \dot{\gamma}^{vp} \frac{\partial F}{\partial \zeta_{ij}}; \qquad \gamma^{vp} = \Gamma^{vp} \left\langle \frac{f}{\zeta_{\ y}^{\ 0}} \right\rangle^N \tag{18}$$

where

$\dot{\varepsilon}_{ij}^{vp}$ = viscoplastic strain tensor

$\dot{\gamma}^{vp}$ = viscoplastic multiplier

N = viscoplastic rate-sensitivity exponent parameter

ζ_y^0 = a yield stress quantity used to normalize the yield surface

The yield surface and plastic potential functions, f and F are defined by Equation 19:

$$f = \eta - \alpha I_1 - \kappa(p); \quad F = \eta - \beta I_1; \quad \eta = \frac{\sqrt{3J_2}}{2}\left[1 + \frac{1}{d^{vp}} + \left(1 - \frac{1}{d^{vp}}\right)\frac{3J_3}{\sqrt{3J_2^3}}\right] \tag{19}$$

where

α and β = pressure-sensitivity parameters

I_1 = the first stress invariant

η = the deviatoric effective shear stress

J_2 and J_3 = second and third deviatoric stress invariants

d^{vp} = distinguishes the viscoplastic response during extension and contraction

The hardening function κ is defined according to Equation 20:

$$\kappa\ p\ = \kappa_0 + \kappa_1\left[1 - exp\ -\kappa_2 p\ \right]; \quad \dot{p} = \left[1 + 2\left(\frac{0.5 + \beta/3}{1 - \beta/3}\right)\right]^{-0.5}\sqrt{\dot{\varepsilon}_{ij}^{vp}\,\dot{\varepsilon}_{ij}^{vp}} \tag{20}$$

where p is the effective viscoplastic strain.

Finally, PANDA uses the hardening-relaxation memory concept (Darabi et al. 2013) to account for the fact that the rate of accumulation of viscoplastic strain changes with increasing number of loading cycles. Use of the hardening-relaxation concept allows for

a more accurate prediction of rutting potential for asphalt concrete mixtures. The model uses static and dynamic hardening-relaxation memory surfaces, $f^{\text{h-r}}$ and $\chi^{\text{h-r}}$, respectively. These parameters are defined in Equation 21:

$$f^{(h-r)} = p - q^{vp} \leq 0; \quad \chi^{h-r} = p - q^{vp} - \left(\frac{\dot{q}^{vp}}{\Gamma^{h-r}} \right)^{\frac{1}{S_1}} \leq 0 \tag{21}$$

where p is the effective viscoplastic strain and q^{vp} is a hardening-relaxation state variable that memorizes the maximum experienced viscoplastic strain for which the hardening-relaxation has occurred. The parameters $\Gamma^{h\text{-}r}$ and S_1 are hardening-relaxation model parameters. An additional model parameter S_2 controls the rate at which the hardening parameter relaxes and is defined by Equation 22:

$$\dot{\kappa}_1 = -S_2 \dot{q}^{vp} \tag{22}$$

Using the PANDA model allowed for better understanding of the material properties that influence permanent deformation and allowed for optimization of mixture performance. This model was applied to the materials and conditions in the full-scale study to simulate the testing computationally. The overall goal was to provide information on important material properties of asphalt concrete and how they relate to permanent deformation when heavy aircraft loads are applied.

Tests to Obtain Material Parameters

Specimen preparation

The asphalt mixture used for the PANDA simulations was sampled during construction of Field Trial 1. The samples were taken from dump trucks delivering the mixture to the Hangar-4 test facility for paving. Samples were collected in 19-liter buckets, sealed, and transferred to the asphalt-testing laboratory. The mixture was reheated and compacted in a SGC using 75 gyrations to produce test specimens. The SGC specimens were 180 mm in height with a 150-mm diameter. They were cut to a height of 150 mm and cored to a diameter of 100 mm for testing. The air void content of the test specimens (approximately 4.0 percent) was similar to the in-place air void content of field-compacted mixture in Field Trial 1. The following tests were performed on specimens to determine material parameters for the model simulations:

- Dynamic modulus
- Repeated Creep-Recovery at Various Stress Levels
- Repeated Creep-Recovery at single stress level using 0.4 s load; 0.4 s unload
- Repeated Creep-Recovery at single stress level using 0.4 s load; 1.0 s unload
- Repeated Creep-Recovery at single stress level using 0.4 s load; 5.0 s unload

Dynamic modulus

Dynamic modulus testing was performed on an Industrial Process Controls (IPC) testing machine. The manufacturer's software was used to record the data. The Superpave Performance Test (SPT) analysis procedure was selected from the available options to determine dynamic modulus and phase angle values from the data. Prior to

testing, the specimens were placed inside the environmental chamber of the test equipment at the test temperature overnight. The test was performed at three temperatures (21, 37, 54°C) and six frequencies (25, 10, 5, 1, 0.5, and 0.1 Hz). No testing was performed at low temperatures since rutting was the primary distress investigated in this study. The load for each combination of temperature and frequency was adjusted so that the resulting microstrain was between 50 and 150. No confinement was used in the dynamic modulus test.

The dynamic modulus and phase angle determined by the IPC software using the SPT analysis procedure were recorded. From these data, the values of the complex compliance D* were determined such that:

$$log\, D^* = -log\, E^* \tag{23}$$

A sigmoidal function was used to fit the experimental data and to obtain the time-temperature shift factor for the mixture according to Equation 24

$$-log\left|D^*\right| = \delta + \frac{\alpha}{1 + exp\left[\beta + \gamma\, log\ \omega_r\right]} \tag{24}$$

where ω_r is the reduced frequency, and δ, α, β, and γ are fitting parameters. The time-temperature shift factor is defined as

$$\alpha_T = \frac{\omega_r}{\omega} \tag{25}$$

where α_T is the time-temperature shift factor and ω is the angular frequency. The fitting parameters were adjusted so that the error between the experimental data and the fitted function was minimized using a Microsoft Excel solver function. Once the time-temperature shift factors were determined for each data point, the linear viscoelastic model parameters were determined. The storage compliance D' and loss compliance D'' were calculated using experimental data such that

$$D' = |D^*| \cos\theta; \quad D'' = |D^*| \sin\theta \tag{26}$$

The storage and loss compliance are described according to a Prony series according to Equation 27

$$D'(\omega) = D_o + \sum_{i=1}^{N} \frac{D_i}{\omega^2/\lambda^2 + 1}; \quad D''(\omega) = \sum_{i=1}^{N} \frac{\omega/\lambda_i D_i}{\omega^2/\lambda^2 + 1} \tag{27}$$

where

N = the number of Prony series coefficients

D_o = the instantaneous compliance

D_i = the i^{th} transient compliance associated with the i^{th} retardation time λ_i

A total of nine coefficients for the mixture were determined by minimizing the error between experimental data and the fitted function using the Microsoft Excel solver function. The values for the transient compliance and retardation time for the mixture at 37°C are given in Table 17. Actual values for the simulations were adjusted according to the time-temperature shift factor.

Table 17. Prony series coefficients

Transient Compliance (1/MPa)		Retardation Time (1/s)	
D1	7.77E-05	$\lambda 1$	2.14E+03
D2	8.46E-05	$\lambda 2$	4.45E+02
D3	1.15E-04	$\lambda 3$	9.30E+01
D4	3.91E-04	$\lambda 4$	1.90E+01
D5	2.54E-04	$\lambda 5$	4.00E+00
D6	6.71E-04	$\lambda 6$	8.00E-01
D7	1.20E-03	$\lambda 7$	2.00E-01
D8	2.15E-03	$\lambda 8$	3.60E-02
D9	1.99E-03	$\lambda 9$	7.50E-03

Repeated Creep-Recovery Test at Various Stress Levels (RCRT-VS)

The repeated creep-recovery test at various stress levels (RCRT-VS) is used to identify the nonlinear viscoelastic model parameters as well as some viscoplastic model parameters. The RCRT-VS test is a repeated creep-recovery test for which the loading and unloading times remain constant throughout the entire test. This test consisted of eight loading blocks. Each loading block contained eight creep-recovery cycles with increasing applied deviatoric stress levels. The loading time for each load application was approximately 0.4 sec. The unloading time was approximately 30 sec. The deviatoric stress level starts from ζ_o in the beginning of the first loading block and increases with the factor of 1.2 for the next deviatoric stress level until it reaches the last creep-recovery within that block. For the first loading block, ζ_o is 0.137 MPa. For the

next loading block, however, the first deviatoric stress level is equal to the third stress level in the previous block. Figure 54 schematically shows the applied stress history for the first two blocks of RCRT-VS test. A chamber pressure of 69 kPa was used for confinement.

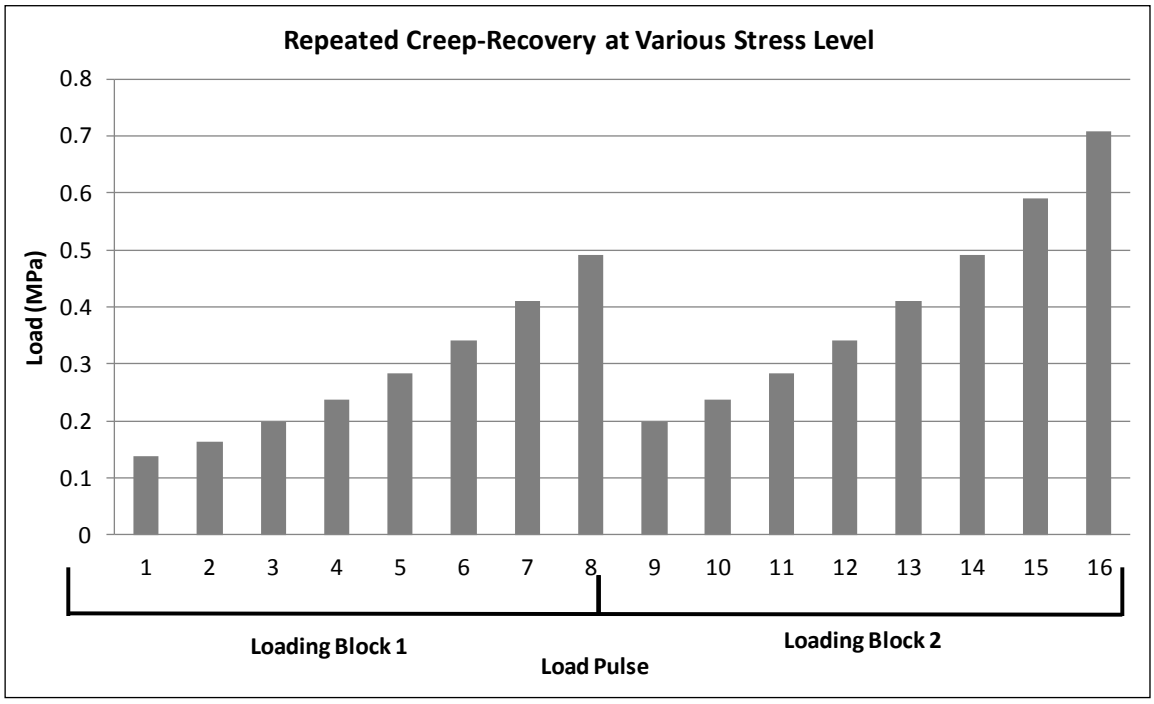

Figure 54. Loading pulse sequence for RCRT-VS test

The nonlinear viscoelastic model parameters were determined from experimental data in the recovery period of the RCRT-VS test. Equation 28 is once again presented to show that the nonlinear viscoelastic strain can be described by the instantaneous and transient compliance.

$$\varepsilon^{nve}\ t = g_0 D_0 \zeta^t + g_1 \int_0^t \Delta D(\psi^t - \psi^\eta) \frac{d(g_2 \zeta^\eta)}{d\eta} d\eta \qquad (28)$$

The value for g_o is assumed to be 1.0 since measuring the instantaneous response of an asphalt mixture is experimentally unachievable. The values for g_1 and g_2 are determined according to the procedure described in the following text.

First, the nonlinear viscoelastic parameter g_2 is determined from data during the recovery period of the RCRT-VS test. During recovery, the accumulation of viscoplastic strain is zero. By using these data, the analysis can be performed on purely viscoelastic strain. An arbitrary point is selected from the data such that $t_o > t_a$ according to Figure 55. By minimizing the error between experimental and analytical data for the

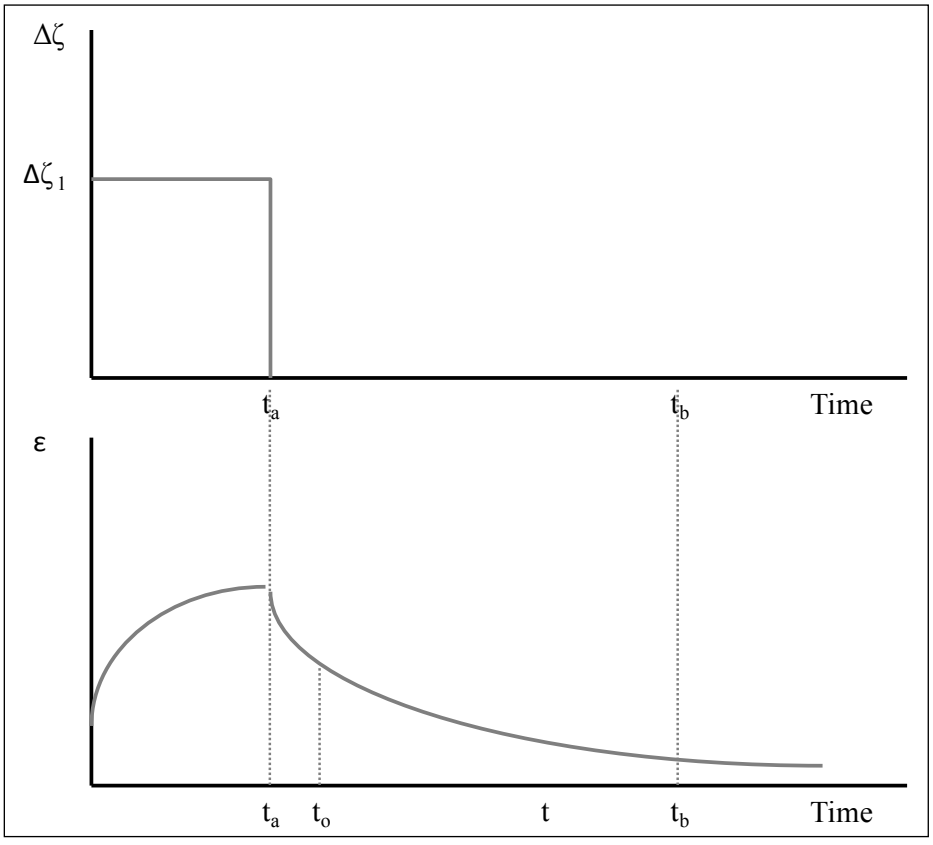

Figure 55. Stress and strain behavior of asphalt concrete during creep-recovery test

change in recovered strain, the value of g_2 is determined. The value for g_1 is then found by minimizing the error between the experimental data and the analytical data modified with the previously determined g_2 value for the full portion of the recovery period (i.e., t_a).

Once the nonlinear viscoelastic model parameters are determined, the RCRT-VS test data is used to determine the viscoplastic model parameters. Several parameters have values that do not vary significantly among asphalt mixtures and can be assumed. These include values for α, β, d^{vp}, and κ_1. A stepwise procedure (AASHTO 2013 draft) is used to determine values for κ_0, κ_2, N, Γ^{vp} by fitting analytical calculations with experimental data.

Repeated Creep-Recovery Test with Constant Loading Time (RCRT-CLT)

The repeated creep-recovery test with constant loading time (RCRT-CLT) is used to identify the viscoplastic hardening-relaxation model parameters. The hardening phenomenon is affected by the resting period between loadings and requires testing at full and partial recovery to accurately capture the behavior. The procedure for extracting the hardening-relaxation model parameters involves identifying the hardening behavior from experimental data for each testing condition and applying the hardening-relaxation model to minimize the error between analytical calculations and experimental data. A detailed stepwise procedure is provided in draft AASHTO protocol (AASHTO 2013 draft). The nonlinear viscoelastic and viscoplastic model parameters determined for the HMA mixture at 25°C and 43°C are provided in Table 18.

Table 18. Model parameters used for PANDA simulations

	g_0	g_1	g_2	α	β	ζ_y^0 MPa	Γ^{vp} 1/s	d^{vp}	N	κ_0 MPa	κ_1 MPa	κ_2	$\Gamma^{vp,s}$ 1/s	S_1	S_2 MPa	S_3
43°C	1	1.1	1.2	0.3	0.25	0.1	0.0012	0.778	1.17	0.0445	1.8	48	1.0E-5	0.2	2.0E5	2.5
25°C	1	2.1	1	0.3	0.25	0.1	0.0008	0.778	1.0	0.0737	1.8	206	1.0E-5	0.2	2.0E5	2.5

Modeling Rutting Behavior Using PANDA

Only the nonlinear viscoelastic, viscoplastic, and hardening-relaxation models in PANDA were used for the analysis. The fatigue damage and moisture damage models within PANDA were not considered because the study focused on properly identifying asphalt mixtures prone to rutting. The aging model in PANDA was not considered because aging typically improves rutting performance by increasing binder stiffness, and the aim of the study was to identify the maximum rutting potential. Simulations were performed using ABAQUS software to determine the rutting potential of asphalt mixtures according to the PANDA model.

The software Panda User Interface (PUI) was used to create ABAQUS input files for simulations of aircraft loads applied to a pavement. The pavement structure and material properties were selected to represent Field-test 1 and Field-test 2 from full-scale accelerated pavement testing. HMA material properties were measured in the laboratory from plant-produced mixtures at the target test temperatures of 25°C and 43°C for the RCRT-VS and RCRT-CLR tests according to the previously described methods. The loads applied in the simulations were representative of the aircraft wheel loads used in field-testing and were simulated by two-dimensional pulse loading.

The first step in using PUI is to select the type of analysis desired (Figure 56). A two-dimensional axisymmetric model with a pulse load was selected for the analysis. A three-dimensional model was not selected because a goal was to simulate a relatively large number of load applications and the three-dimensional model requires significantly more computational time. The two-dimensional model provides a sufficient level of detail for assessing the performance of the HMA under the two conditions used for field-testing.

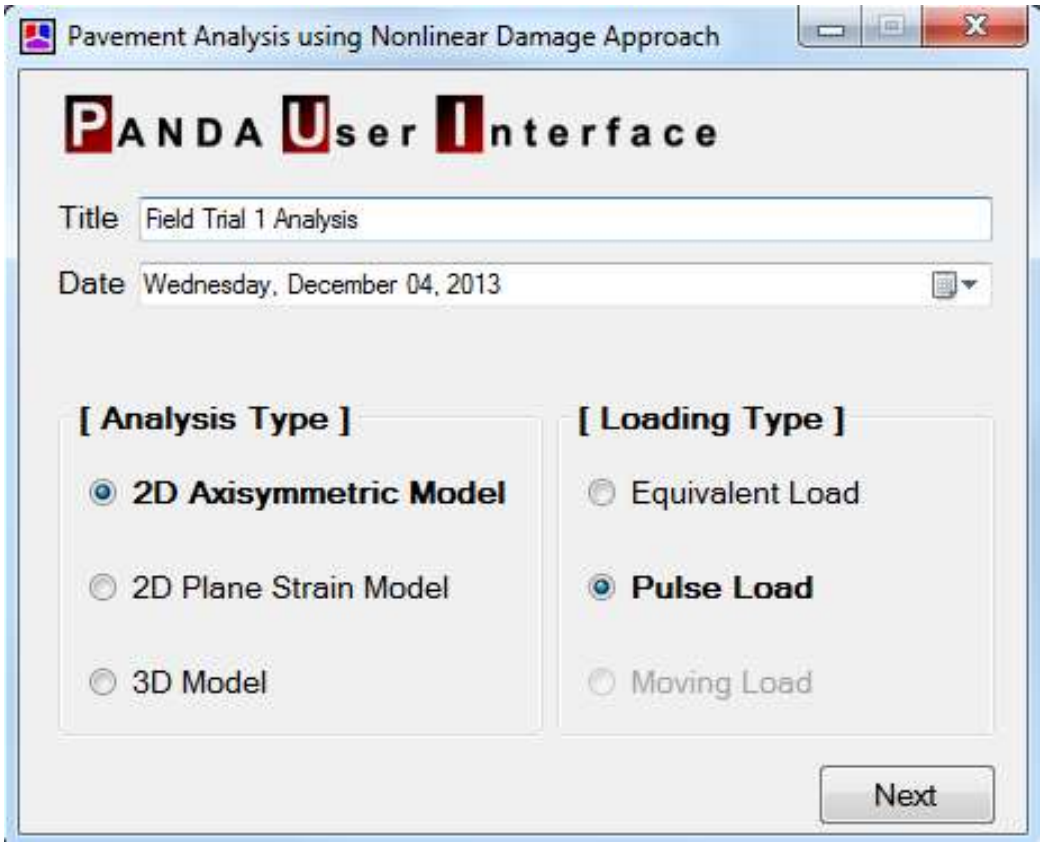

Figure 56. Selecting simulation type in PUI

The second step is to input the pavement structure (Figure 57). Field Trial 1 consisted of four pavement layers; Field Trial 2 consisted of three pavement layers. The appropriate thickness was used corresponding to the structural designs.

The third step is to input the elastic properties of the pavement layers and to select the properties of the asphalt concrete layer that will be used in the analysis (Figure 58). The pavement layers designed for field-testing were relatively stiff to support the intended aircraft loads applied during accelerated pavement testing. The viscoelastic (Figure 59) and viscoplastic (Figure 60) properties of the asphalt concrete were used to identify rutting potential. These properties were identified through laboratory testing.

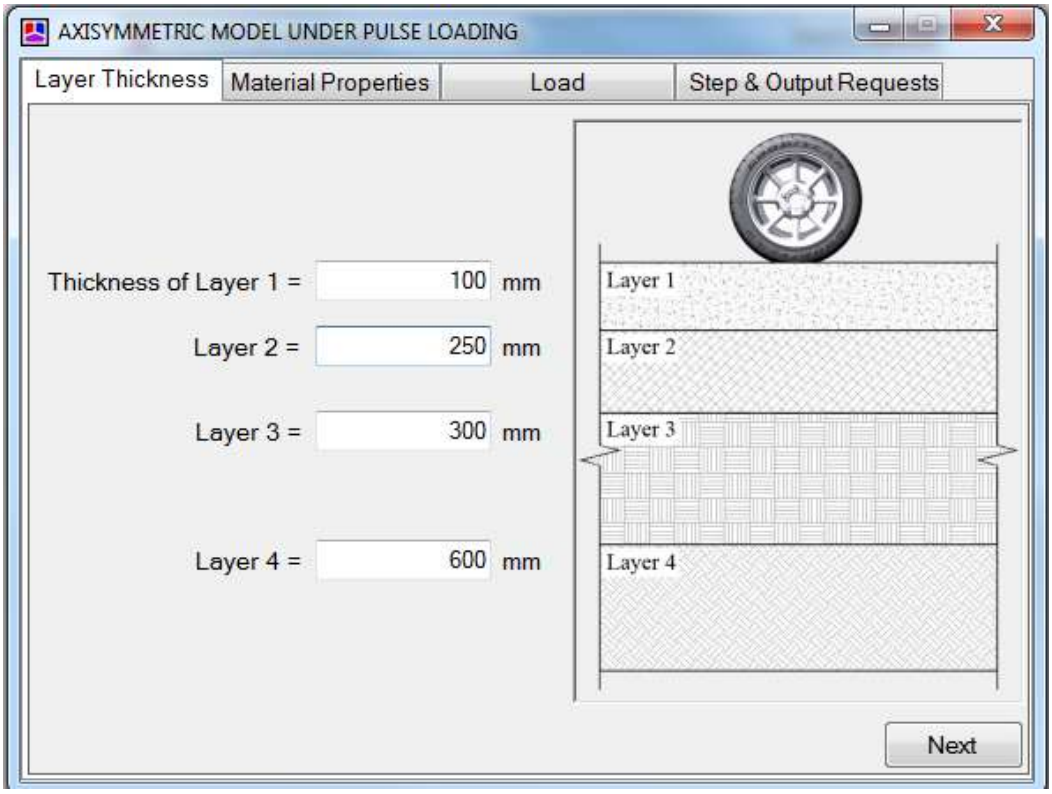

Figure 57. Selecting pavement structure in PUI

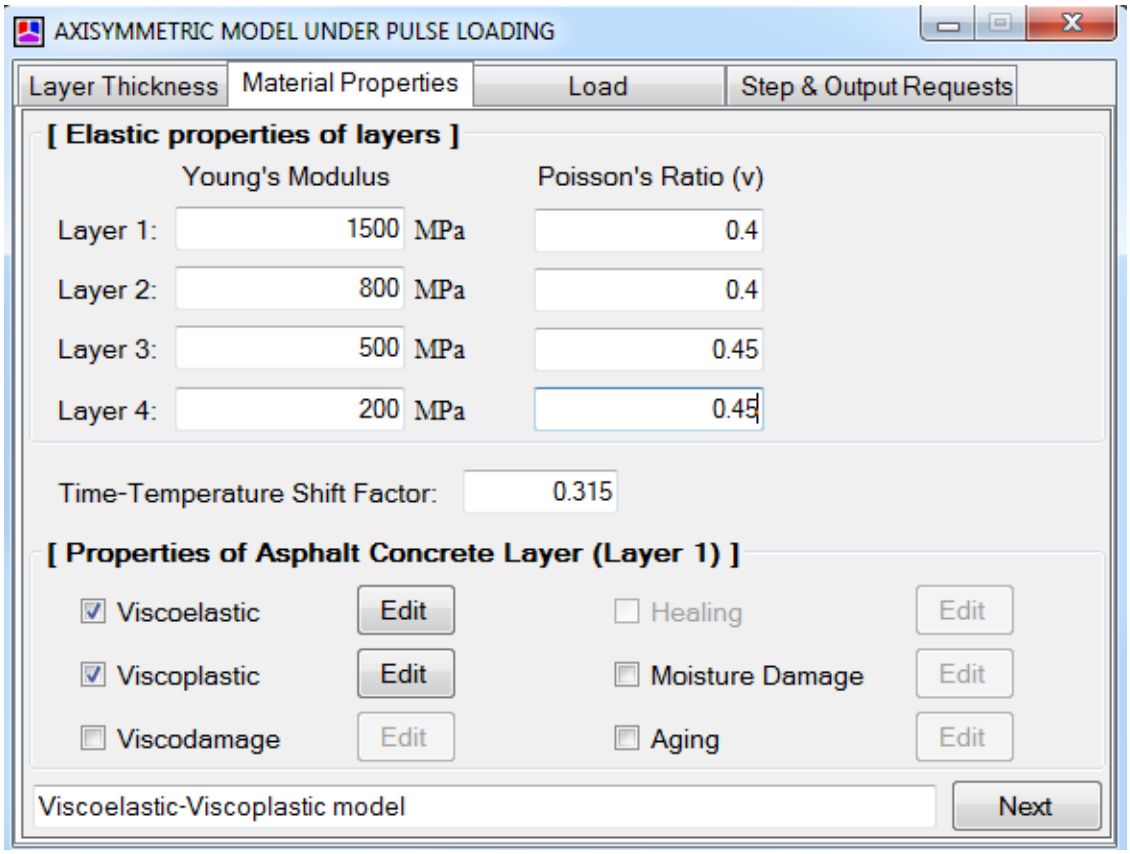

Figure 58. Entering elastic layer properties into PUI

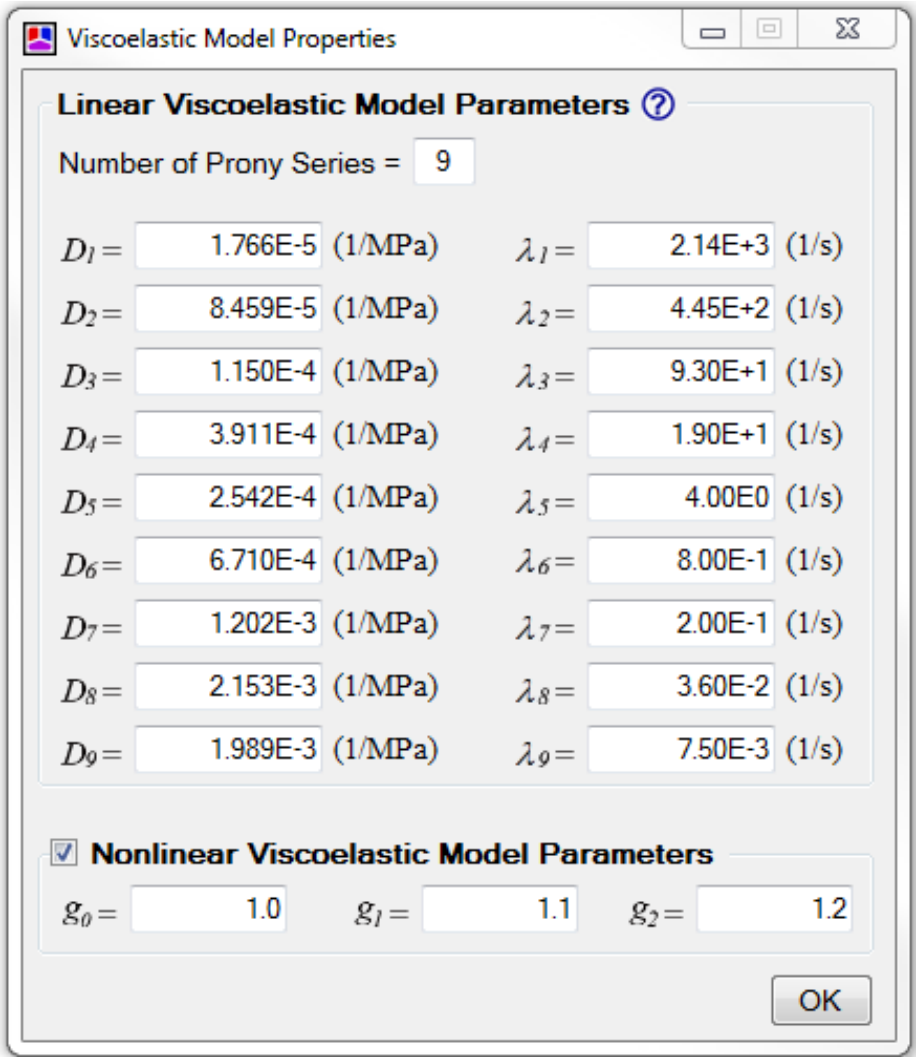

Figure 59. Entering viscoelastic model parameters into PUI

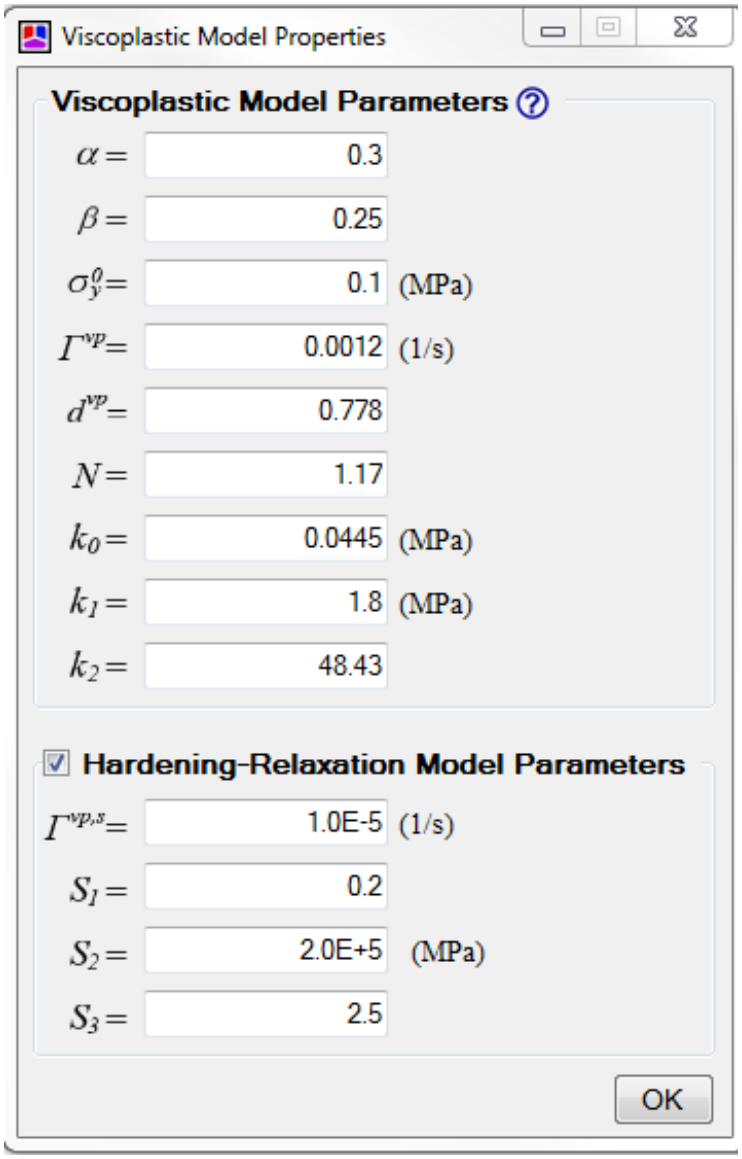

Figure 60. Entering viscoplastic model parameters into PUI

Finally, the loading conditions selected for the analysis were input into PUI (Figure 61). The wheel load and area were selected to represent the vertical loads applied by the HVS during field-testing and the contact area of the aircraft tire used to apply traffic. The loading time and rest periods were selected to allow sufficient time for

viscoelastic strains to recover, but short enough to minimize the computation time for the simulations. A total of 3,000 load pulses were used in the simulations. This number of load applications represented the number of simulated aircraft passes that resulted in significant rutting during Field Trial 1. The input files generated by PUI were run using ABAQUS 6.12.

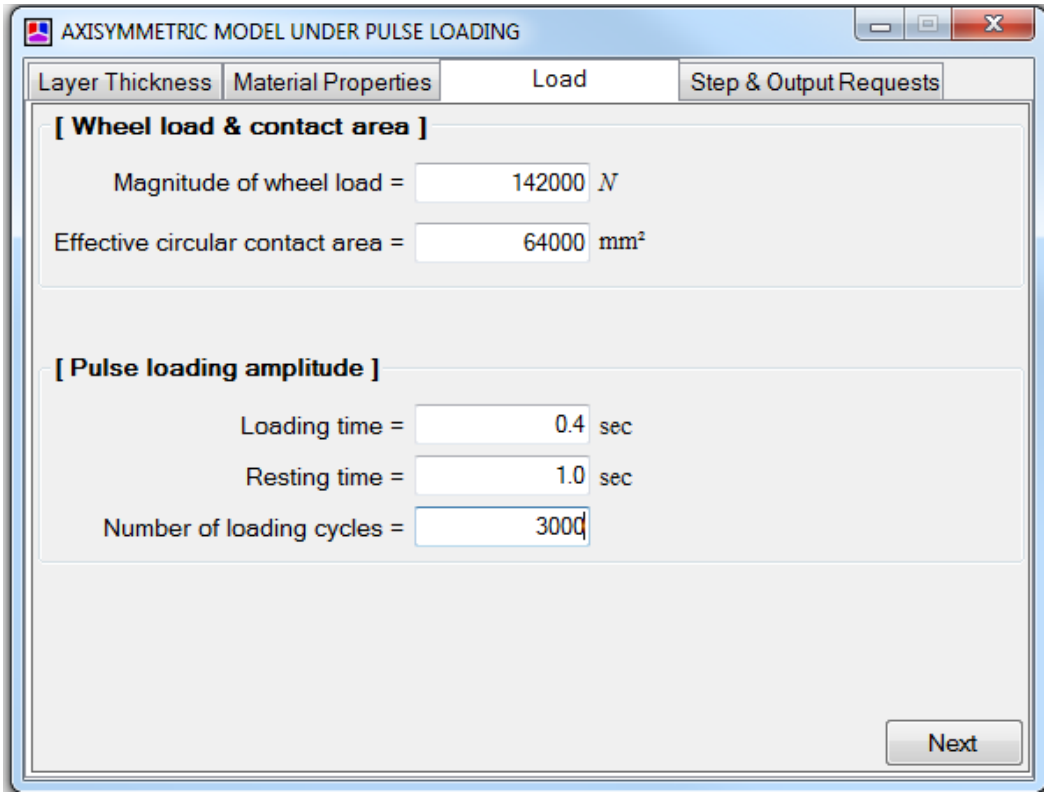

Figure 61. Entering loading conditions into PUI

Discussion of Model Results

Figures 62 and 63 show the viscoplastic strain for the two-dimensional model with accumulating load cycles. Figure 62 is from the analysis representing Field Trial 1 at

43°C; Figure 63 is from the analysis representing Field Trial 2 at 25°C. The magnitude of the viscoplastic strain is noted on the scale at the bottom of the figures. Because of the large differences in viscoplastic strain produced by the model, the scale is different for each figure.

Results in Figure 62 show that the viscoplastic strain developed initially along the edge of the applied load. A progressive increase in the total amount of viscoplastic strain was observed with increasing number of load applications. Viscoplastic strain became more significant in the center of the HMA layer at higher load cycles. The magnitude of the greatest viscoplastic strain was very high and represented significant deformation of the HMA layer. The highest predicted strain was along an upward and outward plane at the edge of the loading area, and the model realistically simulated the shear flow and upheaval observed during full-scale testing.

Simulation results in Figure 63 show that the magnitudes of viscoplastic strains resulting from using the material parameters at 25°C were very small compared to those observed at 43°C. The viscoplastic strain developed first along the surface of the HMA layer directly beneath the loaded area. With increasing number of load cycles, viscoplastic strain began to emerge along the edge of the loading area, similar to the simulations of Field Trial 1 but to a much smaller magnitude. Finally, near the end of the simulation, some viscoplastic strain developed along the bottom of the asphalt layer.

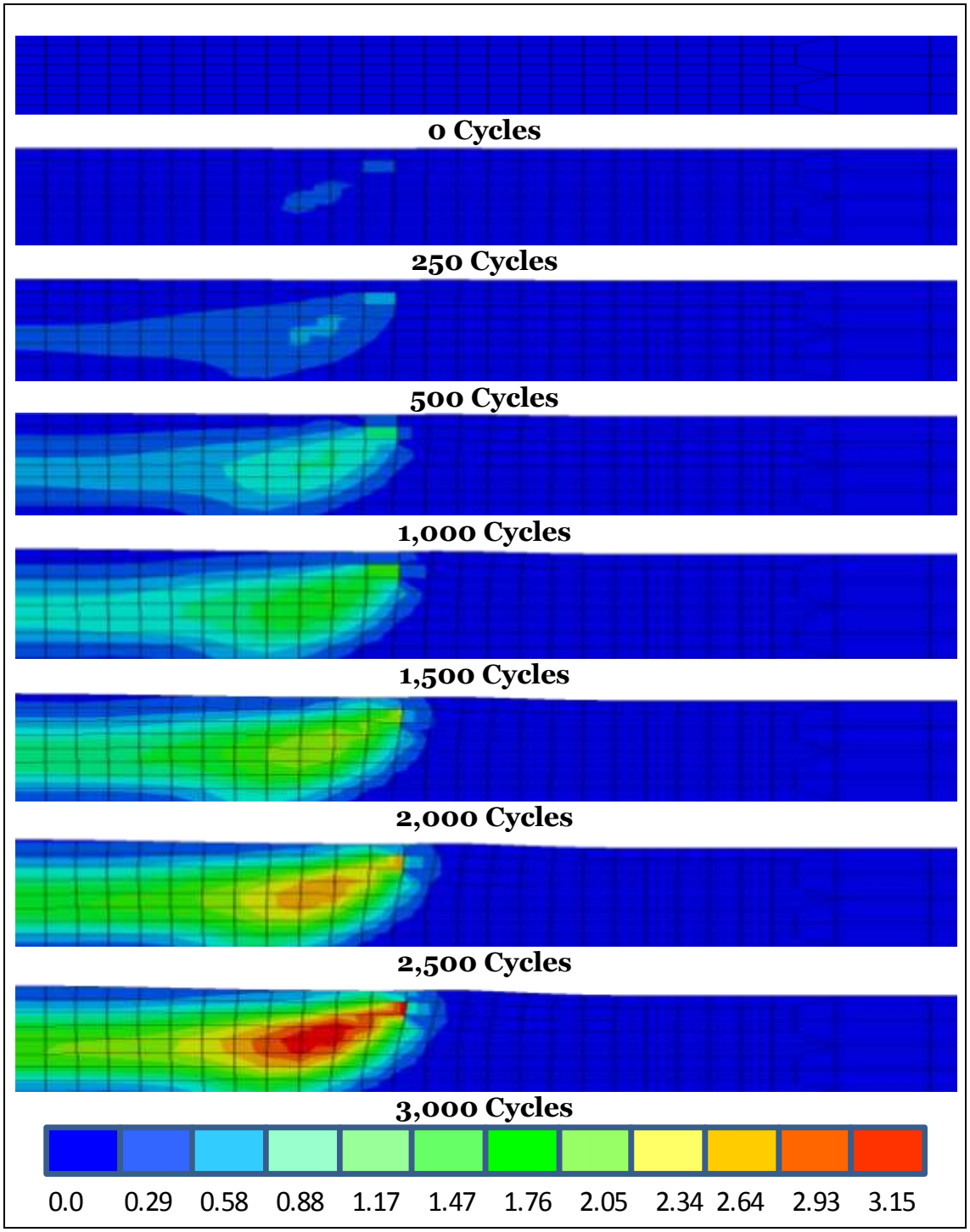

Figure 62. Viscoplastic strain at Field Trial 1 conditions

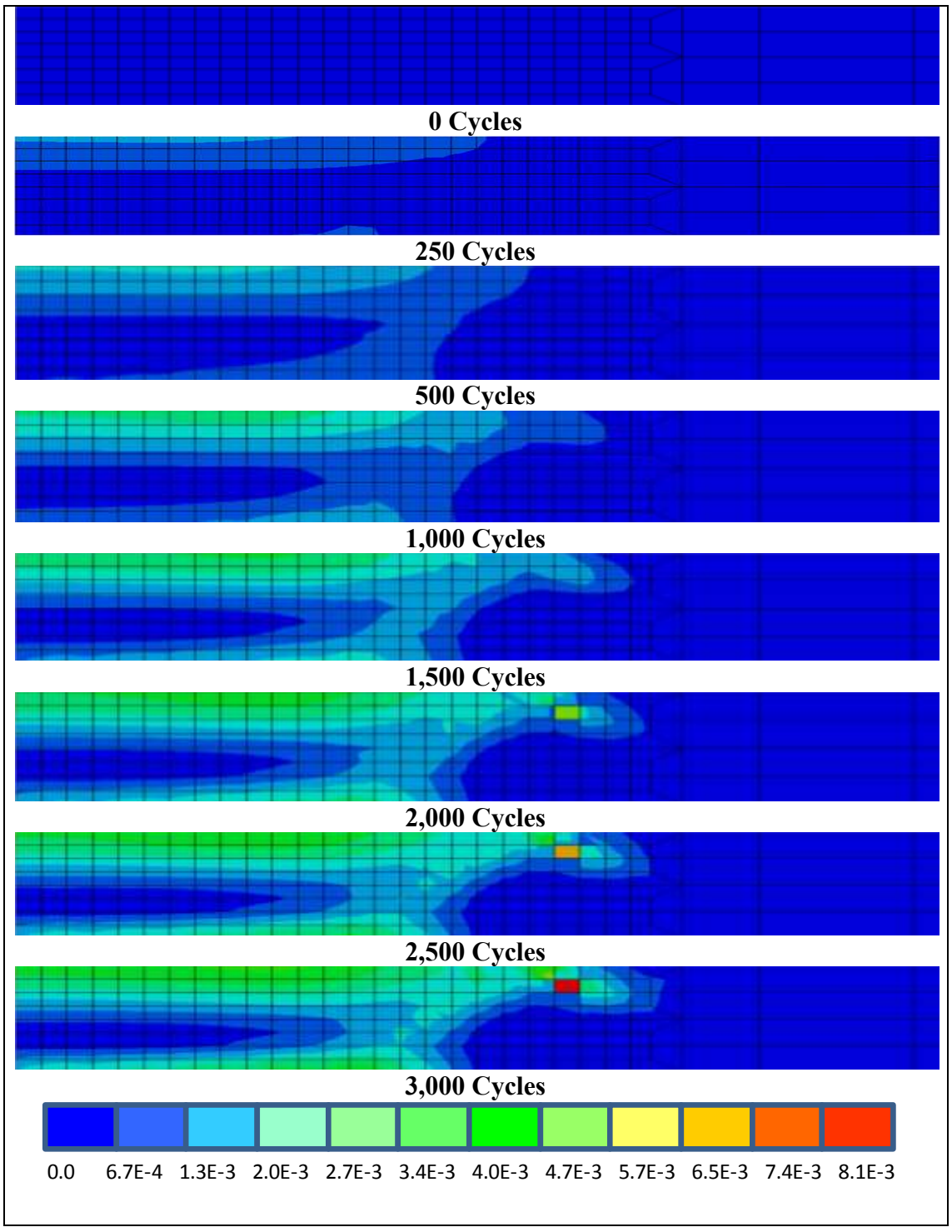

Figure 63. Viscoplastic strain at Field Trail 2 conditions

The total strain in the HMA layer produced very little deformation after 3,000 load cycles.

Actual viscoplastic strain values for each of the elements along the far left vertical axis (center of the load) were extracted using ABAQUS software. The average viscoplastic strain values recorded in the asphalt layer directly beneath the center of the load were 1.28 and 1.61E-05 for the simulations at 43°C and 25°C, respectively. Performing two-dimensional simulations using the PANDA model for the asphalt layer and linear elastic models for the pavement sublayers was not expected to provide a precise measurement of actual rutting because of the variability of the material parameters and the materials used in the constructed pavement. Further, Abu Al-Rub has shown that 2-D simulations produce significantly higher permanent strain than 3-D moving load simulations that more accurately represent the traffic in this study (Abu Al-Rub et al. 2012). However, the model accurately suggests that the propensity for rutting is very different for the two conditions simulated.

Figures 64 and 65 show the nonlinear viscoelastic strain for the two-dimensional model with accumulating load cycles. Figure 64 is from the analysis representing Field Trial 1 at 43°C; Figure 65 is from the analysis representing Field Trial 2 at 25°C. The magnitude of the nonlinear viscoelastic strain is noted on the scale at the bottom of the figures and is the same for each. Positive values represent compression while negative values represent tension.

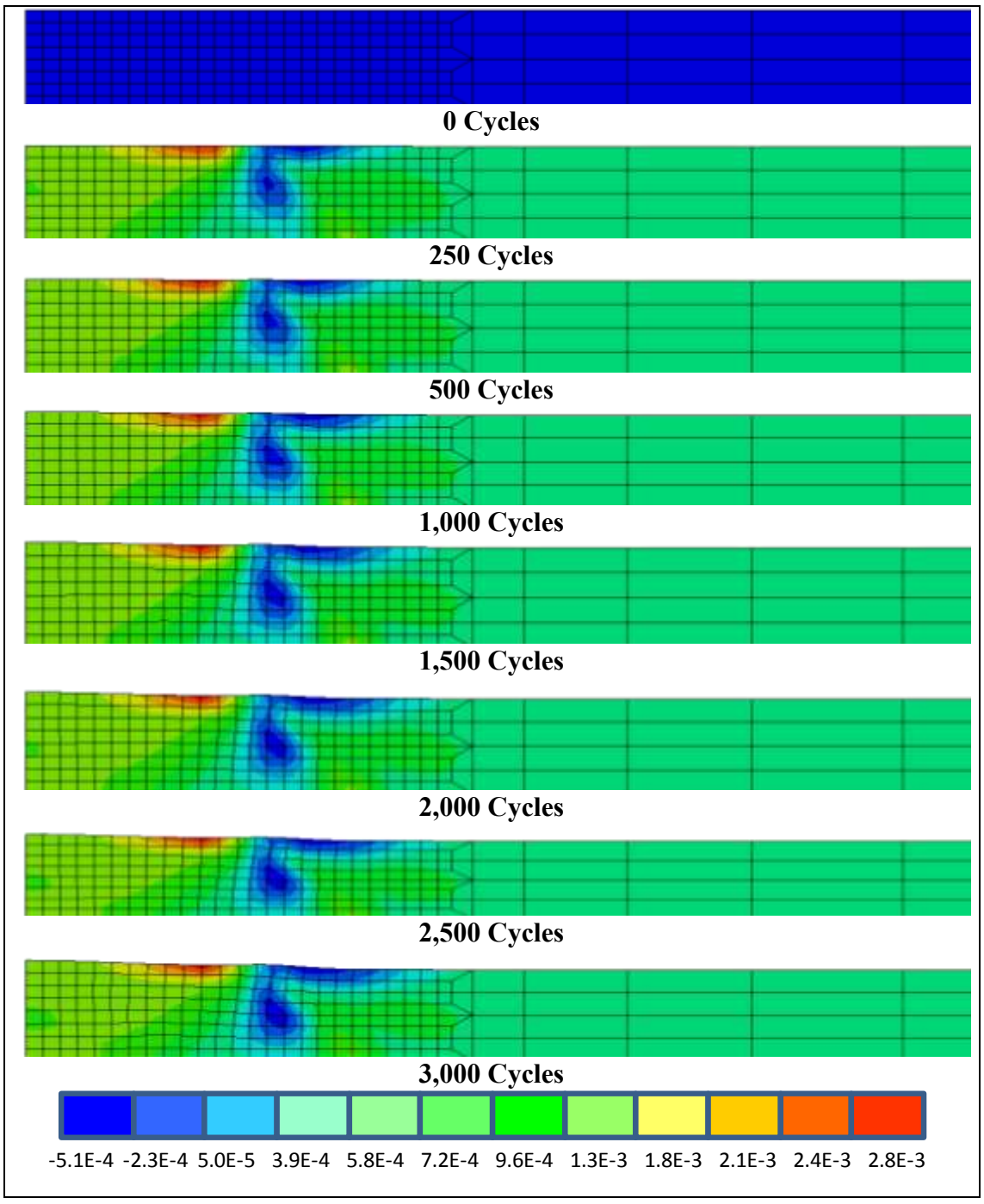

Figure 64. Nonlinear viscoelastic strain at Field Trail 1 conditions

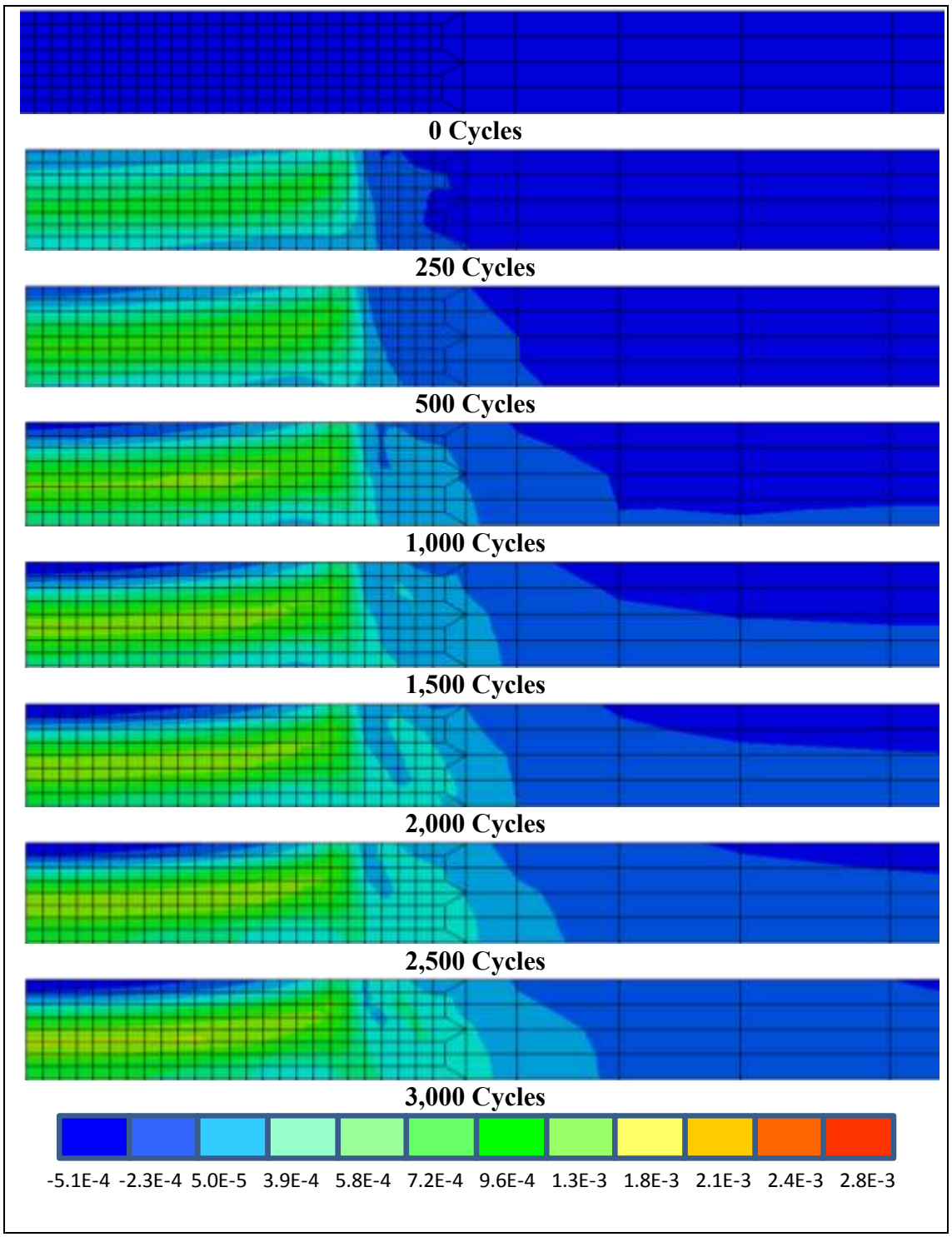

Figure 65. Nonlinear viscoelastic strain at Field Trail 2 conditions

Figure 64 shows that the nonlinear viscoelastic strain increased in magnitude from the center to the edge of the loaded area. The strains were highest at the surface of the HMA layer. Additionally, the area adjacent to the loaded area experienced tensile strain during loading. The overall magnitude of the nonlinear viscoelastic strain was relatively constant with increasing number of load applications. The high stresses represented by a loaded aircraft tire produced fairly high strain levels in the HMA layer.

Figure 65 shows that the magnitude of nonlinear viscoelastic strains resulting from the simulation of the C-17 aircraft tire (Field Trial 2) were lower than those experienced with the simulations of the F-15 tire (Field Trial 1). This result is likely related to the fact that the tire pressure is less than half the magnitude in the second field trial compared to the first, although the material properties at the lower temperature are expected to contribute to the nonlinear viscoelastic response. The nonlinear viscoelastic strain shown in this simulation had the highest magnitude near the center of the HMA layer and dissipated upward and downward. The overall magnitude of nonlinear viscoelastic strain remained relatively constant with increasing number of load cycles, similar to the simulations of Field Trial 1.

The actual nonlinear viscoelastic strain values for each of the elements along the far left vertical axis (center of the load) were determined using ABAQUS. The average nonlinear viscoelastic strain values recorded in the asphalt layer directly beneath the center of the load were 1.06E-03 and 8.90E-04 for the simulations at 43°C and 25°C, respectively. The nonlinear viscoelastic strain was slightly higher for the first field-test condition. Higher strains were expected to result from the much higher tire pressure

simulated during loading. However, the first field-test condition had high accumulation of viscoplastic strains, so a large part of the total strain is not recoverable. Overall, the model provided reasonable nonlinear viscoelastic strain magnitudes for aircraft loads.

Overall, the two-dimensional finite element simulations using the PANDA material model for the HMA layer provided realistic simulations of the response of the pavement system to loading. The PANDA model can be extended beyond its traditional use as a model for simulating highway traffic to assess material responses resulting from applying unique loading conditions of high-pressure aircraft tires. As demonstrated during field-testing, the behavior of HMA can vary widely for a single mixture depending on the temperature and load. At the higher temperature and higher tire pressure conditions of Field Trial 1, the PANDA model predicted viscoplastic strains five orders of magnitude greater than those predicted at Field Trail 2 conditions. These predictions aligned very well with accelerated pavement test results. The data from the simulations suggested that the PANDA model was a useful tool to characterize an asphalt concrete mixture for rutting performance when the loading conditions were accurately estimated.

Many of the model parameters in PANDA are relatively constant among similar asphalt concrete mixtures and can be assumed. For assessing a mixture's rutting potential, results from these simulations indicated the most influential parameters were Γ^{vp} and κ_0. The parameter Γ^{vp} is the viscoplastic viscosity parameter. As expected, this parameter reduces significantly with increasing temperature. Lower viscosity values allow flow to take place, resulting in viscoplastic strain within the material. The

parameter κ_0 is the initial yield stress of the material. This value also decreases with increasing temperature, as expected. The higher temperature reduces the viscosity of the binder and softens the mixture, thus resulting in a lower yield stress.

Comparing material parameters for a single asphalt mixture used for field-testing at two different temperatures and yielding significantly different results provides a standard for comparing and ranking any mixture considered for asphalt concrete airfield pavements. The parameters most influential to rutting have been identified and can be used as a mixture design performance assessment by simulating loading with the PANDA material model.

CHAPTER X

SELECTING THE MOST DESIRABLE PERFORMANCE TEST

The overall goal of this study was to select a performance test to accompany FAA asphalt paving specifications to screen mixtures for rutting potential. Recommendations for acceptable test results were given in Chapter VI for each method studied. These results have been validated through full-scale testing. Additional considerations for selecting the most desirable performance tests are discussed in this chapter.

A desirable performance test is one that produces precise results. Precision refers to the variability of the data produced by running the same test multiple times. The variability of each performance test was studied by preparing and testing twelve specimens of one selected mixture. The 12.5 FGN0 mixture was selected as a representative mixture for testing since its performance was near the median values of the different mixtures considered in this study. Summary statistics for repeated load, static creep, and APA test parameters are shown in Table 19. The coefficient of variation was used to compare the performance tests. The coefficient of variation for dynamic modulus was not measured since a precision statement was recommended in NCHRP 702. The NCHRP study identified the coefficient of variation of low-stiffness mixtures to be between 15 percent and 24 percent, with higher variability in mixtures with larger nominal maximum aggregate sizes.

Table 19. Summary statistics of performance tests

Statistical Measure	Static Creep				Repeated Load				APA RD at 2,300 Cycles
	a	m	FT	TF	a	b	FN	TF	
Average	0.42	0.35	69	191	0.19	0.46	204	517	10
Min	0.39	0.30	52	128	0.11	0.41	143	438	7.3
Max	0.45	0.38	108	325	0.26	0.53	333	634	13.2
Stdev	0.02	0.02	14	50	0.05	0.04	50	67	2
Coeff of Variation	5%	7%	20%	26%	25%	9%	25%	13%	20%
Skewdness	0.126	-0.747	1.882	1.693	0.023	0.925	1.548	0.706	-0.145
Kurtosis	-0.963	-0.601	5.414	4.591	-1.078	-0.527	3.255	-0.969	-1.421
K-S dist	0.158	0.218	0.312	0.283	0.138	0.211	0.196	0.253	0.134

The intercept and slope values from the static creep test had the lowest coefficients of variation, followed by the slope value from the repeated load test. These parameters all had coefficients of variation below 10 percent. The coefficient of variation of the TF value from the repeated load test (13 percent) was much lower than that of the static creep test (26 percent), but the repeated load test FN value was more variable than the FT value from the static creep test. The rut depth after 2,300 APA cycles was considered because this was the number of load cycles at which failure occurred for the worst-performing specimen of the 12.5 FGN0 mixture. The APA rut depth after 2,300 cycles had a coefficient of variation of 20 percent.

Other major factors in selecting the most desirable performance test included the sophistication of the test, level of training required to perform the test, and the time that was required to produce results. Table 20 lists advantages and disadvantages of the different performance tests from this study.

Table 20. Advantages and disadvantages of potential performance tests

Performance Test	Parameter	Test Condition	Advantages	Disadvantages
Repeated Load	Intercept	PG grade high temperature	Rapid test time	Coring and sawing required
	Slope	276 kPa confinement	Slope value has low variability	Standard test equipment and software not available
	Flow number	1380 kPa axial stress		
	tertiary flow	0.1 s load, 0.9 s rest		
Static Creep	intercept	PG grade high temperature	Rapid test time	Coring and sawing required
	slope	276 kPa confinement	Slope value has low variability	Standard test equipment and software not available
	flow time	1380 kPa axial stress		
	tertiary flow			
Dynamic Modulus	|E*|	Temperature and frequency sweep	Rutting prediction algorithms available for master curves	Coring and sawing required
		Unconfined		Requires multiple days to test
APA	cycles to 10 mm rut depth	PG Base Grade	Equipment widely available	Does not measure fundamental material property
		1724 kPa	Short test duration	
		1113 N	Ability to test field cores	
		4,000 cycles	Ability to test specimens from mixture design	

The repeated load test, the static creep test, and the APA tests all required two hours or less, allowing for testing of at least three replicates in one day. The APA tested six specimens simultaneously, providing even greater efficiency. The dynamic modulus test typically required one day for each test temperature, resulting in multiple days to complete testing. To reduce test time, the dynamic modulus could be measured at one temperature (high PG grade) using a single frequency. In this case, the test time would be similar to the other methods.

The repeated load, static creep, and dynamic modulus tests required one additional day for specimen preparation. The test specimens had to be cored and sawn to the test dimensions from gyratory-compacted specimens. Also, the unique size requirements of these test specimens did not allow use of the same specimens that were prepared during the volumetric portion of the mixture design. Further, these performance tests could not be directly used as quality assurance tests after construction because the specimen height required for each of these tests (150 mm) is greater than a typical pavement lift thickness and may be greater than the total pavement thickness. Any of these test methods will likely have different results if the tests are performed on multiple pavement layers stacked into a column.

The APA test can be performed on specimens produced from the volumetric portion of the mixture design if they are sawn to reduce the height from 115 mm to 75 mm. Figure 66 shows an example of performing APA tests on mixture design specimen during this study. The APA curves represent average APA rut depths from two specimens. The APA results are influenced by the binder content of the mixture. For this mixture(3.5 percent air voids), the design binder content was 6.2 percent. Adding additional binder (and subsequently lowering air voids) promotes rutting in the mixture. In this case, insufficient binder (greater than 3.5 percent air voids) also caused the mixture to have higher rutting susceptibility. The mixture produced at the design air void content had the greatest stability and rutting resistance.

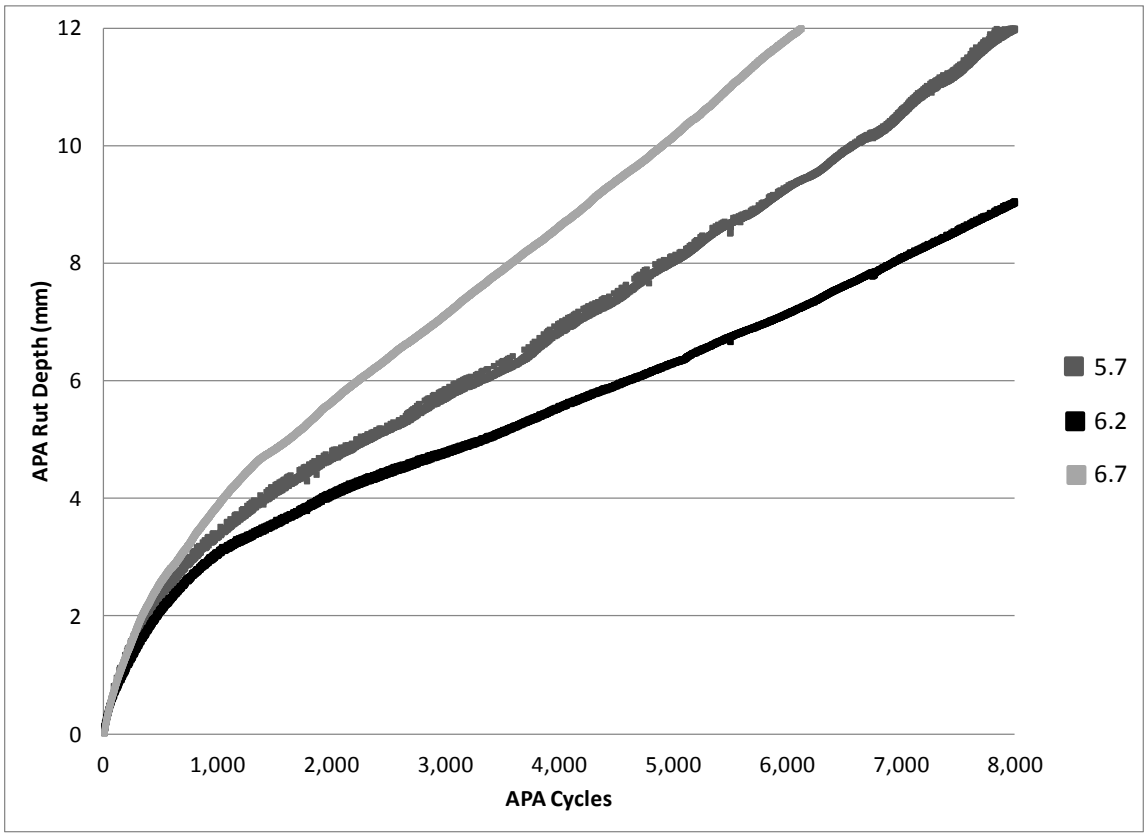

Figure 66. APA test results from mixture design specimens for 19 FGN0 mixture

Ideally, the APA test criterion could eliminate over-asphalting mixtures of marginal quality during mixture design. A specific example is given in Figure 67. In this case, the design binder content was 5.0 percent. Increasing the binder content by 0.4 percent still produced a mixture that would pass the proposed criterion. However, when the binder content was increased by 0.9 percent, the mixture failed the proposed criterion.

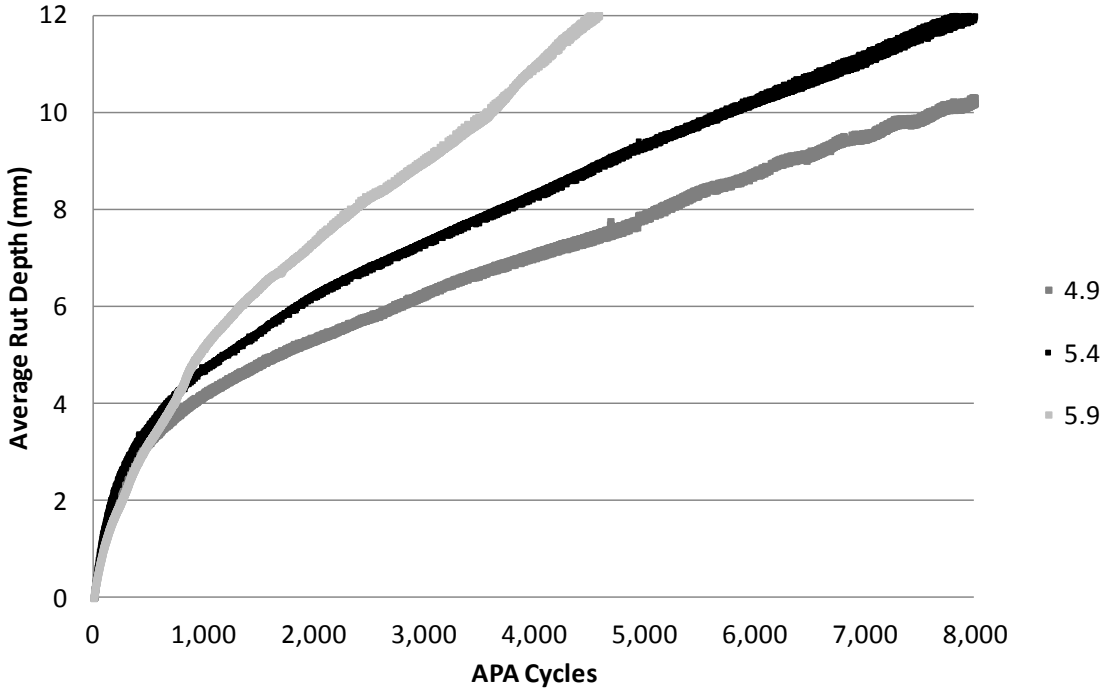

Figure 67. APA test results from mixture design specimens for 12.5 CLS10 mixture

Using mixture design specimens for APA testing eliminates a step in the testing procedure and improves efficiency. Additionally, the APA can be used as a quality assurance test on 150-mm-diameter cores from a constructed pavement. For pavements greater than 75 mm thick, the specimens can be sawn to remove the lower portion. For pavements less than 75 mm thick, a spacer can be placed below the specimen. Because the critical shear stresses applied by the APA are on the surface of the specimen, a 50- to 63-mm surface lift can be tested using the same acceptance criterion.

For these reasons, the APA test is best suited for a performance test in HMA mixture design with potential for use in HMA construction quality assurance. The APA test equipment is widely available and produces very similar rankings to the other

performance tests evaluated by this study. The APA hose pressure can be adjusted to account for varying design aircraft at specific airport locations. The coefficient of variation of the APA test data is similar to FN, FT, and dynamic modulus data. The major disadvantage of the APA is its purely empirical nature. Correlations should be developed between APA test results on laboratory-produced HMA, APA test results on plant-produced HMA, and in-service pavement rutting caused by high tire pressure aircraft.

CHAPTER XI

CONCLUSIONS AND RECOMMENDATIONS

Conclusions

There is a pressing need for a performance test to accompany HMA mixture design for airport pavements. Although the Marshall design method uses an empirical index test, a new design method using the SGC relies only on volumetric properties of the compacted mixture for acceptance. This study investigated the suitability of the repeated load test, static creep test, dynamic modulus test, and APA test for characterizing HMA for airport pavements subjected to high tire pressure aircraft. An asphalt mixture of marginal quality in terms of rutting was constructed and trafficked using an accelerated pavement test device under two different loading and environmental conditions to validate the proposed acceptance limits for the different performance tests. Further investigations of material properties influencing rutting were performed using finite element modeling by simulating aircraft loads on an HMA layer modeled by PANDA. The following conclusions were made from this study:

Although 29 mixtures met all aggregate property and volumetric requirements for use in airport asphalt concrete paving, the performance test results indicated large differences in rutting susceptibility. Resistance to rutting cannot be controlled by these properties alone. A rutting performance test is needed to screen potential paving mixtures.

Repeated load tests on 100-mm-diameter by 150-mm-high cylindrical specimens using a confining pressure of 276 kPa and axial stress of 1380 kPa produced reasonable rankings of mixture performance. Under these test conditions, the onset of tertiary flow ranged from 237 to 1,236 load cycles for mixtures meeting FAA specifications and having a neat binder. Tertiary flow was observed at approximately 50 load cycles for mixtures containing 30 percent natural sand. The onset of tertiary flow occurred between 1,365 and 4,224 load cycles for mixtures meeting FAA specifications and having a polymer-modified binder.

Static creep tests on 100-mm-diameter by 150-mm-high cylindrical specimens using a confining pressure of 276 kPa and axial stress of 1380 kPa produce reasonable rankings of mixture performance. Under these test conditions, the onset of tertiary flow ranged from 63 to 359 sec for mixtures meeting FAA specifications and having a neat binder. Tertiary flow was observed at approximately 8 sec for mixtures containing 30 percent natural sand. The onset of tertiary flow occurred between 533 and 1,534 sec for limestone and granite mixtures meeting FAA specifications and having a polymer-modified binder. Tertiary flow began at 267 and 284 sec, respectively, for the two chert gravel mixtures prepared using a polymer-modified binder.

Dynamic modulus test results alone did not necessarily produce reasonable ranking of mixture rutting performance. A reasonable ranking was produced by using dynamic modulus master curves to determine the modulus of the mixtures at the high PG binder grade (64°C) and 1.0-Hz loading. At lower temperatures and higher loading rates, the stiffnesses of the mixtures were relatively uniform and highly dependent on binder

properties. The differences in moduli were observed only at the conditions when the binder was softest (high temperatures or slow loading rates).

The APA test using a hose pressure of 1724 kPa rapidly damaged HMA specimens. Most mixtures reached the terminal rut depth of 12 mm before 8,000 cycles were applied. None of the mixtures tested in this study had less than 6-mm rut depth after 8,000 cycles in the APA. The mixtures containing 30 percent natural sand reached 12-mm rutting within 1,500 APA cycles.

Of the variables included in this study, the most significant factor influencing permanent deformation was excessive natural sand (30 percent). Mixtures containing excessive natural sand showed significantly reduced performance indices. These mixtures exhibited tertiary flow in fewer than 60 cycles of the repeated load test and in fewer than 10 sec during the static creep test. The dynamic modulus of mixtures containing 30 percent natural sand was less than 5,000 MPa. These mixtures failed the APA test in fewer than 1,500 cycles. Including the mixtures with high sand content helped to identify test results that indicated very poor rutting resistance. The performance indices measured for the mixtures containing 30 percent natural sand were considered to be failing. An acceptance threshold for a performance test should be much greater than the indices measured for these mixtures.

Using a polymer-modified binder significantly increased the performance of all mixtures used in this study according to each of the four performance tests. For airports experiencing frequent loading by aircraft with high tire pressures, using polymer-

modified asphalt binders in the mixture may be necessary to prevent significant rutting from occurring.

Statistical analyses on performance test indices showed the limestone mixtures used in this study provided better rutting resistance than the granite or chert gravel mixtures according to all four performance tests investigated. Further, mixtures containing 30 percent natural sand had the poorest rutting performance according to indices from each of the four tests. According to the analysis of AIMS data, aggregate texture was a greater indicator of rutting performance than was aggregate angularity. The ability of a performance test to statistically differentiate mixture performance is very important to its contributions as a mixture design tool.

Full-scale accelerated pavement testing provided a reasonable validation of the preliminary test acceptance values developed in this study. The asphalt mixture used in the full-scale tests performed at the minimal levels suggested according to each of the four laboratory test methods. When this mixture was trafficked in conditions that promoted high levels of rutting (high temperature and high tire pressure), the mixture performed somewhat poorly. Over 25 mm of rutting developed after only 3,000 wheel load applications. However, when the mixture was trafficked in more moderate loading conditions (moderate temperature and moderate aircraft tire pressure), the mixture performed very well. Very little rutting was attributed to the asphalt concrete layer after 180,000 wheel load applications. Using the recommended performance test threshold acceptance values should produce pavements that perform well under normal field conditions.

Computational simulations of the pavement structure and loading conditions from the full-scale tests replicated in ABAQUS used with the PANDA material model for the asphalt concrete layer produced reasonable predictions of nonlinear viscoelastic strain and viscoplastic strain. The predicted magnitude of the viscoplastic strain was nearly five orders of magnitude greater for the conditions of Field-test 1 (high temperature and tire pressure) compared to the conditions of Field-test 2 (moderate temperature and tire pressure). The magnitude of the viscoplastic strain predicted for Field-test 1 was greater than that observed during the full-scale accelerated pavement testing. However, these simulations considered 2-dimensional pulse loading in one location, while field-testing consisted of a moving wheel load and lateral wander. The nonlinear viscoelastic strains predicted by the model were similar for each loading case. PANDA offered a unique ability to model rutting for any aircraft load since the model simulations were performed in finite element software and the loading conditions were user-defined.

The slope of the static creep data plotted on a log-log scale is the performance index having the lowest coefficient of variation (7 percent). The slope of the repeated load data also has a very reasonable coefficient of variation (9 percent). These indices are less variable than the indices related to the onset of tertiary flow for these tests. The coefficient of variation of the dynamic modulus test is accepted to be approximately 14 percent. The APA has a coefficient of variation of 20 percent. The coefficient of variation should be a reasonable value for a selected performance test to provide statistical confidence in the test results compared to the specified threshold values.

The APA test is the only performance test evaluated by this study that can be performed on specimens produced by the SGC during mixture design because of the required specimen geometries. Additionally, the APA is the only performance test evaluated by this study that could be used for quality assurance on asphalt concrete paving projects because of specimen size and shape. Currently, the APA with the high-pressure equipment option is not widely used. This limits its applicability; however, it may become a viable option in the future.

Recommendations

Based on the results and conclusions from this study, the APA should be considered as a performance test to accompany mixture design for airport asphalt concrete with high tire pressure aircraft traffic. The test should be performed on 150-mm-diameter by 75-mm-high cylindrical specimens. The specimens should be compacted using the design number of gyrations in the SGC and at the design binder content. The air void content of the compacted specimens should be approximately 3.5 percent.

The test temperature should be adjusted to the high temperature of the base PG binder grade. If polymer-modified binders are used to prepare specimens, the test temperature should be that of the unmodified counterpart for a given climate. The APA hose pressure should be adjusted to 1724 kPa. The vertical load applied by the metal rollers should be 1113 N. The test duration should be at least 4,000 cycles, and the terminal rut depth should be set to 12 mm. A preliminary criterion of less than 10-mm rutting after 4,000 APA cycles is recommended for mixture acceptance.

An alternative recommendation for a performance test is the static creep test. The test should be performed on 100-mm-diameter by 150-mm-high cylindrical specimens. The specimens should be compacted in the SGC at the design binder content to achieve an average air void content of approximately 3.5 percent. Specimens can be prepared in the SGC using a 150-mm-diameter mold by compacting to a height of 170 mm. A core saw should be used to cut the specimen to the desired 100-mm diameter. Both ends of the specimen should be cut to reduce the specimen height to 150 mm.

The test temperature should be adjusted to the MMPT according to the procedure described by Witczak for the selected climate. The creep test should be performed in a triaxial cell using a uniaxial loading device. The confining pressure should be adjusted to 276 kPa. The axial stress should be adjusted to 1380 kPa. The data acquisition system should record displacement as a function of time. The static load should be applied until approximately 8 percent strain is achieved or until tertiary flow occurs. The permanent deformation versus time should be plotted on a log-log scale. The slope of the linear region of the data should be used as a performance index. A preliminary criterion of a slope value of 0.45 or less is recommended for mixture acceptance.

It is recommended that the FAA require contractors to submit approved mixture designs and materials for testing according to the selected performance test during a preliminary implementation phase. These submissions should be limited to HMA designed for aircraft with tire pressures exceeding 690 kPa or aircraft gross weight exceeding 267 kN. These submissions should also be limited to surface course materials. Because the recommendations from this study are limited to the materials and tests

evaluated herein, the FAA should validate the test requirements from JMF submissions during the implementation phase, including mixtures with different aggregate types and binder grades.

Further investigations should determine the correlation of the performance test results with actual in-service pavement rutting. The FAA should develop a database of performance test results for surface mixtures placed at multiple airports throughout the United States. Future studies should investigate the rutting that occurred on pavements constructed using these mixtures during the first two years of their service life.

Future work should also include identifying an appropriate criterion for quality assurance testing of plant-produced mixture using the selected performance test. The criterion for quality assurance may be different from the mixture design criterion because of changes to the mixture properties during plant production. Guidance for test frequency, location, conditions, and acceptance criteria should be developed.

The PANDA material model should be further investigated as a tool for predicting rutting performance of asphalt mixtures on airports. Simulations should be performed on the mixture investigated in this study using the 3-dimensional wheel load option to better compare with field measurements. Further enhancements should be made to include lateral wander in the moving wheel load simulations to obtain more accurate predictions of field performance. Additional work should investigate the applicability of the damage model, healing model, and moisture damage model in PANDA to airport pavements.

REFERENCES

AASHTO. 2013. *Calibration of the Pavement Analysis Using Nonlinear Damage Approach (PANDA) Constitutive Model.* AASHTO draft specification.

ABAQUS. 2012. Version 6.12. Providence, RI: Habbit, Karlsson and Sorensen, Inc.

Abu Al-Rub, R.K., M.K. Darabi, C.W. Huang, E.A. Masad, and D.N. Little. 2012. Comparing finite element and constitutive modeling techniques for predicting rutting of asphalt pavements. *International Journal of Pavement Engineering* 13(4):322–338.

Ahlrich, R.C. 1996. *Influence of Aggregate Gradation and Particle Shape/Texture on Permanent Deformation of Hot Mix Asphalt Pavements*. Technical Report GL-96-1, Vicksburg, MS: U.S. Army Engineer Waterways Experiment Station.

Brown, E.R., P.S. Kandhal, and J. Zhang. 2001. *Performance Testing for Hot Mix Asphalt*. NCAT report 1-05, November.

Brown, E.R., B. Prowell, A. Cooley, J. Zhang, and B. Powell. 2004. Evaluation of Rutting Performance on the 2000 NCAT Test Track. In *Journal of the Association of Asphalt Paving Technologists* 73:287-236, Baton Rouge, LA.

Bureau of Public Roads. 1962. *Aggregate Gradation for Highways*. United States Government Printing Office, Washington, DC, May 1962.

Button, J.W., D. Perdomo, and R.L. Lytton. 1990. Influence of Aggregate on Rutting in Asphalt Concrete Pavements. *Transportation Research Record 1259*, TRB, National Research Council, Washington, DC.

Chou, Y.T. 1977. *Analysis of Permanent Deformations of Flexible Airport Pavements*. WES TR S-77-8. Vicksburg, MS: US Army Engineer Waterways Experiment Station.

Christensen, D., T. Bennert, R.D. McQueen, and H. Brar. 2010. Superpave Gyratory Compaction Requirements for FAA's Hot Mix Asphalt Specification. In *Proceedings of the 2010 FAA Worldwide Airport Technology Transfer Conference, Atlantic City, New Jersey, April 2010*.

Collop, A.C., D. Cebon, and M.S.A. Hardy. 1995. Viscoelastic Approach to Rutting in Flexible Pavements. American Society of Civil Engineers. *Journal of Transportation Engineering* 121(1):82-83.

Consuega, A., D.N. Little, H.Von Quintus, and J. Burati. 1989. Comparative Evaluation of Laboratory Compaction Devices Based on Their Ability to Produce Mixtures with Engineering Properties Similar to Those Produced in the Field. In *Transportation Research Record 1228*, Transportation Research Board. Washington, DC: National Research Council, pp 80-87.

Cooley, L.A. Jr., R.C. Ahlrich, R.S. James, B.D. Prowell, and E.R. Brown. 2007. Implementation of Superpave Mix Design for Airfield Pavements. In *Proceedings of*

the 2007 FAA Worldwide Airport Technology Transfer Conference, Atlantic City, NJ.

Cooley, L.A. Jr., R.C. Ahlrich, R.S. James, B.D. Prowell, and E.R. Brown. 2009. *Implementation of Superpave Mix Design for Airfield Pavements*. Airport Asphalt Pavement Technology Program Report 04-03. Auburn, AL.

Darabi, M.K., R.K. Abu Al-Rub, E.A. Masad, C.W. Huang, and D.N. Little. 2011. A thermoviscoelastic- viscoplastic-viscodamage constitutive model for asphaltic materials. *International Journal of Solids and Structures* 48(1):191-207.

Darabi, M.K., R.K. Abu Al-Rub, E.A. Masad, and D.N. Little. 2013. Cyclic Hardening-Relaxation Viscoplasticity Model for Asphalt Concrete Materials. ASCE *Journal of Engineering Mechanics* 139:832-847.

Elliot, R.P., M.C. Ford, Jr., M. Ghanim, and Y.F. Tu. 1991. Effect of Aggregate Gradation Variation on Asphalt Concrete Mix Properties. *Transportation Research Record 1317*. TRB. Washington, DC: National Research Council.

Field, F. 1957. The Effect of Percent Crushed Variation in Coarse Aggregate for Bituminous Mixes. In *Proceedings of Association of Asphalt Paving Technologists,* Volume 27.

Gabrielson, J.R. 1993. Evaluation of Hot Mix Asphalt (HMA) Static Creep and Repeated Load Tests. Ph.D Thesis, Auburn University.

Gaudette, B.E., and R.A. Welke. 1977.*Investigation of Crushed Aggregates for Bituminous Mixes*. Research Report Number TB-58. Michigan Department of State Highways and Transportation.

Hofstra, A. and A.J.G. Klomp. –Permanent Deformation of Flexible Pavements Under Simulated Road Traffic Conditions," Proceedings, Third International Conference on the Structural Design of Asphalt Pavements, London, 1972, pp 613-612.

Huang, C.W., R.K. Abu Al-Rub, E.A. Masad, D.N. Little, and G. Airey. 2011. Numerical implementation and validation of a nonlinear-viscoelastic and viscoplastic model for asphalt concrete mixes. *International Journal of Pavement Engineering* 12(4):433-447.

Huang, B., and X. Shu. 2009. Correlating APA to Field Permanent Deformation for HMA Mixes at the NCAT Test Track. In *Proceedings of the GeoHunan International Conference, 2009.*

Kandhal, P.S., J.B. Motter, and M.A. Khatri. 1991. *Evaluation of Particle Shape and Texture: Manufactured Versus Natural Sands*. NCAT 91-03. Auburn University. Auburn, AL: National Center for Asphalt Technology.

Kim, Y.R., N. Yim, and N.P. Khosla. 1992. *Effects of Aggregate Type and Gradation on Fatigue and Permanent Deformation of Asphalt Concrete*. American Society of Testing and Materials STP 1147. Philadelphia, PA.

Krutz, N.C., and P.E. Sebaaly. 1993. The Effects of Aggregate Gradation on Permanent Deformation of Asphalt Concrete. In *Proceedings of Association of Asphalt Paving Technologists, Vol 62*.

Leahy, R.B. 1989. Permanent Deformation Characteristics of Asphalt Concrete. Ph.D thesis. University of Maryland.

Masad, E., T. Al-Rousan, J. Button, D. Little, and E. Tutumluer. 2005. *Test Methods for Characterizing Aggregate Shape, Texture and Angularity*. NCHRP 4-30A Final Report, Report Number 555. National Cooperative Highway Research Program. Washington, DC: National Research Council.

Mohammad, L.N, Z. Wu, S. Obulareddy, S. Cooper, and C. Abadie. 2006. Permanent Deformation Analysis of Hot-Mix Asphalt Mixtures with Simple Performance Tests and 2002 Mechanistic-Empirical Pavement Design Software. *Transportation Research Record 1970*. TRB. Washington, DC: National Research Council, pp 133-142.

Moore, R.B., and R.A. Welke. 1979. *Effects of Fine Aggregate on Stability of Bituminous Mixes*. Research Report Number 78 TB-34-79F. Michigan Department of State Highways and Transportation.

Panda Parameter Identifier (PPI). 2013. Texas A&M University.

Panda User Interface. (PUI). 2013. Texas A&M University.

Perzyna, P. 1971. Thermodynamic theory of viscoplastcity. *Advances in Applied Mechanics* 11:313–354.

Roberts, F.L., P.S. Kandhal, E.R. Brown, D.-Y. Lee, and T.W. Kennedy. 1996. *Hot Mix Asphalt Materials, Mixture Design and Construction*. Second Edition. Lanham, MD: NAPA Education Foundation.

Rushing, J.F. 2009. Development of Criteria for Using the Superpave Gyratory Compactor to Design Airport Pavement Mixtures. Master's Thesis. Mississippi State University, Mississippi State, MS.

Rushing, J.F., D.N. Little, and N. Garg. 2012. Asphalt Pavement Analyzer Used to Assess Rutting Susceptibility of Hot-Mix Asphalt Designed for High Tire Pressure Aircraft. Transportation Research Record: *Journal of the Transportation Research Board*, No. 2296, pp. 97-105.

Schapery, R.A. 1969. On the characterization of nonlinear viscoelastic materials. *Polymer Engineering and Science* 9:295–310.

Shami, H.I., J.S. Lai, J.A. D'Angelo, and T.P Harman. 1997. Development of Temperature-Effect Model for Predicting Rutting of Asphalt Mixtures Using Georgia Loaded Wheel Tester. *Transportation Research Record 1590*. TRB. Washington, DC: National Research Council, pp 17-22.

Shenoy, A., and P. Romero. 2002. Standardized Procedure for Analysis of Dynamic Modulus Data to Predict Asphalt Pavement Distress. *Transportation Research Record 1789*. TRB. Washington, DC: National Research Council, pp 173-182.

Sotil, A., K.E. Kaloush, and M.W. Witczak. 2004. Reduced Confined Dynamic Modulus Testing Protocol for Asphalt Mixtures. *Transportation Research Record 1891*. TRB. Washington, DC: National Research Council, pp 153-162.

Tran, N.H., and K.D. Hall. 2006. Evaluation of Testing Protocols for Dynamic Modulus of Hot-Mix Asphalt. *Transportation Research Record 1970*. TRB. Washington, DC: National Research Council, pp 126-132.

U.S. Army Corps of Engineers. 1994. *Standard Test Method for Determining Percentage of Crushed Particles in Aggregate*. CRD-C171-94.

U.S. Department of Transportation. 2009. *Standards for Specifying Construction of Airports.* Advisory Circular 150/5370 10 E. Federal Aviation Administration.

Von Quintus, H.L., J. Mallela, R. Bonaquist, C.W. Schwartz, and R.L. Carvalho. 2012. *Calibration of Rutting Models for Structural and Mix Design.* NCHRP Report 719. Transportation Research Board.

Wedding, P.A., and R.D. Gaynor. 1961. The Effects of Using Gravel as the Coarse and Fine Aggregate in Dense Graded Bituminous Mixtures. In *Proceedings of Association of Asphalt Paving Technologists,* Volume 30.

WesTrack Forensic Team. 1998 (June).*Performance of Coarse-Graded Mixes at WesTrack – Premature Rutting*. Final Report.

Witczak, M.W. 1992. A-001 MIDAS Study. Effective Temperature Analysis for Permanent Deformation of Asphaltic Mixtures.

Witczak, M.W. 1996. *Simplified Approach to Determine the Annual Pavement Temperature Distribution.* Work Element 7 – Environmental Effects Mode, Tech Memo 1. College Park, MD: University of Maryland.

Witczak, M.W. 2007. *Specification Criteria for Simple Performance Tests for Rutting*. NCHRP Report 580. Transportation Research Board, National Research Council, Washington DC.

Witczak, M.W., K. Kaloush, T. Peillinen, M.E. Basyouny, and H. Von Quintus. 2002. *NCHRP Report 465: Simple Performance Test for Superpave Mix Desig*n. Transportation Research Board, National Research Council, Washington, DC.

Witczak, M.W. and J. Moulthrop. 2011. *A performance-related specification for hot-mixed asphalt.* NCHRP Report 704. Transportation Research Board, National Research Council, Washington, DC.

Zhang, J., E.R. Brown, P.S. Kandhal, and R. West. 2005. An Overview of Fundamental and Simulative Performance Tests for Hot Mix Asphalt. *Journal of ASTM International* 2(5):1-15.

Zhang, J., L.A. Cooley, and P.S. Kandhal. 2002. *Comparison of Fundamental and Simulative Test Methods for Evaluating Permanent Deformation of Hot Mix Asphalt*. NCAT Report 02-07. Auburn University, AL: National Center for Asphalt Technology.

APPENDIX A

REPEATED LOAD

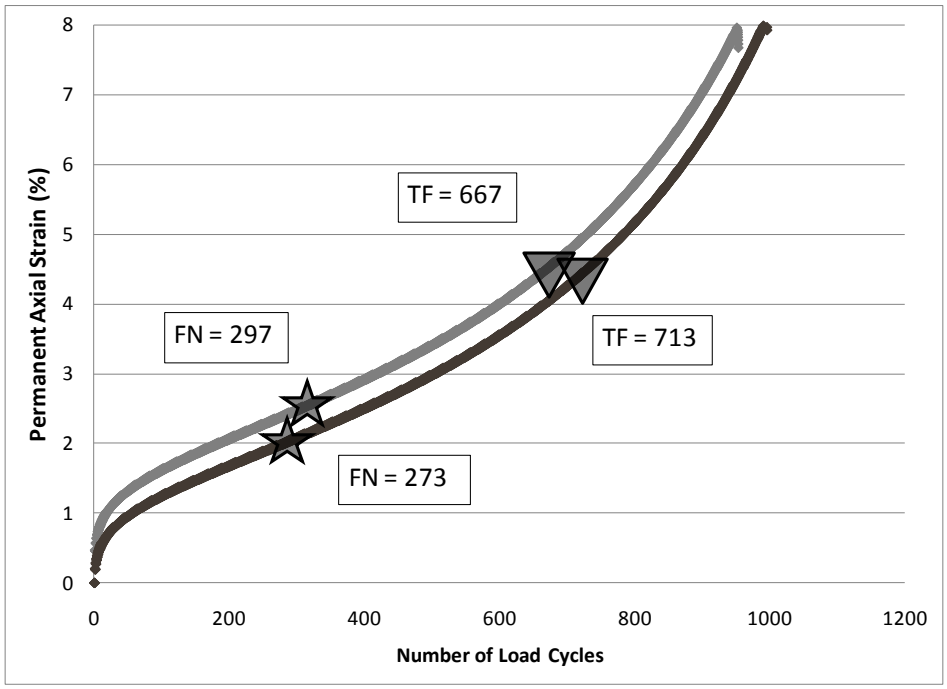

Figure A1. 12.5 FGN0 with PG 64-22

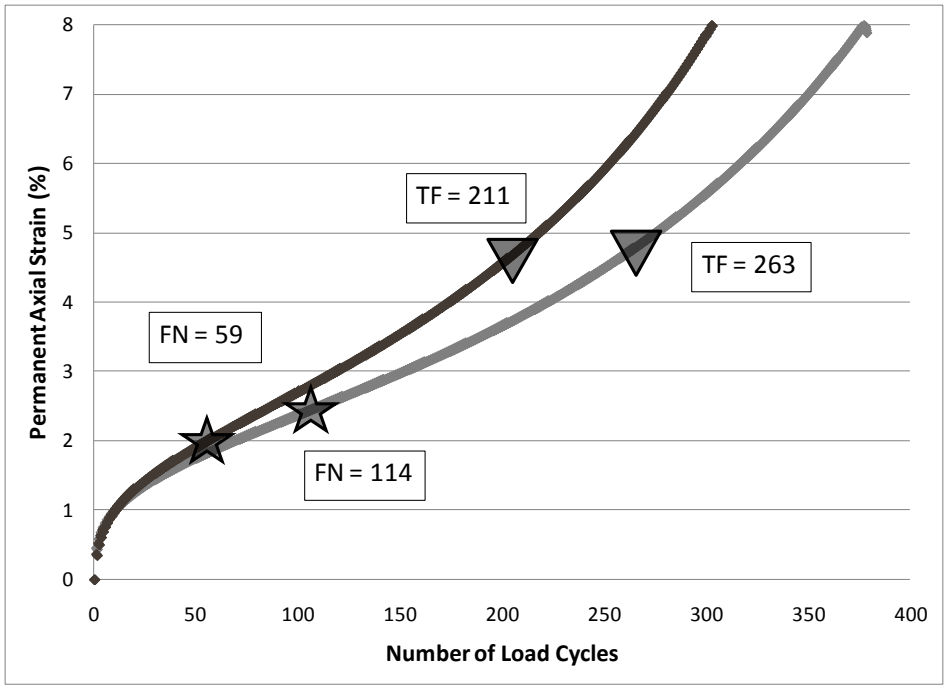

Figure A2. 12.5 CGN0 with PG 64-22

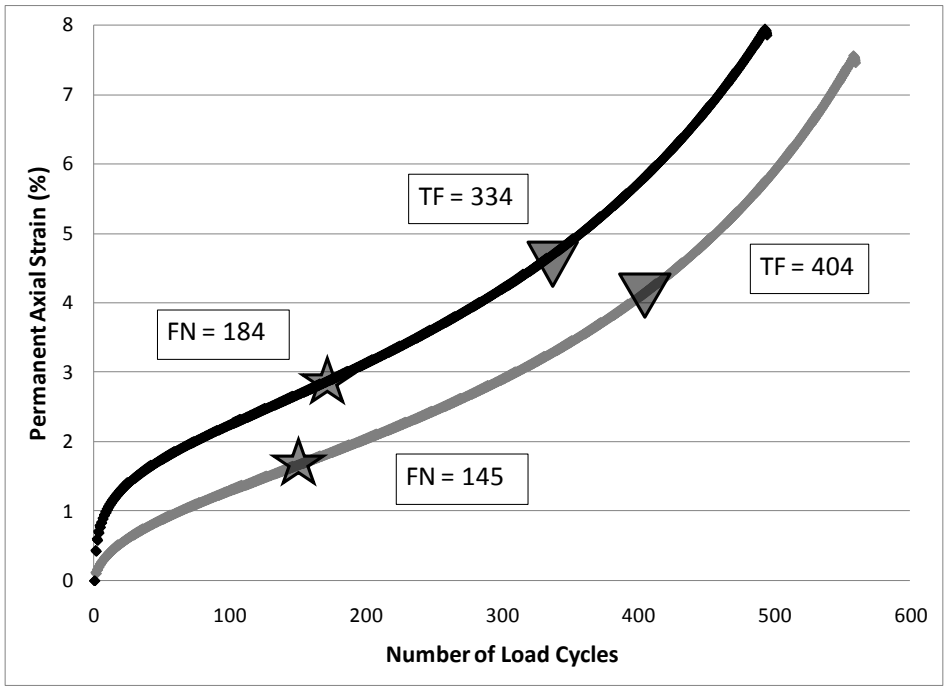

Figure A3. 19 FGN with PG 64-22

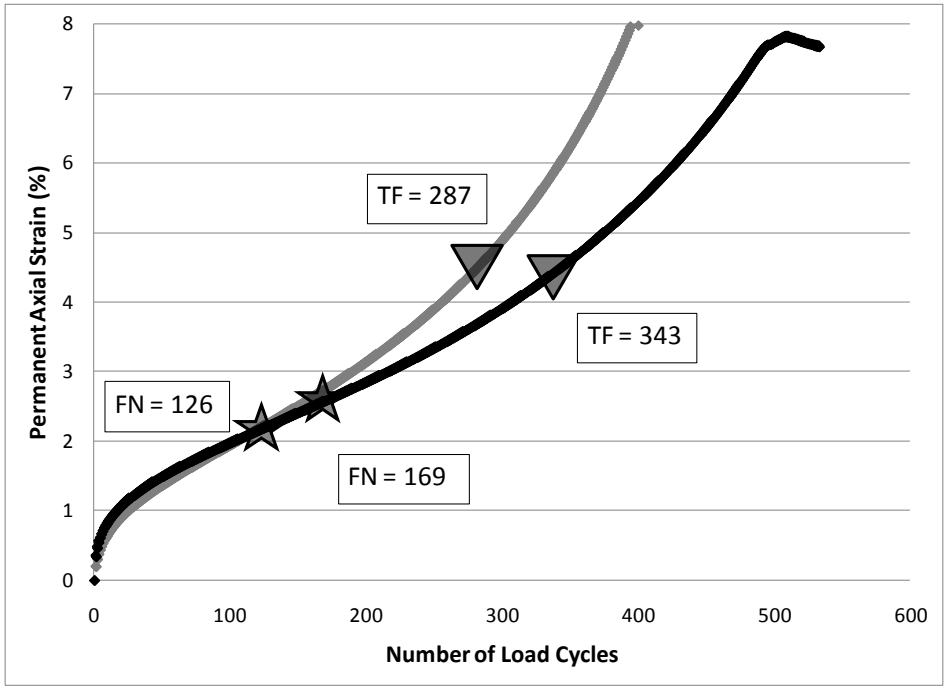

Figure A4. 19 CGN with PG 64-22

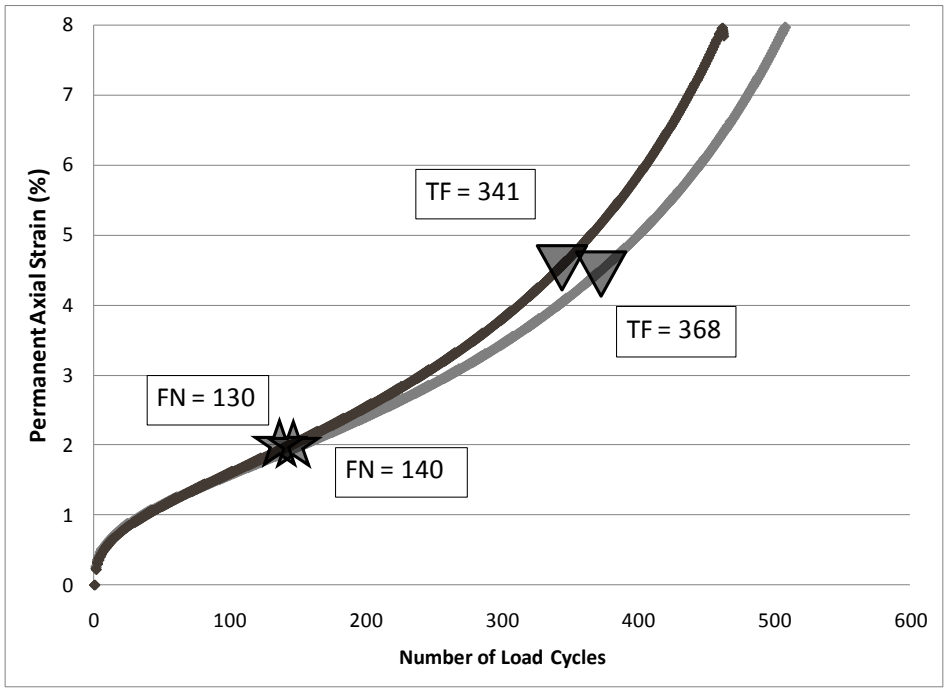

Figure A5. 12.5 FGN10 with PG 64-22

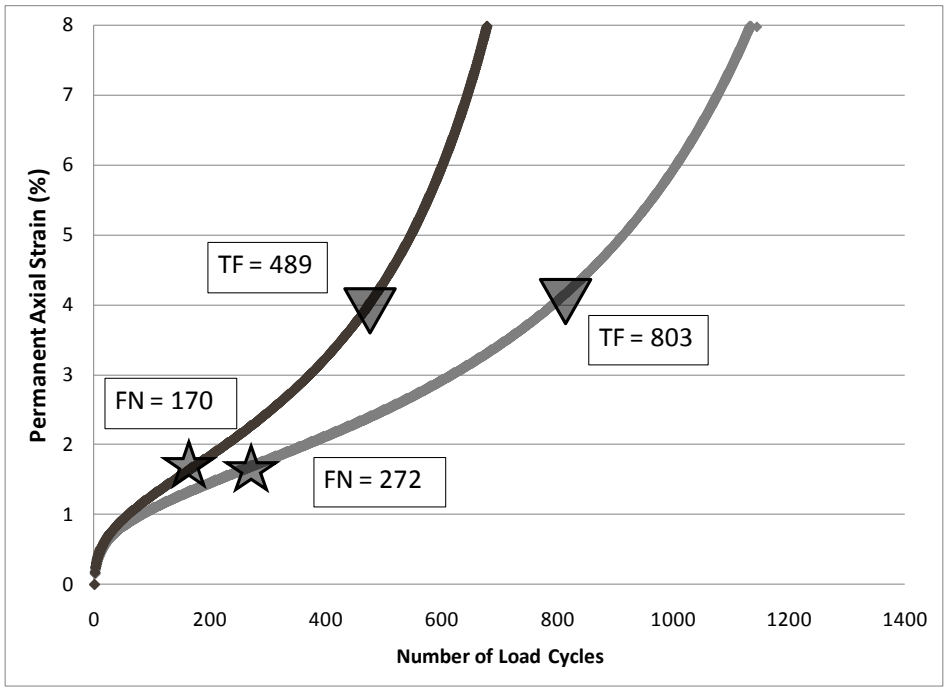

Figure A6. 12.5 CGN10 with PG 64-22

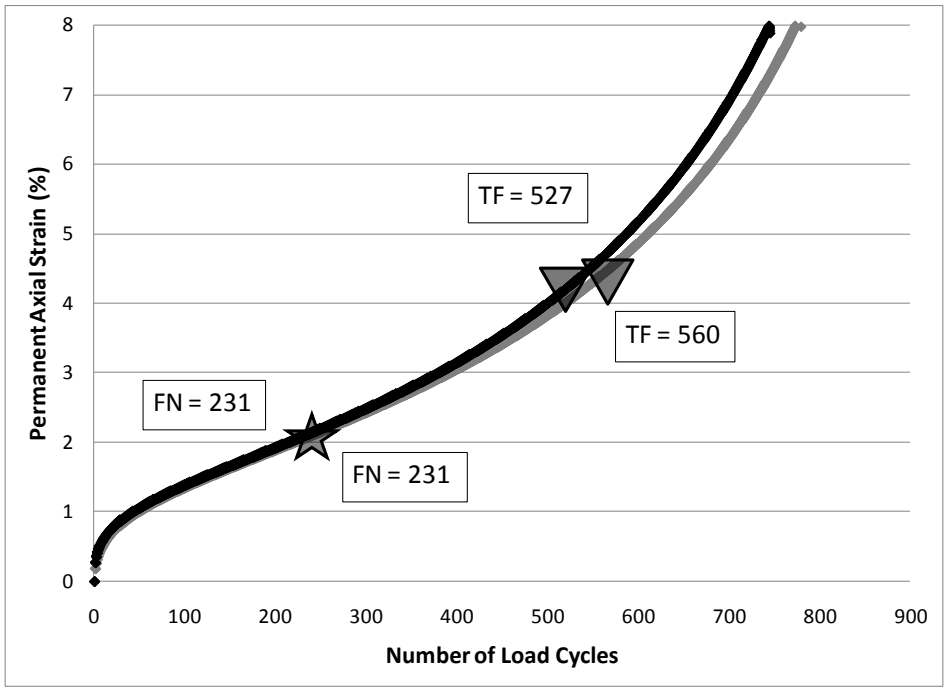

Figure A7. 19 FGN10 with PG 64-22

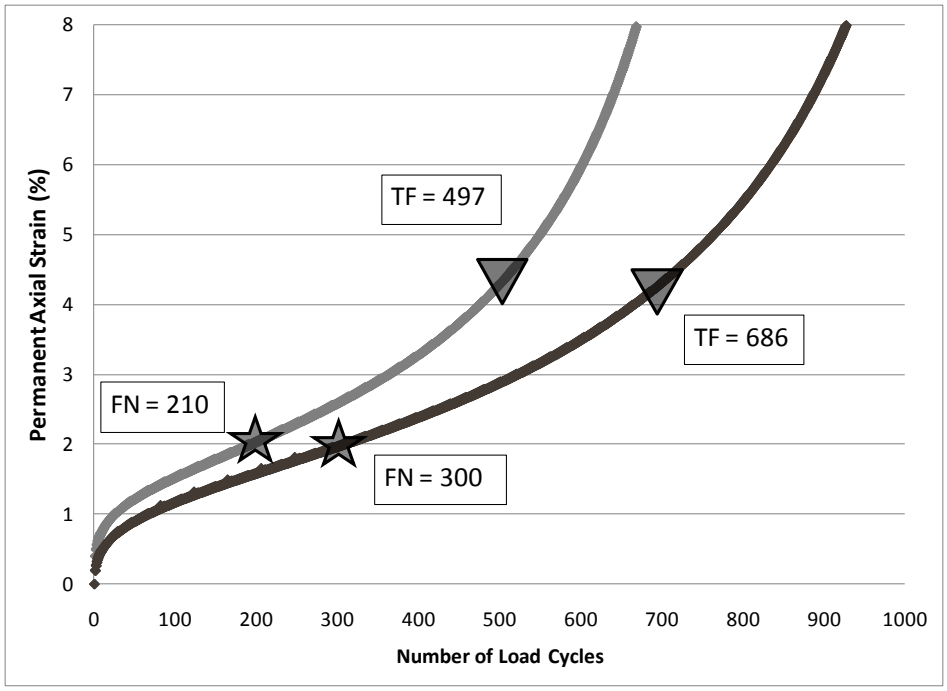

Figure A8. 19 CGN10 with PG 64-22

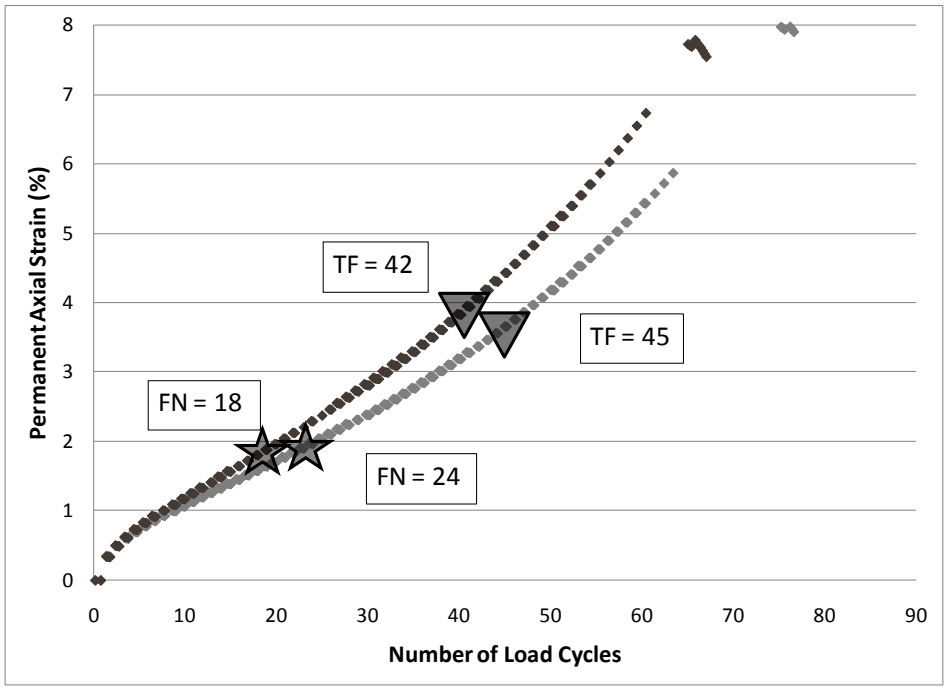

Figure A9. 12.5 FGN30 with PG 64-22

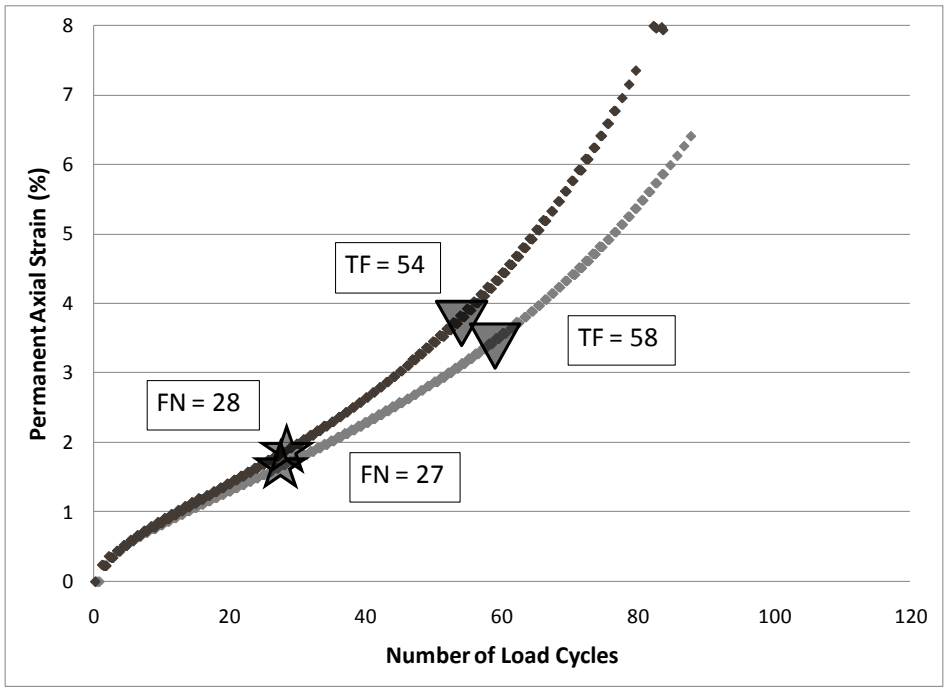

Figure A10. 12.5 CGN30 with PG 64-22

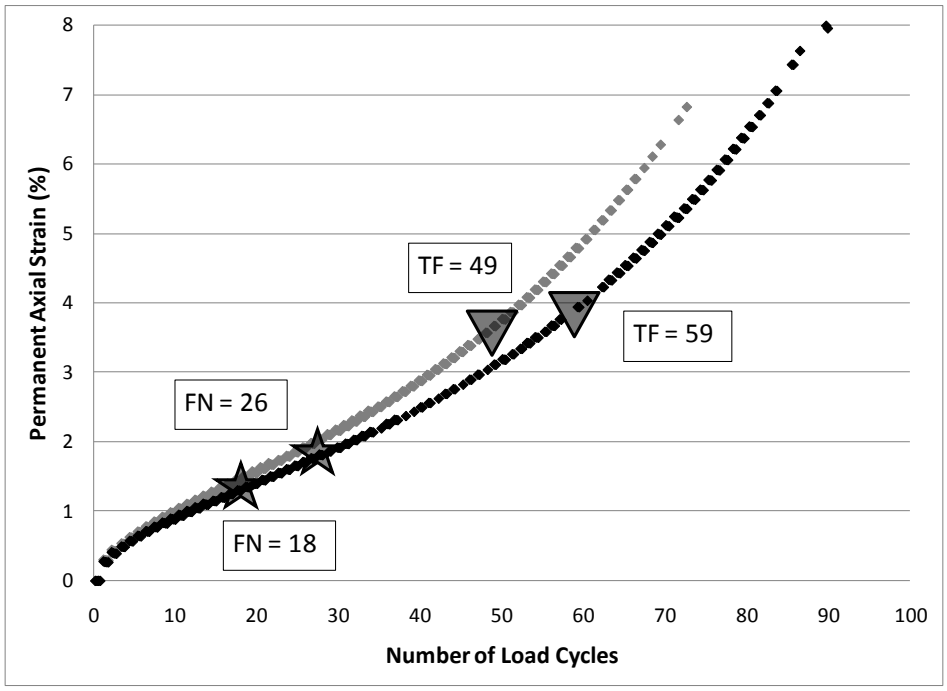

Figure A11. 19 FGN30 with PG 64-22

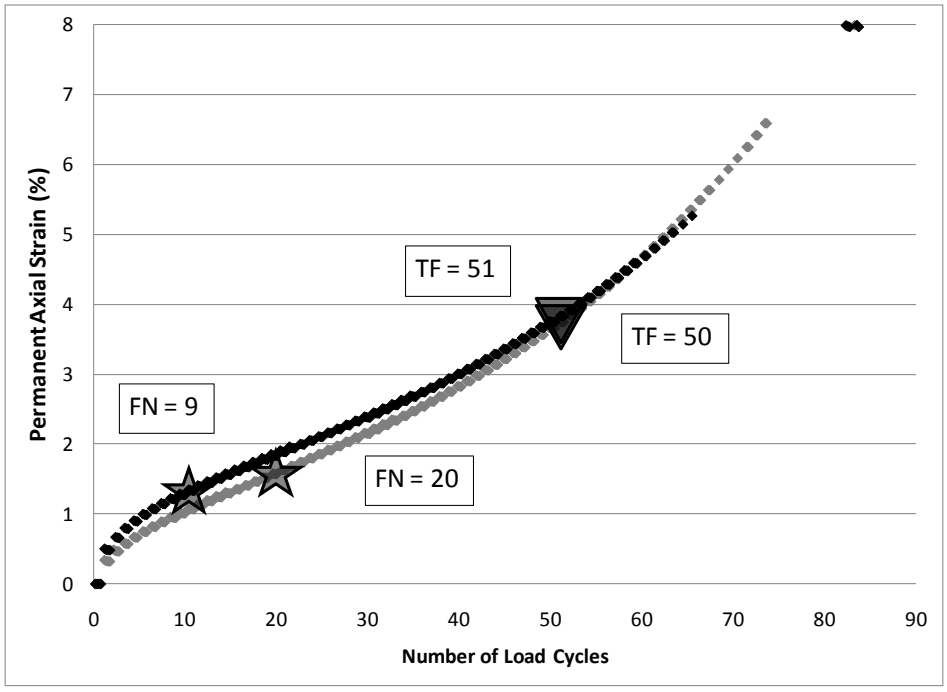

Figure A12. 19 CGN30 with PG 64-22

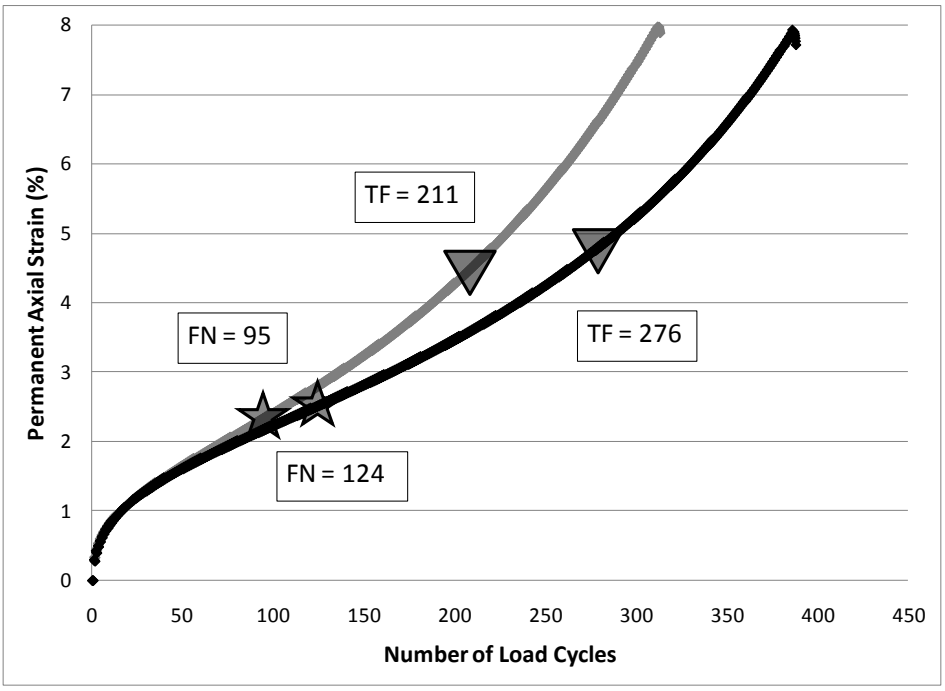

Figure A13. 12.5 GV0 with PG 64-22

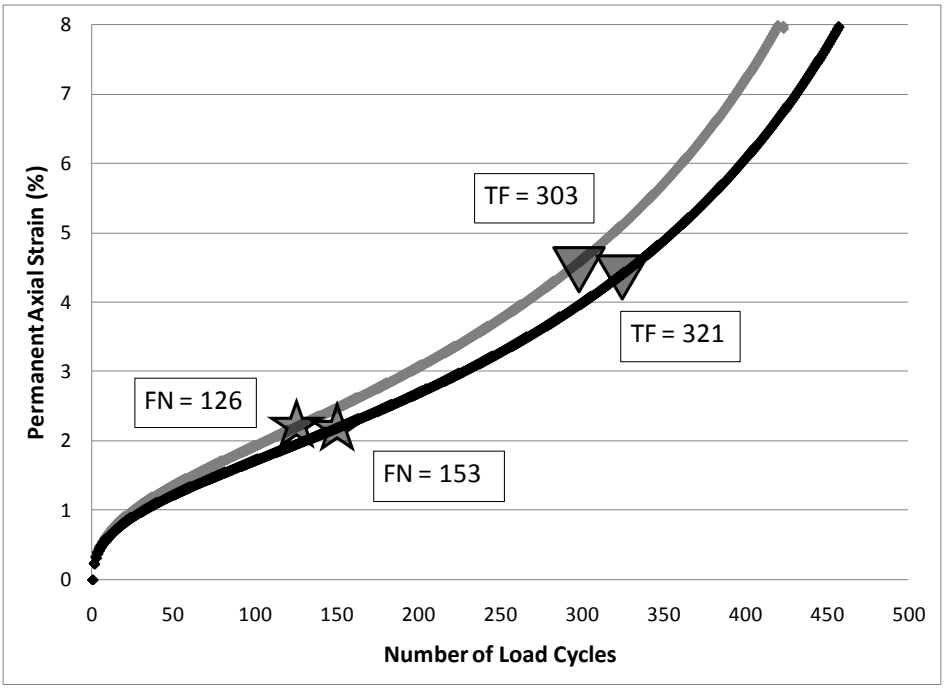

Figure A14. 19 FGV0 with PG 64-22

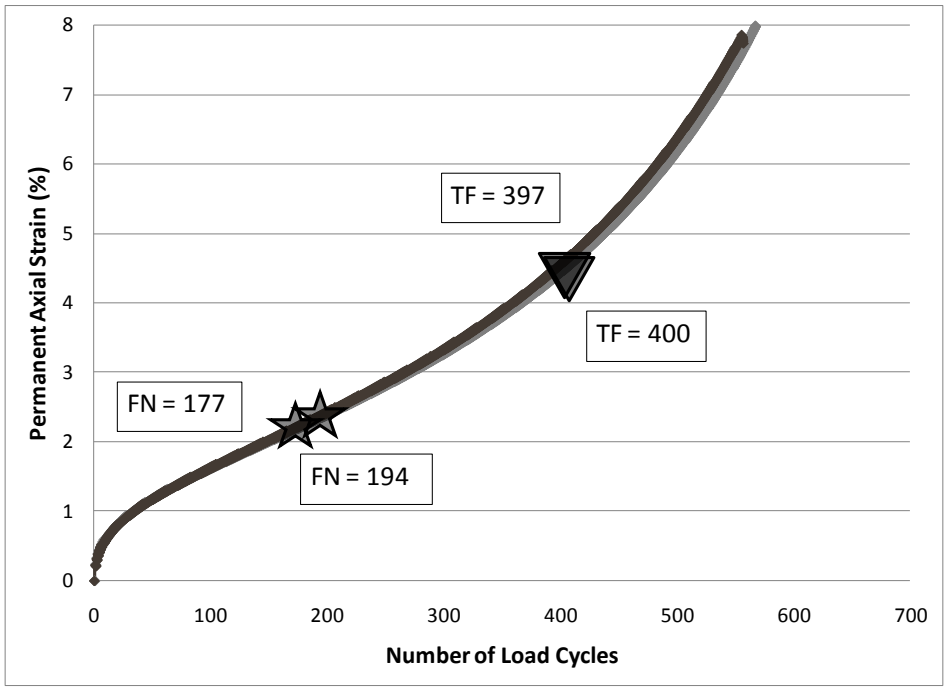

Figure A15. 19 CGV0 with PG 64-22

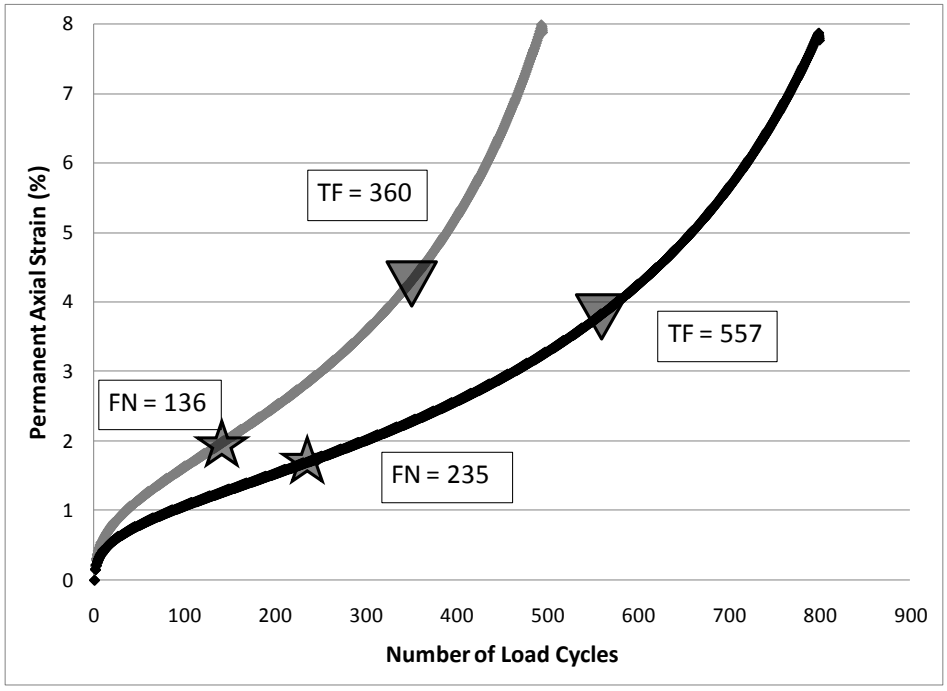

Figure A16. 12.5 GV10 with PG 64-22

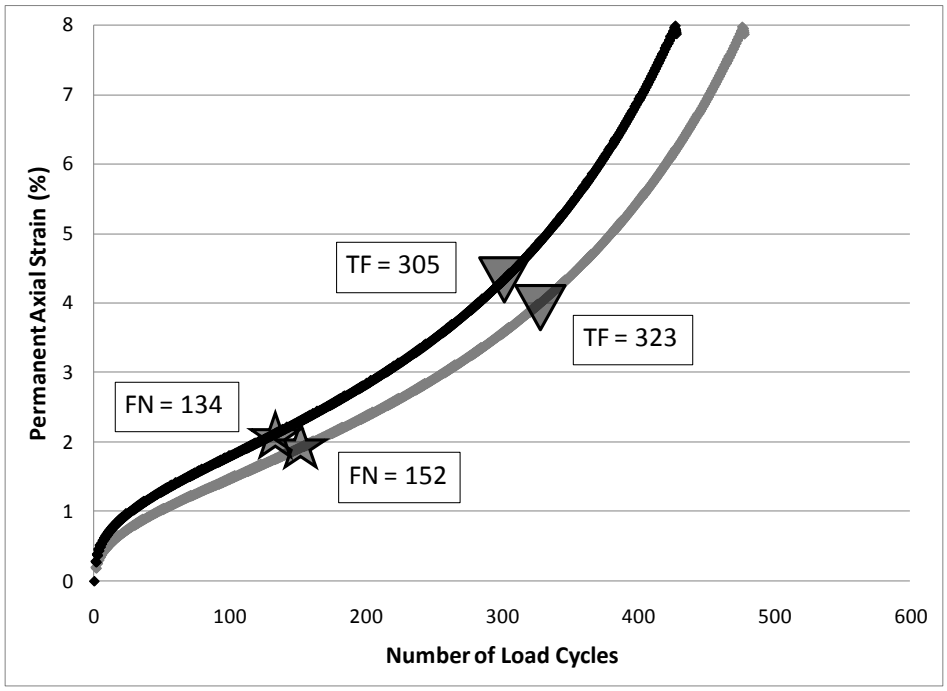

Figure A17. 19 FGV10 with PG 64-22

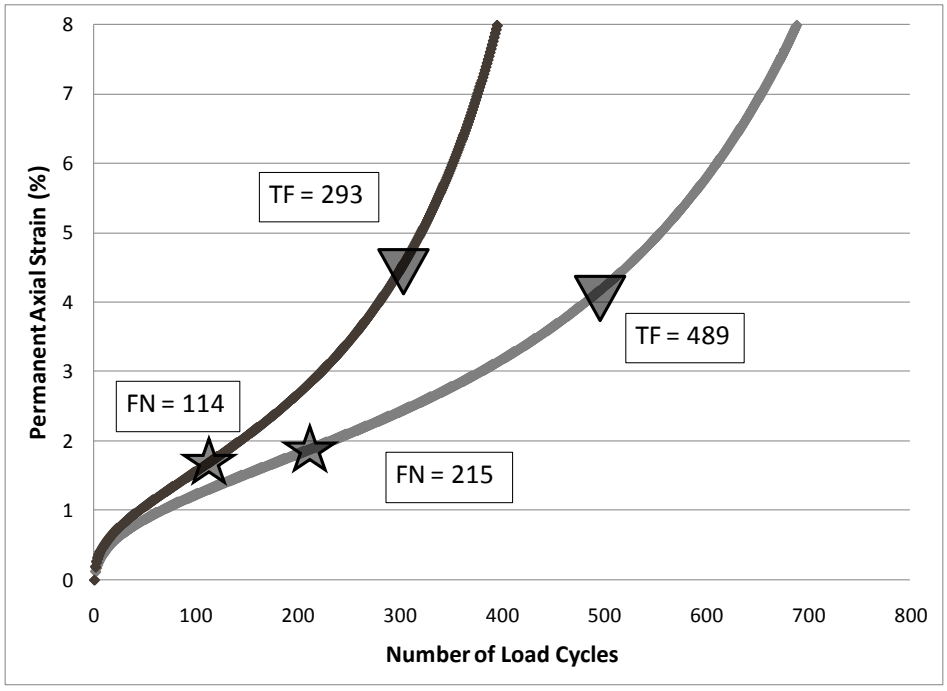

Figure A18. 19 CGV10 with PG 64-22

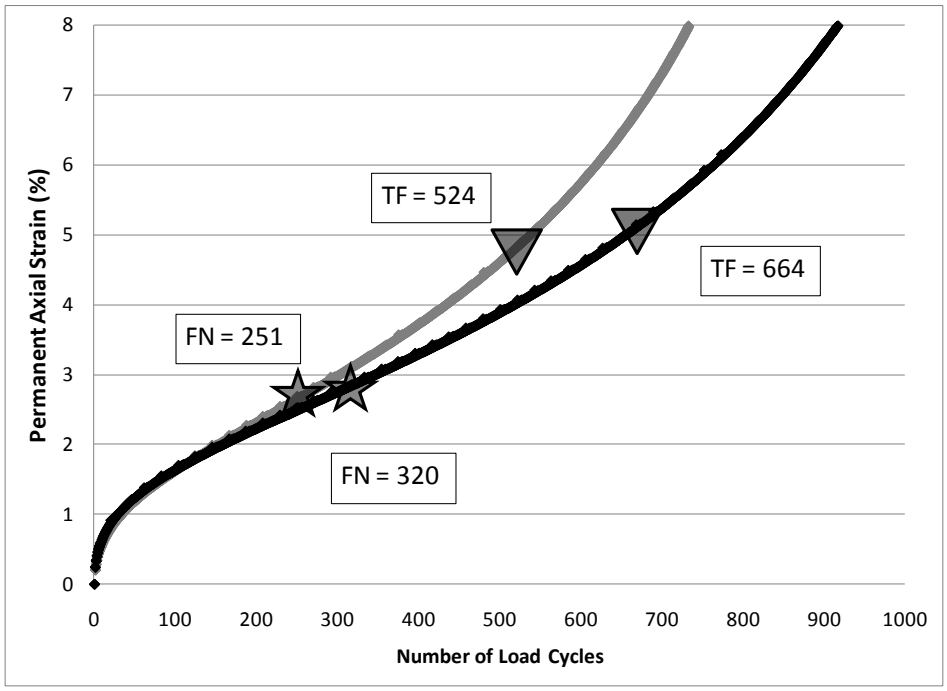

Figure A19. 12.5 FLS0 with PG 64-22

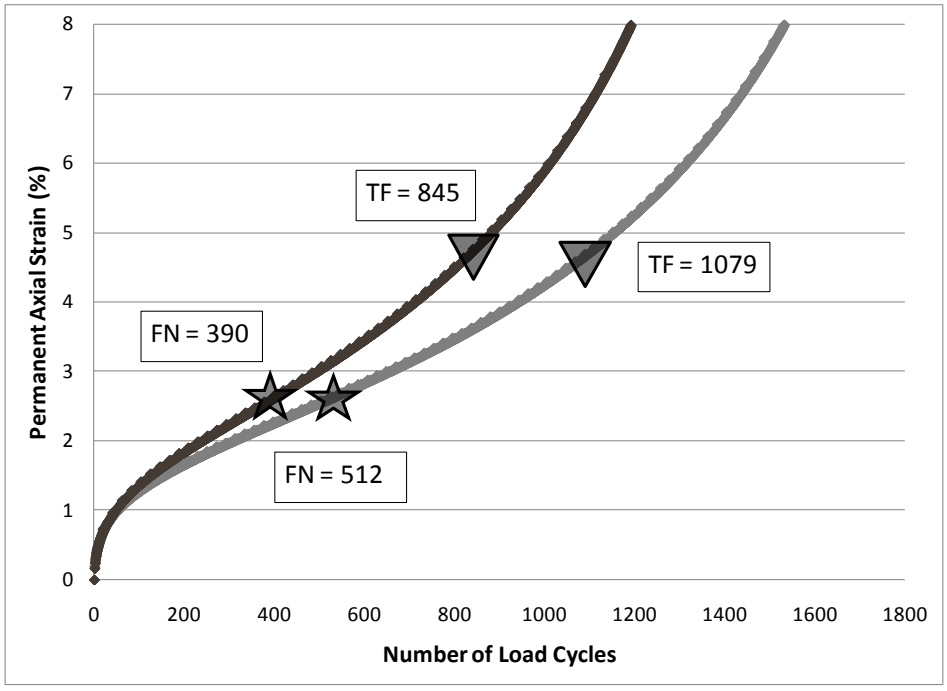

Figure A20. 12.5 CLS0 with PG 64-22

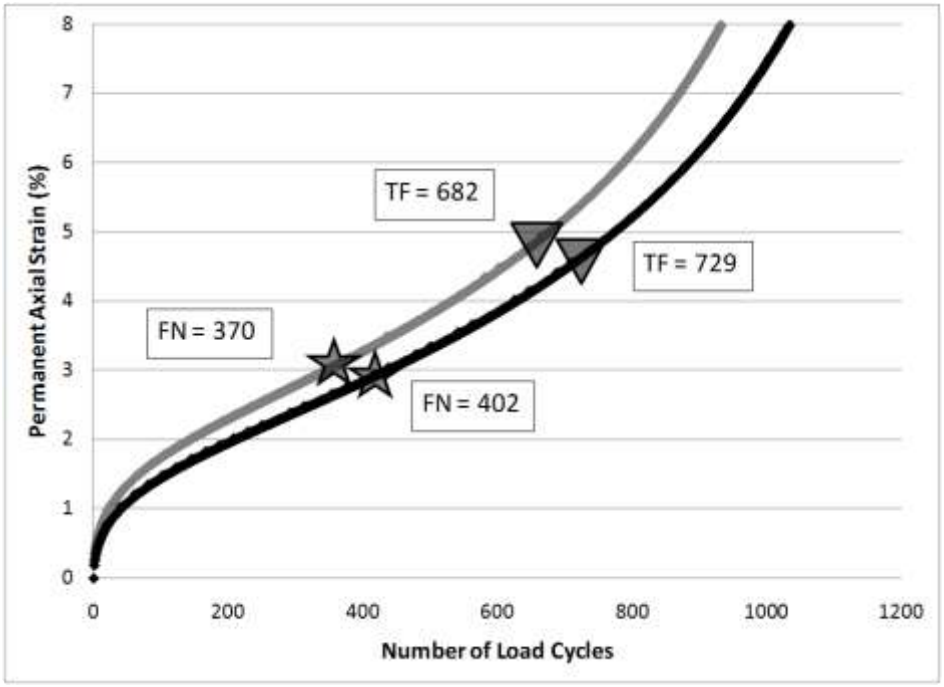

Figure A21. 19 FLS0 with PG 64-22

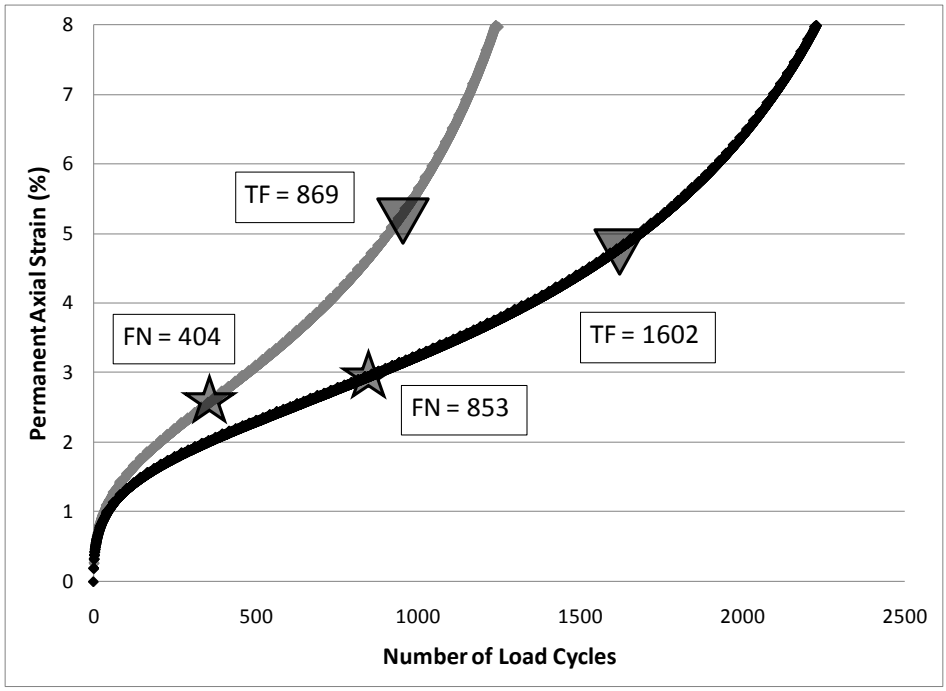

Figure A22. 19 CLS0 with PG 64-22

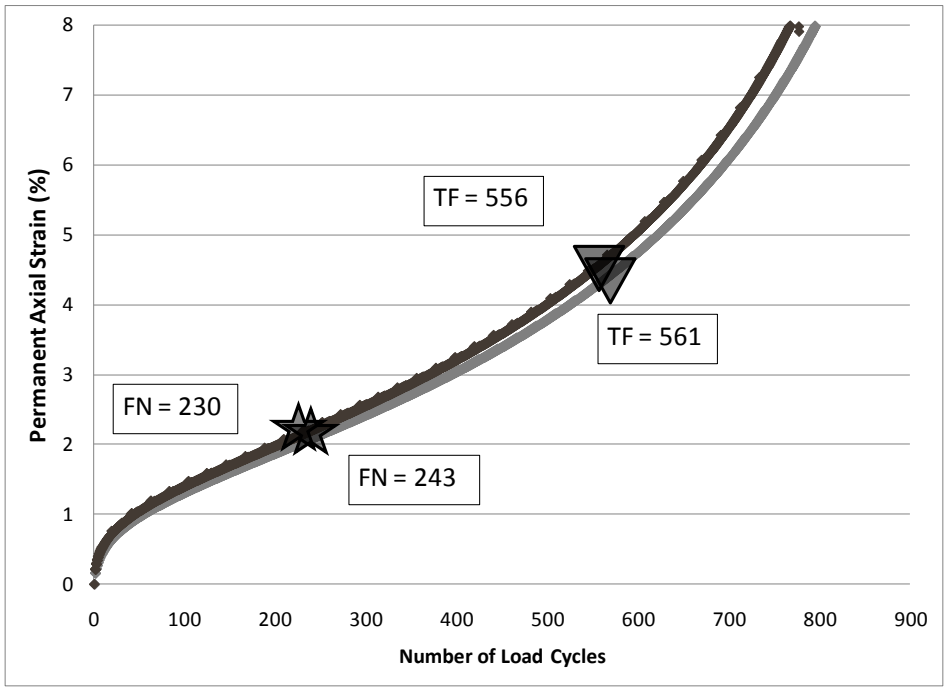

Figure A23. 12.5 FLS10 with PG 64-22

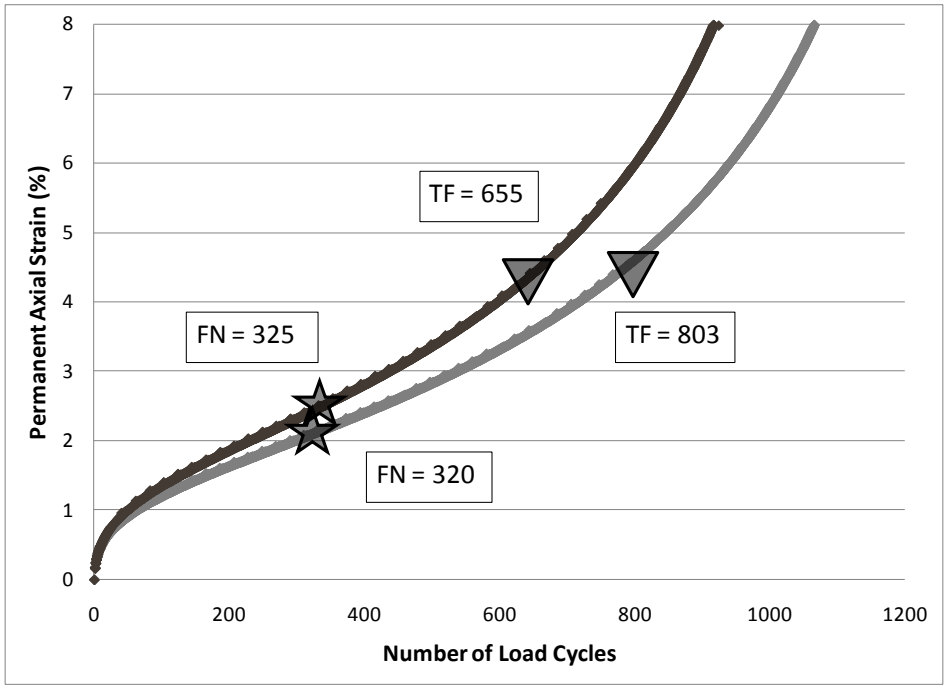

Figure A24. 12.5 CLS10 with PG 64-22

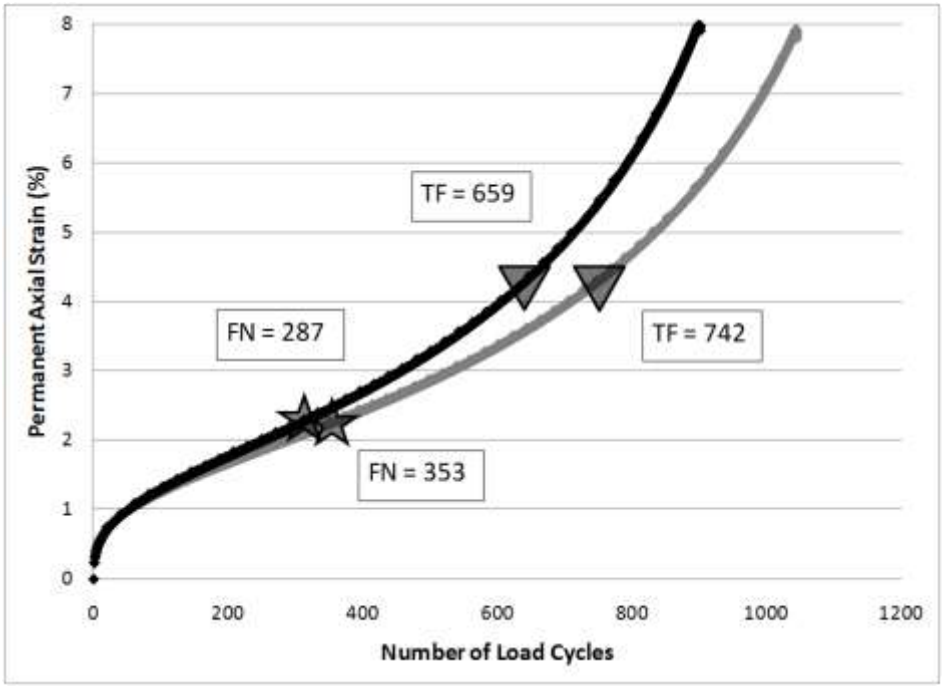

Figure A25. 19 FLS10 with PG 64-22

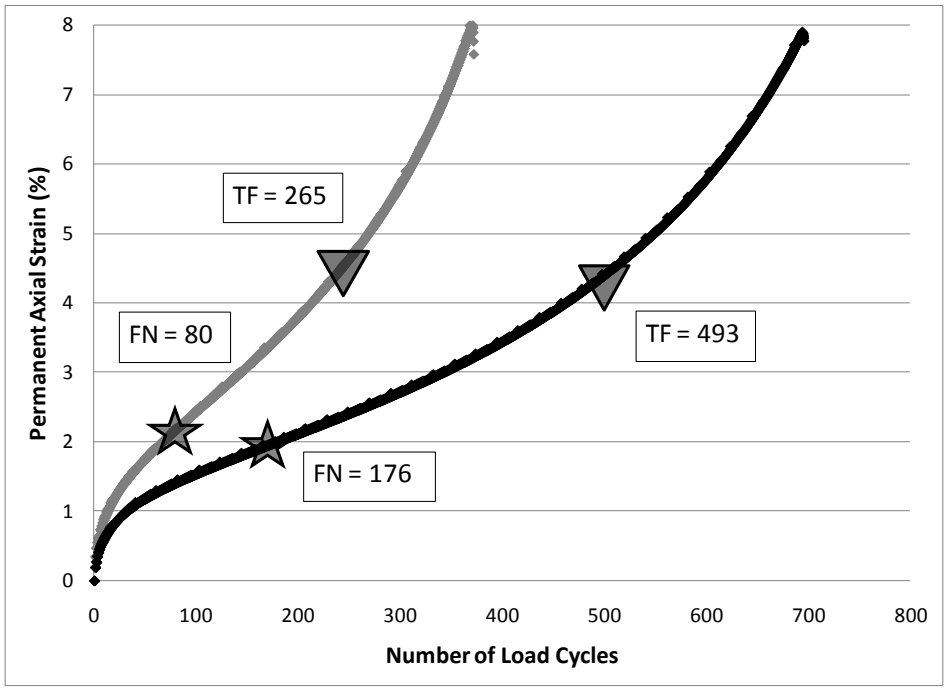

Figure A26. 19 CLS10 with PG 64-22

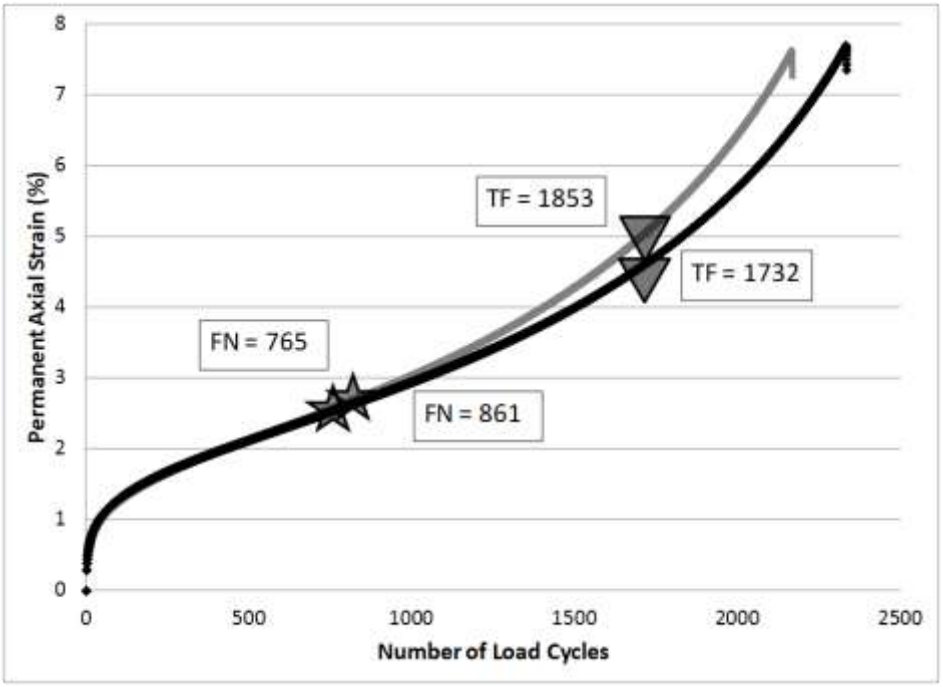

Figure A27. 12.5 FGN0 with PG 76-22

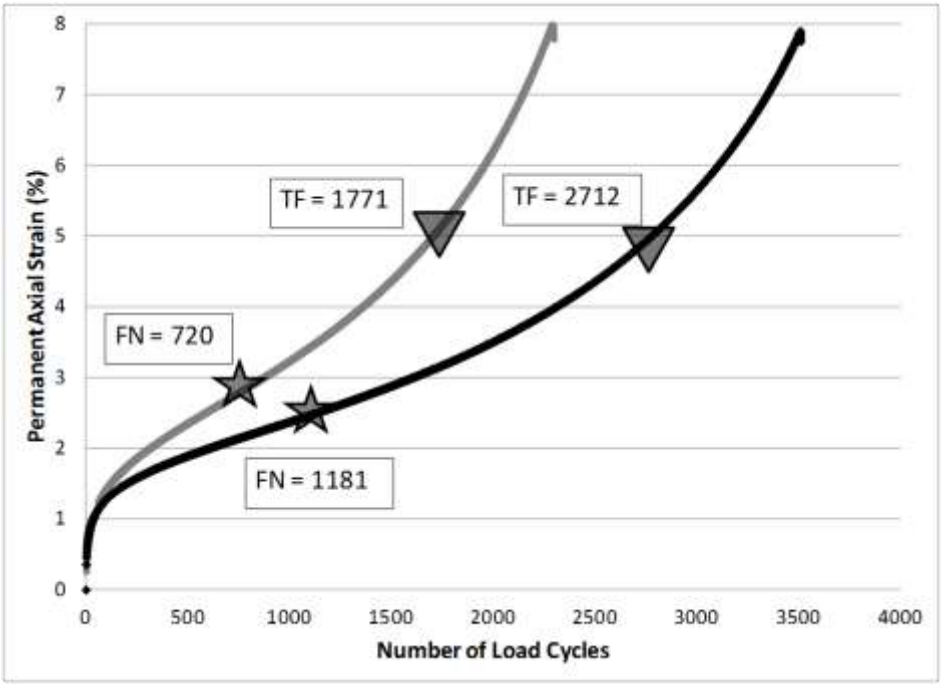

Figure A28. 12.5 CGN0 with PG 76-22

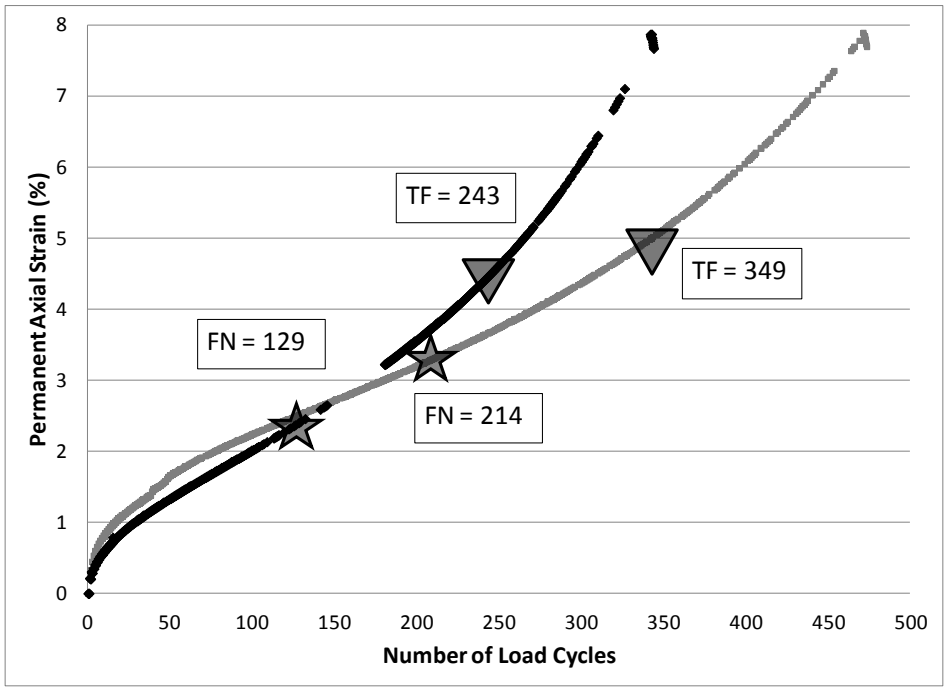

Figure A29. 19 FGN30 with PG 76-22

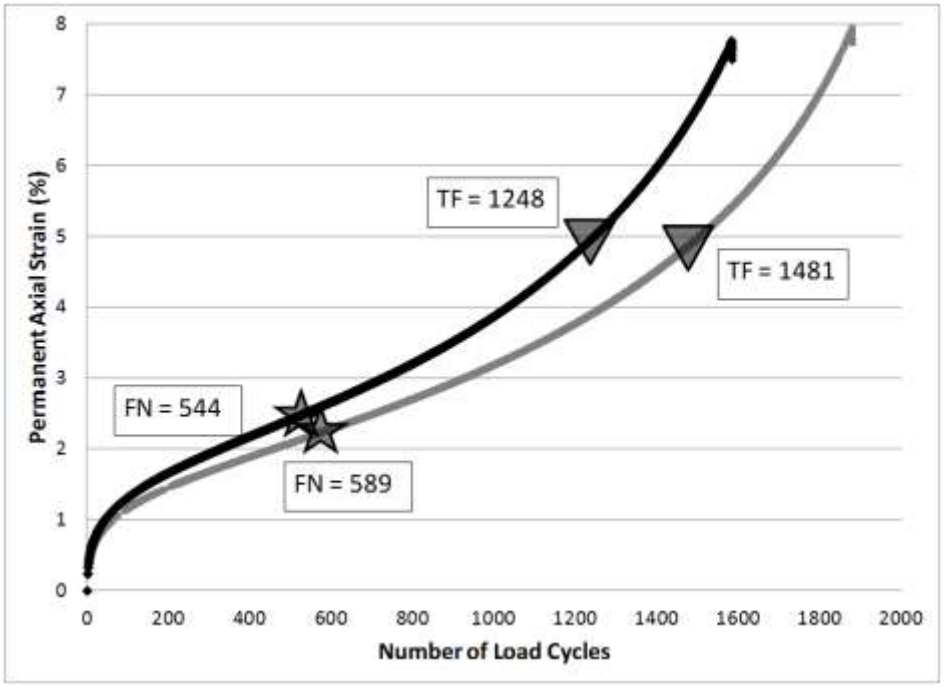

Figure A30. 12.5 GV0 with PG 76-22

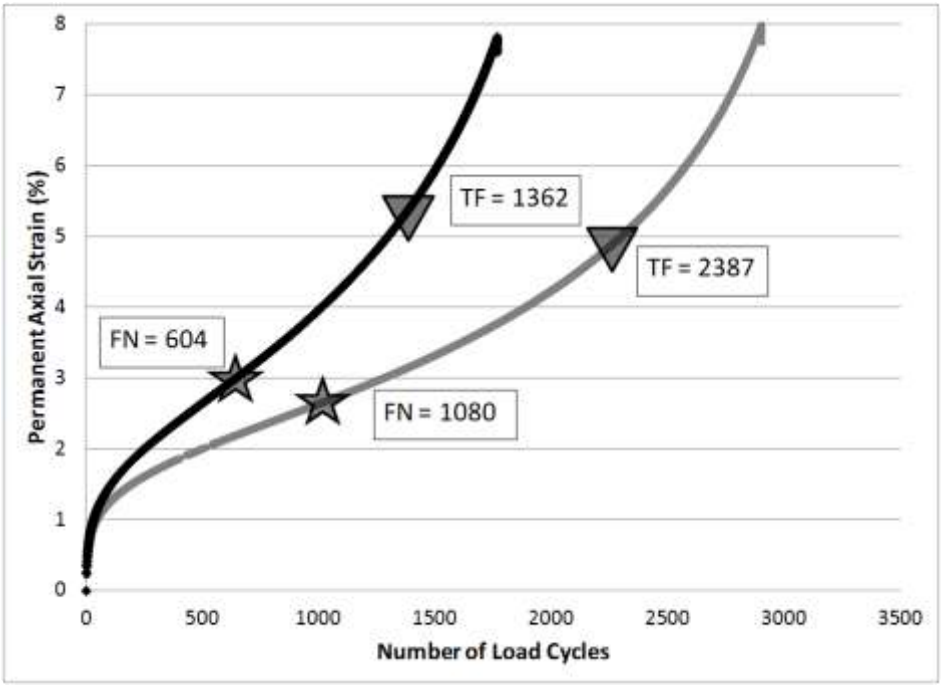

Figure A31. 19 CGV0 with PG 76-22

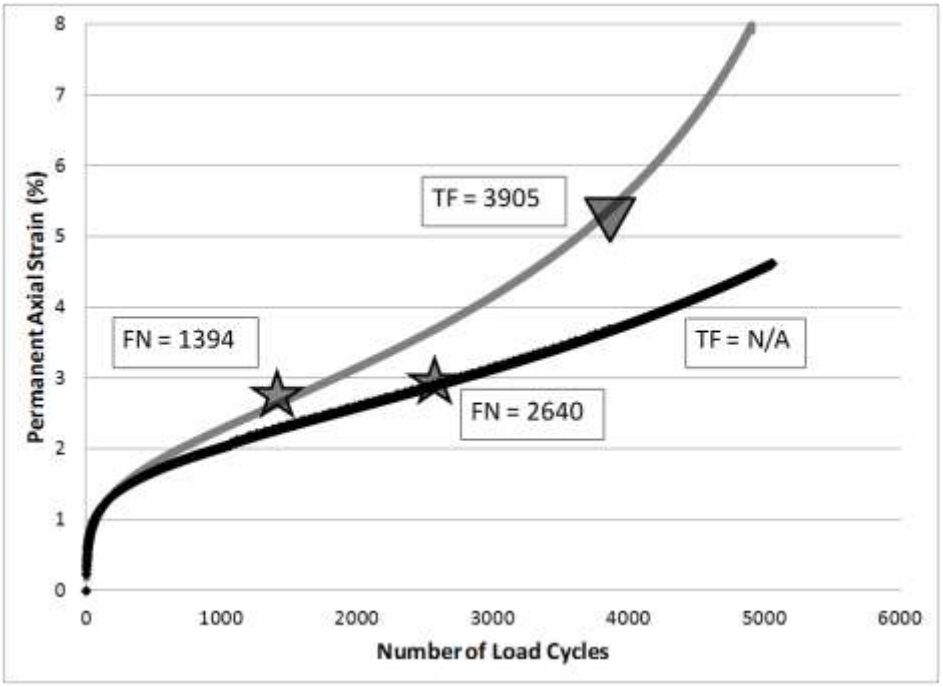

Figure A32. 12.5 CLS0 with PG 76-22

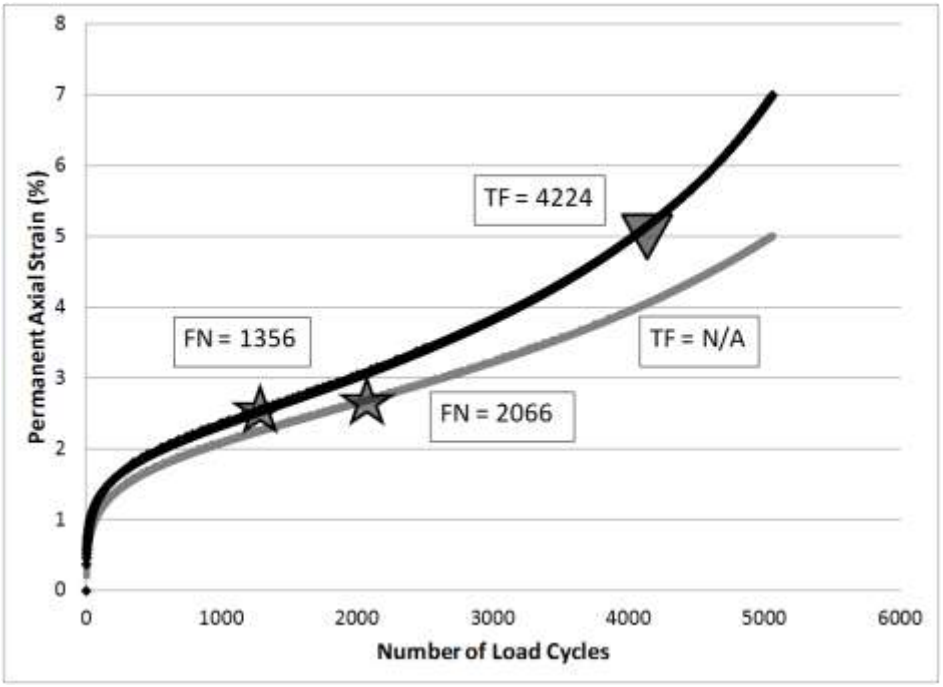

Figure A33. 19 CLS0 wtih PG 76-22

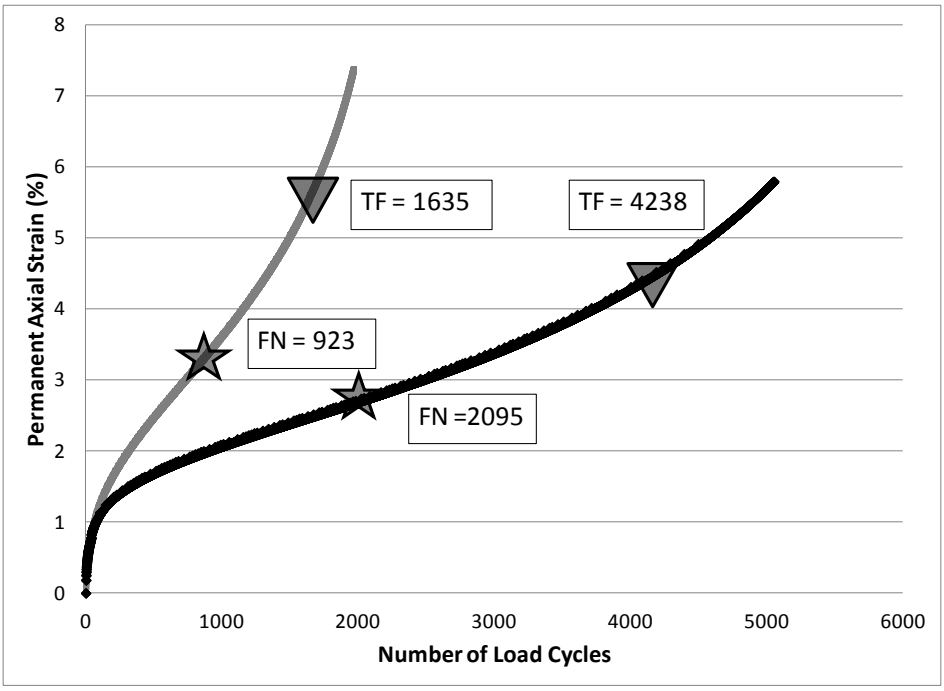

Figure A34. 19 FLS10 with PG 76-22

APPENDIX B

STATIC CREEP

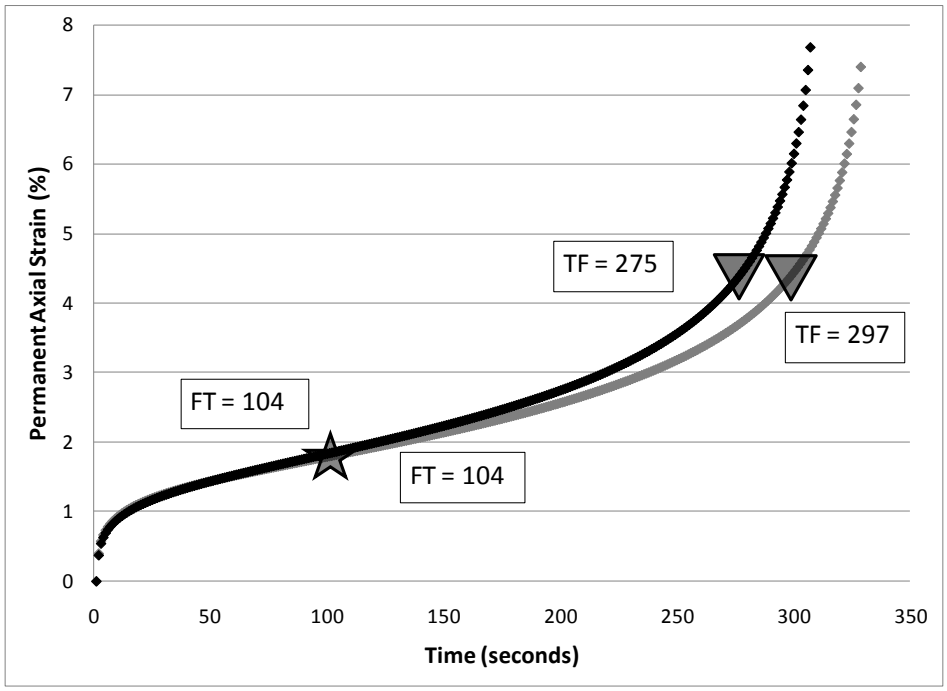

Figure B1. 12.5 FGN0 with PG 64-22

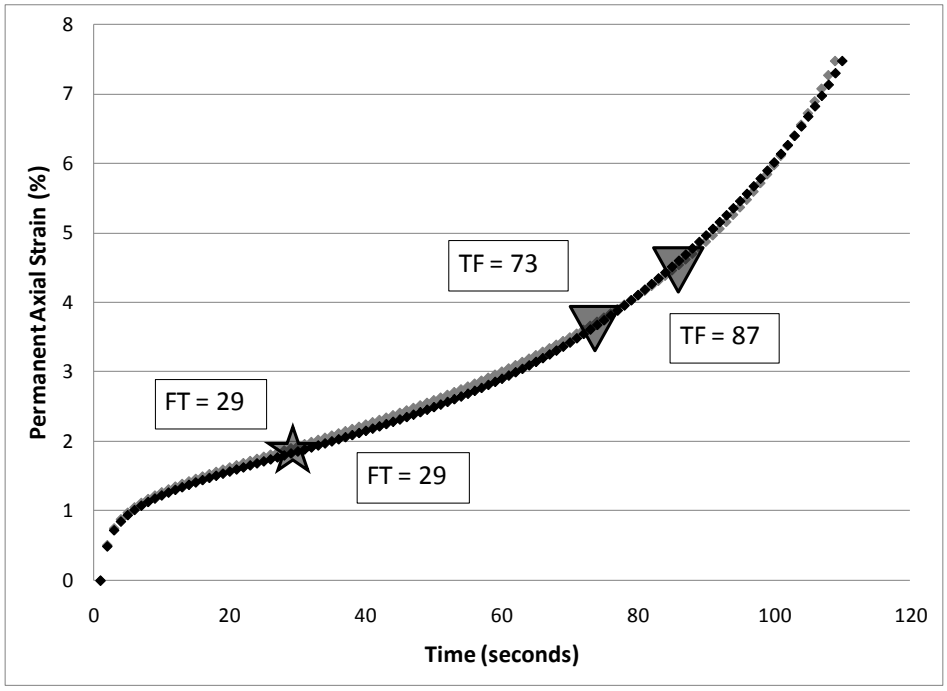

Figure B2. 12.5 CGN0 with PG 64-22

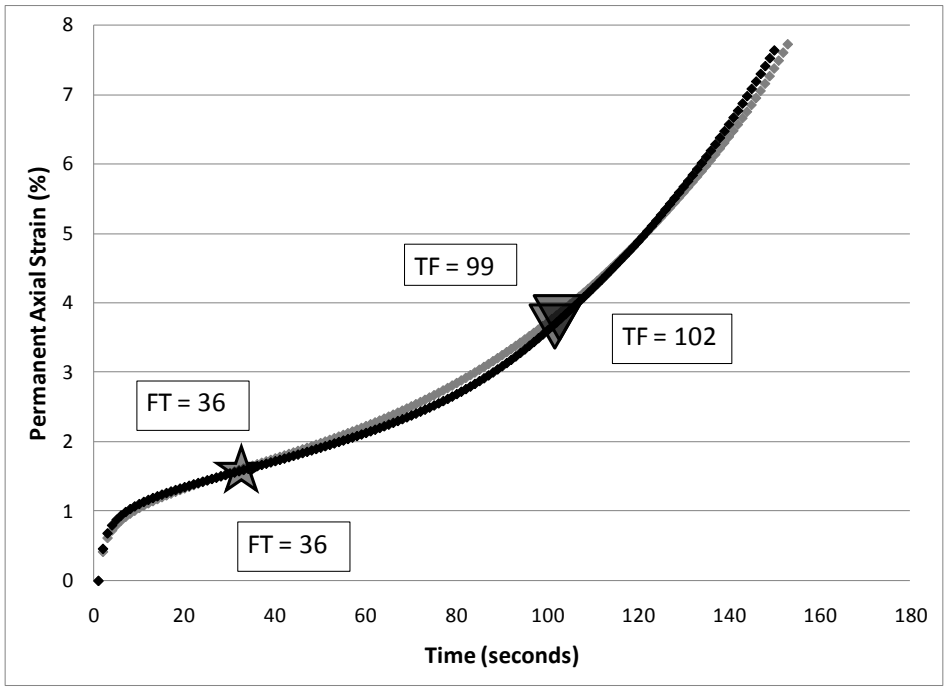

Figure B3. 19 FGN0 with PG 64-22

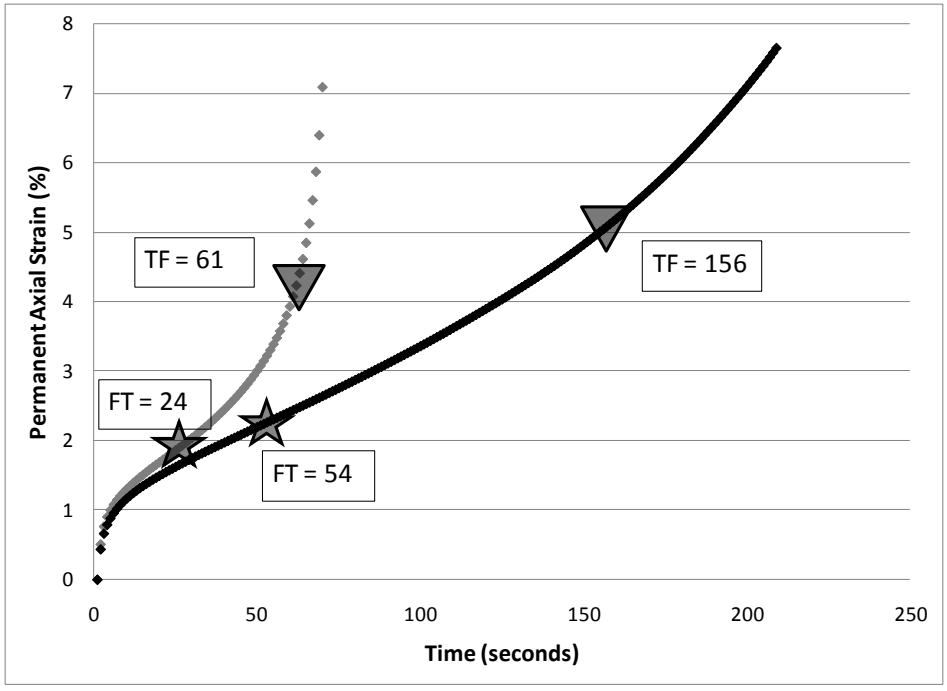

Figure B4. 19 CGN0 with PG 64-22

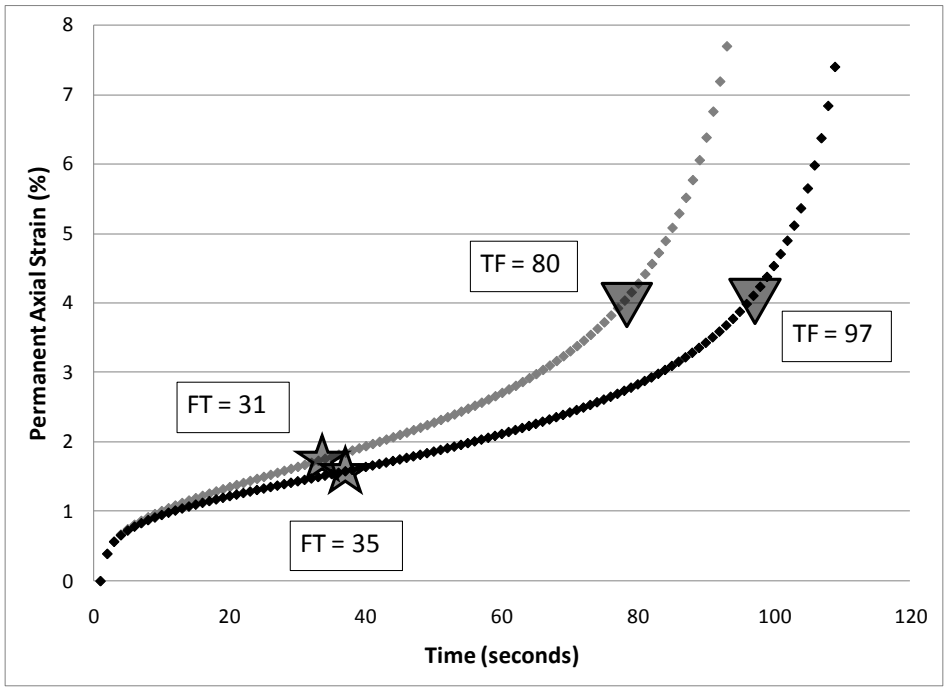

Figure B5. 12.5 FGN10 with PG 64-22

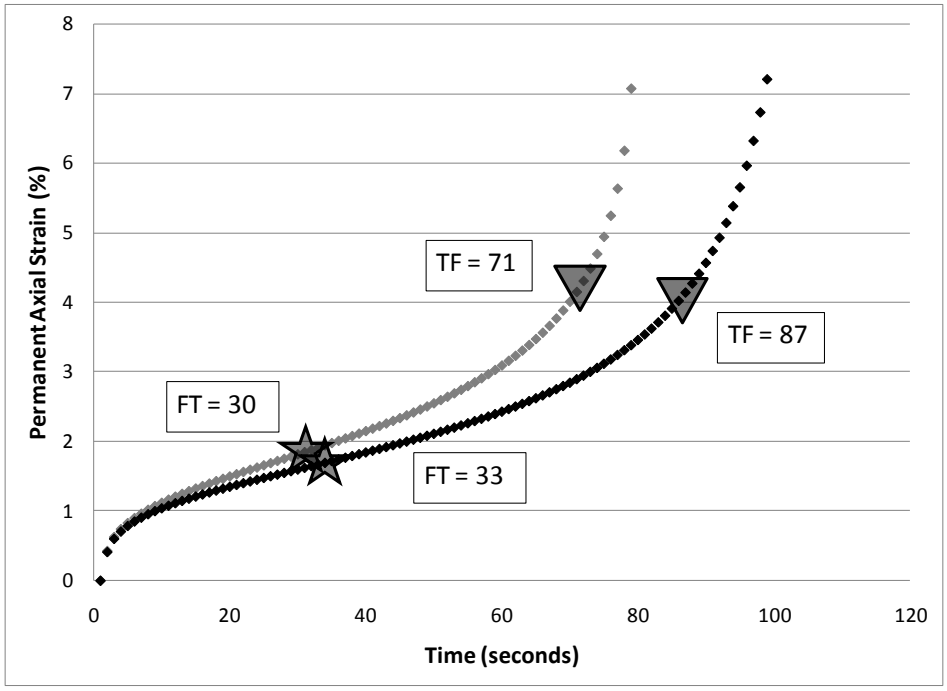

Figure B6. 12.5 CGN10 with PG 64-22

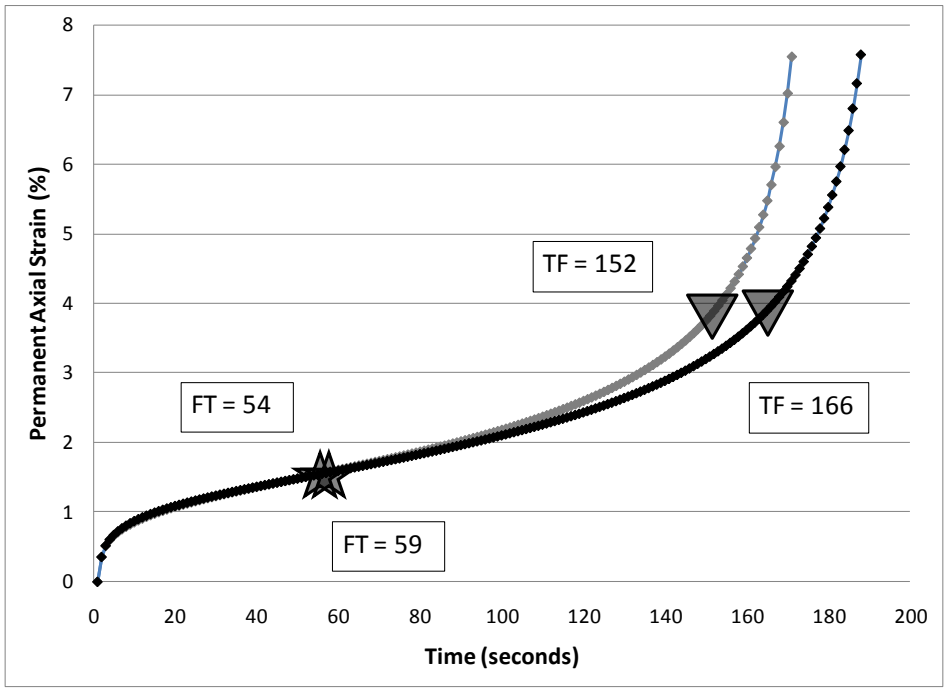

Figure B7. 19 FGN10 with PG 64-22

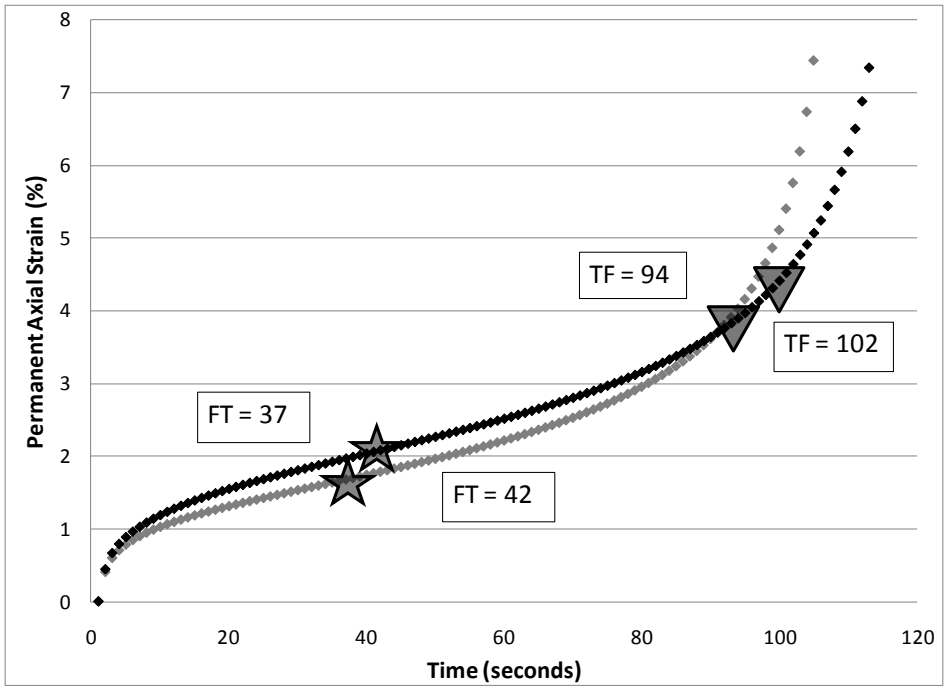

Figure B8. 19 CGN10 with PG 64-22

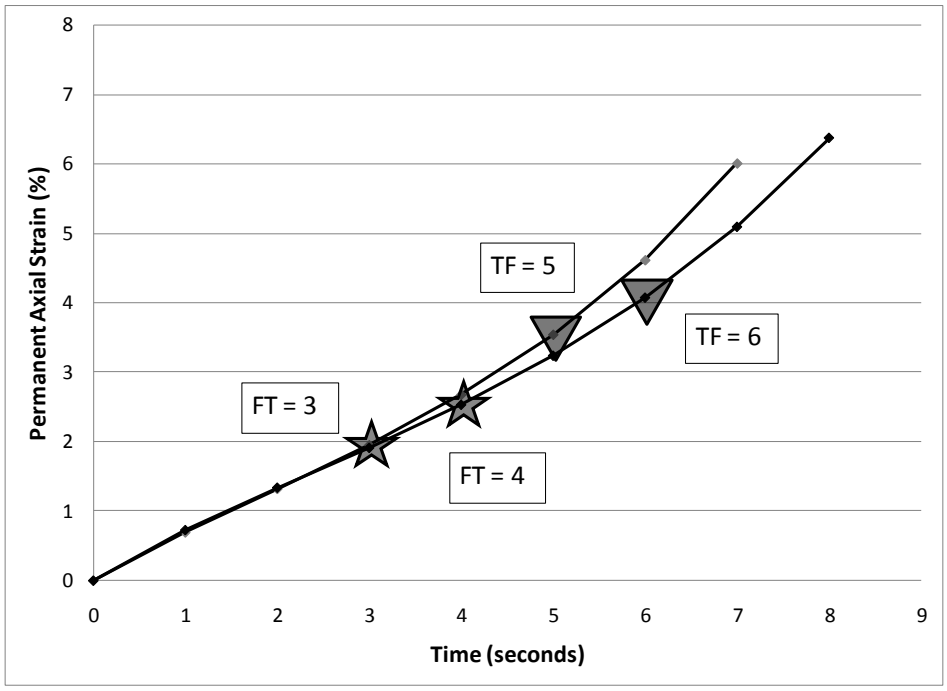

Figure B9. 12.5 FGN30 with PG 64-22

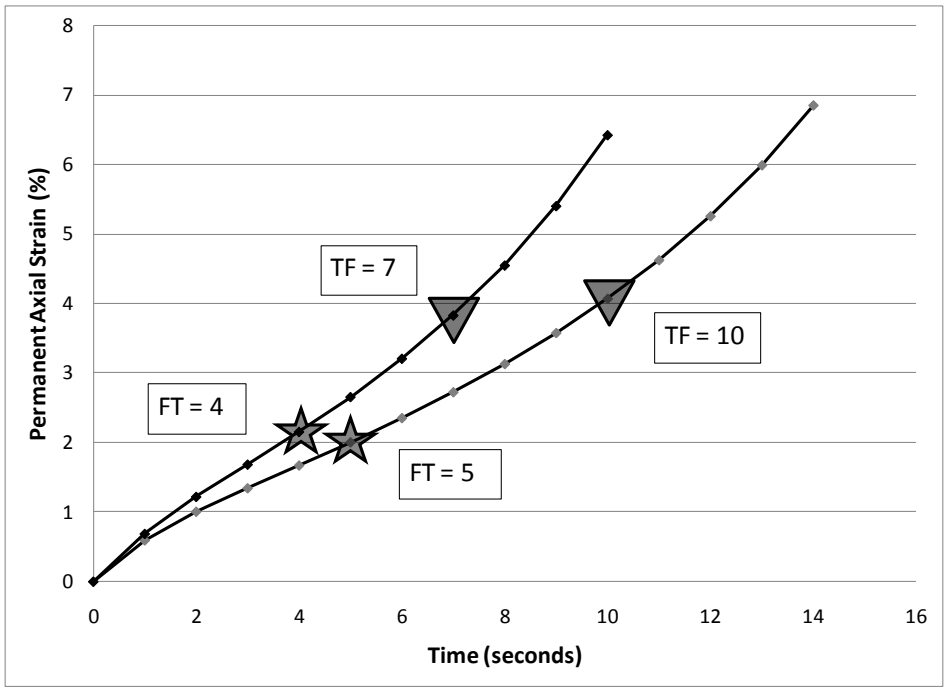

Figure B10. 12.5 CGN30 with PG 64-22

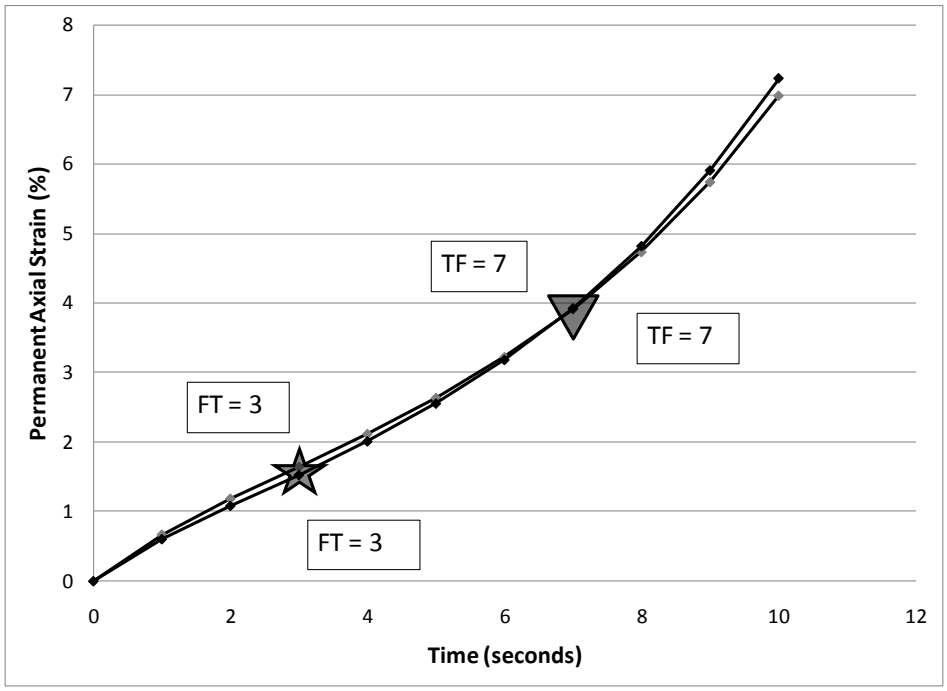

Figure B11. 19 FGN30 with PG 64-22

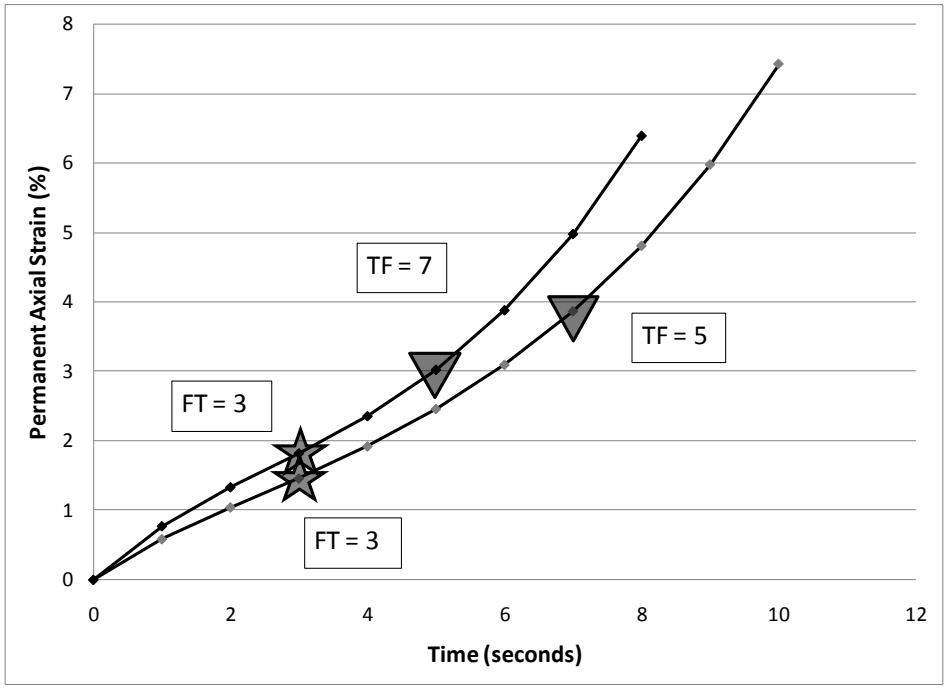

Figure B12. 19 CGN30 with PG 64-22

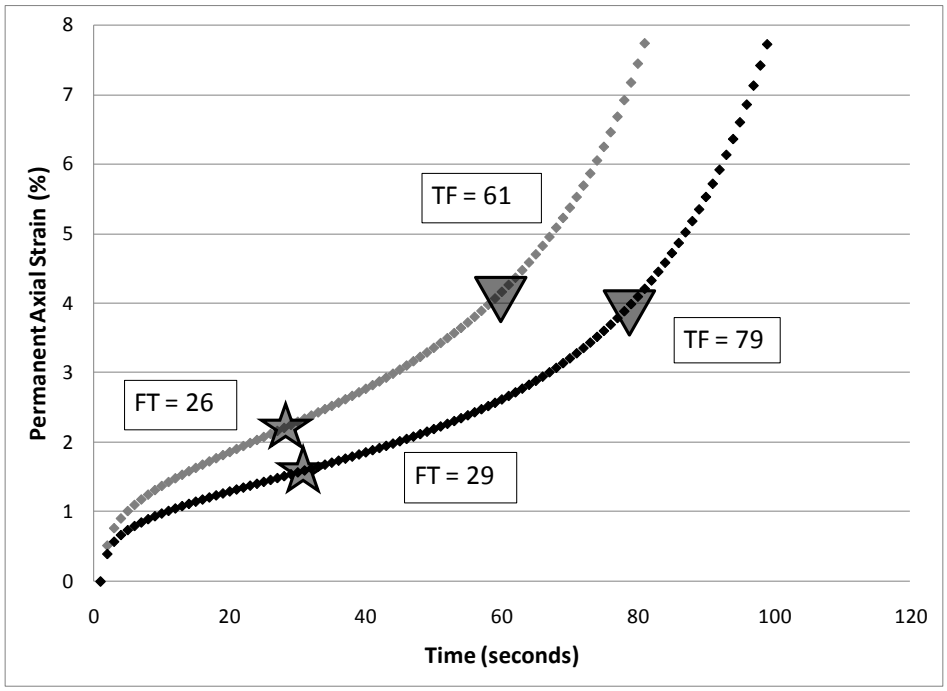

Figure B13. 12.5 GV0 with PG 64-22

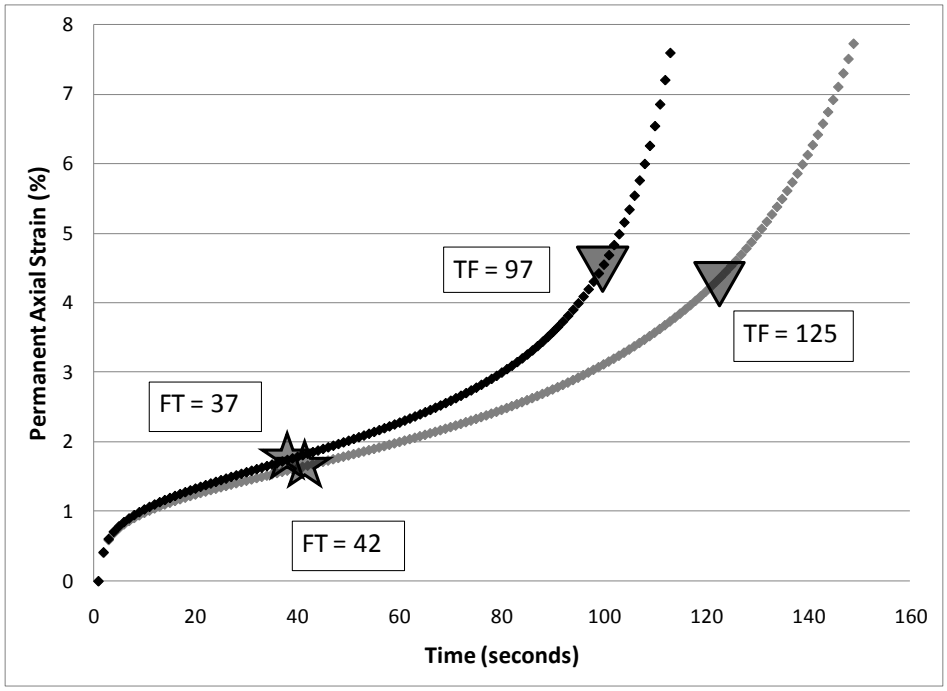

Figure B14. 19 FGV0 with PG 64-22

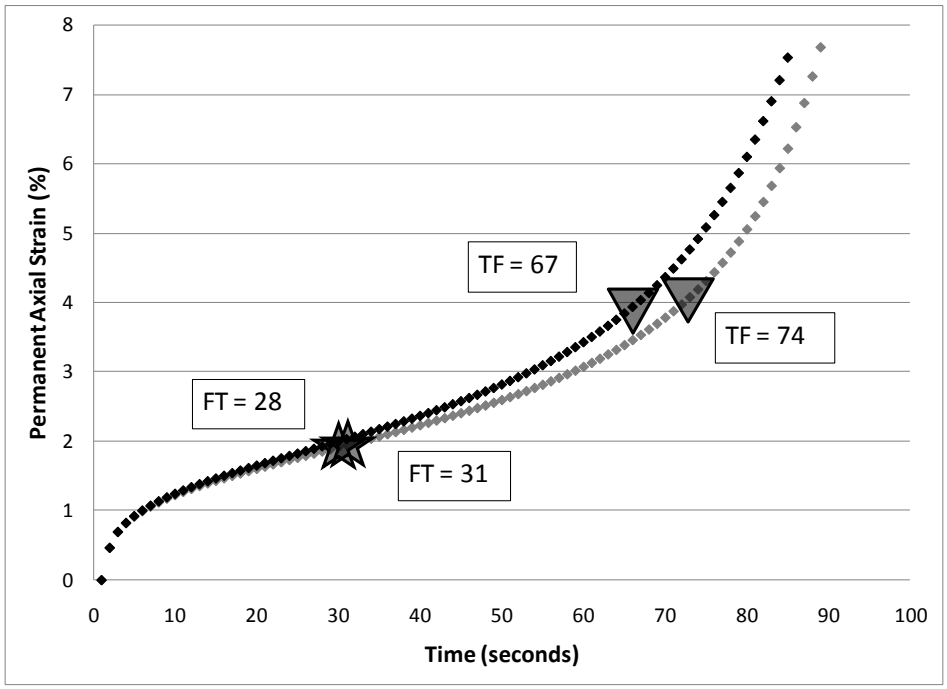

Figure B15. 19 CGV0 with PG 64-22

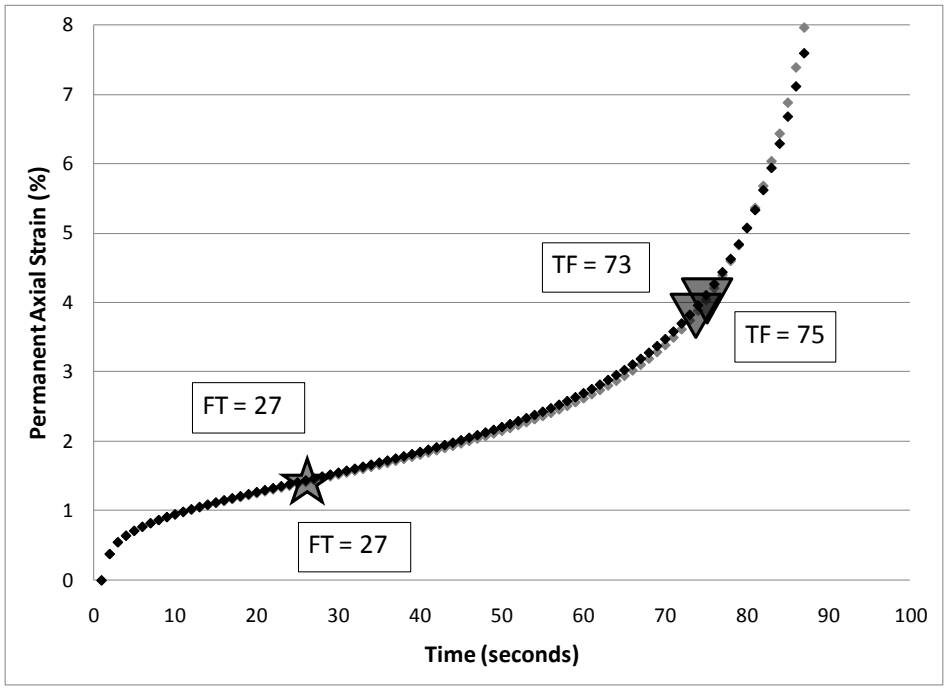

Figure B16. 12.5 GV10 with PG 64-22

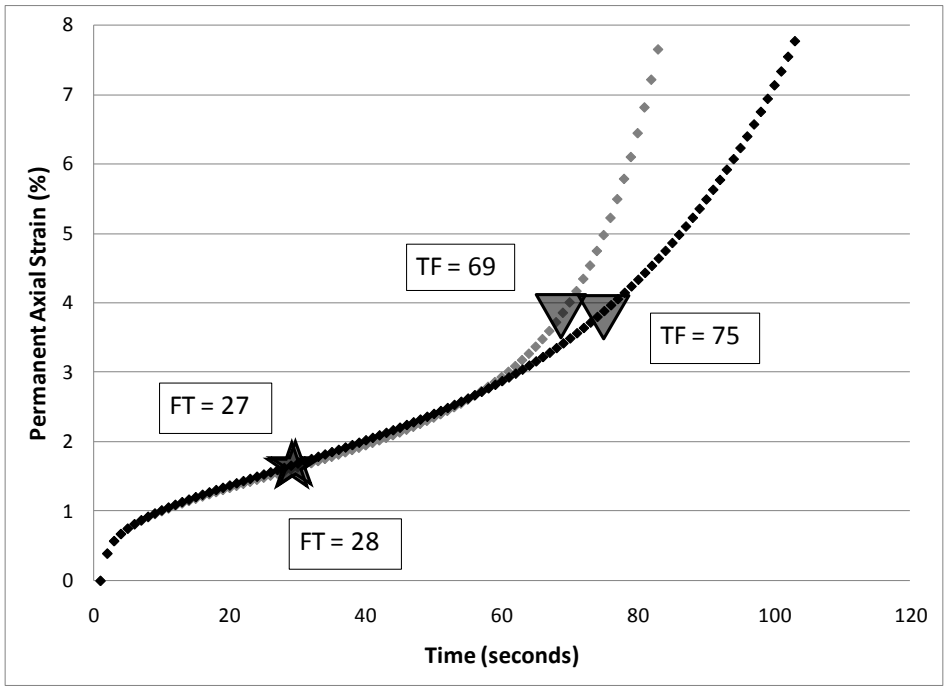

Figure B17. 19 FGV10 with PG 64-22

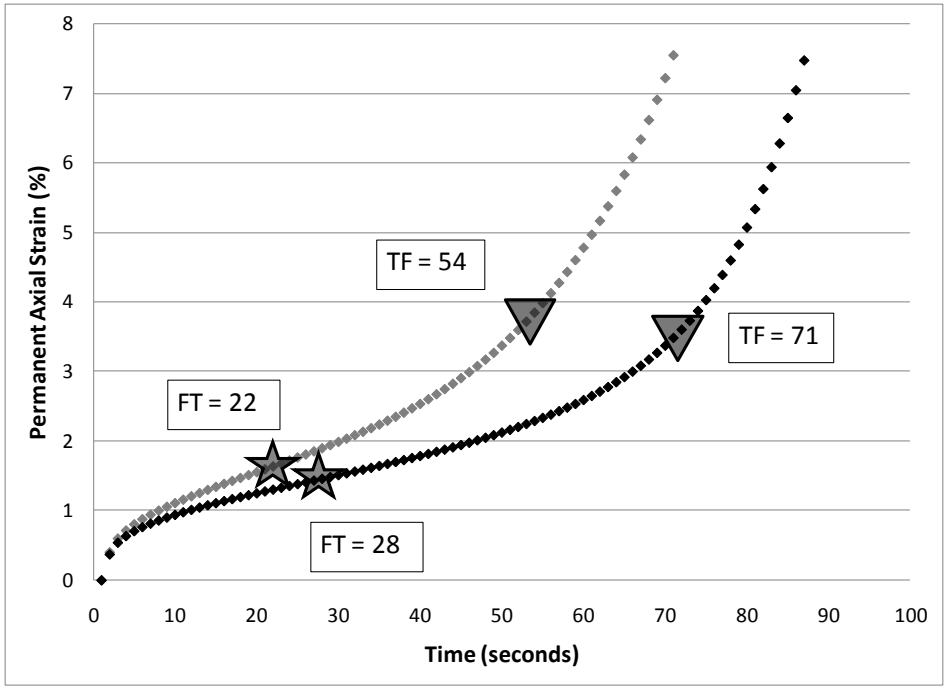

Figure B18. 19 CGV10 with PG 64-22

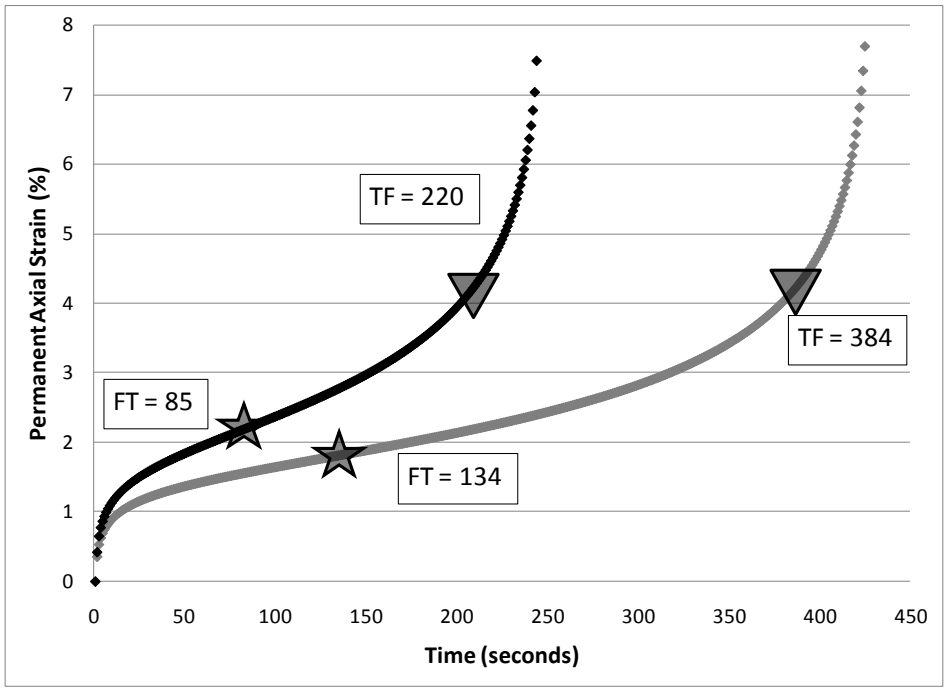

Figure B19. 12.5 FLS0 with PG 64-22

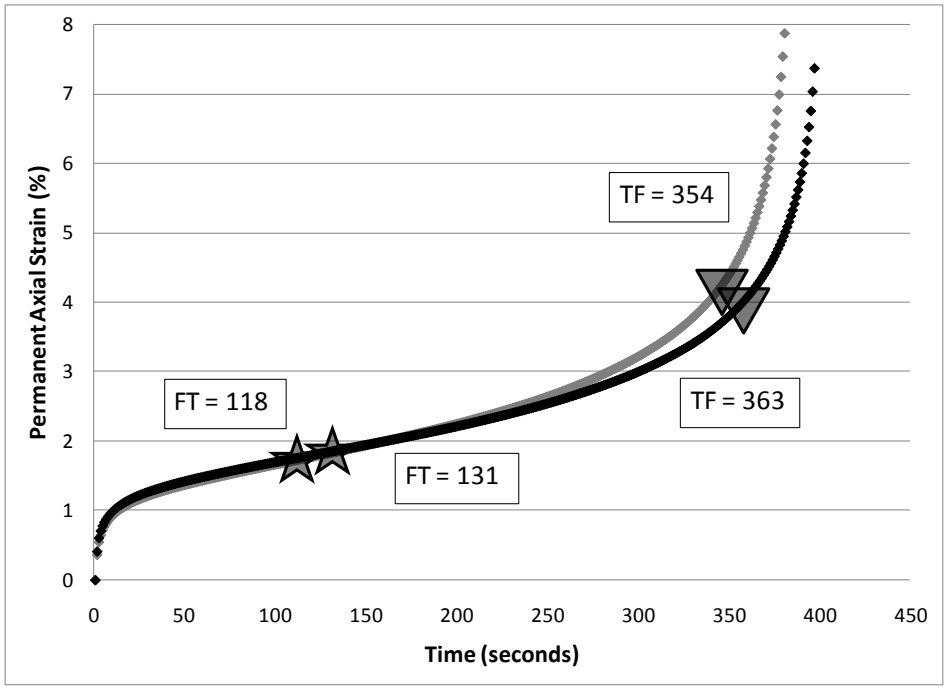

Figure B20. 12.5 CLS0 with PG 64-22

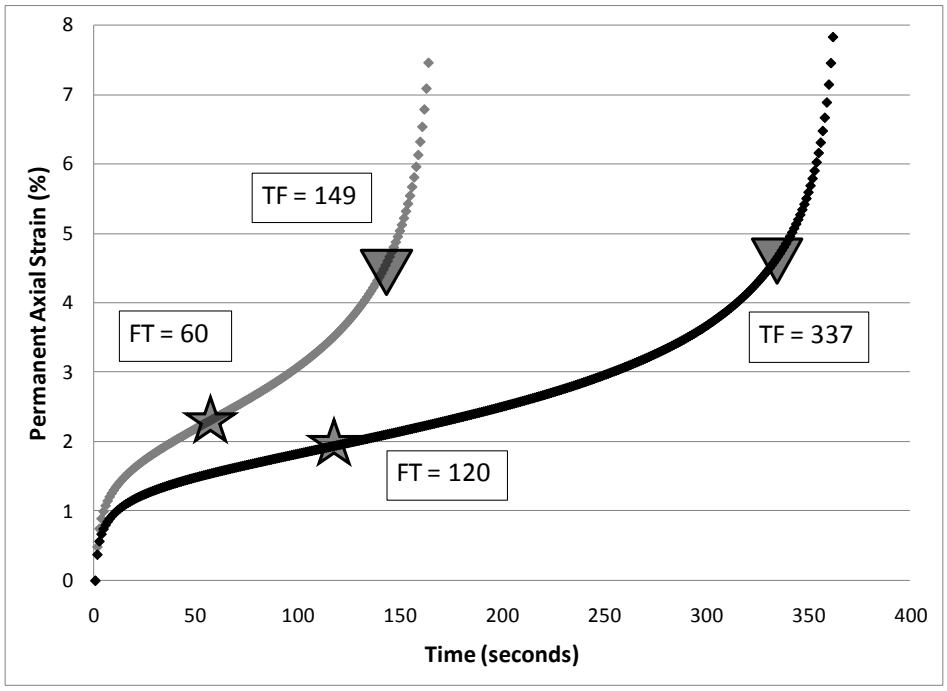

Figure B21. 19 FLS0 with PG 64-22

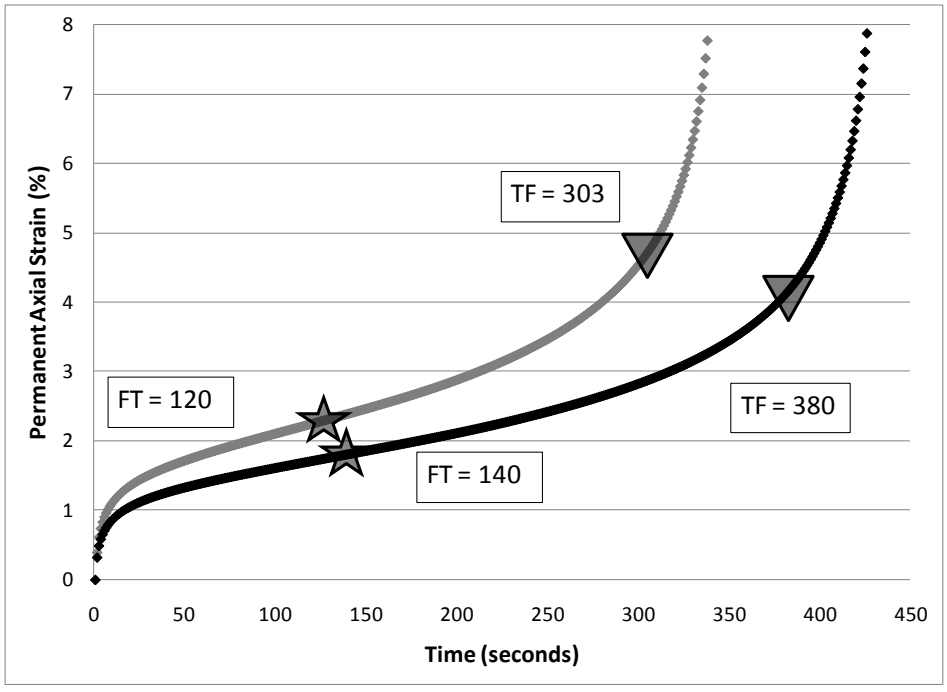

Figure B22. 19 CLS0 with PG 64-22

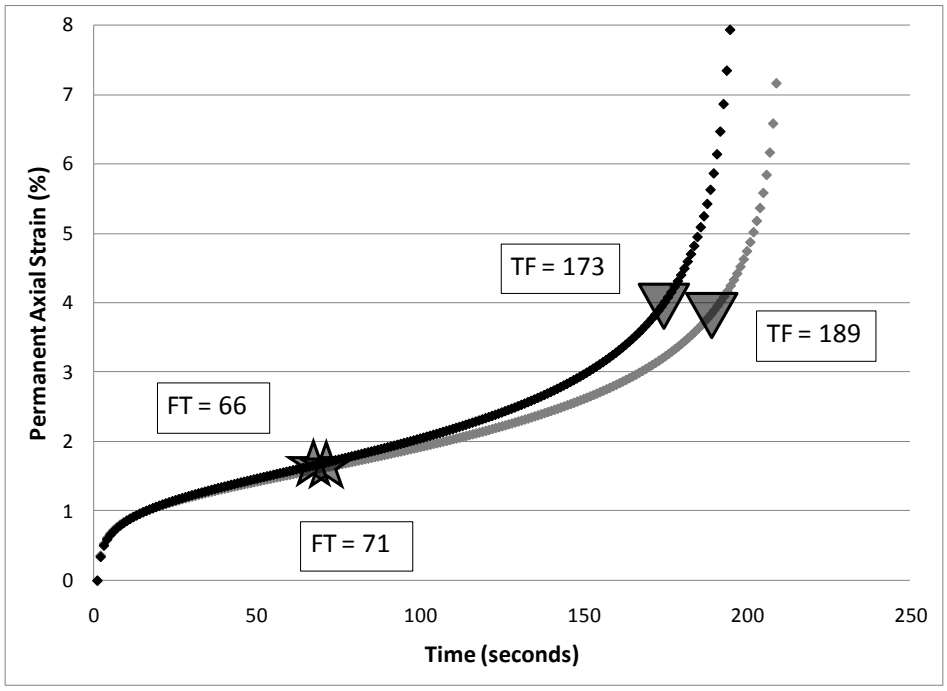

Figure B23. 12.5 FLS10 with PG 64-22

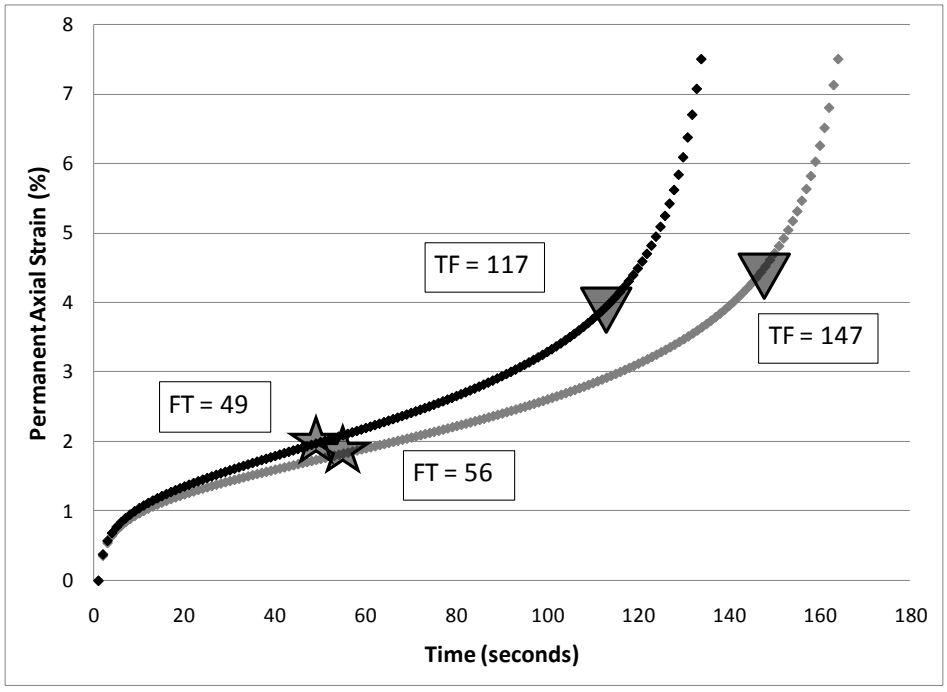

Figure B24. 12.5 CLS10 with PG 64-22

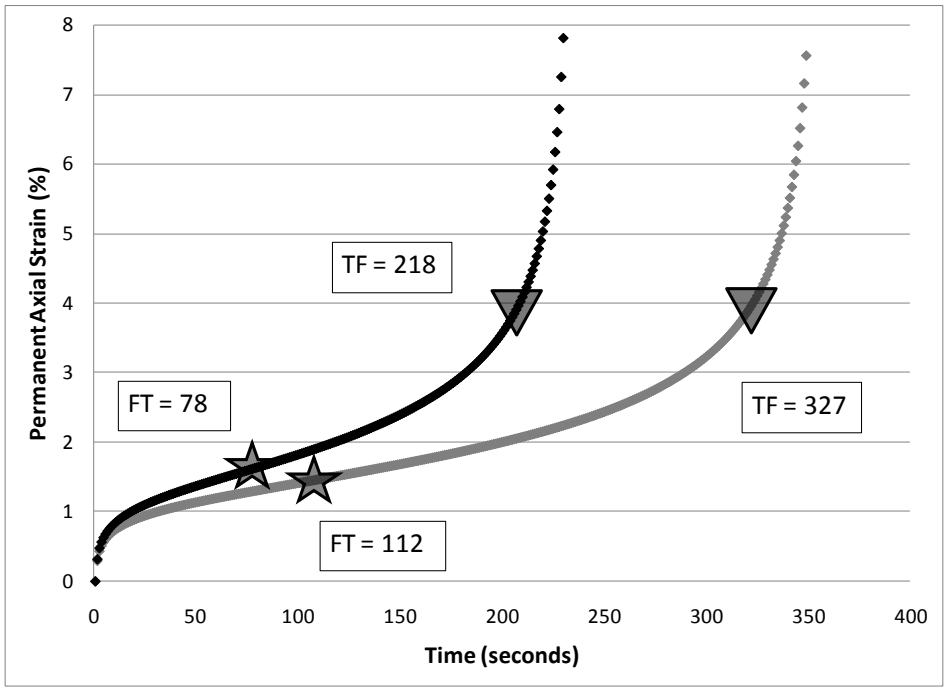

Figure B25. 19 FLS10 with PG 64-22

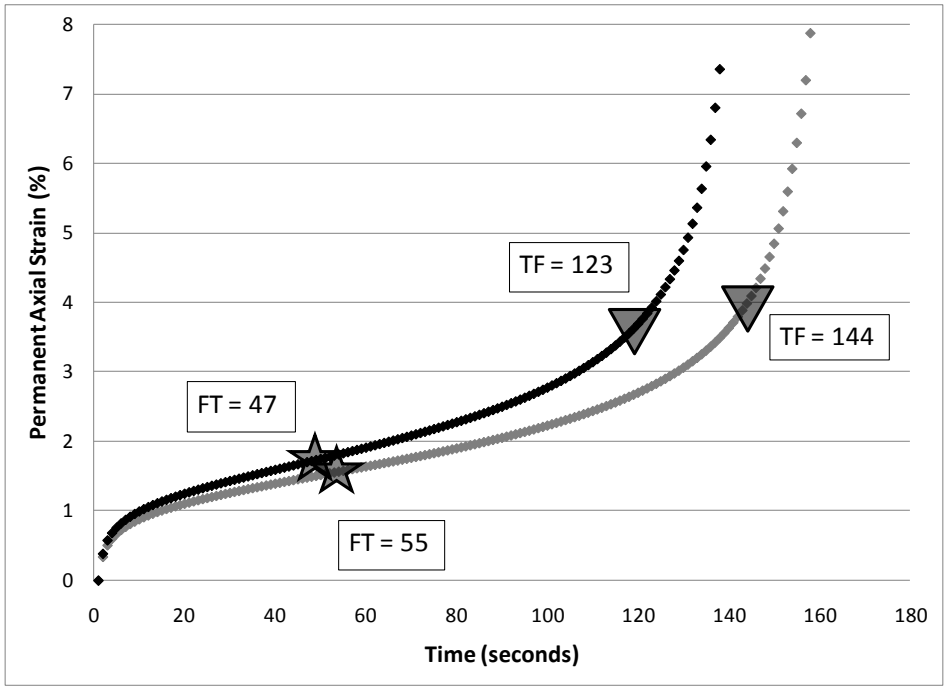

Figure B26. 19 CLS10 with PG 64-22

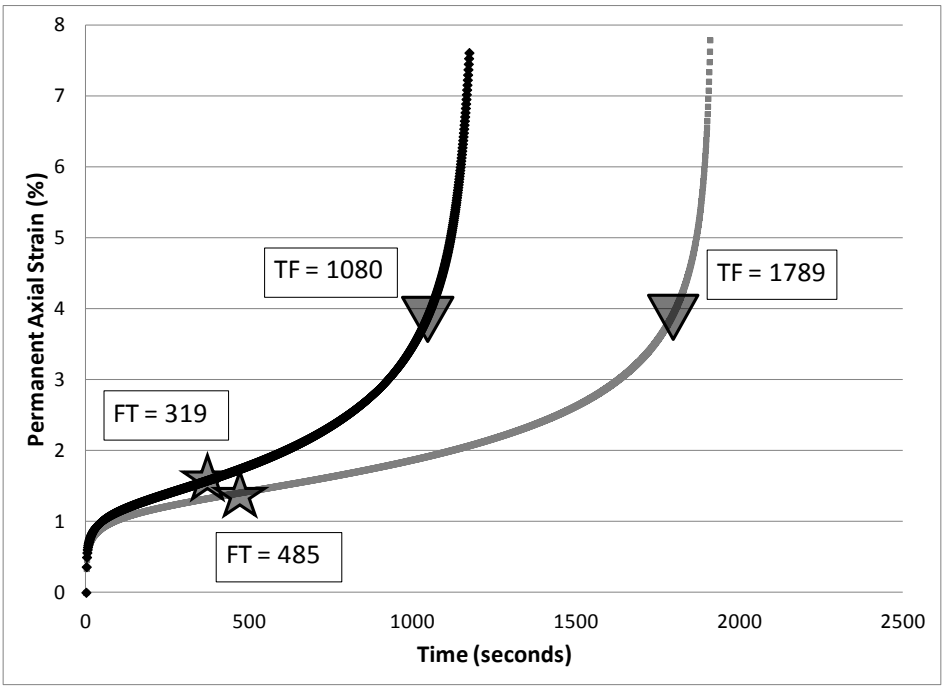

Figure B27. 12.5 FGN0 with PG 76-22

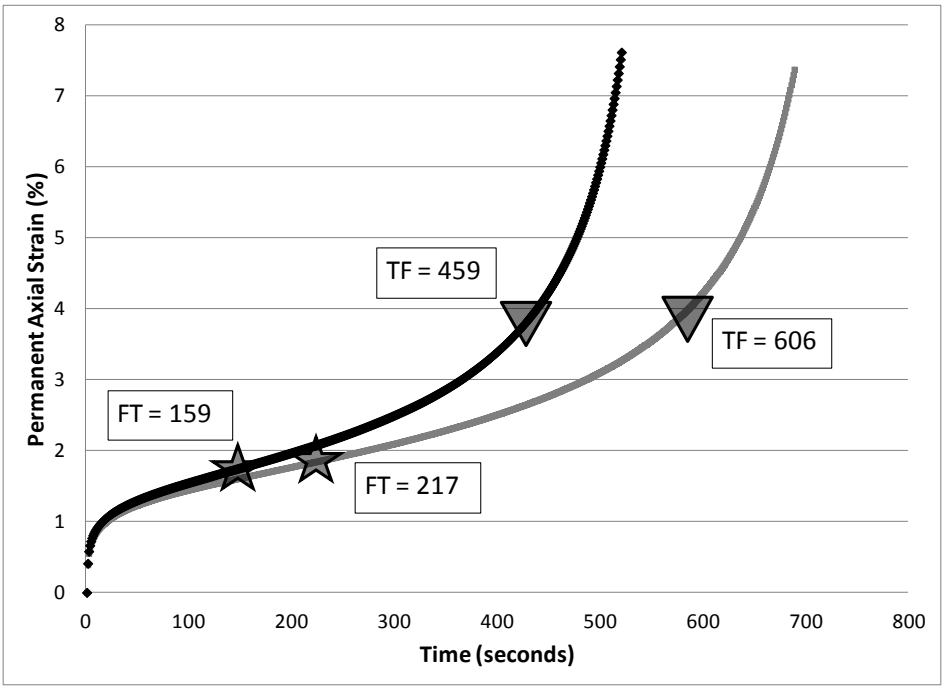

Figure B28. 12.5 CGN0 with PG 76-22

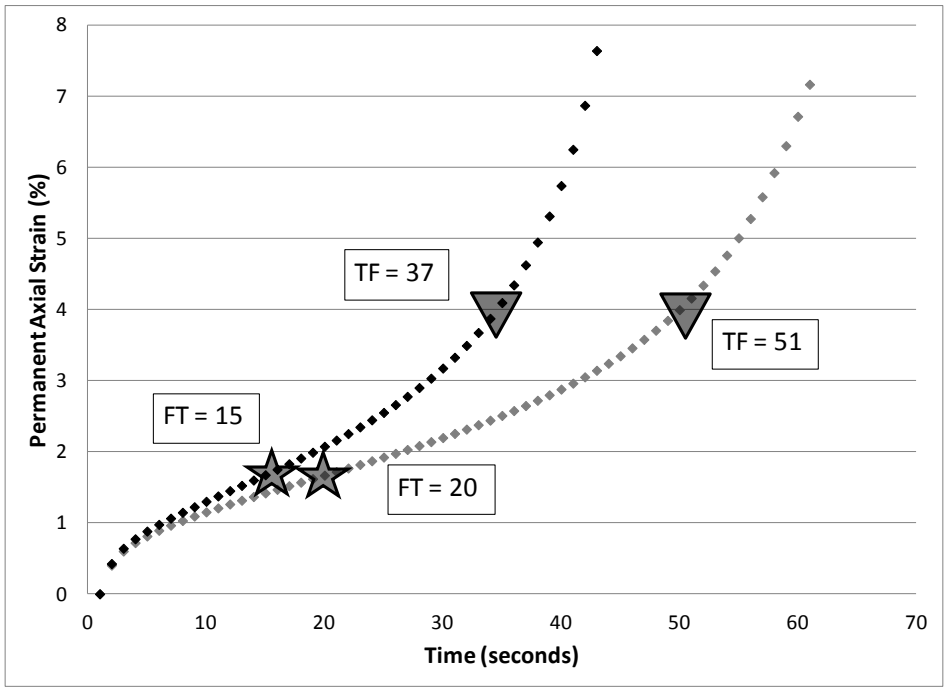

Figure B29. 19 FGN30 with PG 76-22

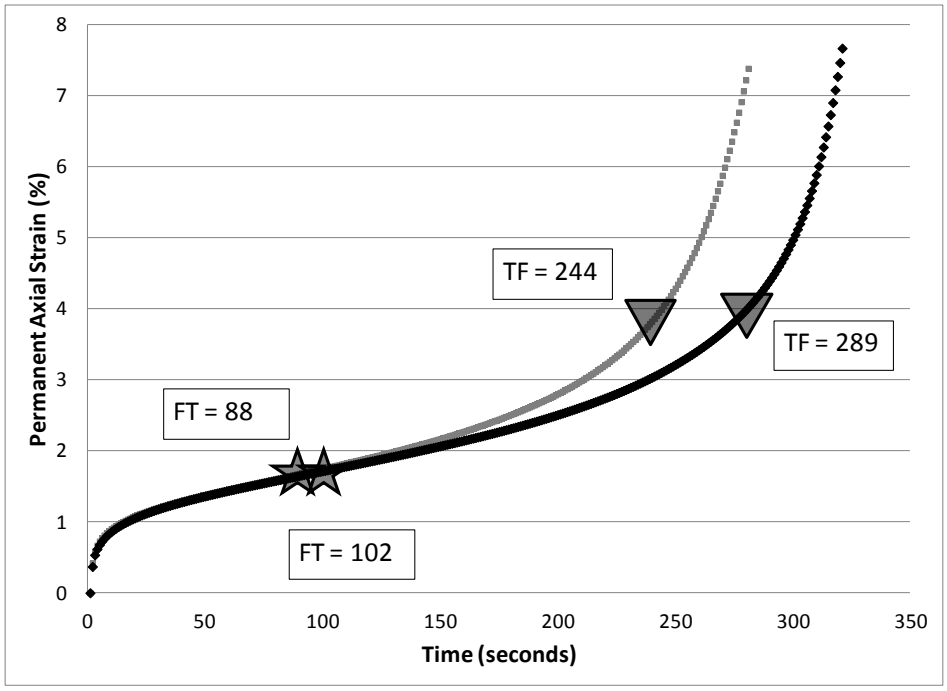

Figure B30. 12.5 GV0 with PG 76-22

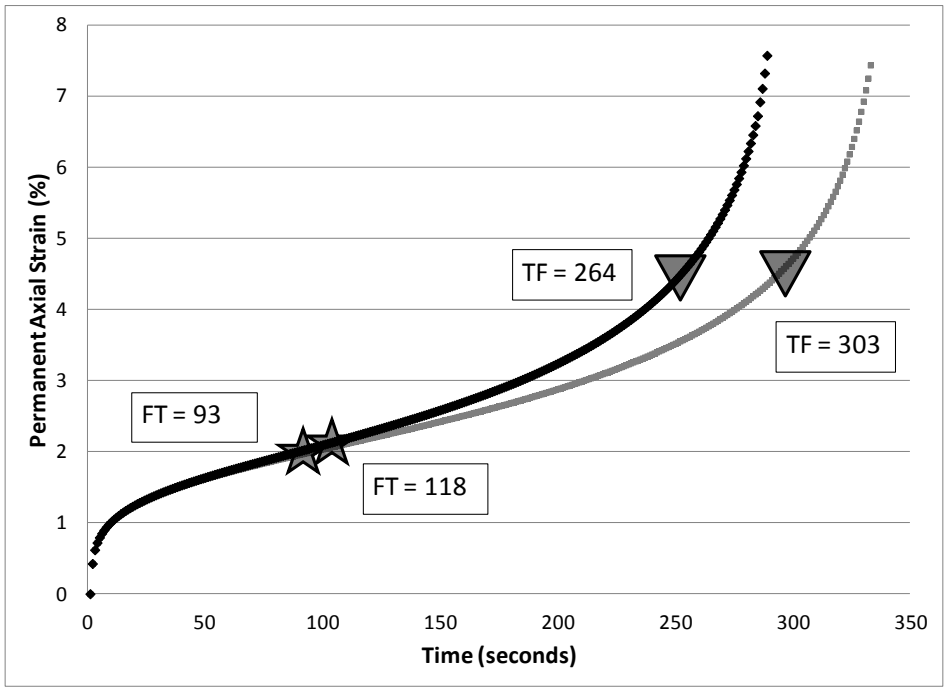

Figure B31. 19 CGV0 with PG 76-22

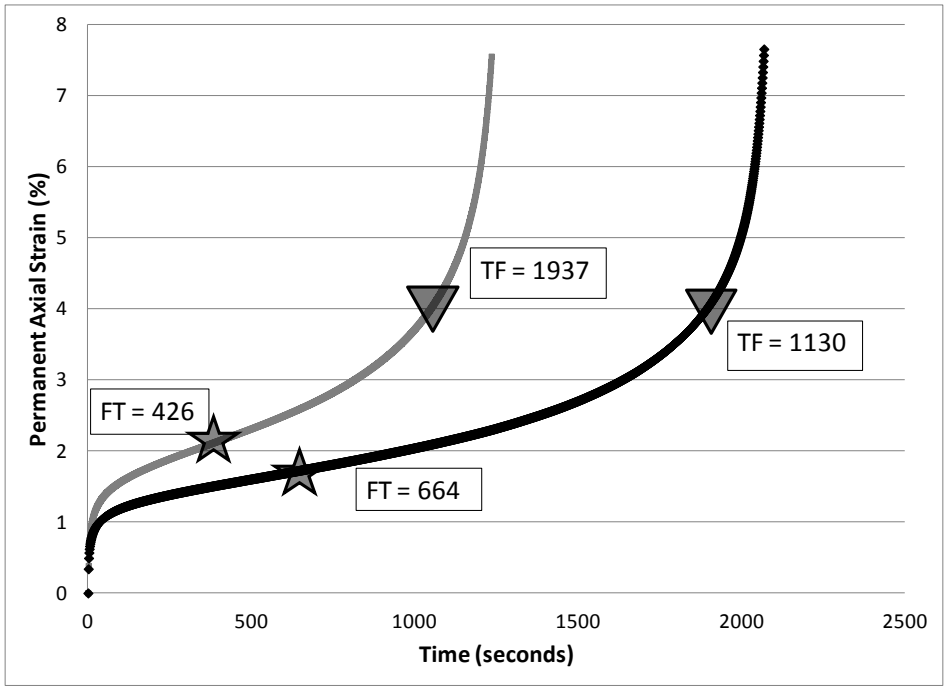

Figure B32. 12.5 CLS with PG 76-22

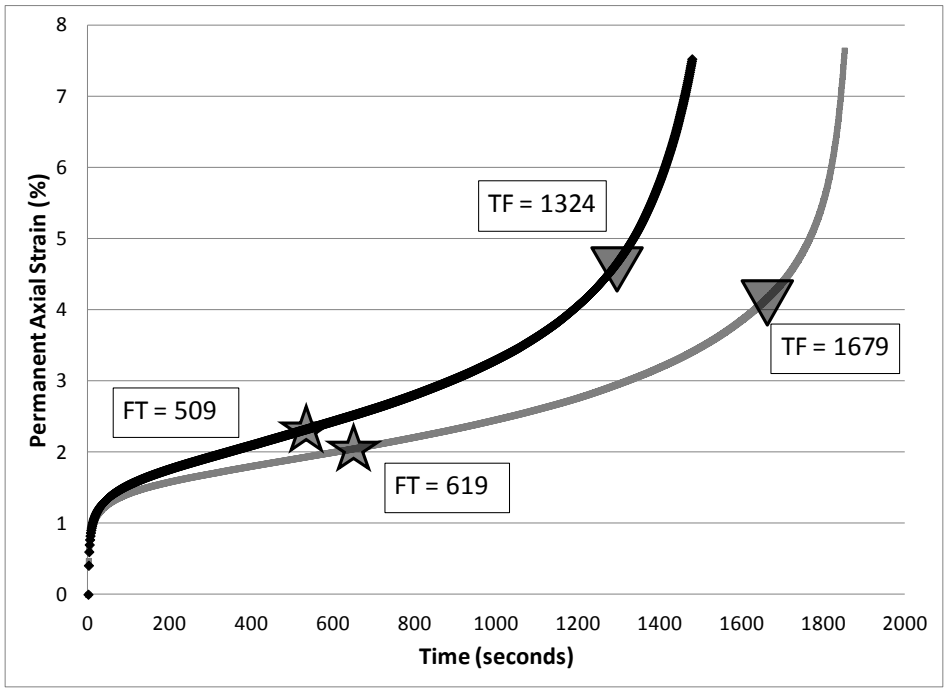

Figure B33. 19 CLS with PG 76-22

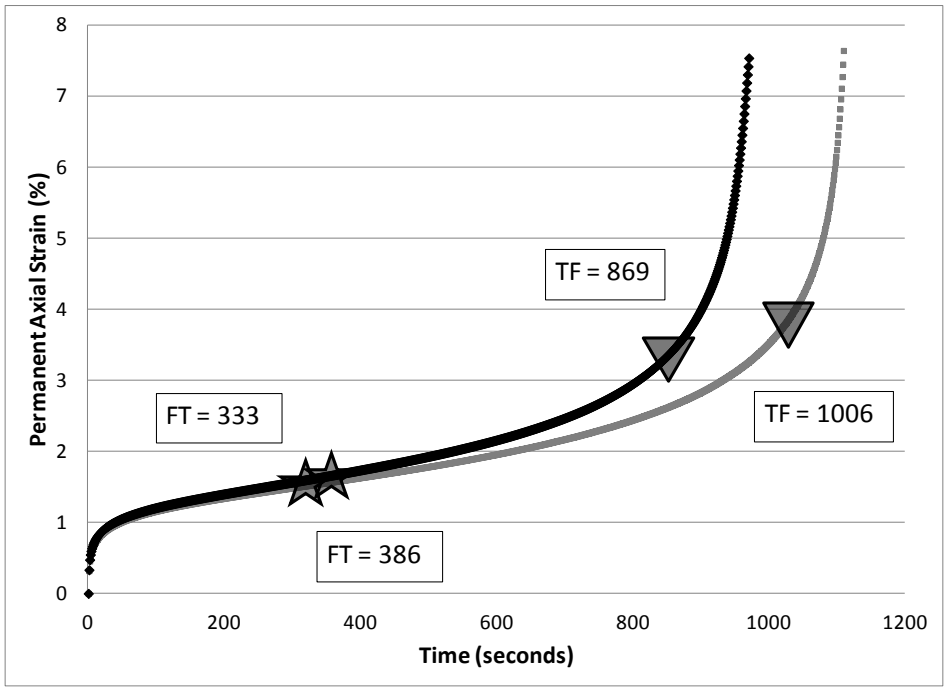

Figure B34. 19 FLS10 with PG 76-22

APPENDIX C

DYNAMIC MODULUS

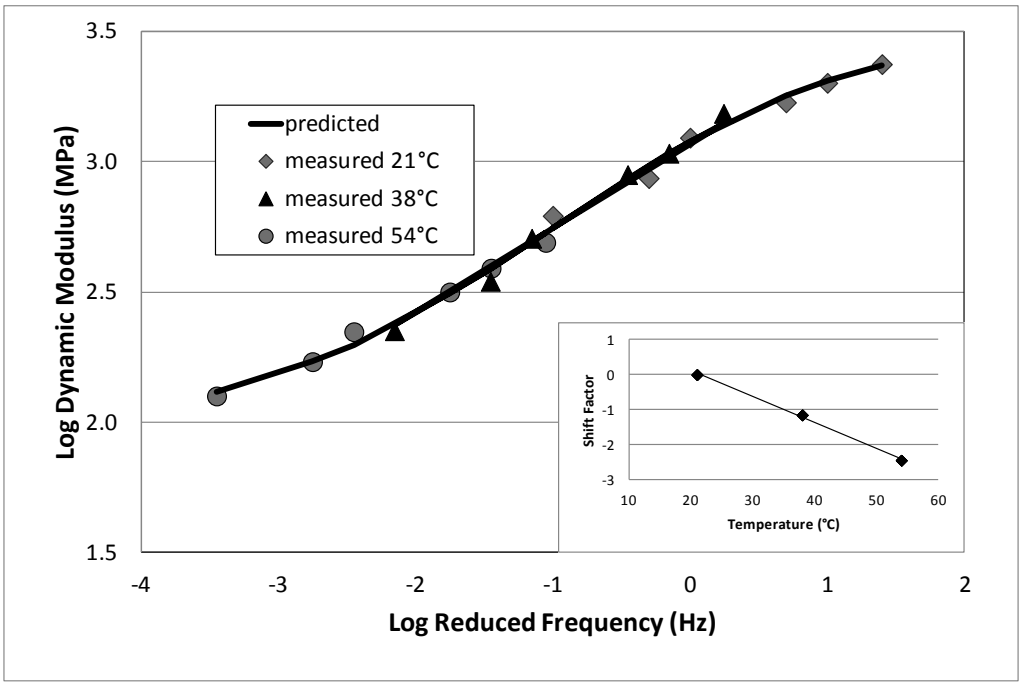

Figure C1. 12.5 FGN0 with PG 64-22

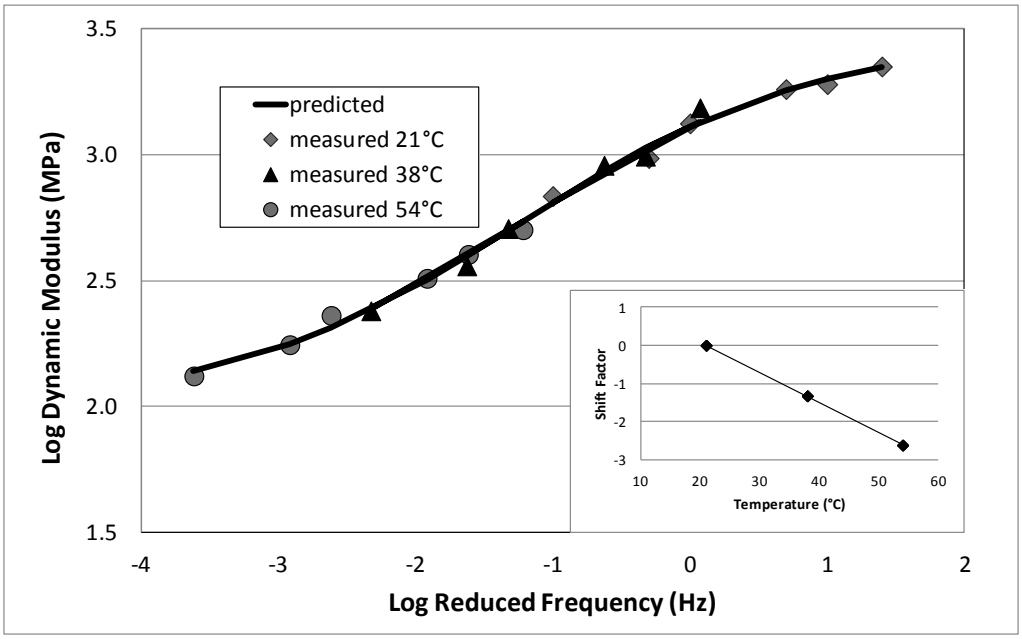

Figure C2. 12.5 CGN0 with PG 64-22

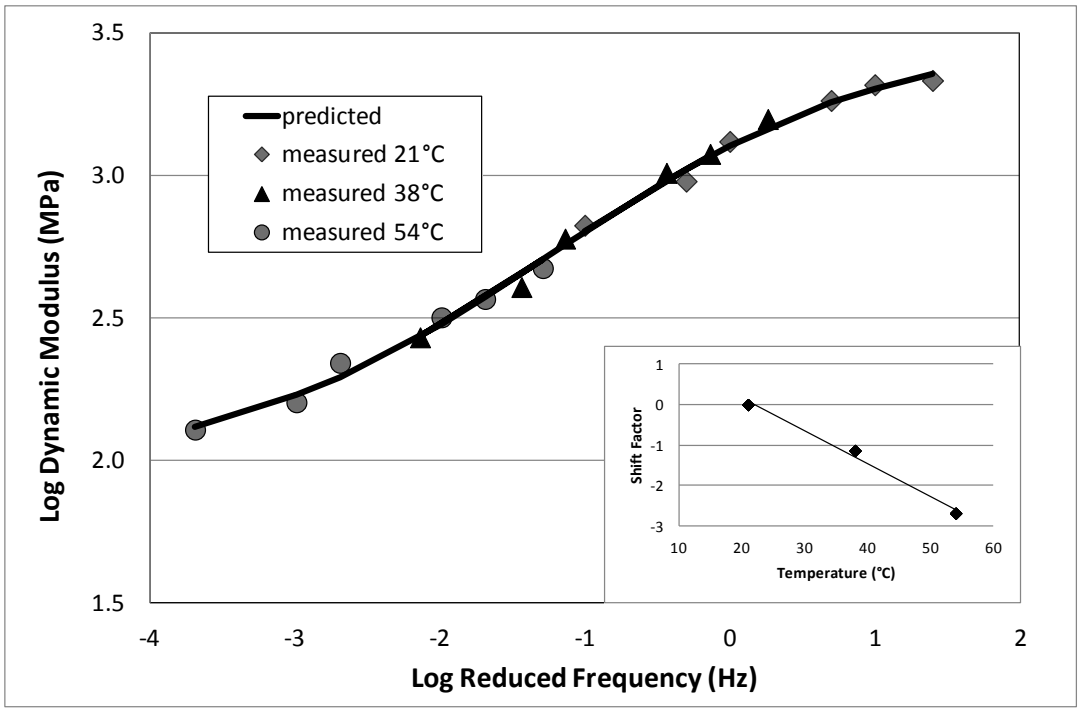

Figure C3. 19 FGN0 with PG 64-22

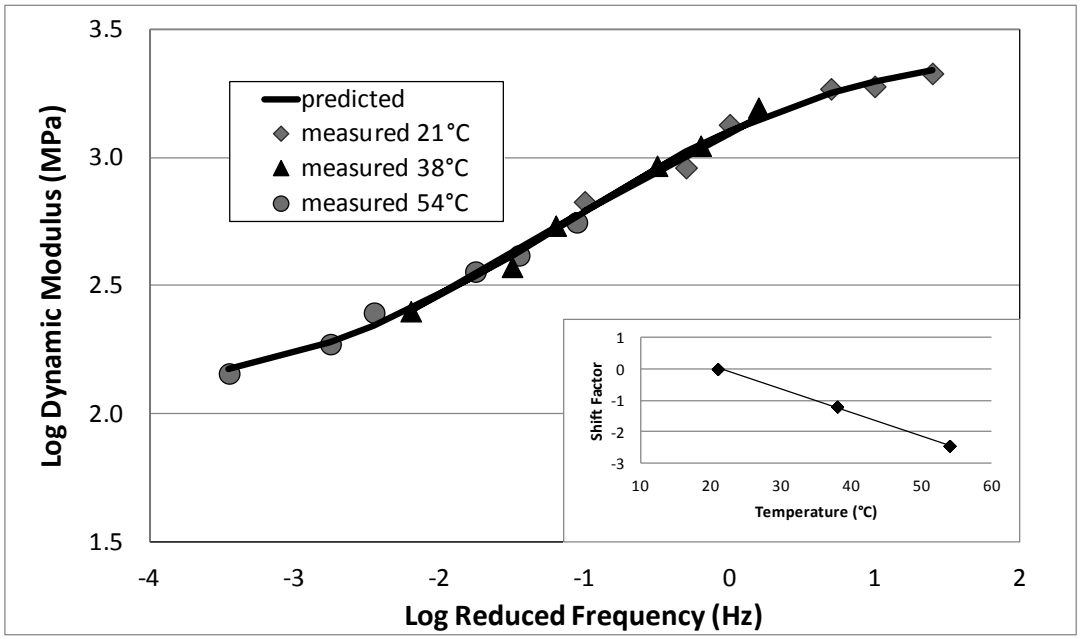

Figure C4. 19 CGN0 with PG 64-22

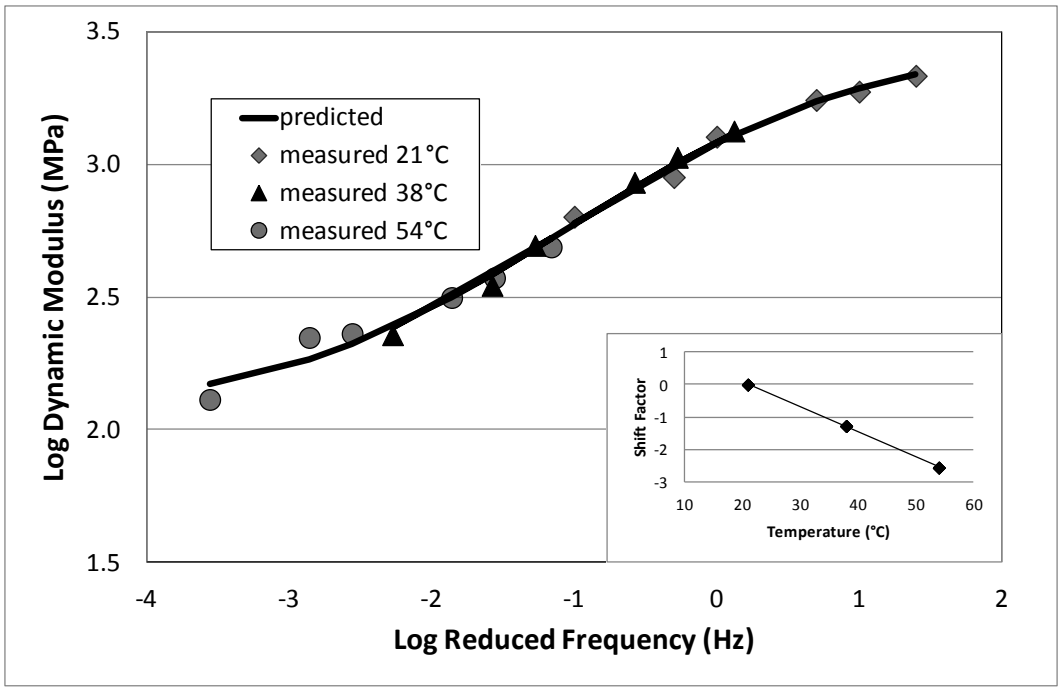

Figure C5. 12.5 FGN10 with PG 64-22

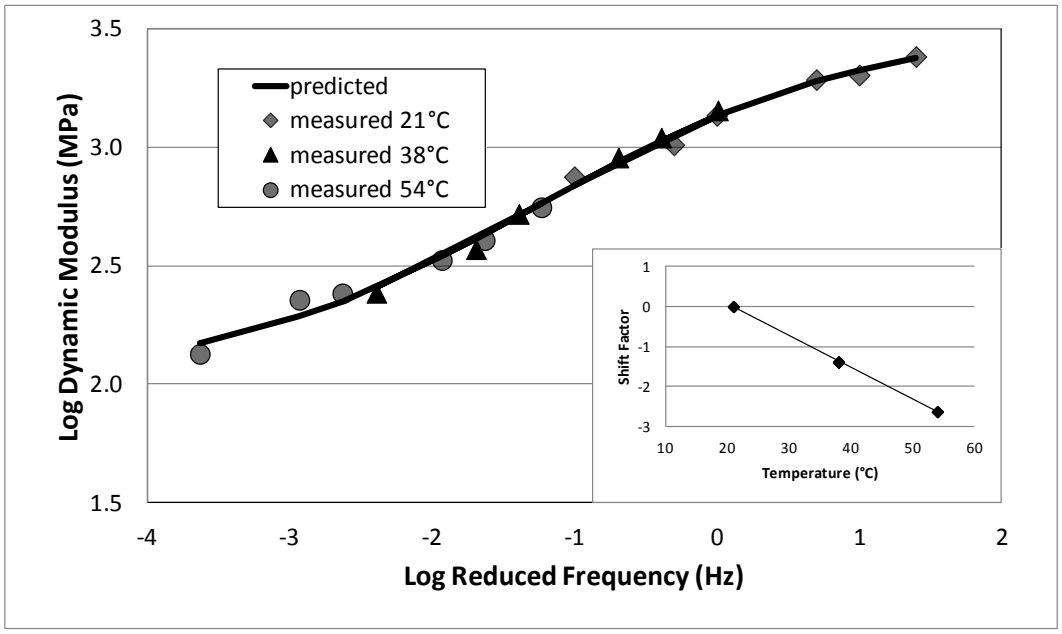

Figure C6. 12.5 CGN10 with PG 64-22

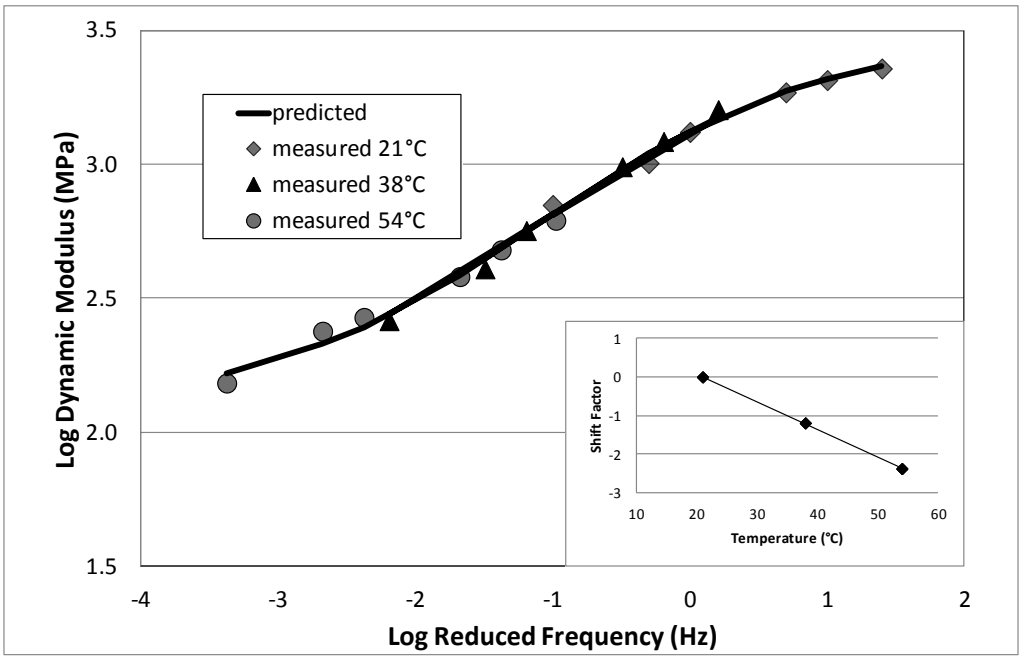

Figure C7. 19 FGN10 with PG 64-22

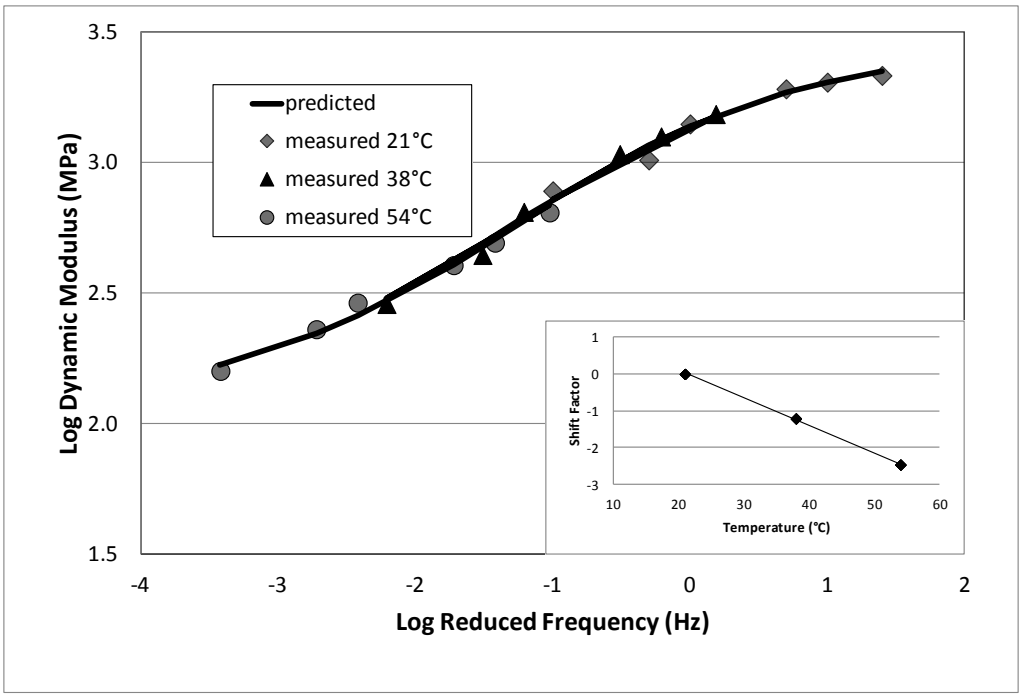

Figure C8. 19 CGN10 with PG 64-22

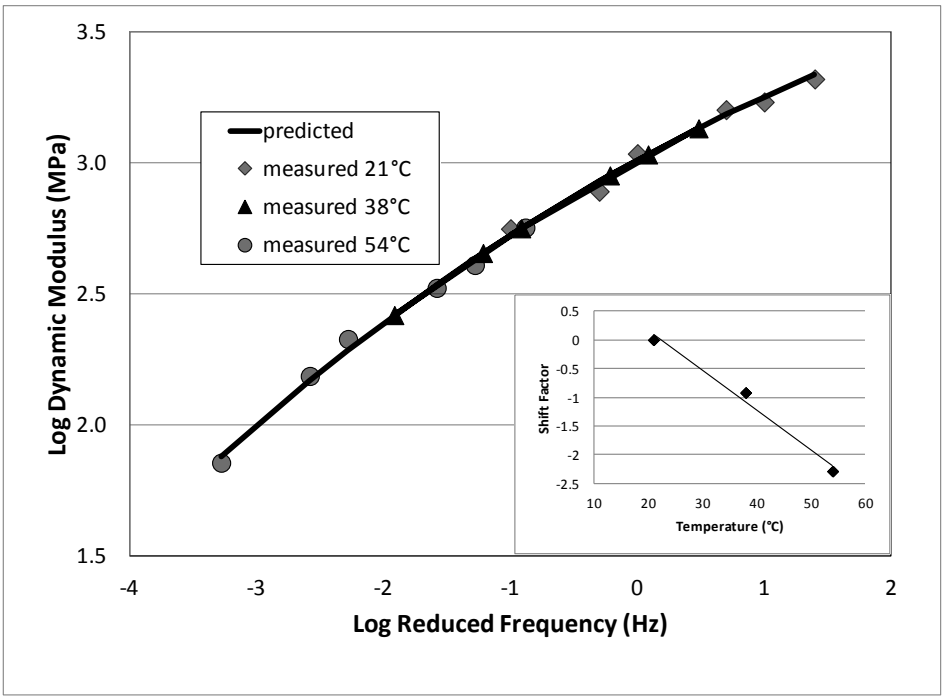

Figure C9. 12.5 FGN30 with PG 64-22

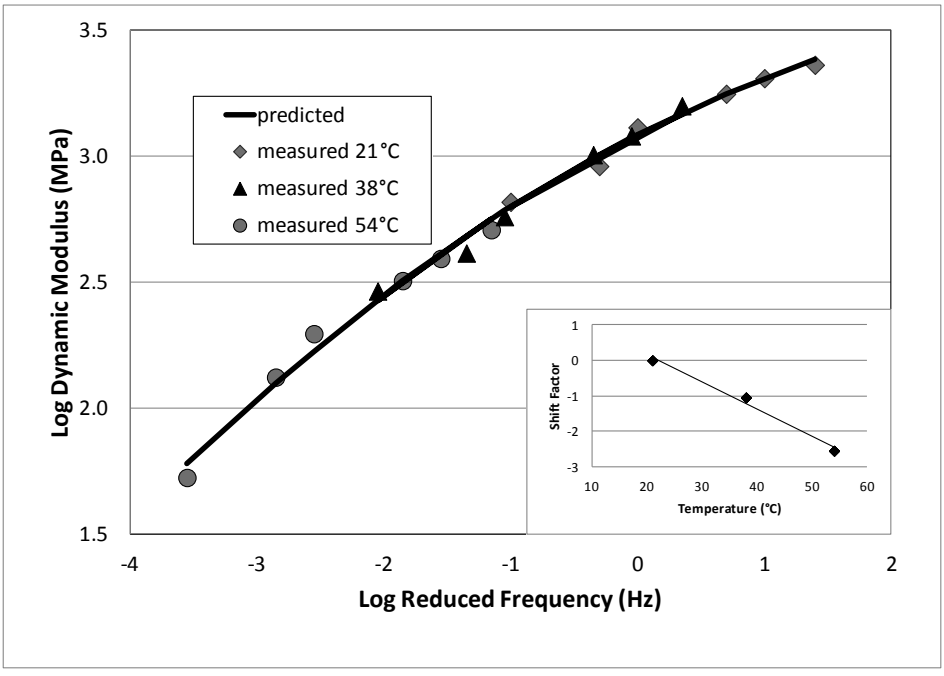

Figure C10. 12.5 CGN30 with PG 64-22

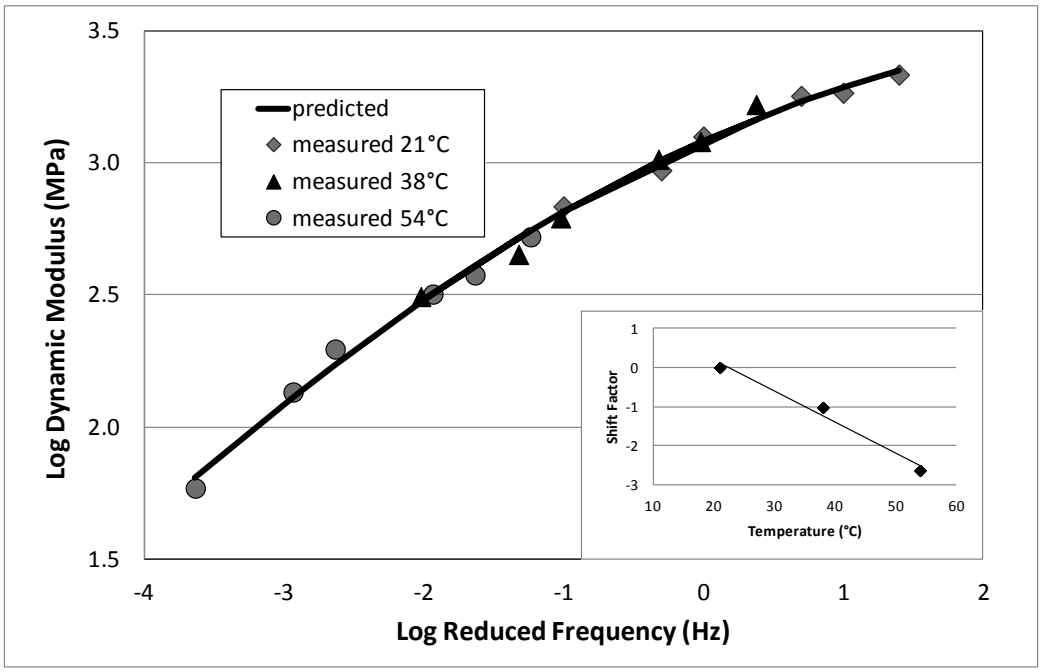

Figure C11. 19 FGN30 with PG 64-22

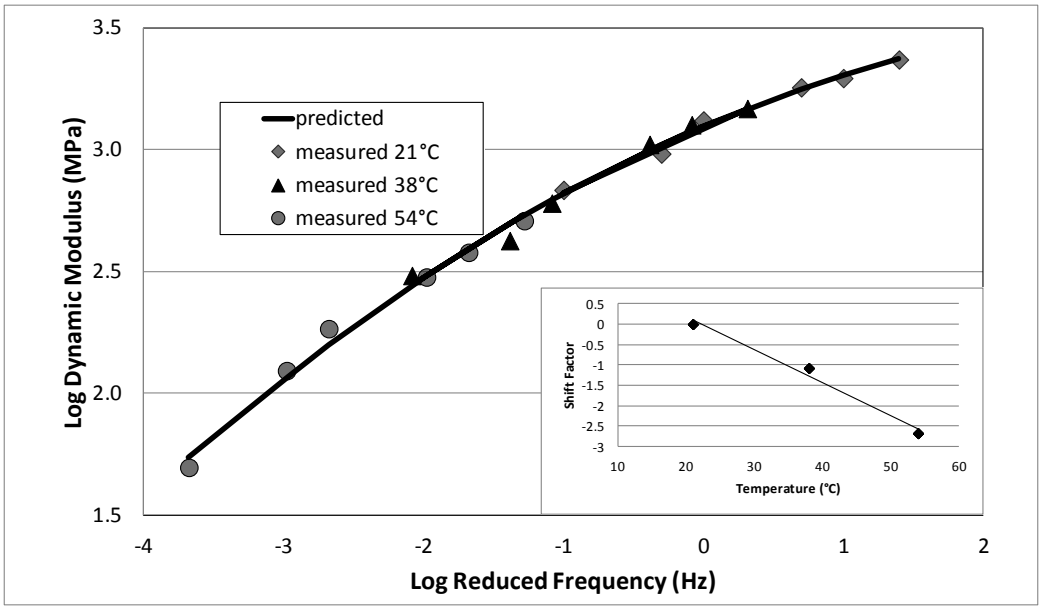

Figure C12. 19 CGN30 with PG 64-22

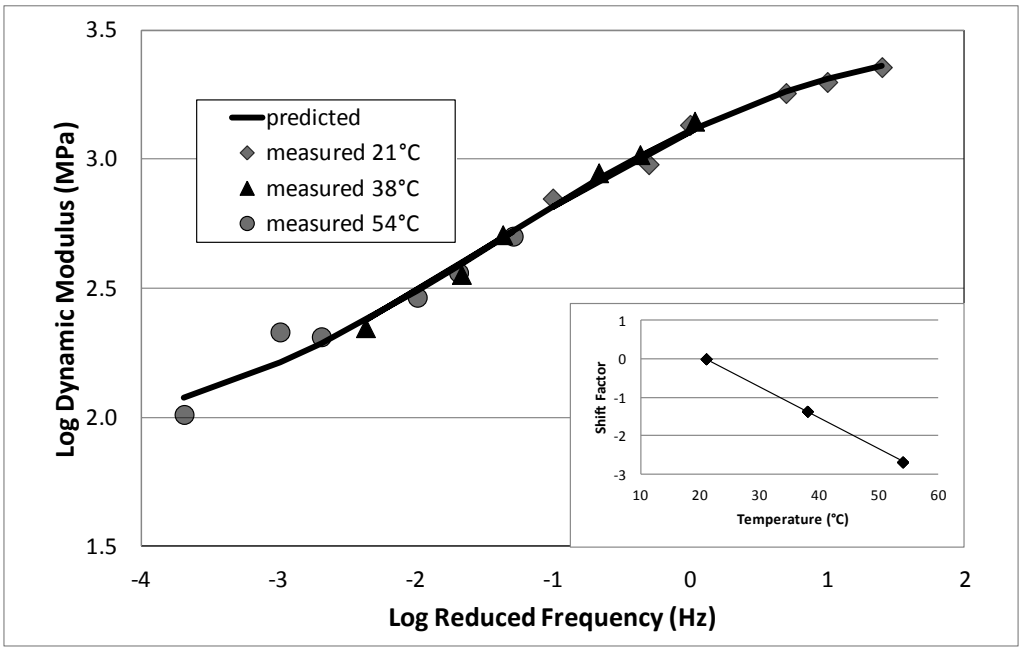

Figure C13. 12.5 GV0 with PG 64-22

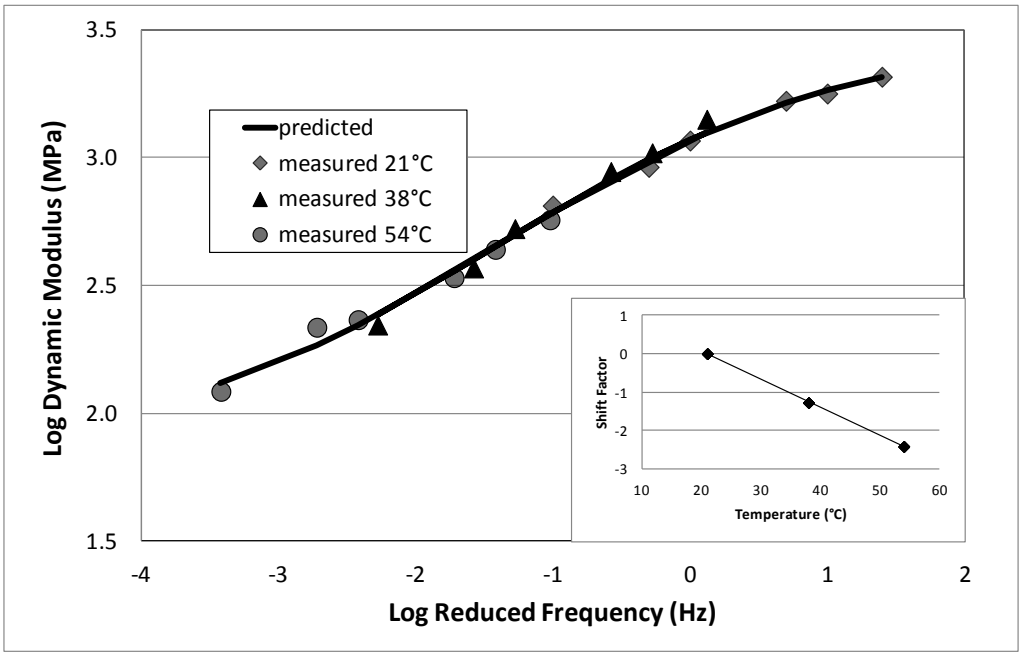

Figure C14. 19 FGV0 with PG 64-22

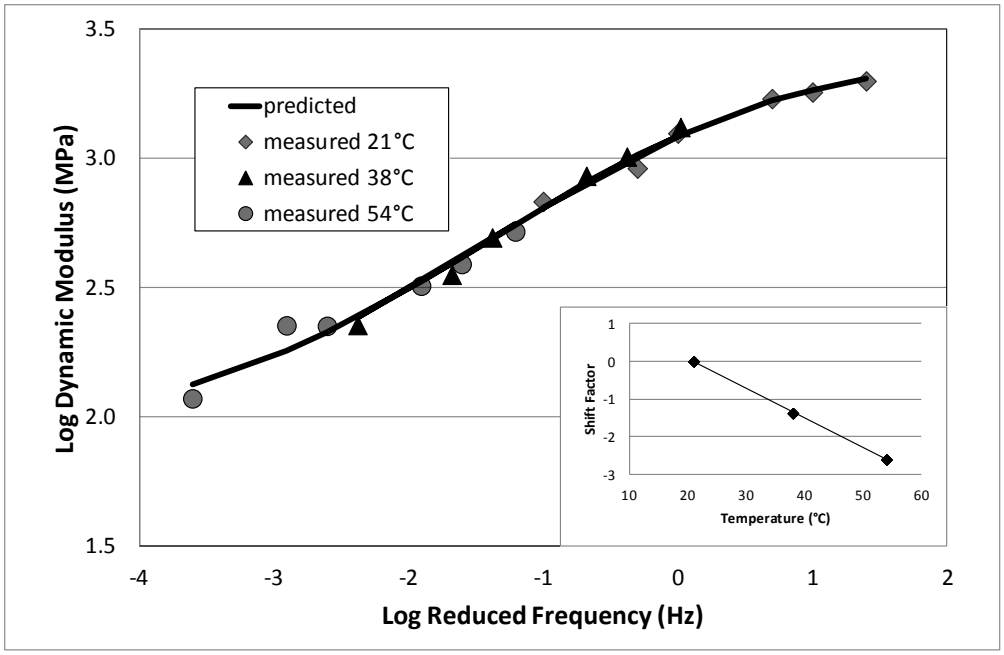

Figure C15. 19 CGV0 with PG 64-22

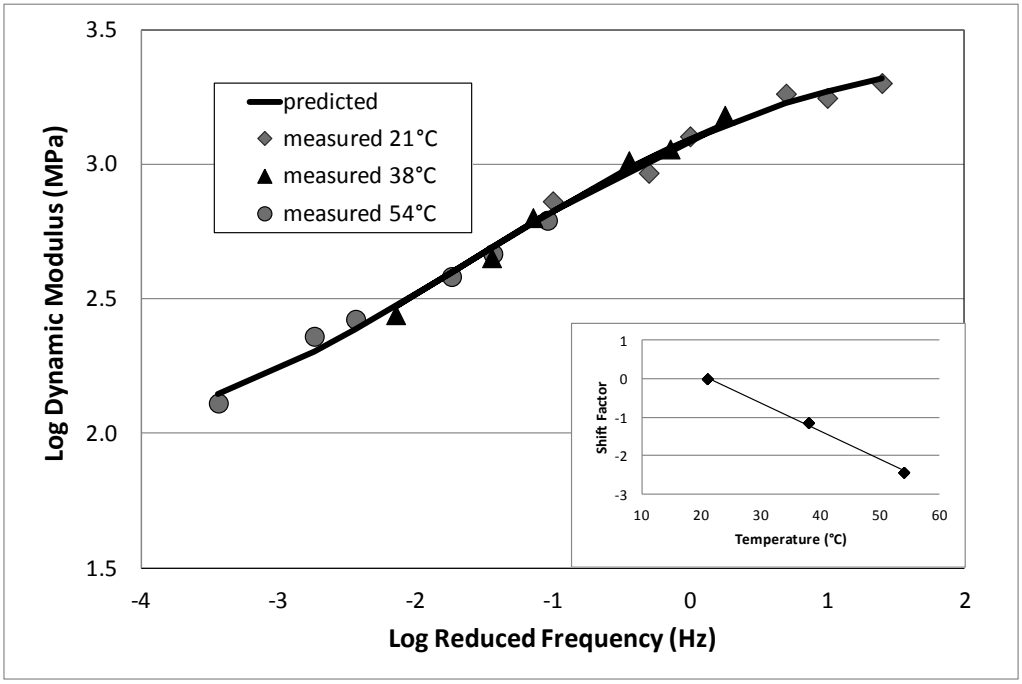

Figure C16. 12.5 GV10 with PG 64-22

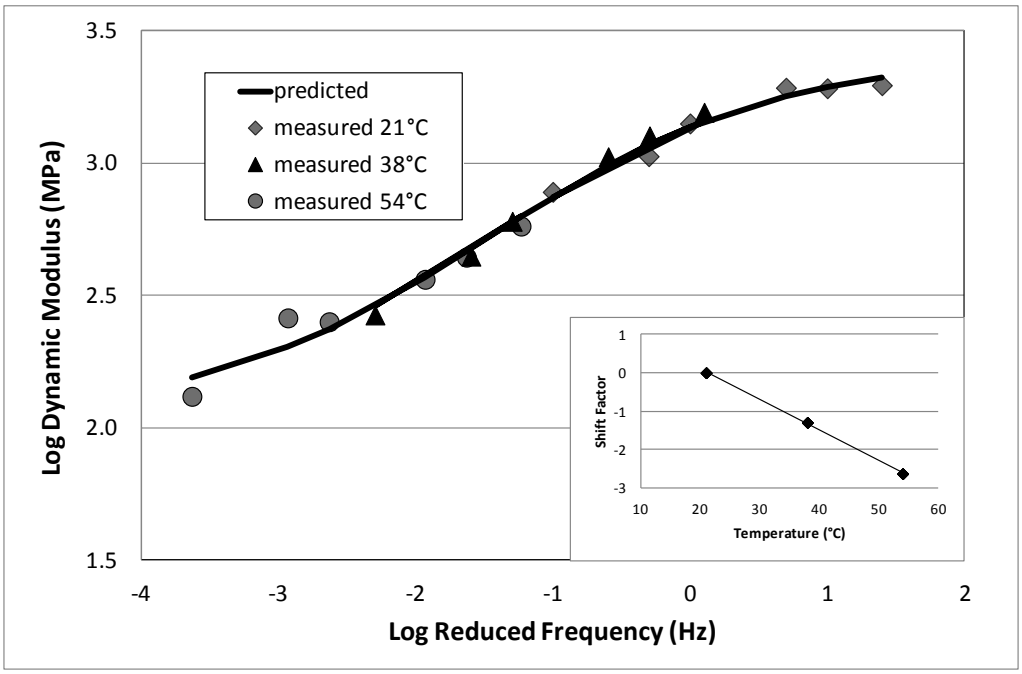

Figure C17. 19 FGV10 with PG 64-22

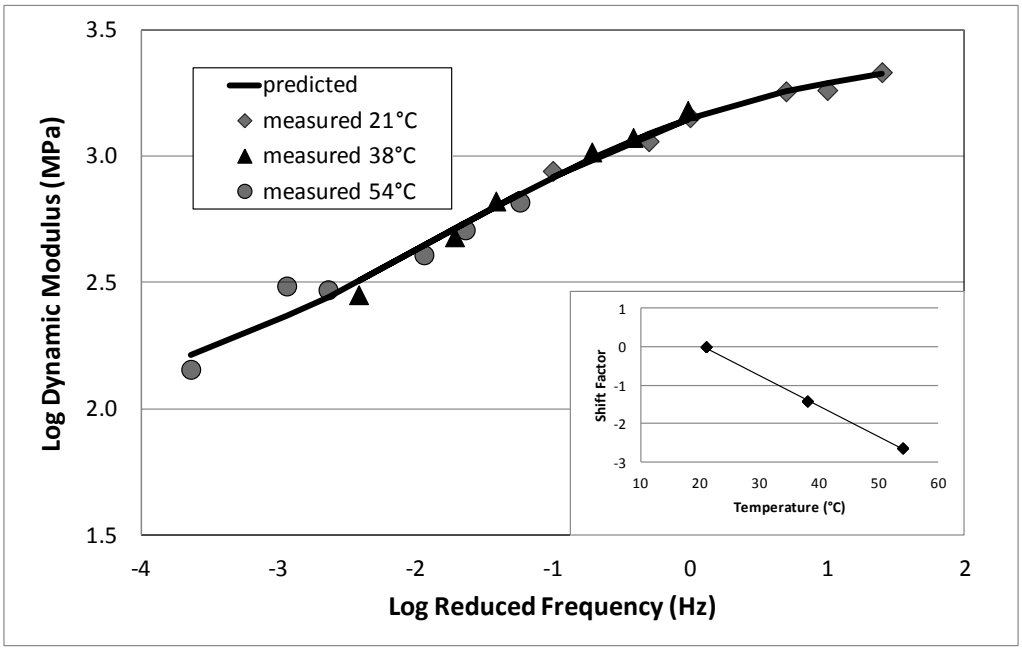

Figure C18. 19 CGV10 with PG 64-22

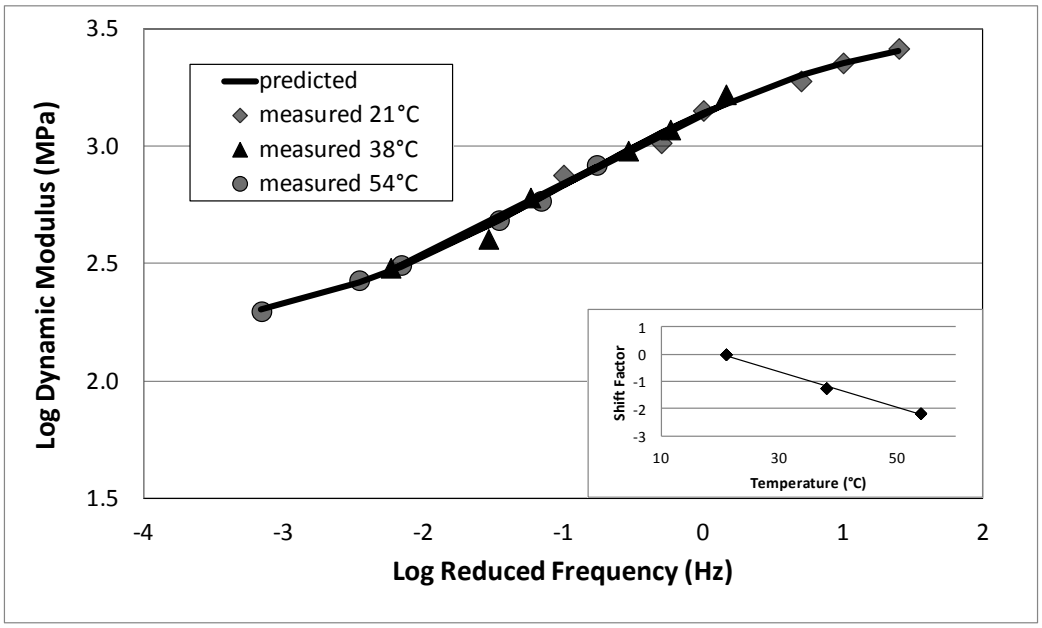

Figure C19. 12.5 FLS0 with PG 64-22

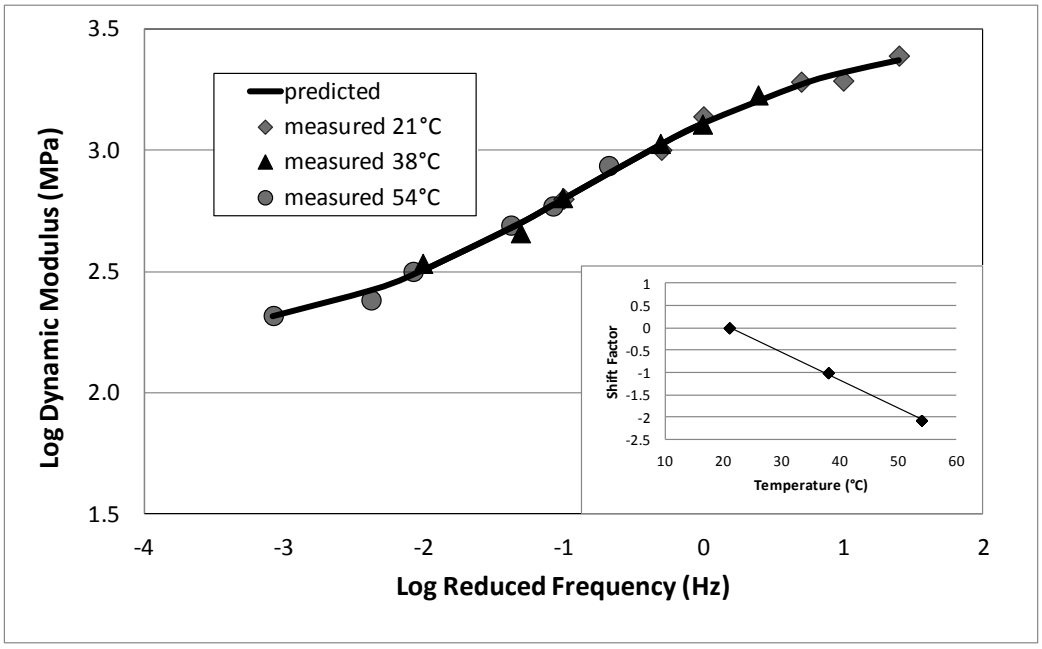

Figure C20. 12.5 CLS0 with PG 64-22

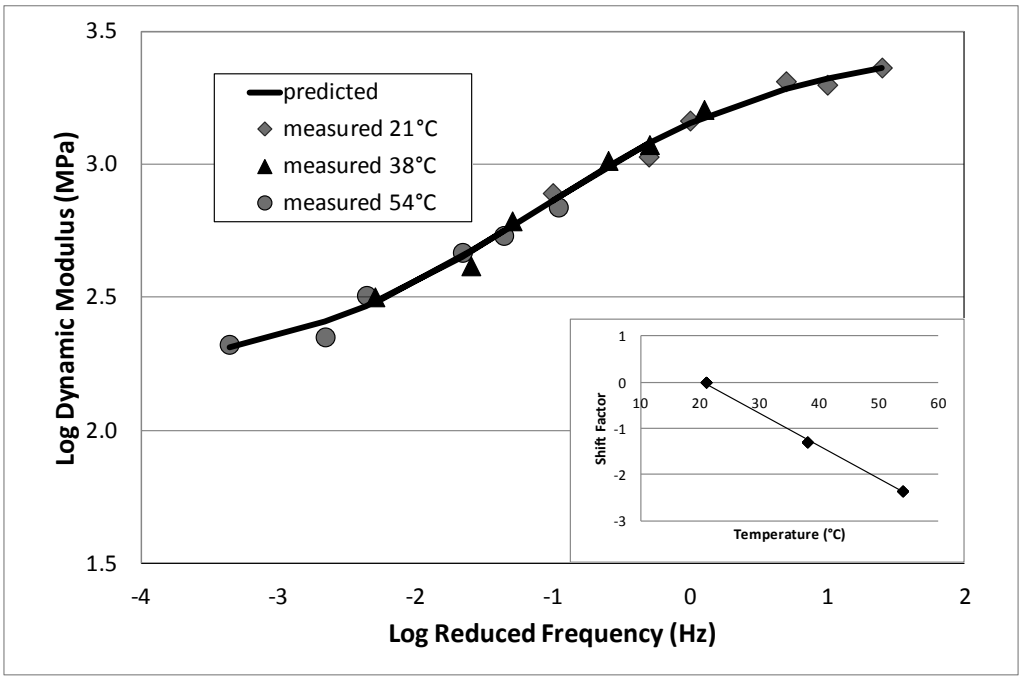

Figure C21. 19 FLS0 with PG 64-22

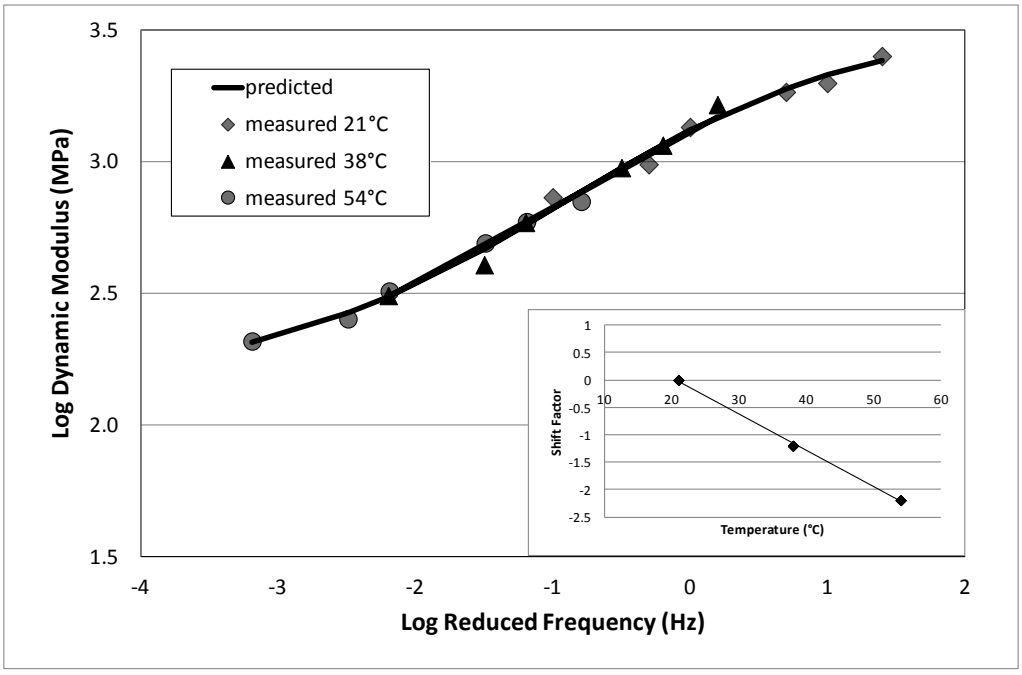

Figure C22. 19 CLS0 with PG 64-22

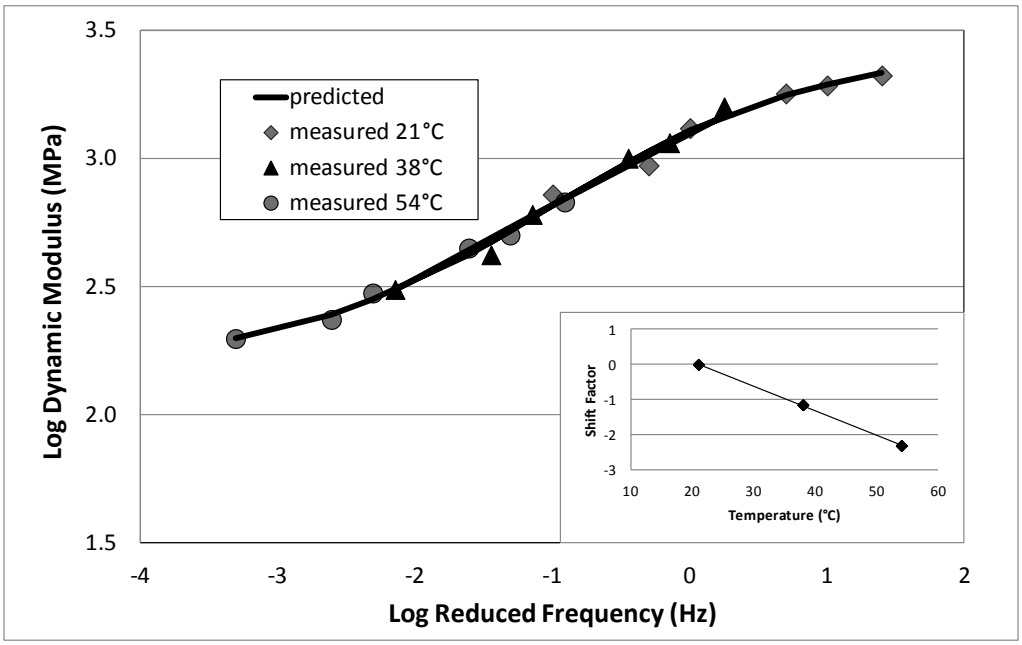

Figure C23. 12.5 FLS10 with PG 64-22

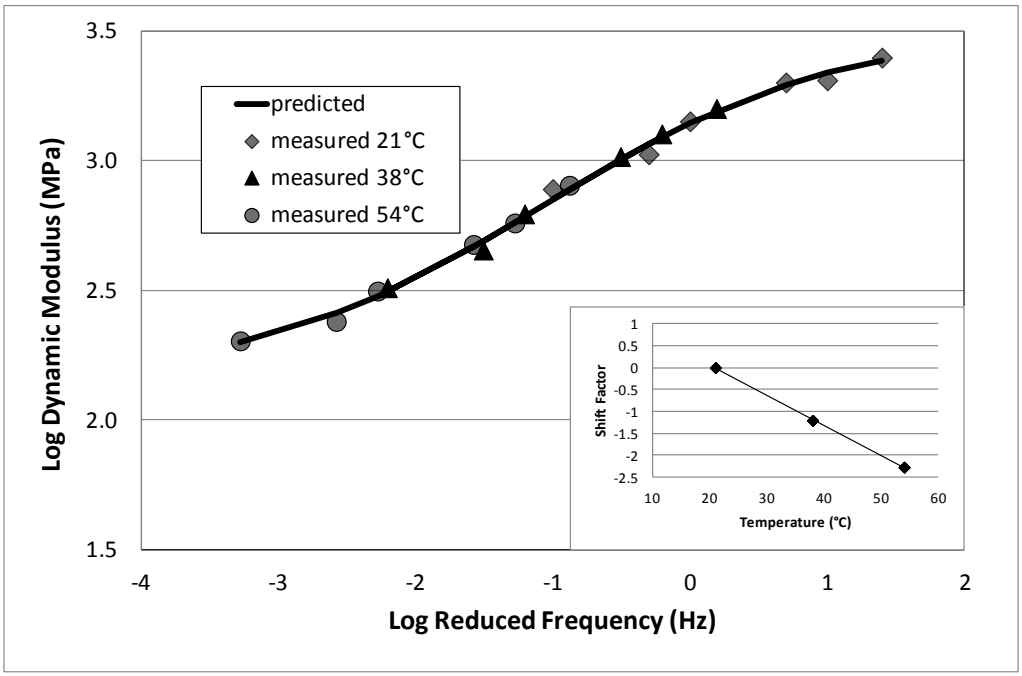

Figure C24. 12.5 CLS10 with PG 64-22

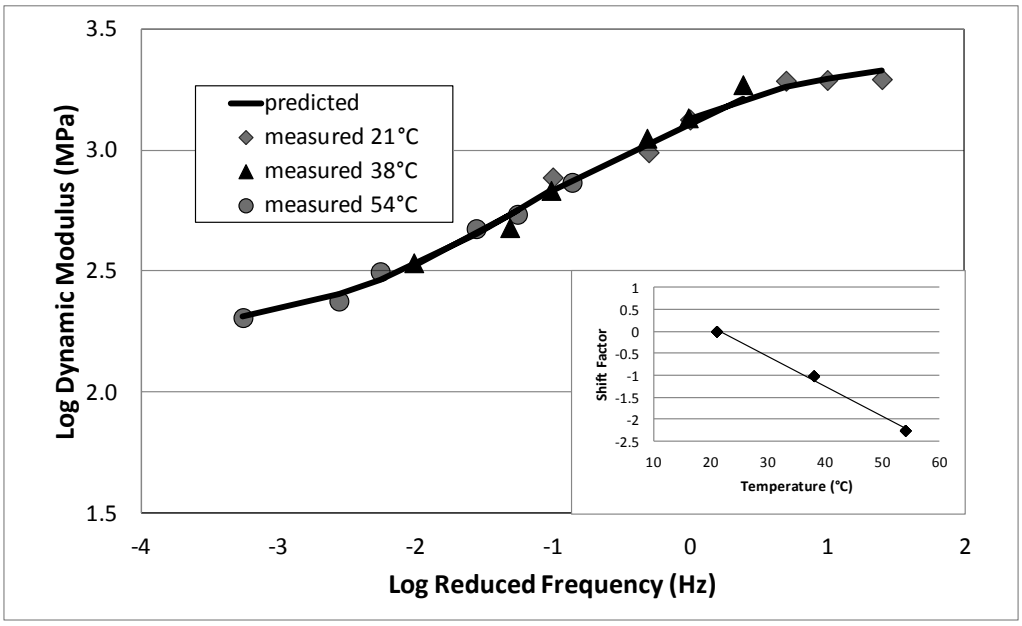

Figure C25. 19 FLS10 with PG 64-22

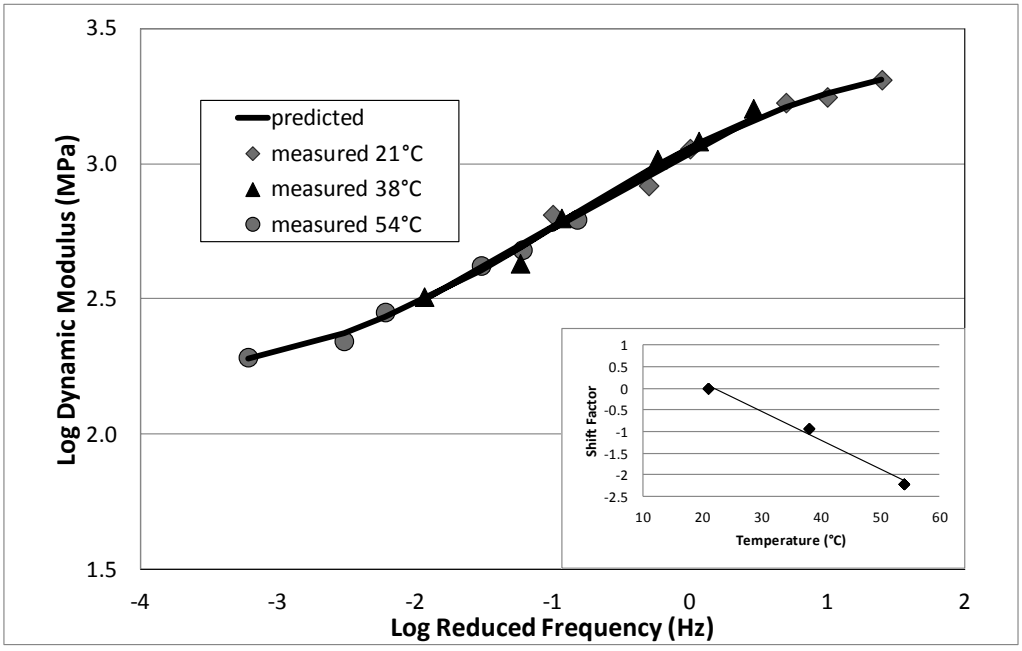

Figure C26. 19 CLS10 with PG 64-22

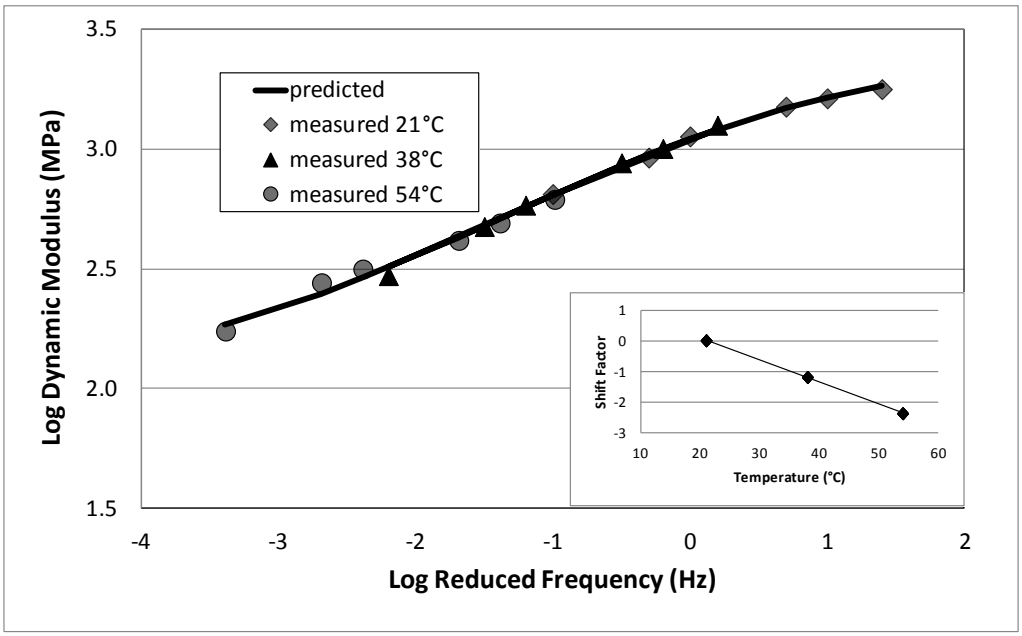

Figure C27. 12.5 FGN0 with PG 76-22

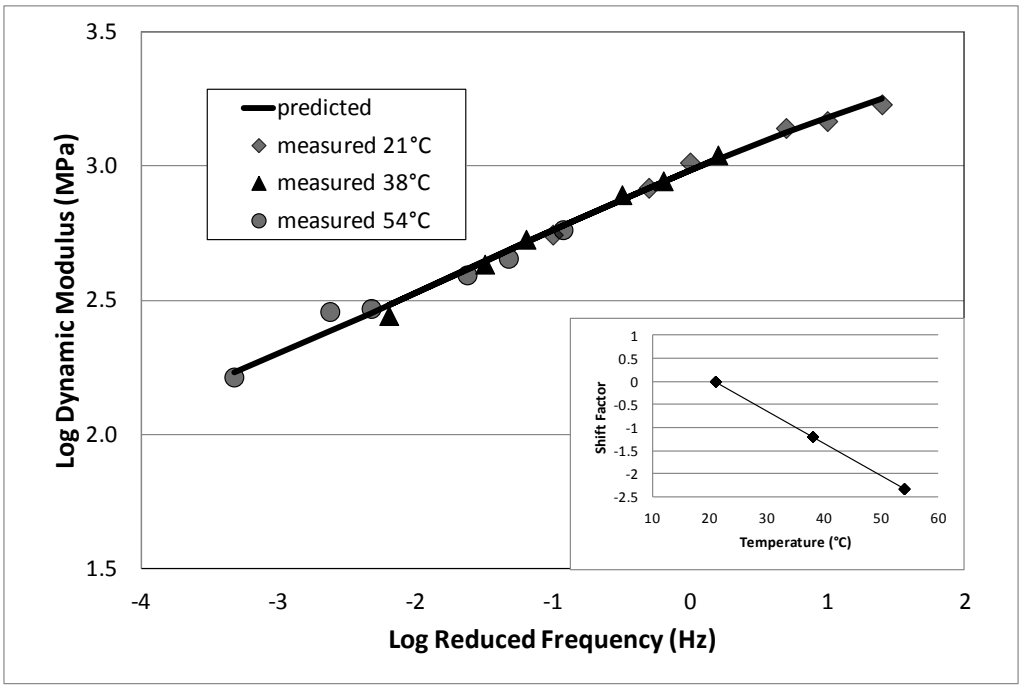

Figure C28. 12.5 CGN0 with PG76-22

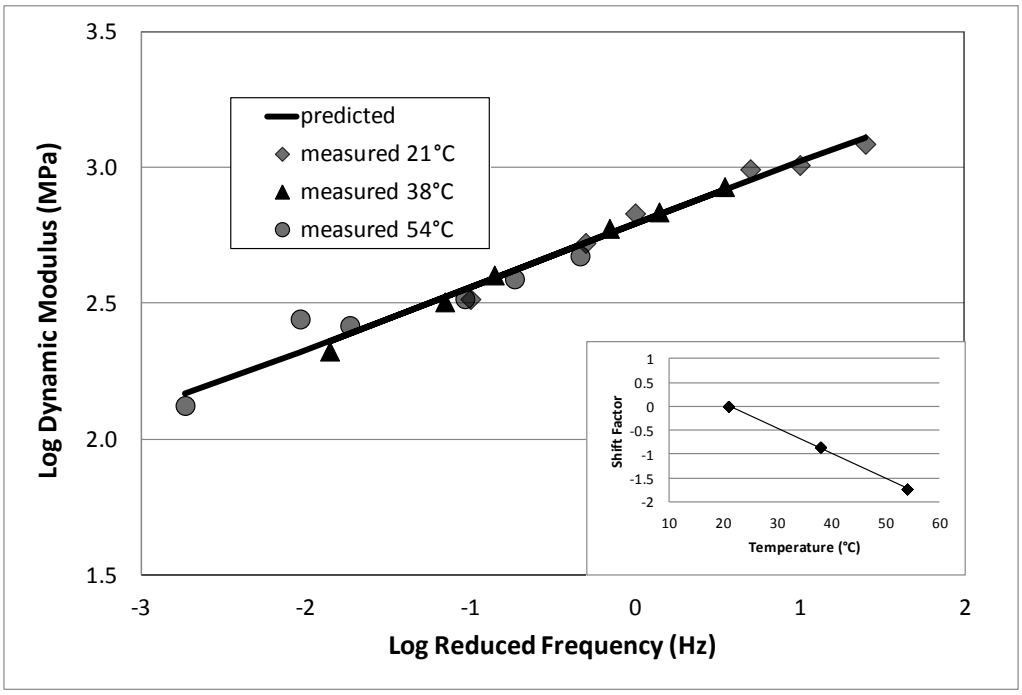

Figure C29. 19 FGN30 with PG 76-22

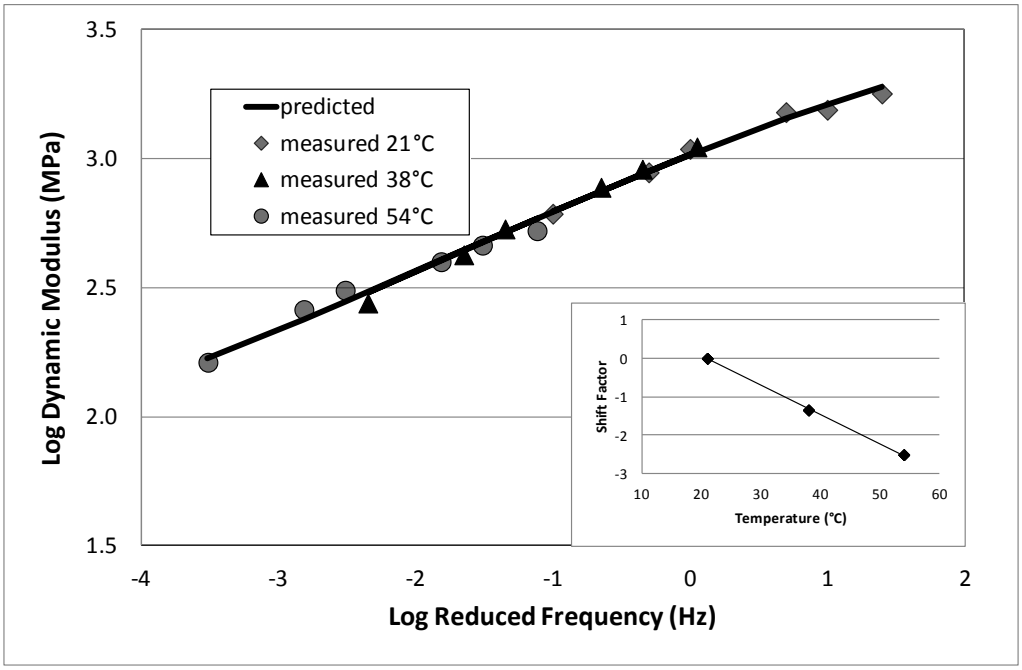

Figure C30. 12.5 GV0 with PG 76-22

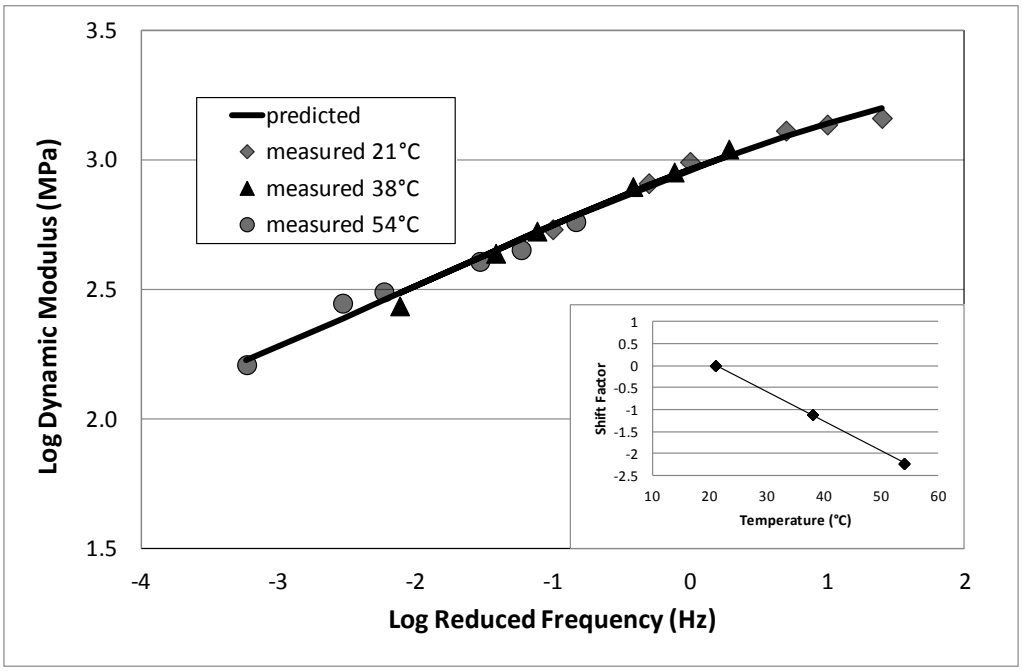

Figure C31. 19 CGV0 with PG 76-22

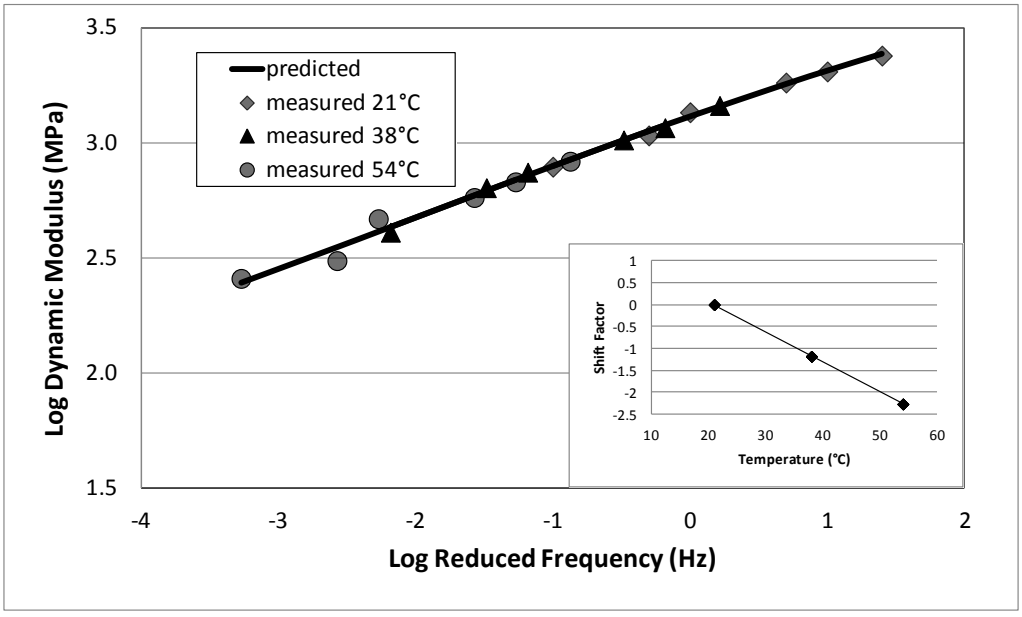

Figure C32. 12.5 CLS0 with PG 76-22

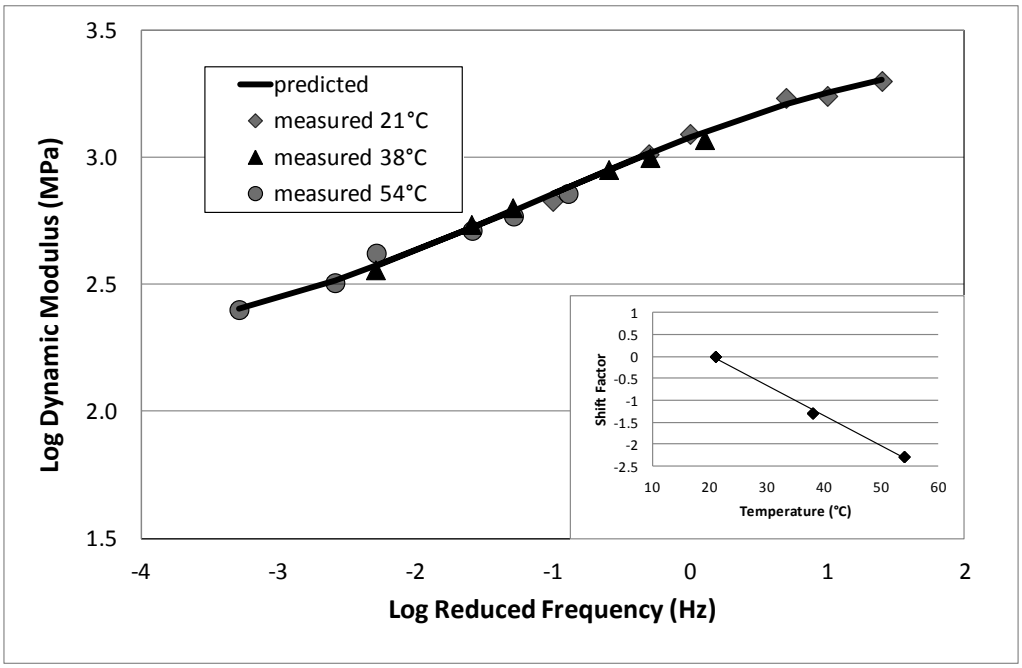

Figure C33. 19 CLS0 with PG 76-22

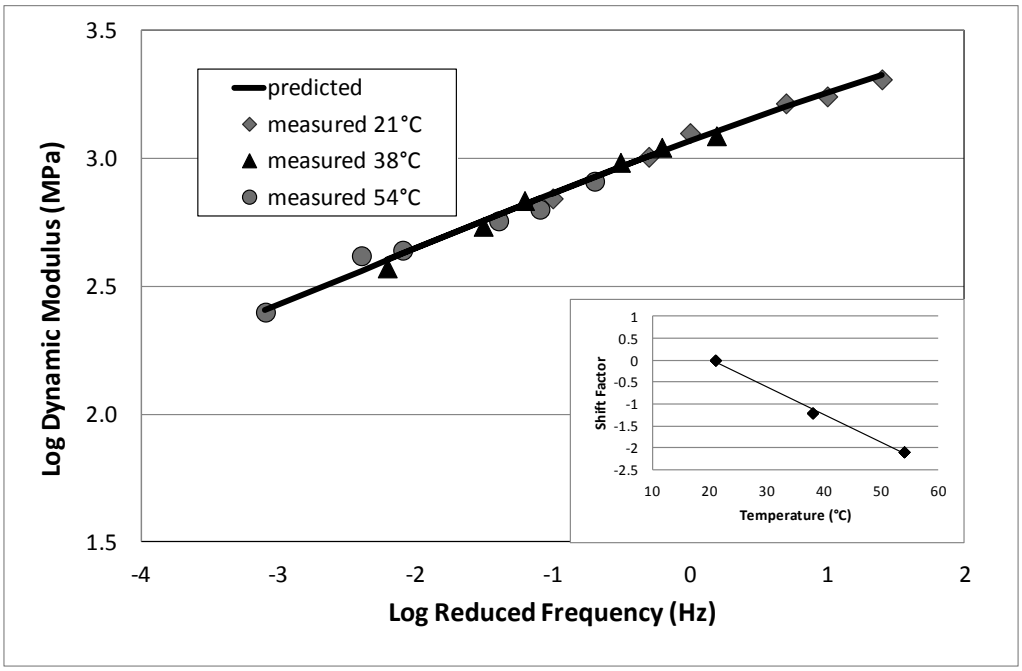

Figure C34. 19 FLS10 with PG 76-22